

SEP 14 1993

# THIN FILM CREEP-FORMING FOR SOLAR THERMAL PROPULSION APPLICATIONS

**Paul A. Gierow**  
**William R. Clayton**  
**James Moore**

**SRS Technologies**  
**990 Explorer Blvd. NW**  
**Huntsville AL 35806**

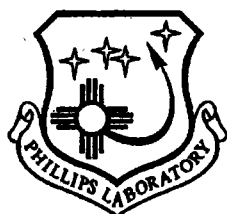
**August 1993**

**Final Report**

Distribution authorized to U.S. Government agencies and their contractors. Critical Technology, August 1993. Other requests for this document must be referred to GL-ACPL/TSR, 5 Polk Ave., Edwards AFB CA 93524-7015.

**WARNING** - This document contains technical data whose export is restricted by the Arms Export Control Act (Title 22, U.S.C., Sec 2751 et seq.) or the Export Administration Act of 1979, as amended. (Title 50, U.S.C., App. 2401, et seq.) Violations of these export laws are subject to severe criminal penalties. Disseminate in accordance with the provisions of AFR 80-34.

**DESTRUCTION NOTICE** - Destroy by any method that will prevent disclosure of contents or reconstruction of the document.



**PHILLIPS LABORATORY**  
**Propulsion Directorate**  
**AIR FORCE MATERIEL COMMAND**  
**EDWARDS AIR FORCE BASE CA 93524-7001**

**NOTICE TO ACCOMPANY THE DISSEMINATION OF  
EXPORT-CONTROLLED TECHNICAL DATA**

1. Export of information contained herein, which includes, in some circumstances, release to foreign nationals within the United States, without first obtaining approval or license from the Department of State for items controlled by the International Traffic in Arms Regulations (ITAR), or the Department of Commerce for items controlled by the Export Administration Regulations (EAR), may constitute a violation of law.
2. Under 22 U.S.C.2778 the penalty for unlawful export of items or information controlled under the ITAR is up to 2 years imprisonment, or a fine of \$100,000, or both. Under 50 U.S.C., Appendix 2410, the penalty for unlawful export of items or information controlled under the EAR is a fine of up to \$1,000,000, or five times the value of the exports, whichever is greater; or for an individual, imprisonment of up to 10 years, or a fine of up to \$250,000, or both.
3. In accordance with your certification that establishes you as a "qualified U.S. contractor," unauthorized dissemination of this information is prohibited and may result in disqualification as a qualified U.S. contractor, and may be considered in determining your eligibility for future contracts with the Department of Defense.
4. The U.S. Government assumes no liability for direct patent infringement, or contributory patent infringement or misuse of technical data.
5. The U.S. Government does not warrant the adequacy, accuracy, currency, of completeness of the technical data.
6. The U.S. Government assumes no liability for loss, damage, or injury resulting from manufacture or use for any purpose of any product, article, system, or material involving reliance upon any or all technical data furnished in response to the request for technical data.
7. If the technical data furnished by the Government will be used for commercial manufacturing of other profit potential, a license for such use may be necessary. Any payments made in support of the request for data do not include or involve any license rights.
8. A copy of this notice shall be provided with any partial or complete reproduction of these data that are provided to qualified U.S. contractors.

## FOREWORD

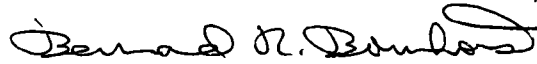
This final technical report was prepared by SRS Technologies, Huntsville AL under Small Business Innovative Research Phase II contract F04611-87-C-0065, for Operating Location AC, Phillips Laboratory, Edwards AFB, 93524-7001. Project Manager for Phillips Laboratory was Kristi Laug.

The report has been reviewed and is approved for release and distribution in accordance with the distribution statement on the cover and on the SF Form 298.



---

KRISTI K. LAUG  
Project Manager



---

BERNARD R. BORNHORST  
Chief, Space Propulsion Branch



---

LAWRENCE P. QUINN  
Deputy Director  
Fundamental Technologies Division

**REPORT DOCUMENTATION PAGE**Form Approved  
OMB No 0704-0188

Public reporting burden for this collection of information is estimated to average 1 hour per response, including the time for reviewing instructions searching existing data sources gathering and maintaining the data needed, and completing and reviewing the collection of information. Send comments regarding this burden estimate or any other aspect of this collection of information, including suggestions for reducing this burden to Washington Headquarters Services, Directorate for Information Operations and Reports, 1215 Jefferson Davis Highway, Suite 1204, Arlington, VA 22202-4302, and to the Office of Management and Budget, Paperwork Reduction Project (0740-0188), Washington DC 20503.

1. AGENCY USE ONLY (LEAVE BLANK)		2. REPORT DATE August 1993	3. REPORT TYPE AND DATES COVERED Final Sep 1987 - Jan 1992	
4. TITLE AND SUBTITLE Thin Film-Forming for Solar Thermal Propulsion Applications			5. FUNDING NUMBERS C: F04611-87-C-0065 FE: 62302F FR: 3058 TA: 006N	
6. AUTHOR(S) Paul A. Gierow, William R. Clayton, and James Moore				
7. PERFORMING ORGANIZATION NAME(S) AND ADDRESS(ES) SRS Technologies 990 Explorer Blvd, NW Huntsville AL 35806			8. PERFORMING ORGANIZATION REPORT NUMBER	
9. SPONSORING/MONITORING AGENCY NAME(S) AND ADDRESS(ES) Phillips Laboratory OLAC-PL/RKAS 4 Draco Drive Edwards AFB, CA 93524-7190			10. SPONSORING/MONITORING AGENCY REPORT NUMBER  PL-TR-93-3001	
11. SUPPLEMENTARY NOTES  COSATI CODE(S):				
12a. DISTRIBUTION/AVAILABILITY STATEMENT Distribution authorized to U. S. Government agencies and their contractors; Critical Technology, Aug 93. All other requests for this document shall be referred to OLAC-PL/TSR, 5 Pollux Drive, Edwards AFB CA 93524-7015			12b. DISTRIBUTION CODE	
13. ABSTRACT (MAXIMUM 200 WORDS) Development of a Solar Powered Rocket depends heavily on demonstrating the technology for light-weight space-deployable solar concentrators. Large parabolic shaped thin film reflectors can be packaged with other solar powered propulsion elements and deployed in low earth orbit. The Solar Powered Rocket Engine is expected to produce specific impulses of 1000 to 1200 seconds. This is over two to three times that of conventional liquid hydrogen/oxygen engines. This performance would significantly improve travel from low earth orbit to geostationary equatorial orbit. The objectives of this Phase II Small Business Innovative Research Program were to support the solar thermal propulsion program through advancing: polyimide materials, fabrication technologies, analytical modeling of concentrators, construction models of doubly curved off-axis parabolic solar concentrators. This research advanced the solar thermal propulsion by enabling fabrication of doubly-curved membrane, off-axis parabolic solar concentrators of low weight/area ratio and high concentration ratio.				
14. SUBJECT TERMS Polyimides, Membranes, Concentrators, Inflatables, Solar Thermal Rocket			15. NUMBER OF PAGES 150	16. PRICE CODE
17. SECURITY CLASSIFICATION OF REPORT Unclassified	18. SECURITY CLASSIFICATION OF THIS PAGE Unclassified	19. SECURITY CLASSIFICATION OF ABSTRACT Unclassified	20. LIMITATION OF ABSTRACT SAR	

# Table of Contents

<b>1.0 — Executive Summary .....</b>	<b>1</b>
<b>2.0 — Introduction .....</b>	<b>3</b>
<b>3.0 — Research Performed .....</b>	<b>5</b>
<b>3.1 — Polyimide Material Testing and Evaluation .....</b>	<b>5</b>
3.1.1 — Literature Survey and Equipment Search .....	5
3.1.2 — Thin Film Material Test Design and Equipment .....	6
3.1.2.1 — Uniaxial Test Apparatus .....	8
3.1.2.2 — Uniaxial Test Procedures .....	10
3.1.2.3 — Method of Cutting Material Samples .....	11
3.1.2.4 — Biaxial Testing of Polymers .....	11
3.1.3 — Polyimide Material Testing .....	13
3.1.3.1 — Preliminary Testing .....	14
3.1.3.2 — Test Data Manipulation Software .....	15
3.1.3.3 — Material Test Results .....	18
3.1.3.4 — Analytical Methods to Represent Test Results .....	28
3.1.3.5 — NASA / Langley Developed Polyimide Materials .....	36
<b>3.2 — Reflector Fabrication Processes .....</b>	<b>37</b>
3.2.1 — Seaming of Flat Sheets, Gores and Combinations .....	37
3.2.1.1 — Seaming of Flat Sheets of Kapton .....	38
3.2.1.2 — Long-Term Film Effects .....	40
3.2.2 — Reflector Construction Without Seams .....	40
3.2.3 — Mandrel Film Curvature Forming Techniques .....	41
3.2.3.1 — Fabrication of Reflector Models Using Creep and Relaxation Forming Techniques .....	41
3.2.3.2 — Liquid Mandrel Centrifugal Spin-Casting of Polyimide Film .....	44
3.2.3.3 — Geodesic Network Mandrel Creep/Relaxation-Forming Study .....	49
3.2.3.4 — Graduated Thickness .....	50
3.2.4 — Reflective Coating of Polyimides .....	52
3.2.4.1 — Aluminum Vapor Deposition .....	53
3.2.4.2 — Electroless Deposition of Silver .....	53
3.3 — Refinement of Analytical Model .....	61
3.4 — Reflector Models .....	75
3.4.1 — Reflector Models Constructed .....	75

3.4.2 — Application of Reflective Coating to Spin-Cast Soluble Polyimide Film .....	81
3.4.3 — Optical Testing Apparatus .....	84
3.5 — Thin Film Heliostat for the Solar Laboratory .....	89
3.5.1 — Thin Film Casting Equipment Design and Fabrication .....	89
3.5.2 — Heliostat Structural Design .....	89
3.5.2.1 — Design of Triangular Segment Support Frame .....	90
3.5.2.2 — Heliostat Interface Designs .....	95
3.5.2.3 — Windshield Discussion .....	96
3.5.3 — Thin Film Process Development .....	96
3.5.3.1 — Evaluation of Electroless Spray Silvering .....	98
3.5.3.2 — Protective Coverings .....	100
3.5.3.3 — Sputtering Coating Study .....	103
3.5.3.4 — Spin-Casting Substrate Joint-Filler Study .....	104
3.5.3.5 — Triangular Substrate Casting .....	106
3.5.4 — Fabrication and Installation of the Thin Film Polyimide Heliostat Segments ...	107
3.5.5 — Summary of Lessons Learned Under Heliostat Contract .....	112
3.5.6 — Installation and Testing of the Heliostat Segments at the Solar Laboratory. ....	119
4.0 — Conclusions .....	121

# List of Figures

Figure 1	Uniaxial Test Apparatus .....	9
Figure 2	Toggle Grip Design .....	10
Figure 3	Computer Test Panel.....	10
Figure 4	Combined Stress Test Apparatus .....	13
Figure 5	Preliminary Kapton Creep Test .....	14
Figure 6	Raw Data Plot of Kapton Creep Test.....	16
Figure 7	Shifted Time = Zero at Point of Loading.....	17
Figure 8	Shifted Displacement of Test Data .....	17
Figure 9	Results of the Zero Macro Run .....	19
Figure 10	Zeroed, Normalized and Smoothed Results .....	19
Figure 11	“Basic” Creep Test of 0.5 mil Kapton .....	20
Figure 12	Kapton Creep Test Data at 1,200 psi and 600°F.....	22
Figure 13	The Mean and Envelope of Error for the Uniaxial Creep Test of Kapton conducted at 1,200 psi and 600°F .....	23
Figure 14	Kapton Creep Test Data at 1,200 psi and 650°F.....	24
Figure 15	Kapton Creep Test Data at 1,200 psi and 700°F.....	25
Figure 16	Kapton Uniaxial Creep Test Performed at 1,200 psi .....	26
Figure 17	Kapton Creep Compliance Curves for Tests Performed at 1,200 psi .....	26
Figure 18	Creep of Aluminized Kapton versus Kapton .....	27
Figure 19	Heat Shrinkage of Materials .....	27
Figure 20	Kapton 1.0 mil Transverse Strain at 1,500 psi.....	29
Figure 21	Relaxation of 1.0 and 0.5 mil Kapton Stain at 5% .....	29
Figure 22	Two Step Load Creep Test .....	30
Figure 23	Master Creep Compliance of Kapton at 1,500 psi.....	31
Figure 24	Master Creep Compliance of Kapton at 1,200 psi.....	32
Figure 25	Master Creep Compliance of Kapton at 2,000 psi.....	33
Figure 26	Master Creep Compliance of Kapton at 500 psi .....	34
Figure 27	Master Creep Compliance Curve .....	35
Figure 28	Film Seaming Method .....	39
Figure 29	Creep-Forming Process to Mandrel .....	43
Figure 30	Reflector Compared to Mandrel Shaping Forms .....	44
Figure 31	Optical Investigation of Focal Point for Off-Axis Reflector Model .....	45

Figure 32	Slicing Paraboloid by Radial Planes .....	45
Figure 33	Projected View of Reflector .....	46
Figure 34	Gore Sections of Off-Axis Reflector .....	46
Figure 35	Comparison of Phase 1 and Phase 2 Analytical Models .....	62
Figure 36	Elements that can be Generated by the Preprocessor .....	64
Figure 37	Examples of Finite Element Model with Elliptic Boundary .....	65
Figure 38	Examples of how the Shape Factor Z Effects the Position of Elements in the Finite Element Model.....	66
Figure 39	Finite Element Gridding Techniques used for Membrane Analysis.....	68
Figure 40	Finite Element Model of Uniaxial Test Speciment using Four Node Shell Elements.....	69
Figure 41	Comparison of Results from Abaqus Simulation and Uniaxial Creep Tests for 1,200 psi Stress .....	70
Figure 42	Comparison of Actual Test Data to Logarithmic Curve Fits for a Test at 500 psi Stress .....	72
Figure 43	Spin Cast Polyimide Film Mounted on Aluminum Support.....	75
Figure 44	Vacuum Deposited Aluminum Thin Film Polyimide.....	77
Figure 45	Formed Thin Film Membrane Using NASA Polyimide.....	79
Figure 46	Slope Error along Radius 1 .....	80
Figure 47	Slope Error along Radius 2 .....	80
Figure 48	Surface Error along Radius 1 .....	81
Figure 49	Surface Error along Radius 2 .....	81
Figure 50	Machined Off-Axis Mandrel for Film Casting.....	82
Figure 51	Aluminum Vapor Deposition Chamber for Step and Repeat Process.....	83
Figure 52	Polyimide Film Mounted on Glass Substrate.....	84
Figure 53	Aluminized Sections of Reflective Polyimide Mounted on Vacuum Chamger .....	84
Figure 54	Geometry of Optical Testing of Primary Mirror .....	85
Figure 55	Thickness Measurement of Polyimide Film.....	87
Figure 57	Curing Oven.....	91
Figure 58	Spin Table and Track System .....	93
Figure 59	Scale Model of Heliostat.....	94
Figure 60	Scale Model of the Option 3D Concept.....	95
Figure 61	Heliostat Test Article .....	97
Figure 62	Tensioning Structure .....	98

Figure 63	Truss Assembly (Concept No. 2).....	99
Figure 64	Truss Assembly No. 2.....	101
Figure 65	Seamed Glass Test Article .....	107
Figure 66	Casting of Thin Film .....	108
Figure 67	Mounting Film on Tensioning Structure .....	109
Figure 68	Silvering the Tensioned Polyimide Film .....	110
Figure 69	Casting Glass .....	112
Figure 70	Release of Silvered Film from Glass .....	113
Figure 71	Tensioning Silvered Film on Glass.....	114
Figure 72	Honeycomb Support Structure.....	114
Figure 73	Film Mounted on Tensioning Structure .....	115
Figure 74	Stretched Membrane Heliostat.....	116
Figure 75	Reflectivity Demonstration .....	117
Figure 76	Segments Ready for Transportation .....	118
Figure 77	Image of Heliostat Segment from Stretched Membrane and Glass Panels .....	119

## List of Tables

Table 1	Test Equipment Search .....	7
Table 2	Uniaxial Material Tests .....	12
Table 3	Test Parameters .....	21
Table 4	“Basic” Creep Test Data Sheet .....	21
Table 5	Material Properties of Kapton and Apical at 20°C .....	28
Table 6	Material Configurations .....	42
Table 7	Materials Constants .....	71
Table 8	Symmetrical Models Constructed.....	76
Table 9	Process Summary for One Segment.....	111

# 1.0 — Executive Summary

This final report documents the work performed under a Phase II Small Business Innovative Research program (SBIR) for the Air Force Phillips Laboratory. The objective of the effort was to build a scientific base of materials and processes data pertaining to high stability polymer films. This supports the solar thermal propulsion program through enabling fabrication of doubly-curved membrane off-axis paraboloidal solar concentrators, of low weight/area ratio and high concentration ratio. To achieve this objective the following tasks were set forth, and are summarized below.

**Task 1:** A data base of the high temperature viscoelastic properties of relevant film materials was developed. In accomplishing this task, a literature search was performed as to materials properties data and testing standards, and a vendor survey of available candidate film materials and suitable test equipment was conducted. Based on these study results, a creep testing/data acquisition/processing system was designed, fabricated and assembled. Extensive uniaxial and limited biaxial testing of candidate film materials viscoelastic properties was performed, and the resulting data was analyzed. The results of the materials characterization task led to the selection of polyimides developed by NASA's Langley Research Center. These polyimides are available in solution form and can be cast on parabolic mandrels to form the desired concentrator shapes.

**Task 2:** Studies concerning specific problem areas of the application of viscoelastic forming and spray/spin casting procedures to solar concentrator fabrication processes were conducted. This involved relating in general the data accumulated in Task 1 to the configuration/materials/processes design of models to be built under Task 4. Evaluation of gore/sheet seaming and gore versus seamed-sheet creep-forming options was per-

formed. Evaluating and minimizing seam and film imperfection effects on concentrator performance were addressed. Time, temperature, stress, effects on dimensional stability concerns, and investigating processing options such as mandrel-controlled creep/relaxation forming versus temperature-distribution-controlled pressure/creep-forming and spray/spin casting/curing on shaped mandrels were investigated.

**Task 3:** An analytical model for the membrane creep-forming process was developed and adapted. It was initially intended primarily to support the temperature-profile-controlled uniform-pressure creep-forming process, but the design includes the capability of describing and monitoring all other viscoelasticity-dependent film curvature forming processes, as well as the possible extension of the model predict on-station mechanical and thermal behavior of operational deployed thin film concentrators.

**Task 4:** Preliminary physical models were built in support of the foregoing tasks, and design studies were done to delineate problem areas key to the application of this technology to the design, fabrication, and deployment performance testing of scaled-down and full scale solar rocket compatible concentrators. An additional effort to expand the casting and curing of large polyimide membranes was added to the original contract. The objectives of the additional effort were to demonstrate the capability to spin cast and coat large area polyimide reflectors and deliver the reflectors to the Solar Laboratory for evaluation. The work performed enabled the advancement of casting and reflective coating large one-piece concentrators. The procedures developed under this task will be used in the near future for fabrication of concentrators to be used for Solar Thermal Propulsion.

## 2.0 — Introduction

The development of Solar Powered Propulsion systems depends heavily on the technology demonstration of lightweight space deployable solar concentrators. Large elliptically shaped thin film reflectors can be packaged with other solar powered propulsion systems and deployed into low earth orbit. The Solar Powered Propulsion system could produce specific impulses on the order of 1,000 seconds. This performance would significantly improve travel from low earth orbit to geostationary equatorial orbit. A significant step in demonstrating the feasibility of large lightweight deployable concentrators has been taken under this contract. SRS has successfully demonstrated a thin film casting and coating technique on large 15 foot triangular sections that has significant promise for extrapolation to large sections that can be used in solar propulsion systems.

The success of the solar thermal rocket program is predicted on the availability of compactly-stowable off-axis paraboloidal solar concentrators of very large area, very low weight, and very high concentration ratio. The most obvious candidate technology for such concentrators is that of inflation deployed/inflation rigidized thin polymer membrane structures. Regardless of whether the reflective surface of a thin membrane concentrator is supported and tensioned by gas pressure, electrostatic force,

or drying rigidized structure there is strong advantage in utilizing a precise doubly curved membrane rather than relying on pressure-shaping and/or gore configuration shaping of flat or singly curved film elements into a reflector membrane assembly. Depending on the support tensioning utilized, the doubly curved formed membrane reduces the gas inflation pressure, electrostatic potential, or supporting structure mass. For all the above techniques, the available forces are at a premium. For inflation rigidization, gas leakage mass flow rate through a given set of micrometeoroid punctures is directly proportional to the pressure required to configure the film. A 10:1 reduction in such configuring pressure requirement and consequent leakage rate could have decisive mission implications. Spray casting of NASA Langley polyimide films permits precise double curvature forming operations not readily accomplished otherwise in polymer films of high stability. The objective of this contract was to establish the film configuring processes on a sound engineering basis by building a scientific groundwork of quantitative data on material viscoelastic properties and related forming/assembling procedures, for high stability films judged to be suitable candidates for the solar thermal rocket application.

## 3.0 — Research Performed

### 3.1 — Polyimide Material Testing and Evaluation

The objective of this task was to generate a materials properties handbook comprised of families of curves fully describing the properties of thin polymer film materials. The properties of interest to the solar concentrator application, were in the regions of temperature, time, and stress directly relevant to creep and/or relaxation forming doubly curved thin film materials. Extensive materials test were performed with "off-the-shelf" polyimides. Large variances in material properties were discovered as a result of the materials testing. The material properties varied with brand, thickness and batch. Alternative materials were investigated as a result of the materials test program. NASA supplied polyimides were tested and found to have properties equivalent to that of Kapton. The NASA materials also had better atomic oxygen resistance and could be cast and cured in the laboratory to the desired shape. The following section describes the test apparatus that was designed for performing the tests. The testing philosophy, the apparatus design, and test methods, as well as test results, are also presented.

#### 3.1.1 — Literature Survey and Equipment Search

A literature survey was conducted to determine the state-of-the-art in the area of thin film material characterization and analytical modeling. Numerous resources, including Redstone Science and Information Center, NASA RECON Aerospace Database, and AIAA Technical Information Service, were used to find pertinent literature. The literature survey resulted in the development of

an in-house creep-forming library consisting of over forty publications.

A review of literature obtained yielded a great deal of useful information. It was found that one of the best sources of information about the creep of thin films comes from publications about the design of high altitude meteorological balloons. These high altitude balloons are usually made of thin polyethylene film and experience loading conditions that are somewhat analogous to the loading conditions that will be used to fabricate solar concentrators. During a balloon launch, the balloon experiences thermal and pressure gradients as it ascends through the atmosphere. Therefore, balloon designers have addressed some of the problems associated with modeling and characterizing thin viscoelastic films under pressure and temperature loading. Another source of useful information comes from studies of injection molding techniques for manufacturing plastic components. There are several publications regarding the finite element modeling of this viscoelastic process. The literature survey also identified several computer software packages that might be useful in modeling the creep-forming process. The availability and limitations of this software were investigated. The information obtained from this literature survey was used to assure that state-of-the-art technology was incorporated into the design procedure.

A search for testing standards was performed using the American Society for Testing and Materials (ASTM) Standards. Standards of mechanical testing for plastics, films, and metals were considered in the search. A preliminary analysis of the metals standards revealed they were inadequate for thin films such as Kapton. Further investigation uncovered four standards which were considered. These were: D674-56,

Testing Long-Time Creep and Stress Relaxation of Plastics Under Tension or Compression Loads at Various Temperatures; D638-84, Tensile Properties of Plastics; D1204-54, Measuring Changes in Linear Dimensions of Nonrigid Thermoplastic Sheeting or Film; and D882-83, Tensile Properties of Thin Plastic Sheeting. The standards include testing apparatus definition, type of test specimen, number of tests, material conditioning, testing rate, and calculations.

Some test equipment needed, including the oven, was available from Phase I testing. This oven was modified to allow the test apparatus to be set-up and the oven to be mobile, eliminating jolting inaccuracies after the apparatus is in position for testing. Grips were needed to clasp the material and were merited on slippage minimization and an even stress distribution. A specimen cutter was necessary to produce specimens with straight, clean, parallel edges with no visible imperfections. When using thin films, the cutting task must be carefully executed to avoid tear and shear which would invalidate the test results. Extension indicators were designed to minimize stress on the specimen at the contact points of the material and the indicator.

ASTM specifies that test specimens must consist of strips of uniform width and thickness at least 2 inches longer than the grip separation used. A width-thickness ratio of at least eight should be used. The specimen edges should be parallel to within 5% of the width over the length of the specimen between the grips.

ASTM D882 was adhered to for constant strain rate tests. The apparatus was equipped with a device for recording the tensile load and the amount of separation of the grips; both of these measuring systems were accurate to  $\pm 2\%$ . The rate of separation was determined by the percent elongation at material breakage and the initial distance between the grips. For an elongation at break less than 20% and 5

inches gauge length, ASTM requires a constant strain rate of 0.5 in/in/min.

A test equipment search was performed to identify companies which supply materials testing equipment needed for the testing of thin polymers. Several criteria were used in evaluating the applicability of the test items. *Table 1* is a listing of the companies contacted, the items of interest from each, and whether or not they met the specified requirements. The search supported our theory that it would be necessary to design and construct the test apparatus by using separate testing components due to the inadequacy of currently available material testing systems. When contacting the equipment companies it was realized most of the testing equipment was designed for materials larger, thicker, or easier to handle than the thin film polyimides. The candidate testing apparatus must be capable of handling 0.3 mil polyimide film; however, it must not impart any loads or constraints on the film.

Companies were contacted for availability of such items as grips, extensometers, load cells, pressure transducers, and material cutters. The high temperature oven used in Phase I was used in Phase II. The sources for the names of companies contacted were the Thomas Register and Standardization News. All literature material received from the companies were reviewed for applicability in creep testing. Design ideas which were useful were gained from the equipment search.

### **3.1.2 — Thin Film Material Test Design and Equipment**

The task objectives were to generate a materials properties handbook comprised of families of curves fully describing the viscoelastic properties of relevant thin polymer film materials. The most direct application of this handbook was to provide the data to be used in the analytical modeling and the subsequent application of that mod-

**Table 1 Test Equipment Search**

Company	Equipment	Cost Compliance	Availability <i>Lead time less than 2 months</i>	Film Thickness Capability (0.3 mil)	High Temperature Capability		No Imparted Load	Equipment Too Large	No Response
					Standard	Option			
AOR Inc.	Extensometer					✓			
	Grips			✓			✓		
Applied Test Systems	Furnace	✓		✓	✓				
GSI	Testing Machine			✓			✓		
Detroit Testing Machine	Testing Machine						✓		
Frost Controls	Testing Machine						✓		
Grif Grips	Grips	✓		✓	✓				
ISR	Extensometer	✓					✓		
Instron	Testing Machine			✓	✓		✓		
Interlaken Technology	Extensometer								✓
Lloyd	Grips	✓	✓		✓		✓		
	Extensometer								
MTS	Testing Machine			✓		✓	✓		
	Grips					✓	✓		
Optron	Electro-Optical Extensometer			✓	✓		✓		
Sama Corp.	Strain Measurement								
SATEC	Testing Machine			✓		✓	✓		
	Extensometer	✓				✓			
Testing Machines Inc.	Optical Extensometer			✓	✓		✓		
Theta Industries	Extension Measurement								
Tinius Olson	Testing Machine							✓	
Zwick	Grips	✓		✓	✓		✓		
	Extensometer					✓	✓		
	Testing Machine			✓		✓	✓		

FinRepFig3.1-01-dr2

eling to optimization of the fabrication processes for the experimental model fabrication and subsequent follow-on work.

The design and construction of the test equipment was critical in order to assure accurate test results. Two test equipment configurations were used, one for the uniaxial tests and the other for the combined state of stress tests. The test results yielded curves of both uniaxial and limited biaxial strain data for a large array of test parameters. The thin films tested were Dupont H Kapton, UPILEX R&S, and API-CAL polyimide film with thicknesses of 1, 0.5 and 0.3 mils, non-metallized and metallized. NASA-developed polyimides were also evaluated for material property characteristics.

### 3.1.2.1 — Uniaxial Test Apparatus

The thin film test apparatus shown in *Figure 1* is comprised of a testing machine, temperature chamber, and data logging/processing system. The complete design drawings for this apparatus are shown in Appendix A. The testing system is capable of performing materials characterization tests such as:

- Relaxation
- Creep
- Constant strain rate
- Modulus of Elasticity determination
- Thermal Expansion measurements
- Cylinder pressurization (Biaxial) tests

Material tests performed with the apparatus adhere strictly to the appropriate ASTM testing procedure. The instrumentation devices are calibrated and traceable to NBS specifications. A time proportioning controller regulates temperature control in the temperature chamber for temperatures up to 800 °F. The data acquisition system includes a Macintosh II computer which collects and stores data from several instrumentation devices. The instrumentation devices indicate the testing parameters such as

oven temperature, load, pressure, and strain of the material during the test.

The load beams shown in *Figure 1* are balanced on low friction bearings which allow the grips to impart a load on the film. A load cell is used to measure the force of an applied load and also for calibration purposes. The grips which hold the thin film are toggle grips which increase the crimping force as the sample is stressed higher. The grips are a unique design which allows the test technician/engineer to load the samples in the test apparatus easily. The design of the toggle grips is shown in *Figure 2*.

A temperature chamber was used for determining the thermal expansion/contraction coefficient. The temperature chamber was also used for investigating the recovery of residual stresses due to the manufacturing process of the thin films. For example, Kapton recovers residual stresses in the rolled direction when elevated to high temperatures.

The computer data control system is configured to perform creep testing at high temperatures for long periods of times. A representative test computer screen that was used for the testing is shown in *Figure 3*.

The test equipment design incorporated an extensometer that has sensor arms with clamps on the ends. The clamps were tightened at a low force around the material so as not to influence the specimen. A 6-inch sample length between the grips with a 4-inch gauge length between the extensometer sensor arms was used in the uniaxial tests. By incorporating the extensometer in the test equipment design, ASTM 882-83 Standards were met which call for strain measurements to be made between the grips. The grips that held the polyimide film were toggle grips which increase the crimping force as the sample is stressed higher. A load cell was used for calibration of the testing equipment to a known applied weight, and to deter-

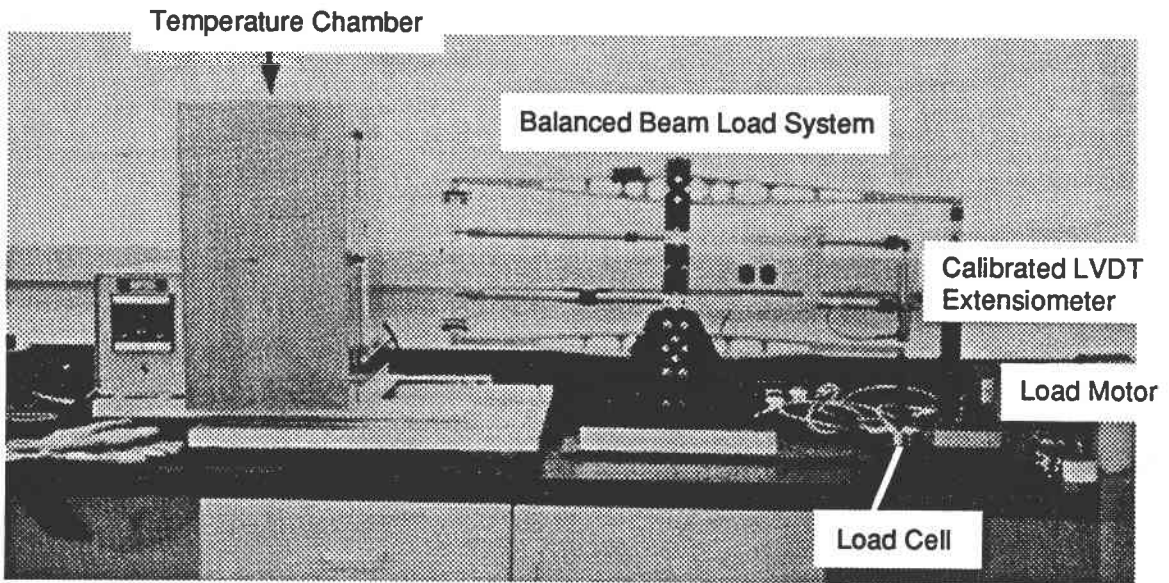
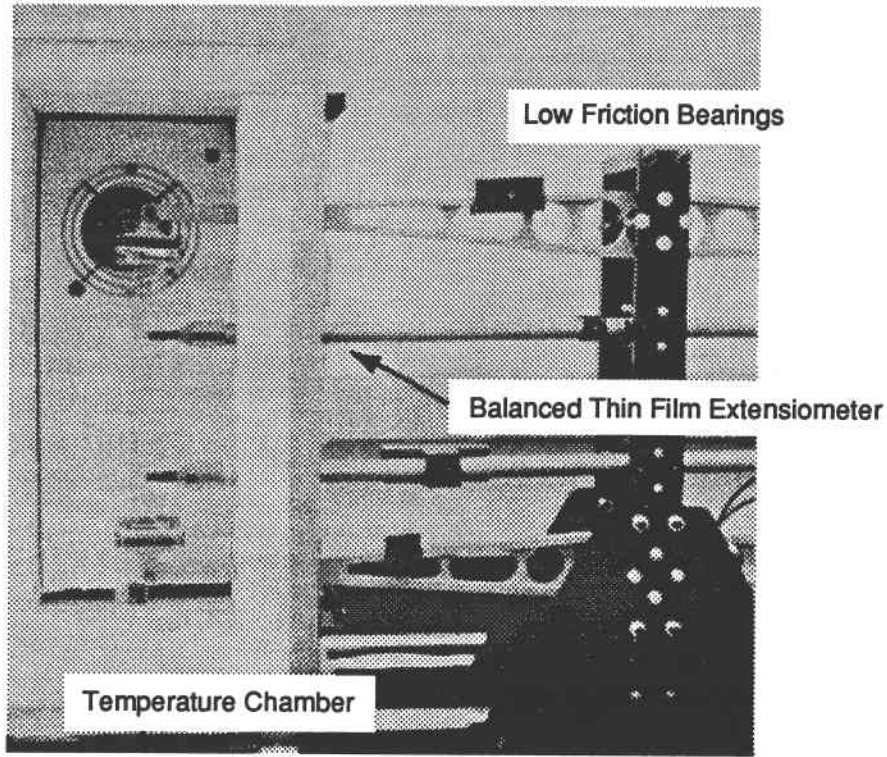


Figure 3.1-02

Figure 1 Uniaxial Test Apparatus

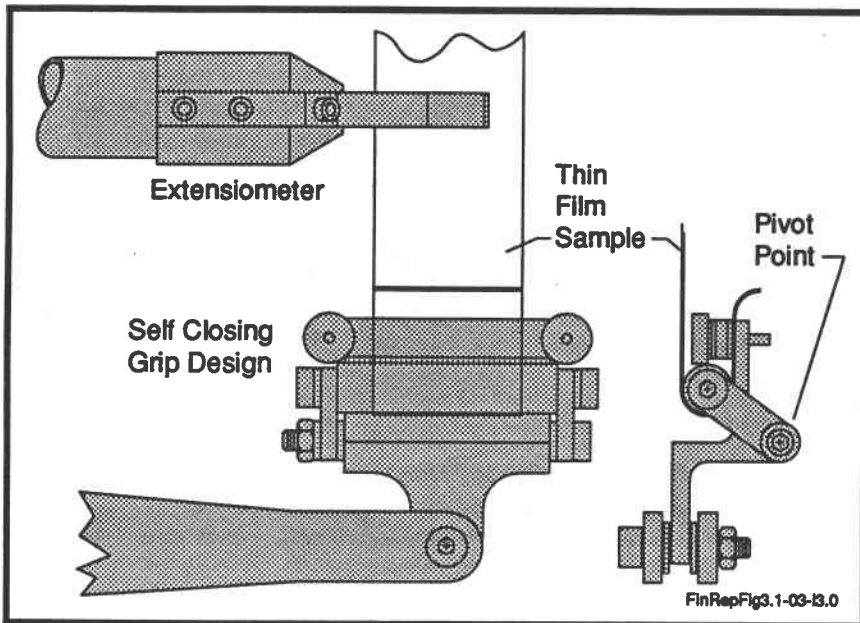


Figure 2 Toggle Grip Design

facility was dedicated for the creep-forming testing effort. An efficient laboratory set up was designed to allow for both combined stress and uniaxial tests. A computer control system was used in the laboratory to initialize testing and monitor the temperature chamber conditions, specimen loading conditions and strains, and other parameters relating to the specific test being performed.

### 3.1.2.2 — Uniaxial Test Procedures

Creep compliance testing, relaxation modulus testing, and constant strain rate creep testing are mathematically equivalent and interchangeable for ideal linear vis-

mine the onset of loading the polyimide film during creep tests. The load cell was also used in the relaxation and constant strain rate tests.

The analog data taken from the extensometer and load cell was recorded and stored by means of the computer data acquisition system. This test equipment design eliminated the concern of sample slippage in the grips, grip thermal effects, thermal expansion of the test hardware, and grip weight.

The laboratory clean room

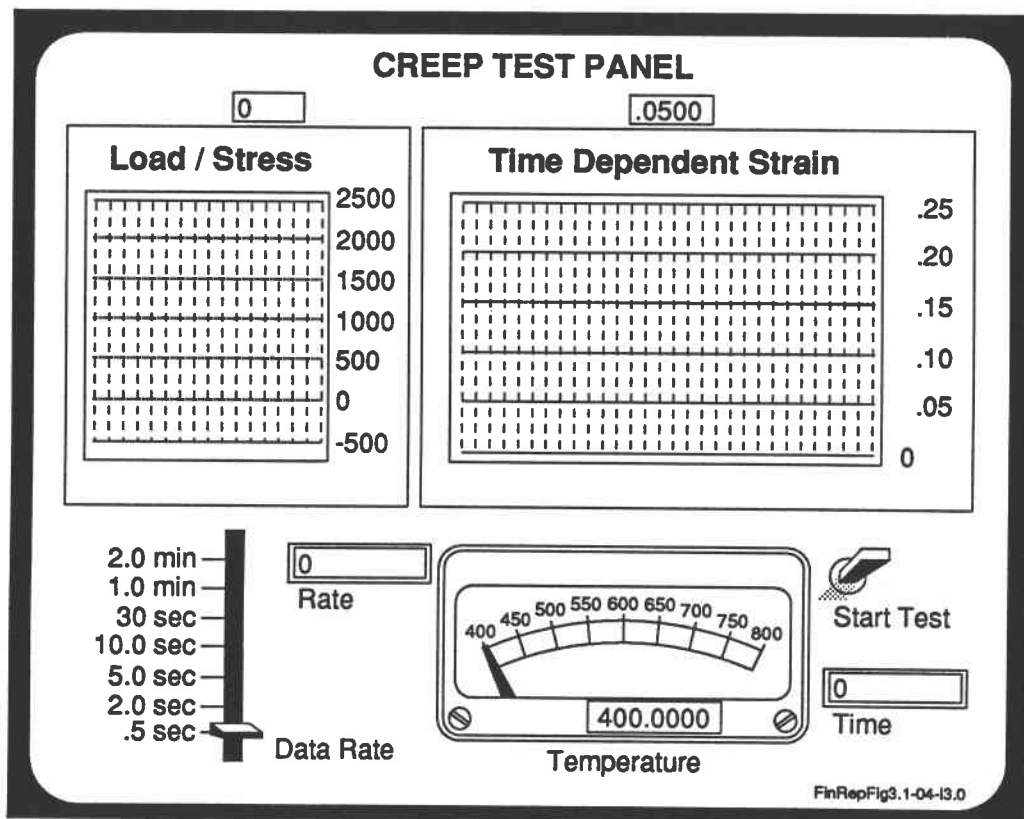


Figure 3 Computer Test Panel

coelastic materials. Polyimides appear to be a reasonable approximation of a linear viscoelastic material. It is reasonable to measure in detail only creep compliance which is the most directly relevant and the easiest to measure. The other parameters only need to be measured in sufficient detail to provide justification and correlation factors for analytically recasting the data into other formats.

The materials tests performed are shown in *Table 2*. A "test status" was determined for each test description and test condition. The "test status" refers to the number of polyimide samples that were tested at identical conditions. Five identical samples were tested when a test is classified as a "basic" test. The results of the "basic" test were a plot of the average data from the five samples and reporting standard deviation. For tests with a "correlation/exploratory" test status, two identical tests were performed at the test conditions. Both test specimen results with a "correlation/exploratory" test status were plotted. An additional "voting" test was performed in the event of a 20% data spread.

The test samples were principally Dupont H Kapton, UPILEX R&S, and APICAL polyimide film. The samples were unmetallized of 1, 0.5, and 0.3 mil thickness. Polyimide samples were cut at a width of  $1" \pm 0.02"$  with a dual razor blade fixture. An effort was made to minimize handling of the gauge length region of the samples with fingers, and exposure to dust, solvents, or water. Because of the hydrolysis weakening sometimes observed in polyimide film exposed to water at elevated temperature, high temperature hydrolysis testing was performed. These results were then compared to the common creep tests with similar oven temperatures and loads. The results of exploratory testing of the polyimide appear in *Appendix A*.

### 3.1.2.3 — Method of Cutting Material Samples

The uniaxial and combined stress tests required several samples of material. The sample size was 1" x 10" for the uniaxial tests. A method that produces straight "clean" cuts along the edges of the material was desired so that effects due to imperfections during testing were minimized. Consistent sample sizes were required in order to ensure repeatable test results. Although apparently simple, cutting consistent sample sizes with "clean" cuts was quite difficult when working with thin materials. Several cutting methods with the 0.3, 0.5 and 1 mil material samples were investigated. One such method which is widely used in solid propellant testing involves using a die to punch out the sample. This method for thin materials such as KAPTON tended to provide rough edges along the length of the sample. A proficient method for cutting the material was developed through testing several cutting techniques. The backing material that is used beneath the polyimide has proven to be a factor in the cutting procedure. Using a semi-hard rubber backing material along with a dual razor blade tool appeared to be the most efficient method for achieving a good sample. A dual razor blade tool was designed which consisted of two metal blocks with the razor blades attached at an angle to each of the blocks. The weight of the blocks provided a consistent load on the blades as they moved across the specimen.

### 3.1.2.4 — Biaxial Testing of Polymers

There are presently no universally accepted and standardized combined stress tests for polymer thin films. An extensive literature search for previous biaxial tests on thin films was conducted. A pressurized cylinder test appears to be the simplest, most direct, and most versatile combined stress test. Several combinations of stress conditions can be achieved using cylindrical specimen tests. The designed test appa-

**Table 2 Uniaxial Material Tests**

Paragraph in Proposal	Test  Description		Test Conditions			Samples				Test Status  Number of Repetitions	Number of Samples Required							
			Stress Levels, psi	Oven Temp- erature °F	Other	Vendor Material	Thick- ness -Mils	Batches	Roll Direc- tion		Dupont				Uplex or Apical			
											0.3, A	1 B	0.5 A	1 B	0.3, A	1 B	0.5 A	1 B
3.1.1.1.A	Basic Creep Compliance	Basic Data	1,500	550, 650	—	Dupont Uplex	0.3, 0.5 1.0	2	X, Y	Basic (5)	20	20	20	20	20	20	20	20
3.1.1.1.A	Heat Shrinkage and Recovery	Supplementary Data	500, 3,000	500, 600, 700	—	Dupont Uplex	0.5	1	X	Basic (5)			30				30	
3.1.1.1.B	Iterative Creep and Hot Recovery		1,500	500, 600, 700	3 Times	Dupont Uplex	0.5	1	X	Correlational (2)			6				6	
3.1.1.1.C	Iterative Creep and Cold Recovery		1,500	500, 600, 700	3 Times	Dupont Uplex	0.5	1	X	Correlational (2)			6				6	
3.1.1.2	Rupture Elongation		3,000, 4,500	500, 600, 700	—	Dupont Uplex	0.5	1	X	Correlational (2)			12				12	
3.1.1.3A	Rapid Creep Compliance		1,500	500, 600, 700	—	Dupont Uplex	0.5	1	X	Correlational (2)			6				6	
3.1.1.3B	Constant Strain Rate Rapid Recovery		1,500	500, 600, 700	0.5, 0.05, 0.005 in. / sec.	Dupont Uplex	0.5	1	X	Correlational (2)			18				18	
3.1.1.4	Heat Shrinkage		1,500	500, 600, 700	—	Dupont Uplex	0.5	1	X	Correlational (2)			6				6	
3.1.1.7	Relaxation Modulus		3,000	500, 600, 700	—	Dupont Uplex	0.5	1	X	Correlational (2)			6				6	
3.1.1.8A	Metallization Effects on Creep Compliance		1,500	500, 600, 700	—	1	0.3, 0.5	2	X, Y	Correlational (2)	12	12	12	12	12	12	12	12
3.1.1.8B	Metallization Effects on Iterative Creep		1,500	500, 600, 700	3 Times	1	0.3, 0.5	1	X, Y	Correlational (2)	12		12		12		12	
3.1.1.9A	Aluminum Creep		1,500	500, 600, 700	—	1	0.5	1	X	Correlational (2)			6					
3.1.1.10	Polyester Creep Compliance, Heat Shrinkage, and Recovery		1,500	500, 600, 700	—	1	0.5	1	X	Correlational (2)			6					

FinRepFig3.1-05-dr2

ratus is shown in *Figure 4*. The test equipment is capable of applying uniaxial, pressurized, and torque loads to the specimen. Limited material testing was done with the biaxial test apparatus design. The results of the uniaxial testing led to use of NASA Langley polyimides. Biaxial material tests could be done in the future with this test apparatus. The following suggestions are made for testing films in a biaxial

state. Because of the difficulty of making nonperturbing strain measurements, the motion of the cylindrical specimen was measured by movement of the specimen end grips for measurement of torsional shear and "Y" direction strain. For future testing, strain-dot position, optical tracking tests, or tests with tab attachments to the extensometer might be used for post test measurements to indicate the typical

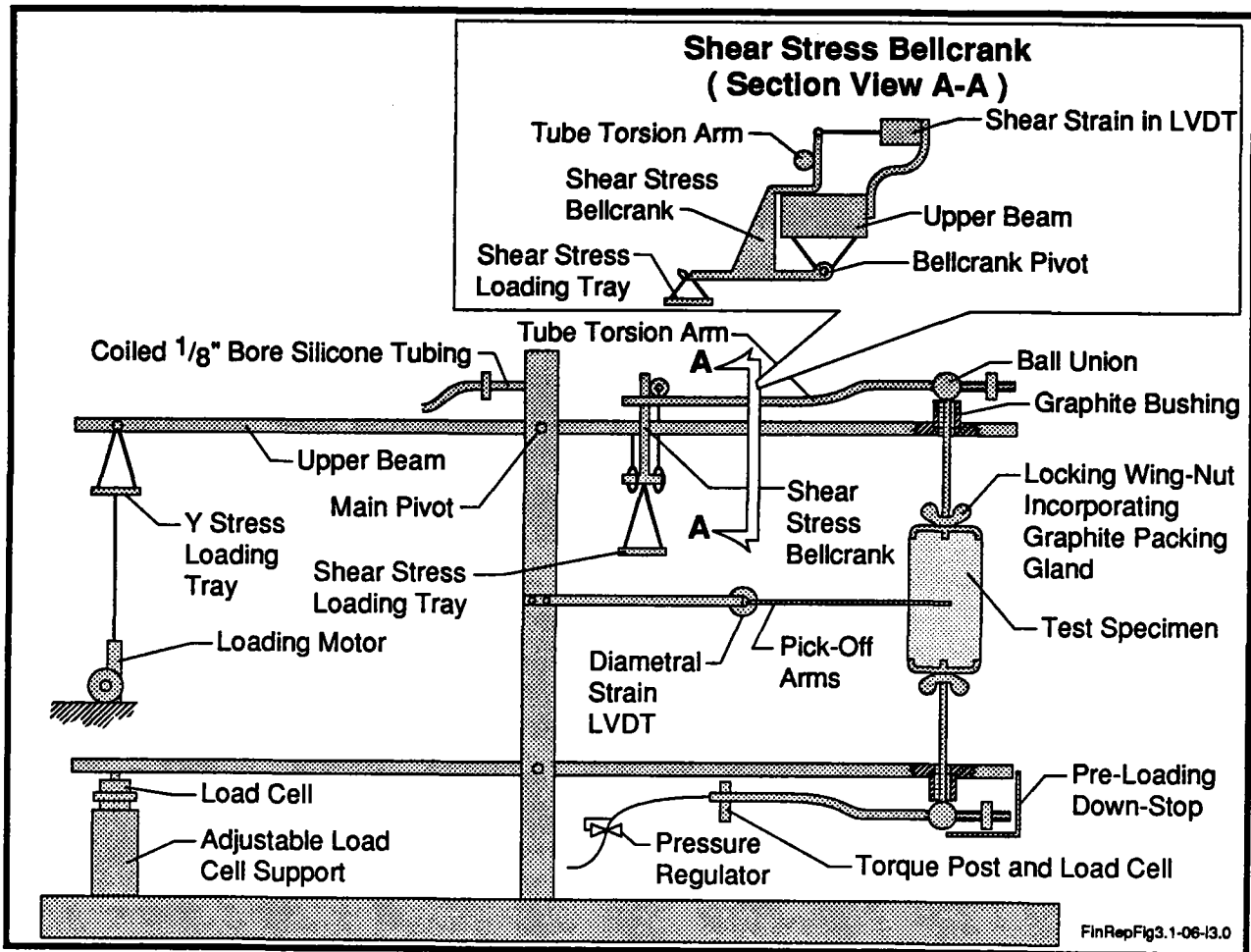


Figure 4 Combined Stress Test Apparatus

magnitude and direction of the errors introduced by using the testing machine jaw motion to indicate specimen strain. A remote sighting optical cathetometer concept could be used for correlating specimen end grip strain measurements to specimen central region strain. A traveling cross hair telescope of a cathetometer would sight the dots through an oven wall window. Vertical and horizontal motion of the dots would define the axial, circumferential and torsional shearing strain.

The correlation of uniaxial test data to a biaxial stress state was investigated through obtaining actual biaxial strain data. The primary objective of these tests was to determine the effect of a biaxial stress state on the uniaxial creep

compliance. The test results were used for the purpose of deriving a factor that could be applied to the uniaxial test data. The time/temperature/load dependent factor was used for analytical modeling of inflatable reflector creep-forming process involving combined biaxial tension and shear stress. Therefore, absolute magnitude data was less important in this test than ratio data, for differing stress conditions applied to similar test specimens in similar apparatus.

### 3.1.3 — Polyimide Material Testing

The following section describes the material testing done under this task with the test equipment fabricated and assembled. Several methods were used to reduce the data that was taken.

Creep compliance curves were generated for Kapton material. Comparisons were made between different thicknesses of material, varying batches, and manufacturers. The large variation in test results led to the evaluation and selection of NASA developed polyimides for advanced development of the inflatable concentrator.

### 3.1.3.1 — Preliminary Testing

Preliminary tests were performed using 0.3 mil Kapton type H. Thermal expansion, heat shrinkage, strain and the recovery process following creep of the Kapton were investigated using the completed test apparatus. The preliminary creep tests of the Kapton were performed at a stress of 1,500 psi and a temperature of 600°F. *Figure 5* depicts actual test data taken during a preliminary test. Initially the Kapton was inserted into the oven unloaded; the thermal expansion of the material occurred immediately with heat shrinkage occurring over a longer time. The results of the Kapton thermal expansion taken by the test

instrumentation were repeated by removing the sample from the temperature chamber, allowing the sample to cool, then placing the sample back into the temperature chamber as depicted in *Figure 5*.

Upon loading of the sample, an instantaneous elastic strain was recorded, followed by primary creep of the material. A constant secondary creep rate was recorded by the apparatus following primary creep. The sample was then unloaded and hot recovery was recorded while the sample was in the temperature chamber. Finally, the sample was removed from the temperature chamber and the thermal contraction of the material was recorded. These preliminary test results indicate a dramatic improvement in the testing apparatus as compared to Phase I results.

Several qualitative creep tests were performed to verify and support further modifications/improvements to the testing procedures developed. The tests also served as a means

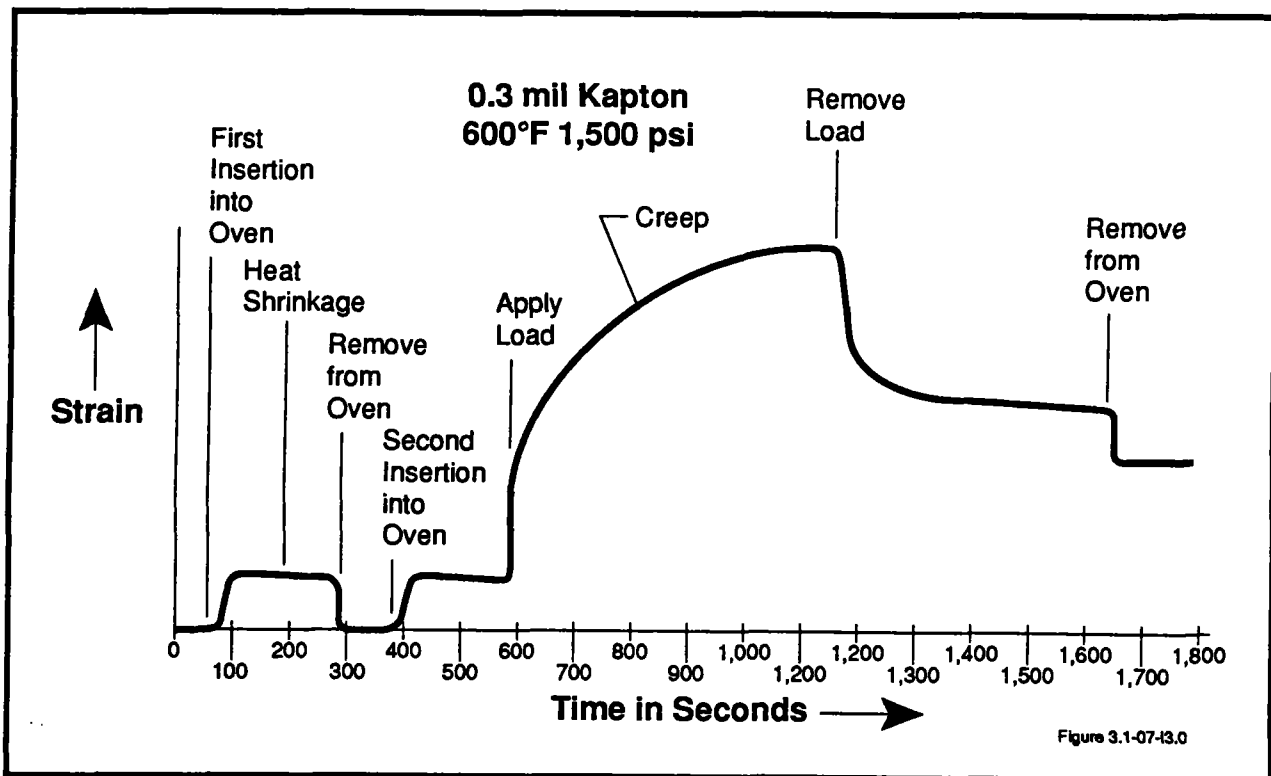


Figure 5 Preliminary Kapton Creep Test

for encountering possible errors in the test design/apparatus that would need correcting before formal testing was initiated. Some tests indicated varying results in magnitude of strain for identical creep test conditions. After further investigation it was determined that these discrepancies were a result of inconsistent temperatures in the testing chamber and the differences could be eliminated by requiring a one hour oven heat up before formal creep tests were performed. The temperature gradient over time was further minimized by reducing the large step heat input from the heating elements to a longer cycle time with the step heat input reduced.

Creep testing also revealed a strong correlation between initial heat shrinking and the hot recovery process of the material following creep. The two processes appeared to hold similar time constants for strain relieving of the material. Extensive formal testing subsequently numerically verified the preliminary qualitative results.

Regions of the Basic Creep Test consisted of: thermal expansion, heat shrinkage, primary creep, secondary creep, and recovery. Variations in the test parameters effected the regions of creep results. The test parameters including temperature, load, creeping time, recovery process and recovery time could be varied to yield different results. The qualitative tests performed included variations in the test parameters. For the qualitative tests the load and temperature were held constant (600°F and 1,500 psi) in order to make comparisons relating to the recovery process and stability of the material following creep. Evidence from the tests supported the importance of the recovery process to the final strain of the material and its stability. As expected, the hot recovered tests yielded the lowest final strain with the largest apparent stability. From the cold recovery tests, the strain that was "frozen in" to the material began to recover upon re-entering the

test sample into the temperature chamber. The recovery process appeared to continue as if the material had been hot recovered in the oven immediately after creep. The results of these tests led to many interesting questions regarding the degree of "frozen in strain" that can be useful to a stable creep-formed material at a range of operating temperatures.

The coefficient of thermal expansion of Kapton was determined from creep tests conducted. Constant stress tests at room temperature were conducted to determine the modulus of elasticity of Kapton Type H. Both results are in good agreement (10%) of the handbook value. The relative agreement between handbook and actual test values of the elasticity and thermal expansion coefficient supported the accuracy of the testing apparatus and instrumentation for material characterization.

The overall results of the qualitative tests enabled SRS to re-evaluate the test schedule and make changes to the testing procedure in order to gain the largest amount of useful information possible by the most efficient method. Repeatable test results were of primary importance and critical to the validity of the testing method and apparatus. Weekly calibration checks of the apparatus were done throughout formal testing. A more detailed discussion of the qualitative testing performed is included in the appendix.

### **3.1.3.2 — Test Data Manipulation Software**

A method for reducing test data was developed during the contract. Several uniaxial tests were performed at identical conditions to investigate reliability in test equipment and repeatability of tests as specified in ASTM Standards. A normalization procedure was needed to average and statistically evaluate up to five identical tests. The results of the normalization program were used to calculate average creep

compliance curves for a range of operating temperatures and loading conditions.

During material tests, the computerized data acquisition system wrote the test parameters to a data file, in a spreadsheet format, for further data reduction and analysis. The EXCEL spreadsheet program, written by Microsoft, was used on the Macintosh II to create various programs (macros) to perform data manipulation of the test data in spreadsheet form. The macros were written to zero the time scale of the test data upon initiation of the load on the material, eliminate extraneous data from the displacement, and normalize time scales for tests at identical testing parameters. *Figure 6* represents typical raw data from two uniaxial creep tests with both time and displacement scales not correctly shifted for proper analysis. The offset displacement was a result of the actual placement of the strain displace-

ment arms on the test apparatus. The time recorded for the raw data was the time that the computer started taking data before the sample was inserted into the temperature chamber. The ZERO macro shifted the time scale to time = 0 at the instant the test sample was loaded (*Figure 7*). The displacement shift correction was determined by averaging the data points before the material was inserted into the oven and subtracting the average from the raw displacement data (*Figure 8*). *Figure 9* indicates the results of using the ZERO macro on two sets of raw data.

A normalization program was written to obtain desired displacement, load or temperature data points at specified time intervals for tests of particular interest. The normalization was accomplished by selecting a base time for one test and using a step type interpolation method

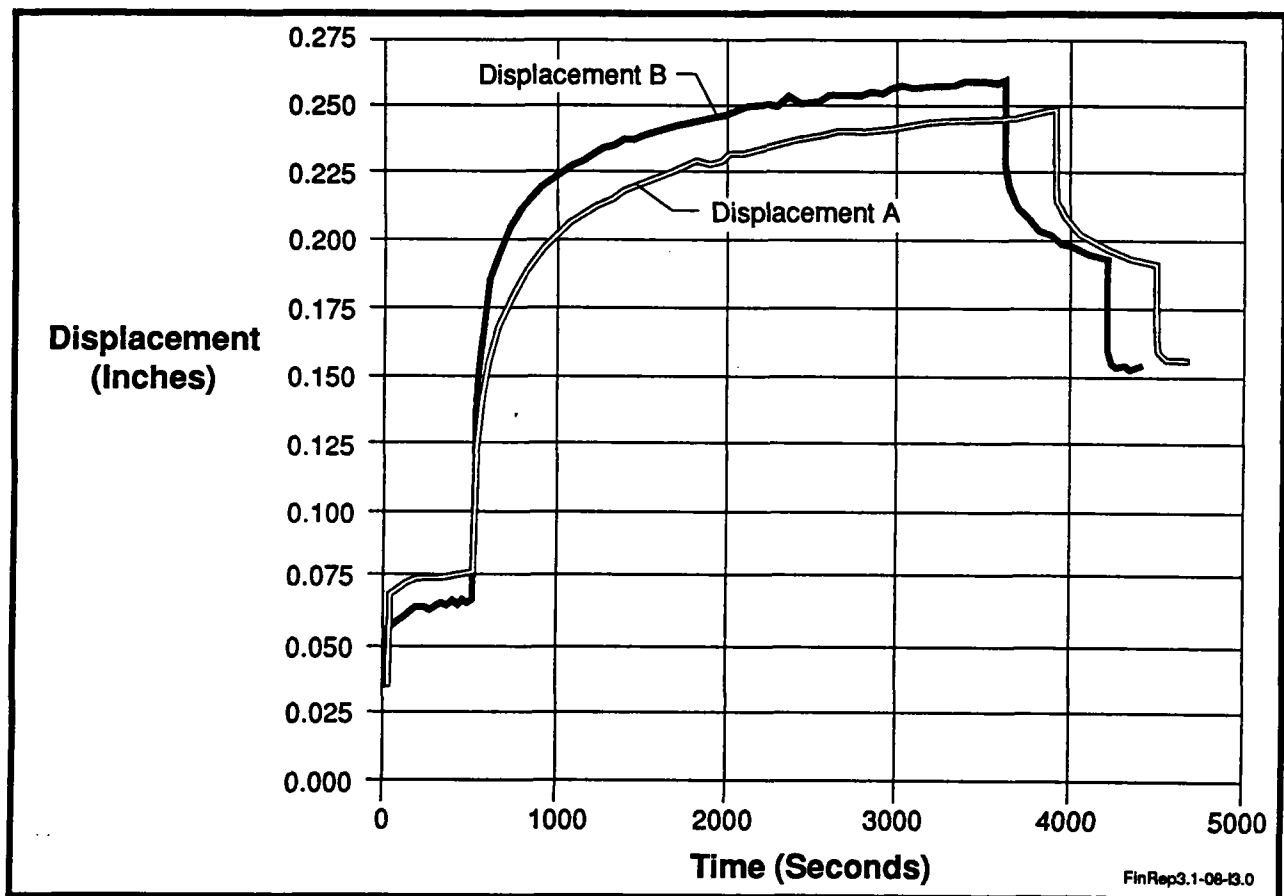


Figure 6 Raw Data Plot of Kapton Creep Test

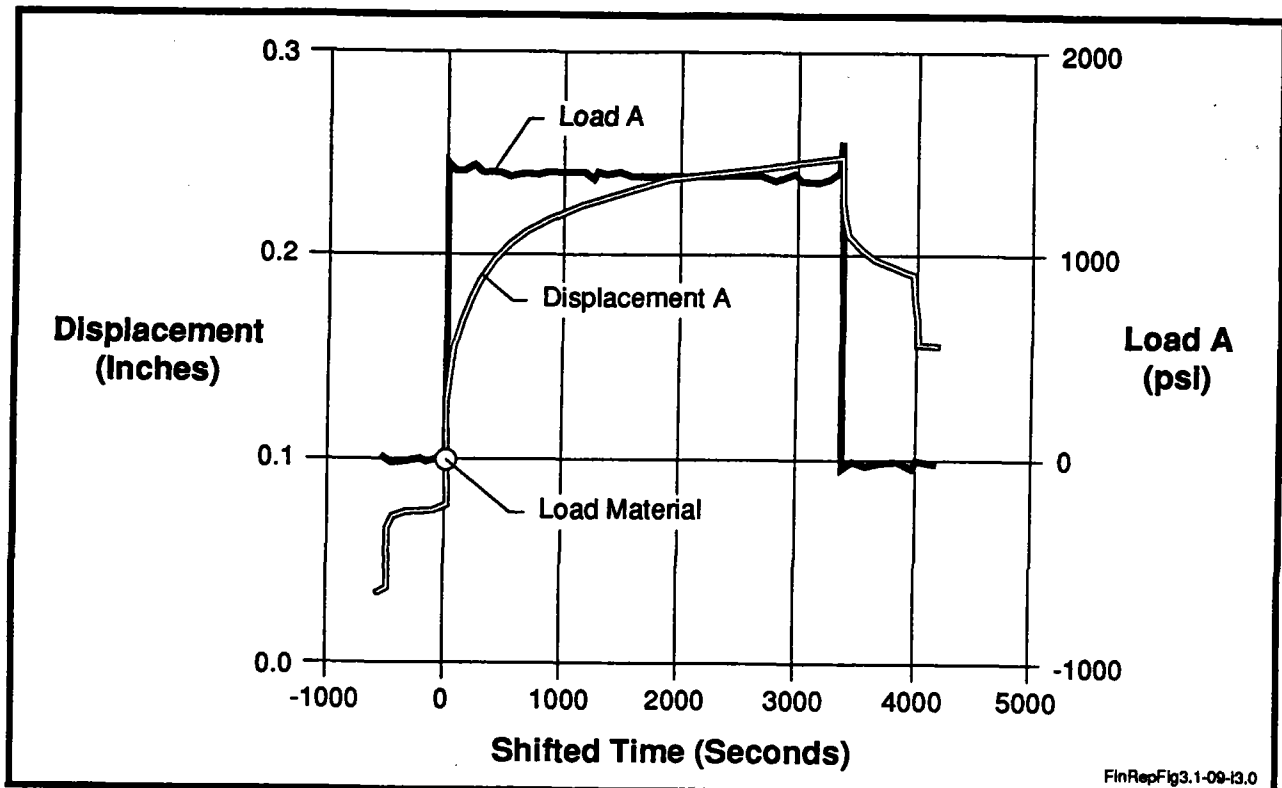


Figure 7 Shifted Time = Zero at Point of Loading

FinRepFig3.1-09-13.0

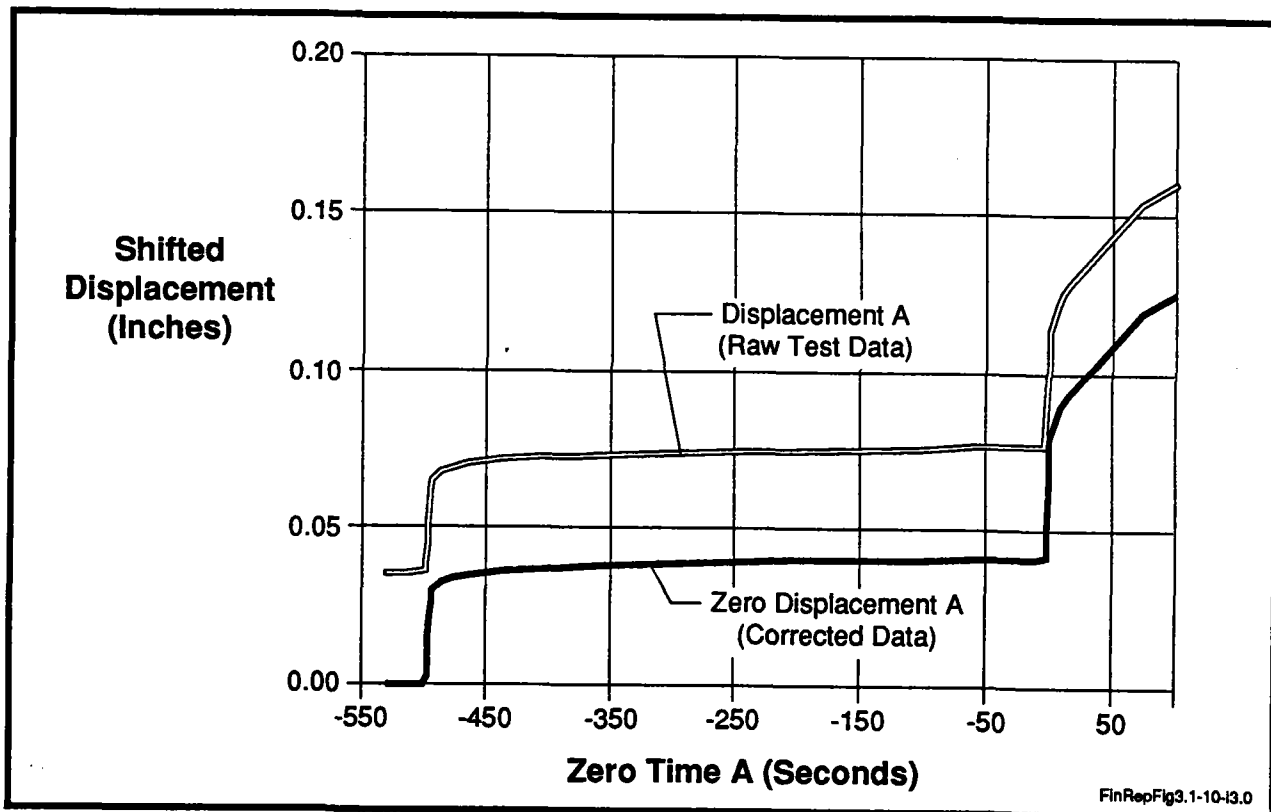


Figure 8 Shifted Displacement of Test Data

FinRepFig3.1-10-13.0

between data points of other data sets with different time intervals. *Figure 10* depicts a final graph of data for two tests of normalized time scale displacement values. The data, as shown in the figure, was normalized which enabled a displacement relationship between the two sets of data at specified times to be investigated. This program was used extensively to average uniaxial creep or relaxation test data at identical testing parameters. A smoothing macro was also written by using a weighted average algorithm to smooth raw test data.

### 3.1.3.3 — Material Test Results

“Basic” creep tests were performed with each type of polyimide material being tested at the prescribed conditions taken from the test plan. *Figure 11* represents an actual “Basic” test with 0.5 mil Kapton. The plot was generated from the data acquisition system which stored stress, strain, and temperature conditions relating to the specific times during the creep test. Three plots can best describe the “Basic” creep tests. The first plot in *Figure 11* represents the thermal expansion, heat shrinkage, and load application of the material preceding primary creep. Time was assumed to be zero at the application of the load in order to relate identical tests to the creep process. The second graph represents the entire creep test including the primary, secondary and final creep strain. The third plot investigates the recovery process with an expanded time scale over the area of interest. This plot depicts elastic recovery, hot recovery, and thermal contraction of the material upon removal from the oven. Each test performed was included in the Creep Handbook. The information from each test was represented in graphical form for easy identification of results. Identical tests were performed to investigate the reliability of repeatable tests. A statistical average of test results for identical conditions with error analysis was per-

formed to enhance and indicate the reliability of the test results. Comparison plots between testing parameters on identical materials were included in the creep handbook. The comparison plots depict the importance of each parameter (stress, temperature, creep, and recovery time) to the creep-forming process. Creep properties of different materials tested were also plotted to indicate differences or similarities between materials.

Kapton, Apical, and Upilex uniaxial test specimens were aluminized by vapor depositing aluminum onto the specimens in a vacuum chamber. The metallized samples were subjected to test conditions similar to the unmetallized materials. The results of the tests (discussed subsequently) revealed minor effects of the aluminum on the creep properties of the polyimides.

Results of the uniaxial creep tests indicated a varying creep compliance at a constant temperature, for varying loads, indicating that the material was a non-linear viscoelastic material. Subsequent testing and analysis, discussed subsequently, indicated that this apparent non-linearity is largely an artifact due to residual stresses from roll-processing of the materials. The uniaxial creep tests performed were numerically reduced in order to calculate the material properties at a range of temperatures and loads. The information from each test was represented in graphical form for easy identification of results. The creep tests were performed at typical creep-forming temperatures and loading conditions for reflector construction. *Table 3* depicts the loading conditions and temperatures at which the uniaxial creep tests were performed. All combinations of these parameters were used in the uniaxial creep tests.

The data taken for each test was included in the Creep Handbook. A “basic” creep test sheet for 0.5 mil KAPTON, shown in *Table 4*, is for a stress level of 1,200 psi and temperatures of 600°F, 650°F, and 700°F. The test sheet indi-

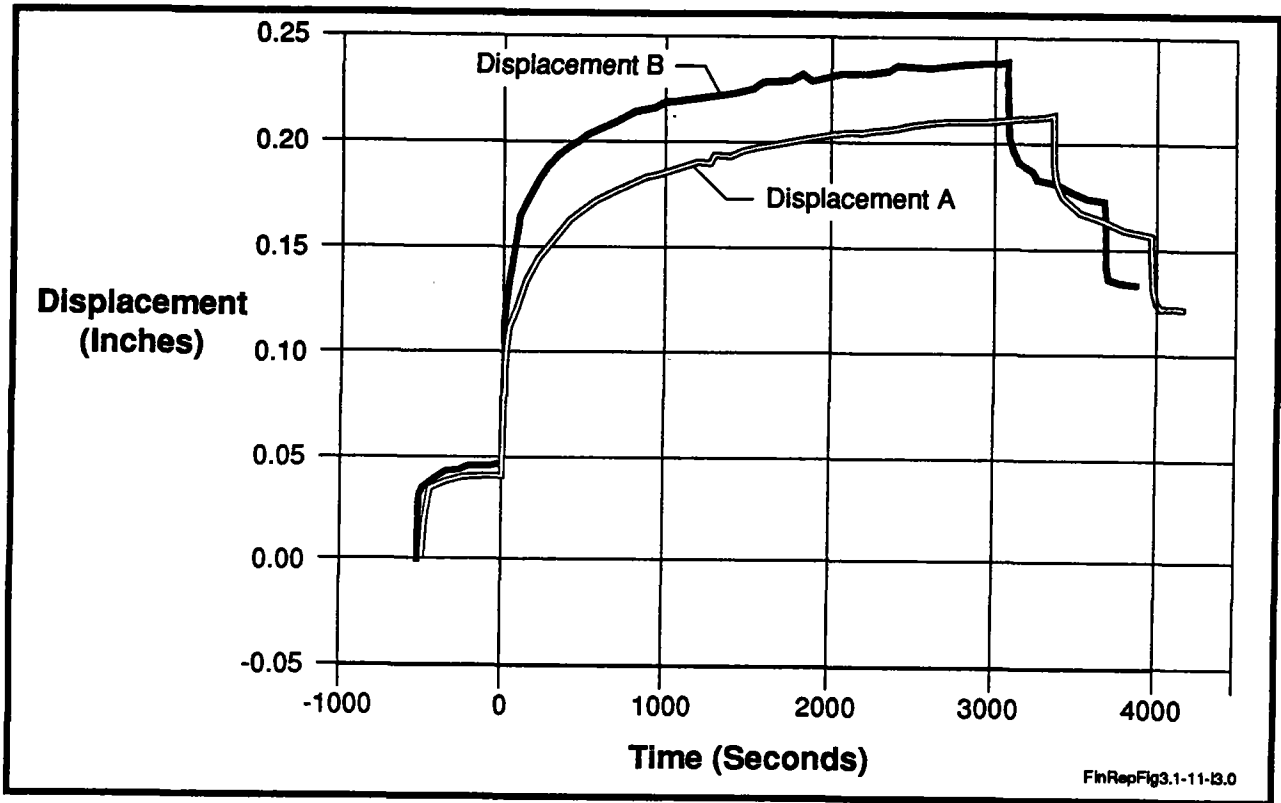


Figure 9 Results of the Zero Macro Run

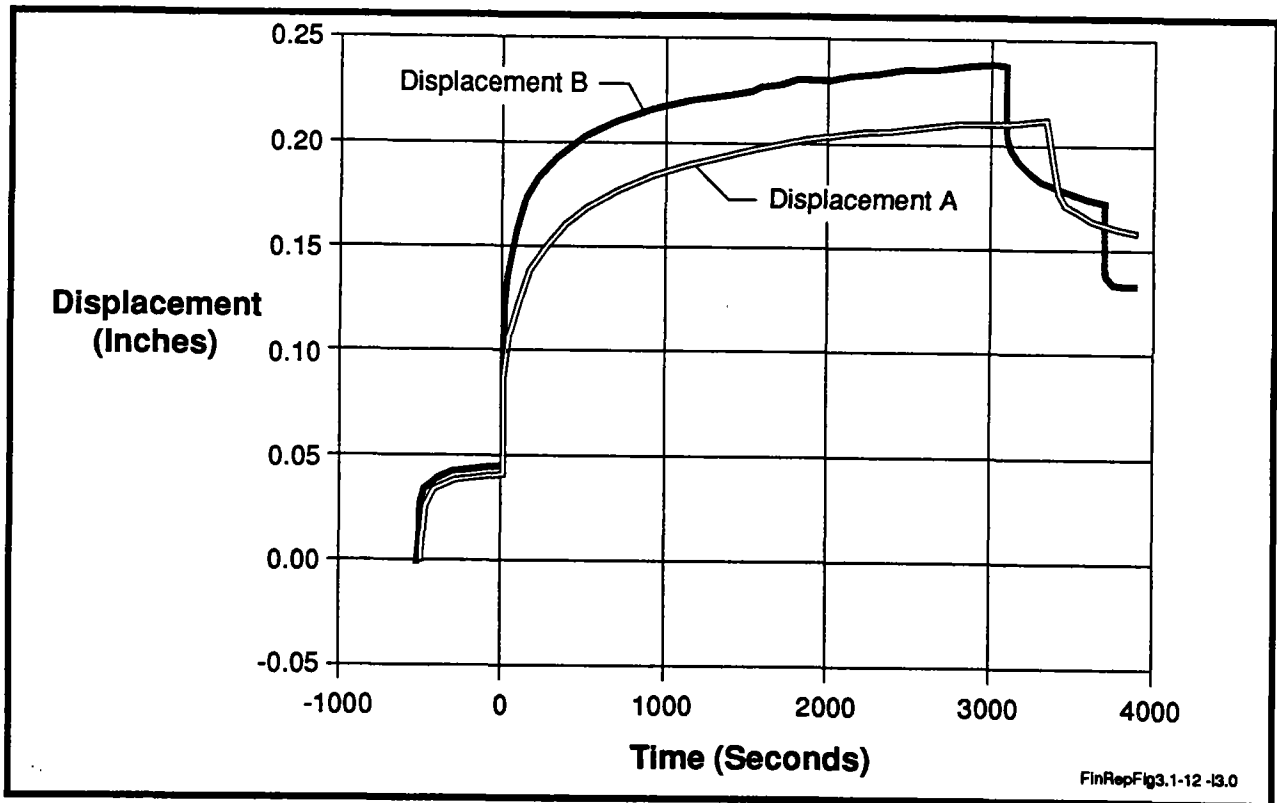
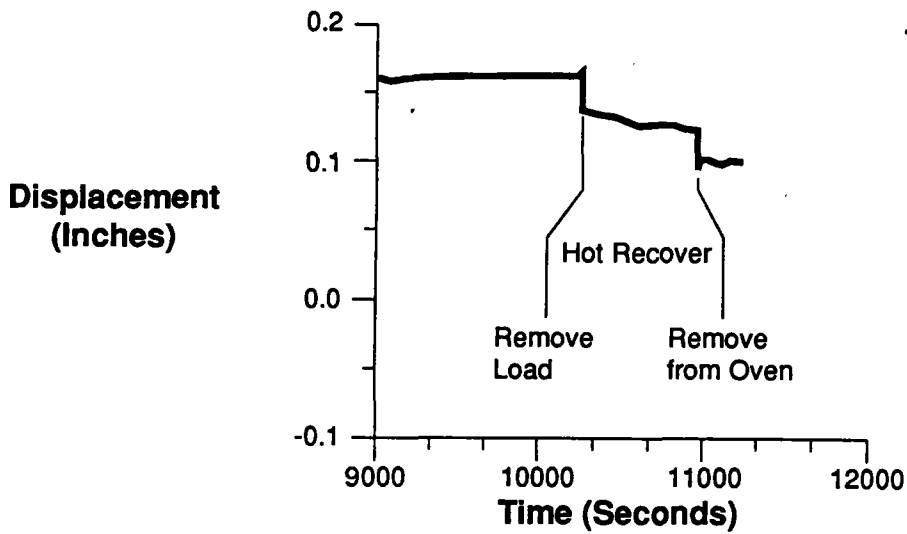
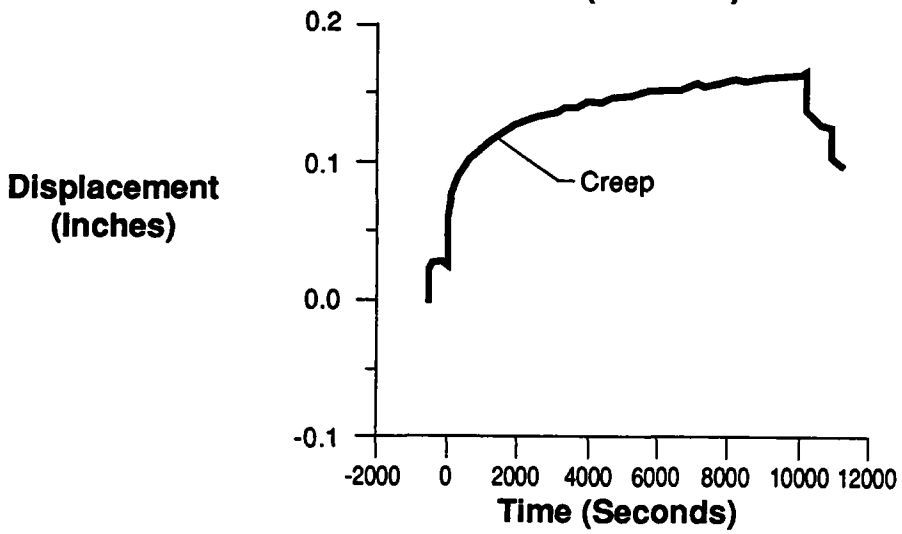
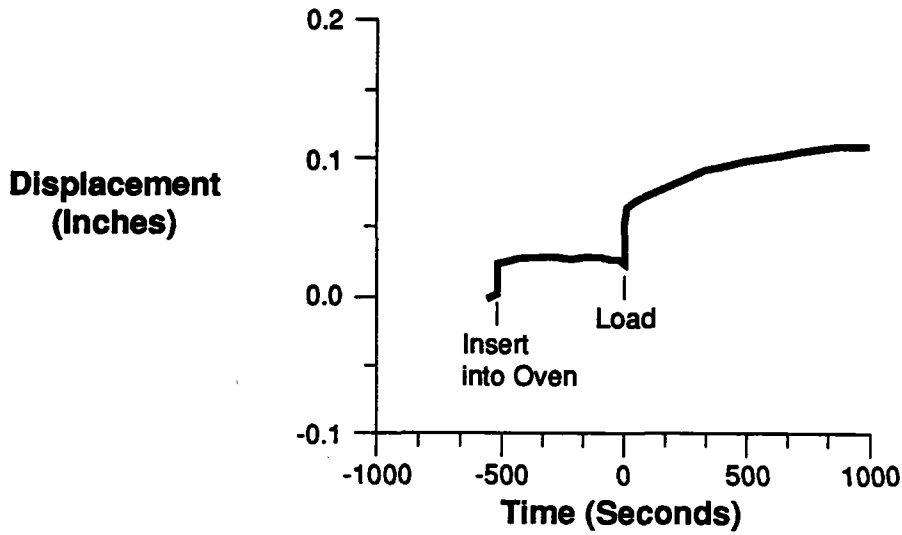


Figure 10 Zeroed, Normalized and Smoothed Results



**Test Conditions**  
1500 psi 600°F

FinRepFig3.1-13-13.0

Figure 11 "Basic" Creep Test of 0.5 mil Kapton

**Table 3 Test Parameters**

Temperature	Stress Level
500°F	500 psi
550°F	1,200 psi
600°F	1,500 psi
650°F	2,000 psi
700°F	—

FinRepFig3.1-14-dr2

cates the test number, test conditions, and the date on which each test was performed. *Figure 12* depicts the results of three tests at 600°F. The graphical representation indicates the repeatability of the tests. Zero time was considered to be at the point when the material was initially stressed. The initial strain of the material (time < 0) was the thermal expansion of the material. The material was unloaded and allowed to recover for 500 seconds at time = 3,000 seconds. Finally, the material was removed from the oven and the final strain was recorded. A time normalization procedure and statistical evaluation for the tests (shown in *Figure 12*) was done to numerically and graphically indicate the repeatability of the test results. *Figure 13* shows a plot of the mean of the three tests performed and an envelope of error for the tests. The mean curve was used for analytical assessment of the creep properties in Task 3. The normalization procedure and statistical evaluations were done for all tests performed to date. *Figures 14* and *15* indicate tests results for temperatures of 650 and 700°F. The

results of the creep tests for a constant load of 1,200 psi and varying temperatures is shown in *Figure 16*. The final creep strains for the material following recovery are indicated in the figure and are increasing with temperature. *Figure 17* represents the creep compliance of the material tested. The results from this figure indicate that horizontal shifts in the time scale might yield a good representation of time-temperature equivalence. Similar graphs are presented in the Creep Handbook which indicate the relationship between strain and varying constant stress conditions at constant temperatures. Vertical shift factors can be applied to yield a master creep compliance curve to predict the material response for a wide variety of temperature-time-stress conditions.

Uniaxial creep tests were performed with aluminized 0.5 mil Kapton and compared to past un-aluminized Kapton test results. Creep compliances for the aluminized material were nearly identical to the Kapton test results. *Figure 18* depicts the test results for both types of material. The deviation in the results shown was primarily due to the recovery of the residual stresses in the aluminized Kapton. Heat

**Table 4 "Basic" Creep Test Data Sheet**

Material: Kapton Stress: 1,200 psi Thickness: 0.5 mm			
Temperature (°F)	Test Time (sec)	Test Number	Date
600	3,000	KH1012T-100-600-A	5/19/88
600	3,000	KH1012T-100-600-B	5/23/88
600	3,000	KH1012T-100-600-C	6/08/88
650	3,000	KH1012T-100-650-A	5/17/88
650	3,000	KH1012T-100-650-B	5/17/88
650	3,000	KH1012T-100-650-C	5/20/88
700	3,000	KH1012T-100-700-A	5/20/88
700	3,000	KH1012T-100-700-B	5/24/88
700	3,000	KH1012T-100-700-C	5/26/88

FinRepFig3.1-15-dr2

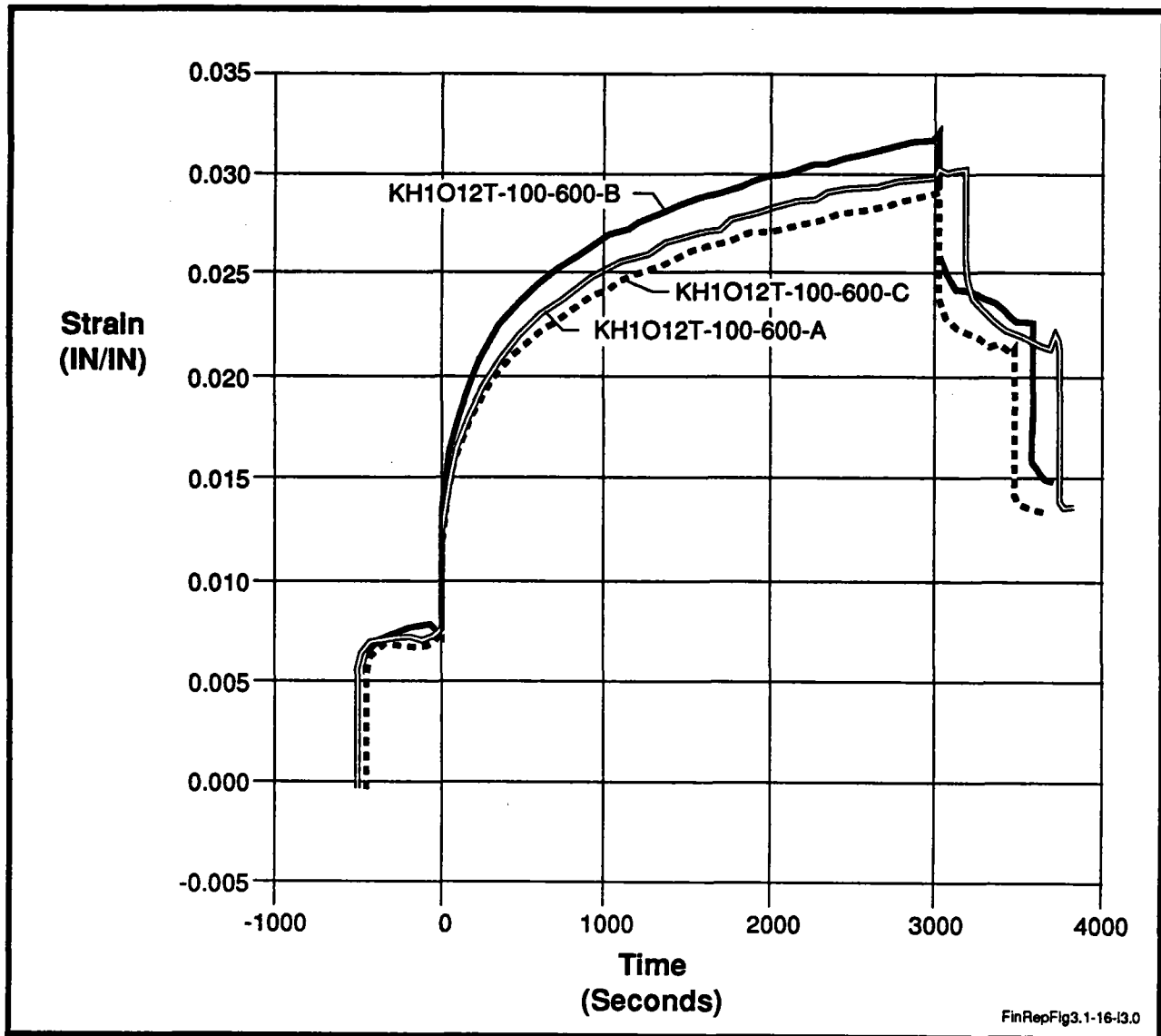


Figure 12 Kapton Creep Test Data at 1,200 psi and 600°F

curing the material at the forming temperatures unloaded eliminated the heat shrinkage differences shown in *Figure 19*.

Biaxial tests were completed and evaluated. Pure uniaxial stresses and combined biaxial stresses were applied to several cylindrical test specimens at the creep-forming conditions. Axial strain of the material was measured for comparisons with uniaxial creep results. Biaxial tests with 1 mil Kapton yielded small amounts of axial creep with no apparent primary creep. Biaxial tests with 0.5 mil material

yielded final creep strains similar to uniaxial tests. Elastic-viscoelastic analogy was applied to the elastic solutions of a cylinder inflated with a constant pressure or a purely axial load using Laplace transformations to eliminate the time parameter. Uniaxial creep compliance data combined with other material properties was used to approximately predict the axial strain of the material under the biaxial state of stress. The method proved useful for prediction and comparison of the actual test results.

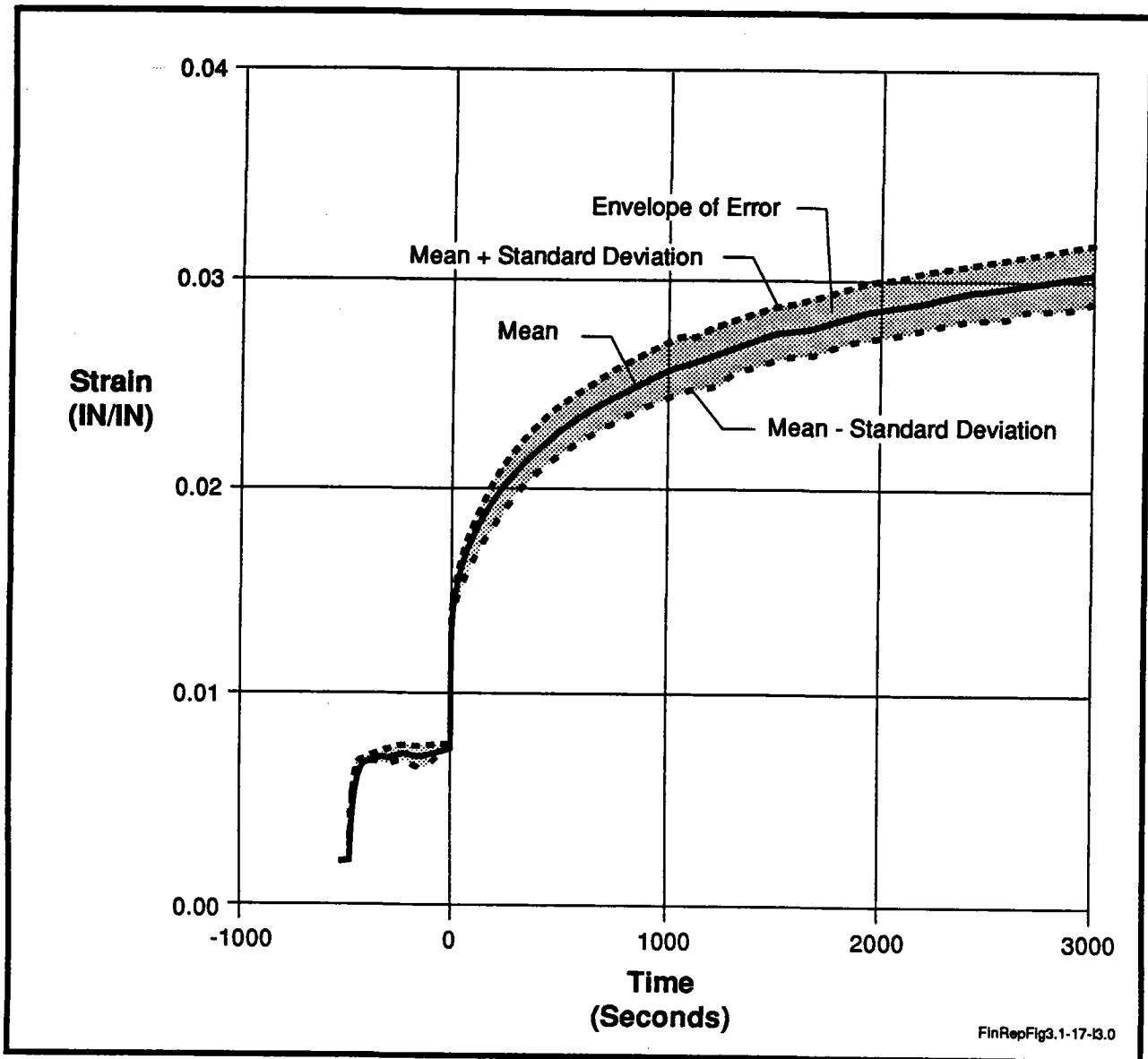


Figure 13 The Mean and Envelope of Error for the Uniaxial Creep Test of Kapton conducted at 1,200 psi and 600°F

### Comparison of Apical and Kapton

The physical properties for Kapton and Apical at room temperature are shown in *Table 5*.

From the material properties in the table it appeared that the two materials would have similar creep properties. Basic creep tests performed at SRS revealed that the two materials were dramatically different with respect to thermal stability (creep resistance). Following insertion into the oven, both materials thermally expanded similarly. Upon loading of the

samples the elastic deformation also appeared to be similar. The plastic deformation of the materials following elastic deformation was dramatically different. Kapton underwent a steep primary creep rate, while Apical stabilized with nearly no creep. Investigation of the total creep curves indicated that Apical did not creep as much as Kapton did for the given loading conditions. The results implied that Apical was a much more stable (creep resistant) material than Kapton.

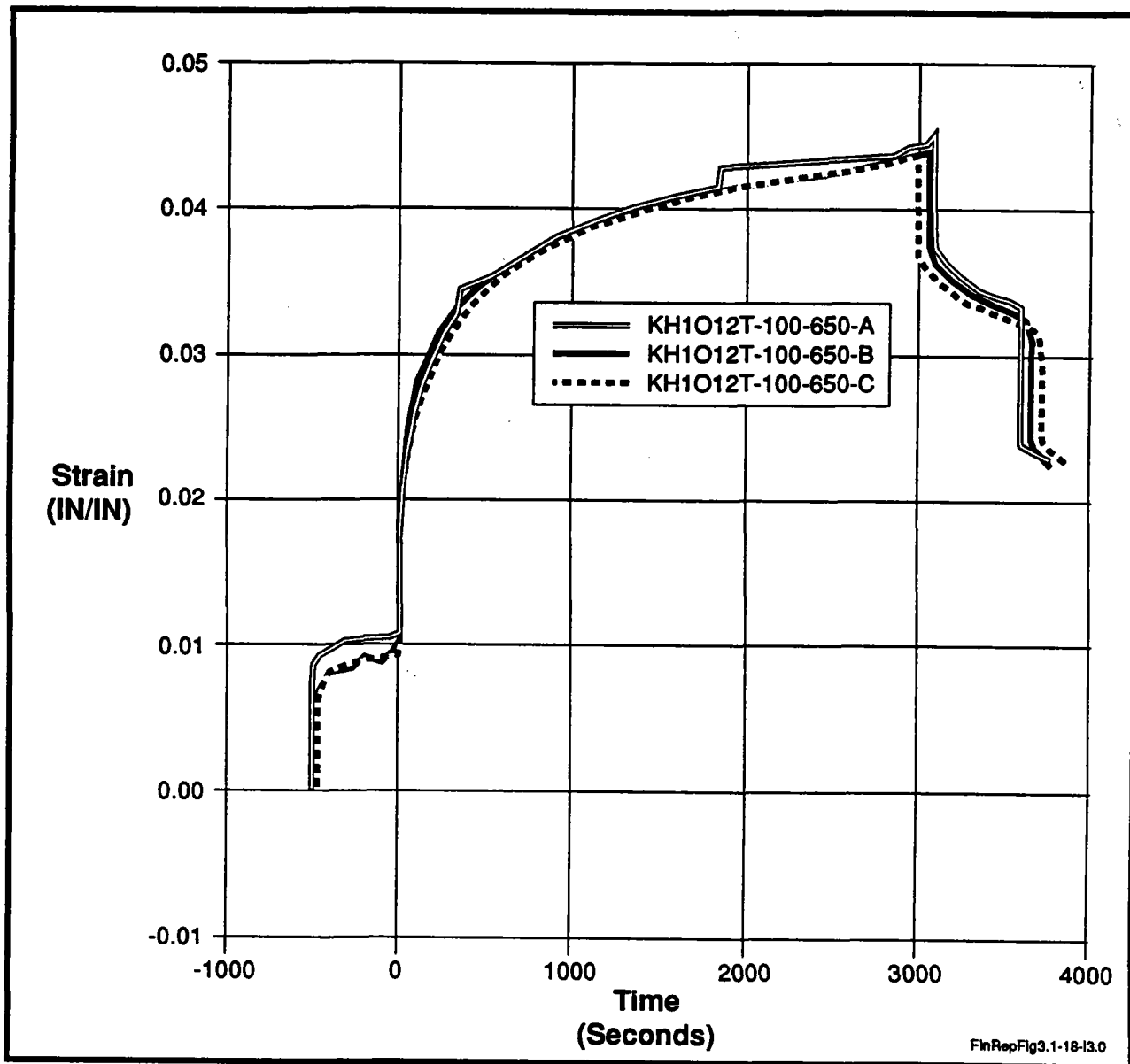


Figure 14 Kapton Creep Test Data at 1,200 psi and 650°F

SRS's creep test comparison conclusions supported Apical's claim that a thermally stable material could be produced by altering the processing parameters of a material with a nearly identical chemical composition. Apical, which has the same chemical composition as Kapton, undergoes a different processing procedure than Kapton. This makes Apical a superior thermally stable material. This fact made Apical less appealing to the creep-forming process.

#### Comparison of 1 and 0.5 mil Kapton

Uniaxial creep and relaxation tests were performed using Kapton with a thickness of 1 mil. The results of the tests indicate that there are dramatic differences in 0.5 mil and 1 mil Kapton with respect to creep-forming the material into an off-axis reflector. *Figure 20* indicates creep of 1 mil Kapton at a stress level of 1,500 psi and temperature of 650°F. The maximum creep strain of the material during the test was less than two percent. The final

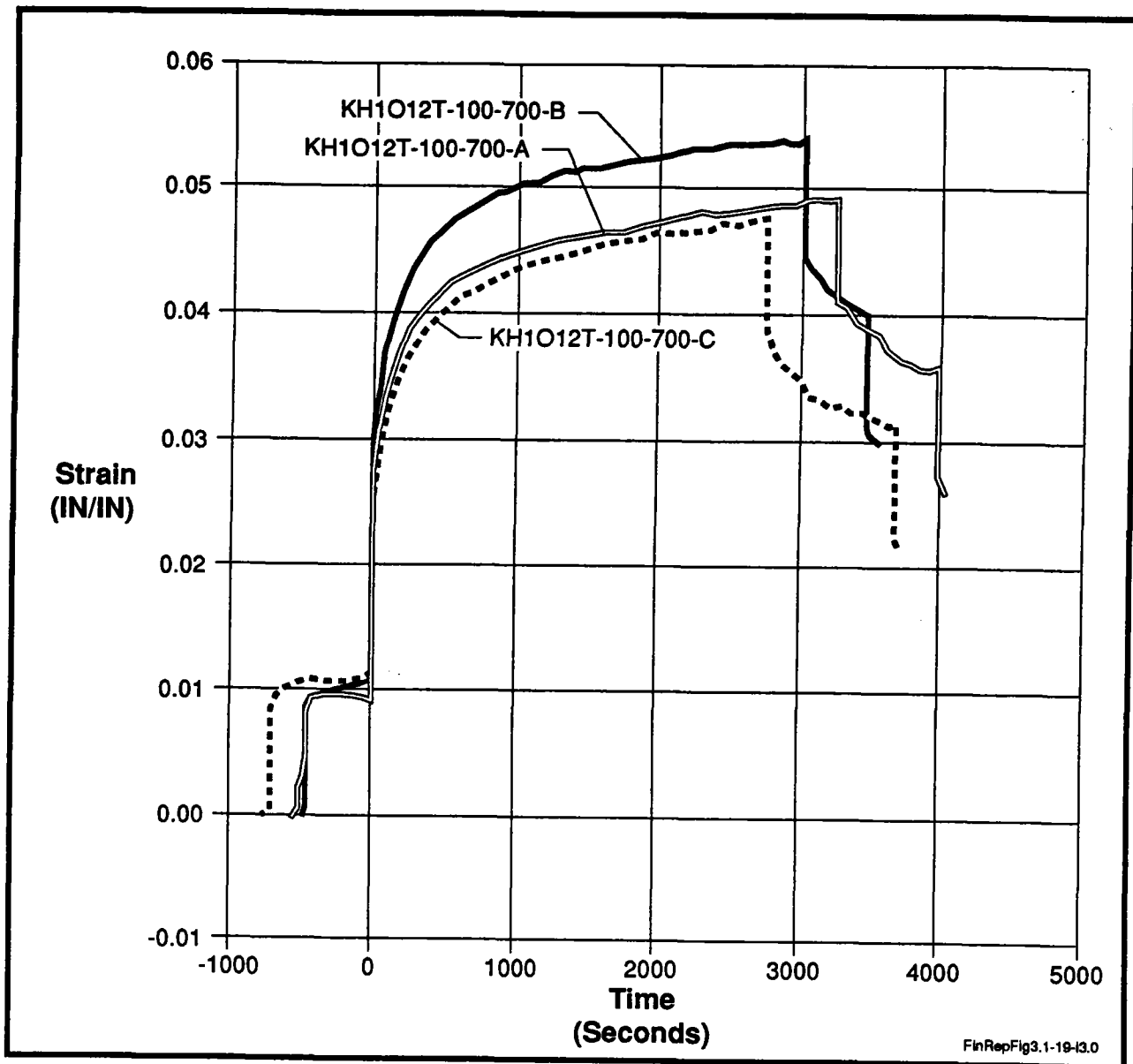


Figure 15 Kapton Creep Test Data at 1,200 psi and 700°F

strain following recovery was nearly zero percent. The graph indicates that the material has no permanent deformation under loading conditions which yield a permanent set for 0.5 mil material. Relaxation tests also indicated that the 1 mil Kapton material was not suited for relaxation forming because of the lack of stress relaxation and a large recovery of the deformation upon releasing the material. *Figure 21* depicts a five percent strain relaxation test for both 1 mil and 0.5 mil Kapton material. The

amount of material stress relaxation determined the degree of strain recovery of the material upon releasing the material from a constant strain of five percent. The figure illustrates that the 1 mil material did not stress relax and subsequently a large portion of the strain was recovered upon releasing the material until zero stress exists. By contrast, the 0.5 mil material relaxed and did not recover as much strain, resulting in the desired permanent set. The test results raised many questions with regard to the

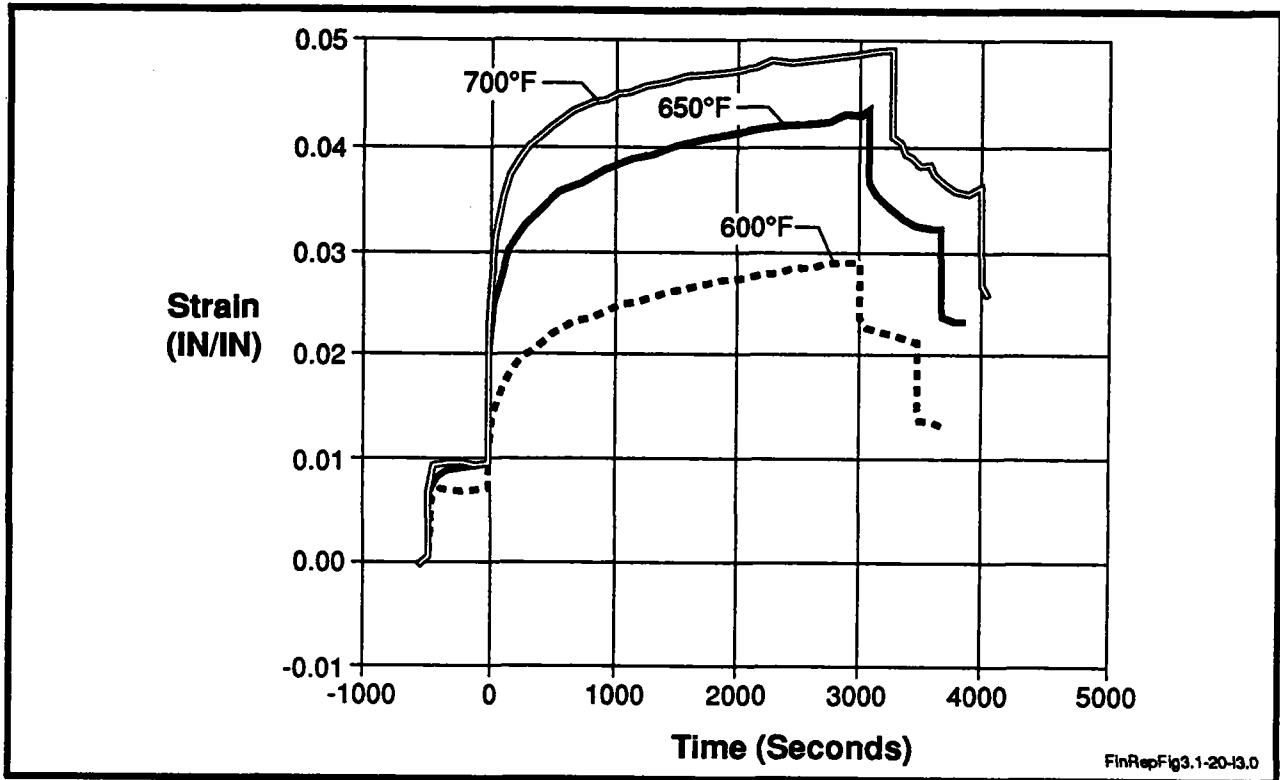


Figure 16 Kapton Uniaxial Creep Test Performed at 1,200 psi

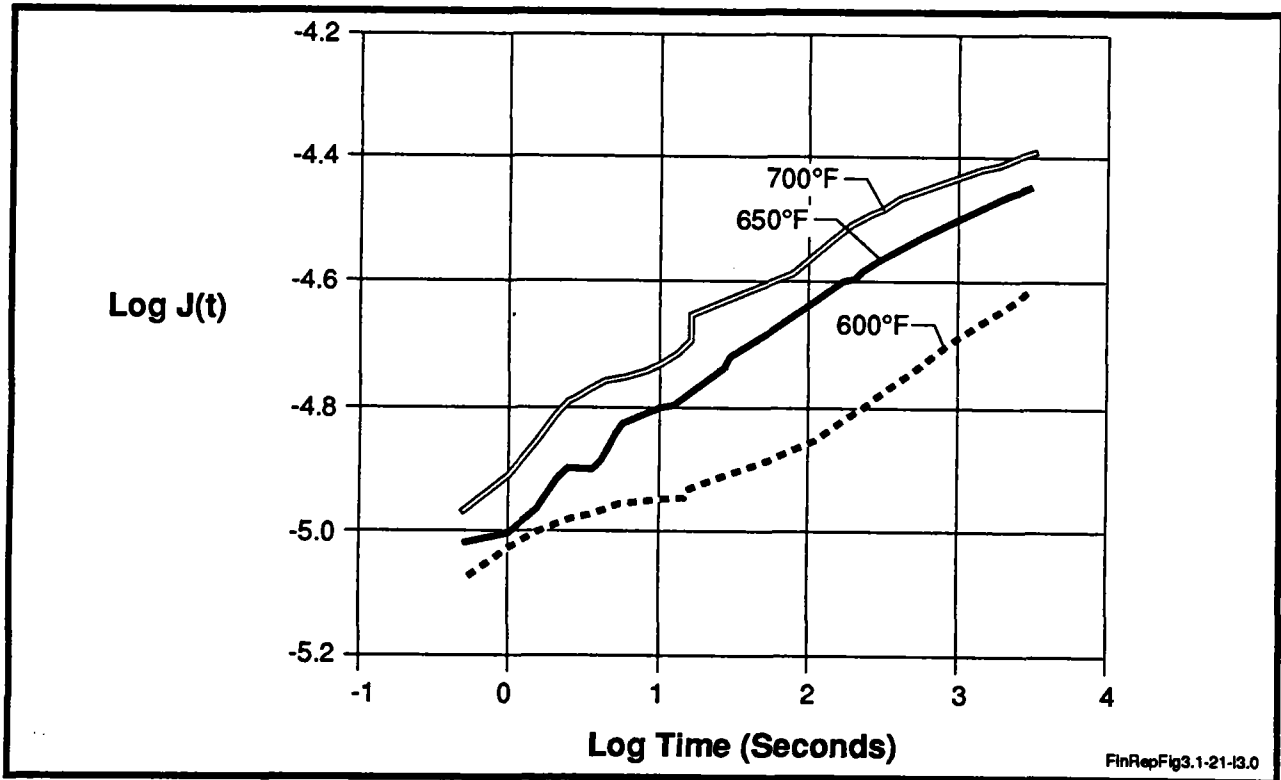


Figure 17 Kapton Creep Compliance Curves for Tests Performed at 1,200 psi

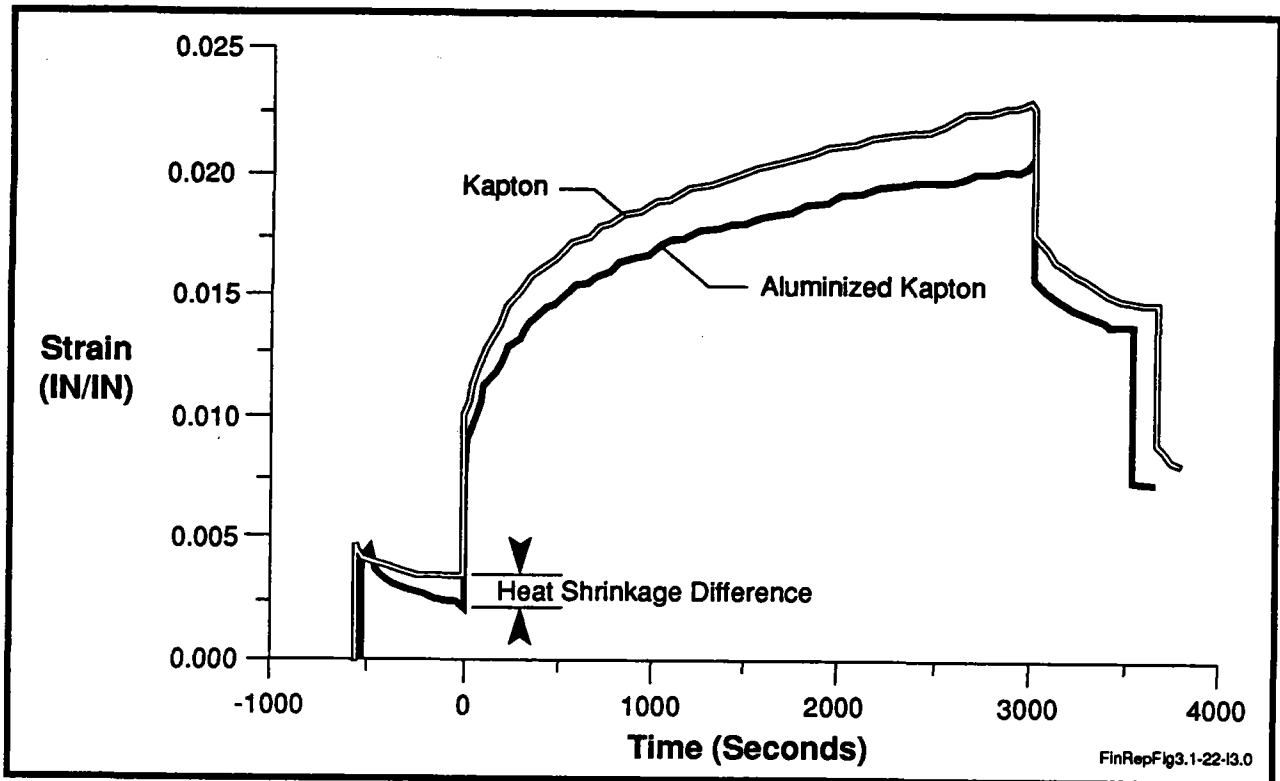


Figure 18 Creep of Aluminized Kapton versus Kapton

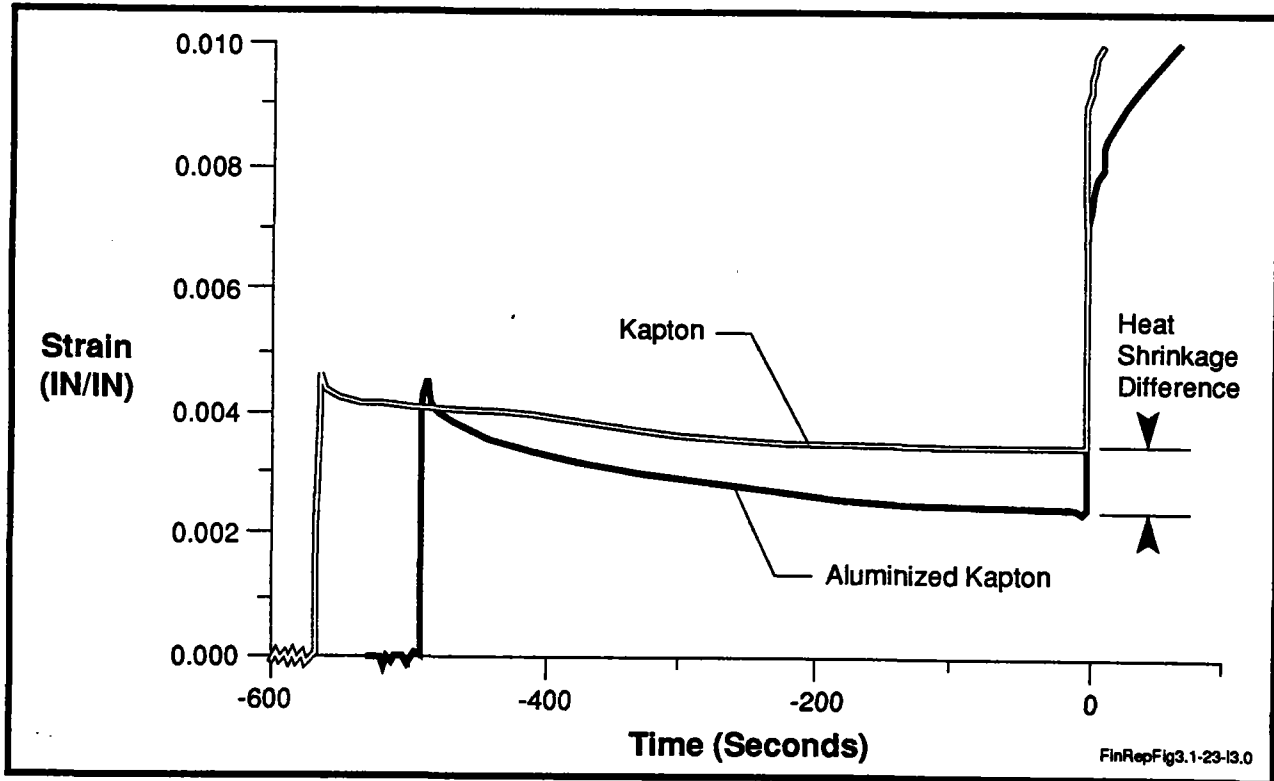


Figure 19 Heat Shrinkage of Materials

**Table 5 Material Properties of Kapton and Apical at 20°C**

	<b>Apical *</b>	<b>Kapton *</b>
Tensile Modulus (psi)	460,000	430,000
Ultimate Strength (psi)	35,000	20,000
Stress at 5% Elongation (psi)	13,000	13,000
Coefficient of Linear Expansion (in/in/°C)	$2.1 \times 10^{-5}$	$2.1 \times 10^{-5}$

Figure 3.1-24-1B8 \* Data taken from manufacturer's data sheet

material properties of the 1 mil Kapton at the creep-forming temperatures. Material processing differences during manufacturing account for the varying material properties for the 0.5 and 1 mil Kapton. The 0.5 mil material is not heat cured as long as the 1 mil material during the manufacturing process. A darker amber color results due to the increased curing time of the 1 mil film. Long term creep tests with 0.5 mil Kapton material resulted in a similar amber appearance. Further testing of the long term crept 0.5 mil film indicated properties similar to the 1 mil film. Long term creep-forming (24 hrs.) was not measurable because of the material properties changes at the elevated creep-forming temperatures.

### Multiple Step Creep Tests

Material characterization tests performed during the task included multiple step load creep tests. Linear viscoelastic theory is derived from the superposition principle of a "linear material". A "linear material" can be described by defining the total time dependent strain as a function of the sum of the stresses applied to the material at the respective times, multiplied by the creep compliance of the material. The time dependent strain can be written as:

$$e(t) = (S1 + S2) * J(t)$$

where S1, S2 = stress levels

J(t) = creep compliance

e(t) = strain.

For the case which S1 is applied at t1 and S2 is applied at t2, the total strain can be approximated by the relation:

$$e(t) = S1 * J(t1) + S2 * J(t2 - t1)$$

This theory is referred to as the Boltzmann's superposition principle.

Kapton material was subjected to a two step loading process to further investigate the linearity of the material. Separate strain data for creep tests at 650°F and 500 and 1,200 psi were used to predict the strain response of the material for an initial load of 500 psi applied to the material with an additional load of 1,200 psi added after a 1,000 second interval. The predicted time dependent strain was calculated by using the superposition theory. An actual test was then performed and compared to the predicted results. The results are shown in *Figure 22*. The material strain predictions consistently followed the test data which indicates linearity of the material at the testing conditions.

### 3.1.3.4 — Analytical Methods to Represent Test Results

Time-temperature equivalence theory for thermorheologically simple materials was applied to the test data. Horizontal shift factors were calculated for each stress level at a base temperature of 600°F. *Figure 23* indicates the method for obtaining the shift factors for time-temperature equivalence for a 1,500 psi stress

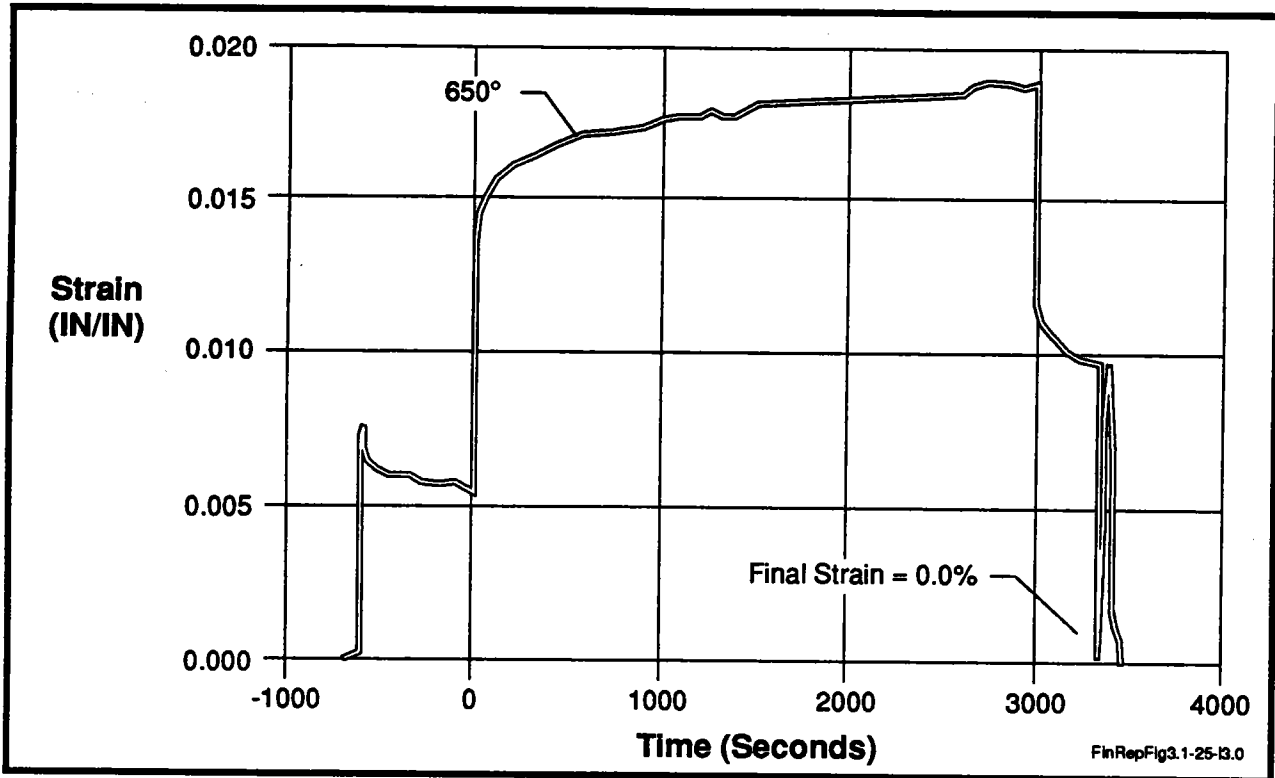


Figure 20 Kapton 1.0 mil Transverse Strain at 1,500 psi

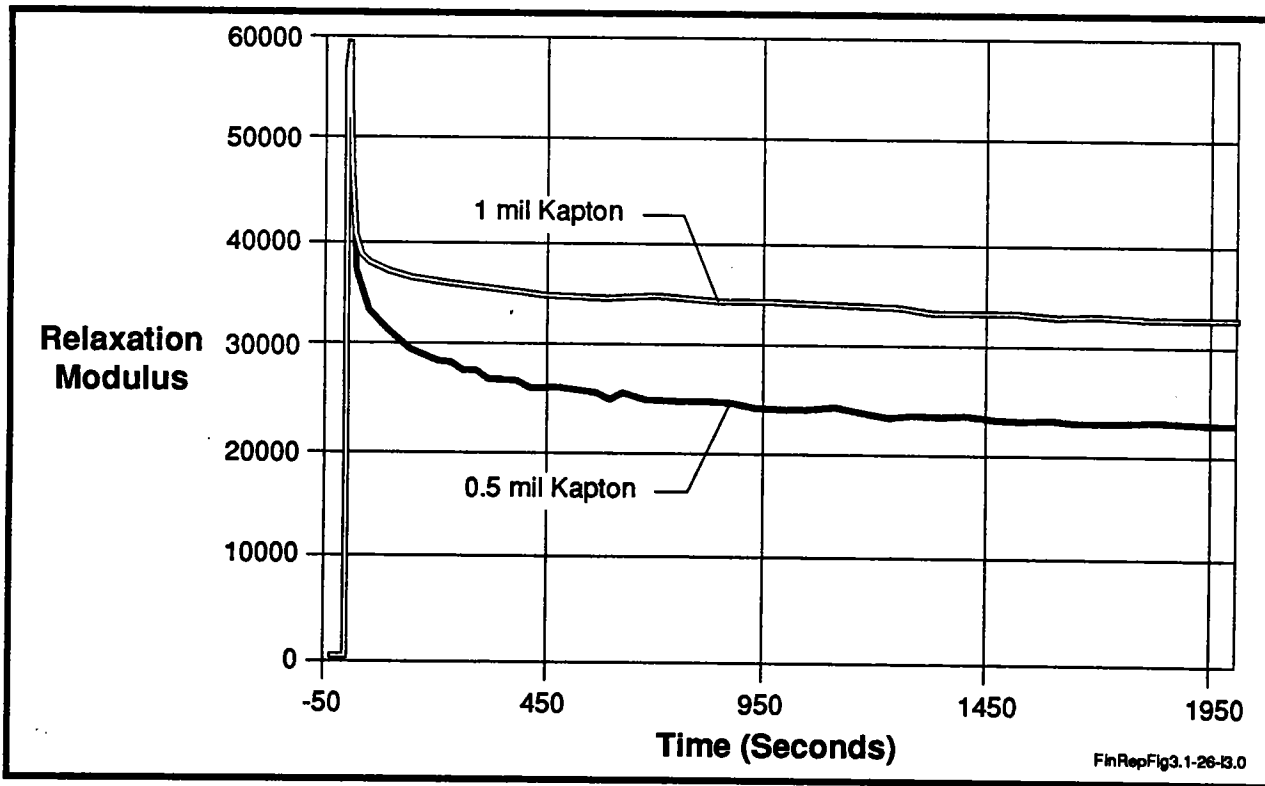


Figure 21 Relaxation of 1.0 and 0.5 mil Kapton Strain at 5%

on the material. A series of constant stress creep tests were done at each temperature shown in the figure. The creep compliance, defined as the time dependent strain divided by the constant stress, was plotted as a function of log time. For thermorheologically simple materials, an increase in temperature would be related to an increase in time. Thus, for a higher test temperature relative to a base temperature, the creep compliance curve can be shifted horizontally to the right along the log time axis. Similarly, for a material tested at a lower temperature relative to a base temperature, the compliance curve would be shifted toward the left of the horizontal time scale. Using the shift factors for a material exhibiting this phenomena enables one to generate a master creep curve with a time scale orders of magnitudes larger than the relatively short testing time at the reference temperature. This is accomplished by performing tests at higher and lower temperatures than the reference temperature and then applying the time-temperature superposition principle to shift the curve and generate a master creep curve for the stress level. *Figure 24*, *Figure 25*, and *Figure 26* indicate application of the horizontal shift factors to the 500 psi, 1,200 psi, and 2,000 psi stress levels. It is interesting to note that the shift factors that were calculated are entirely separate for each stress level, but are similar for identical temperatures. The similarities indicate that at the range of temperatures tested (500°F–700°F), the material somewhat exhibits the characteristics of a thermorheologically simple material.

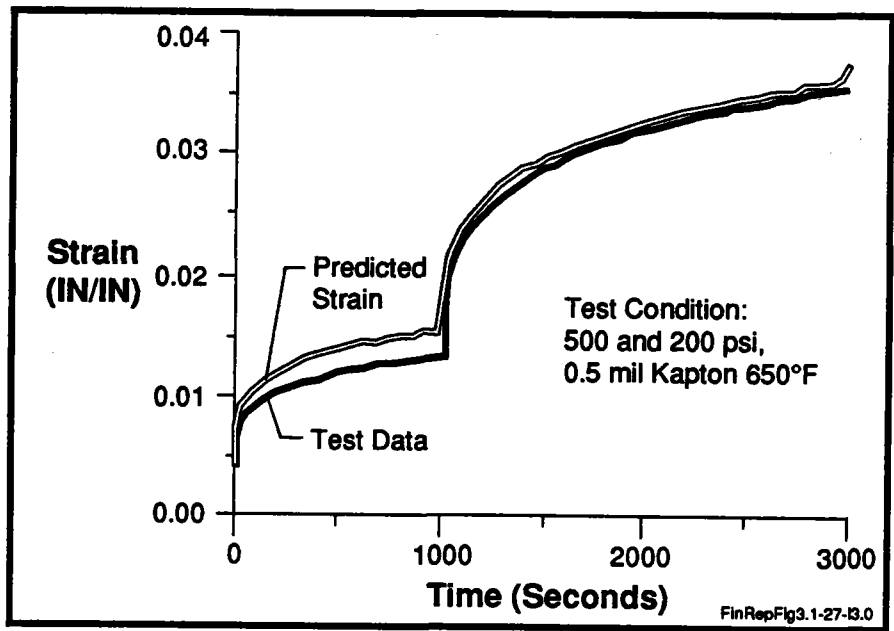
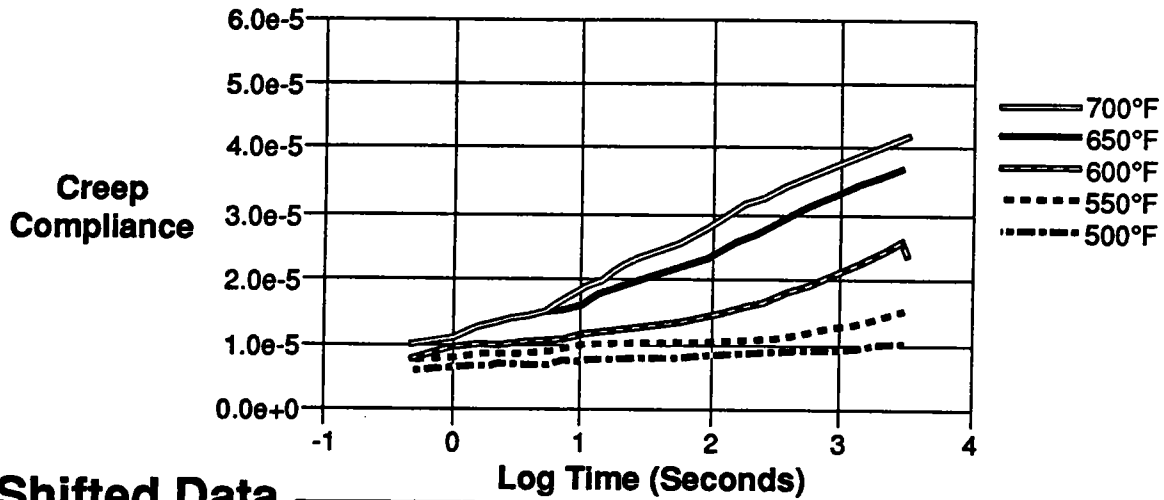


Figure 22 Two Step Load Creep Test

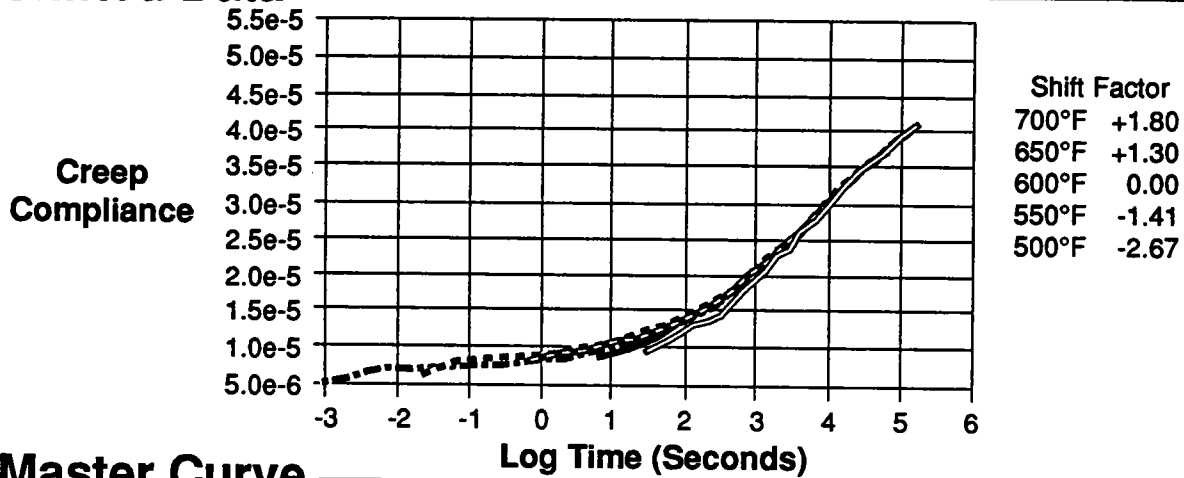
A linear viscoelastic material tested in uniaxial tension will yield the same creep compliance curves for varying constant stress levels. Several materials that are non-linear in nature which exhibit large deformations (50%-300% strain) before failure can be treated as linear over a limited strain (<10%) range. *Figure 27* depicts the master creep curves generated from *Figure 24*, *Figure 25*, and *Figure 26* on the same scale. It is apparent from the figure that the material behaves linearly for stress ranges between 1,200 psi and 2,000 psi. For the stress level of 500 psi the shape of the compliance curve appears similar to the other stress levels, but shifted vertically. The results of these tests give a good indication of the material's response to a uniaxial stress rate for a range of creep-forming temperatures and stresses. The material creep compliance curves can be applied to the creep-forming process in order to determine creep-forming time, relaxation time, and temperature needs to achieve the desired off-axis shape.

An objective of Task 1 testing was to develop constitutive relations for KAPTON and other polyimides at the creep-forming temperatures and loads, which would allow for the

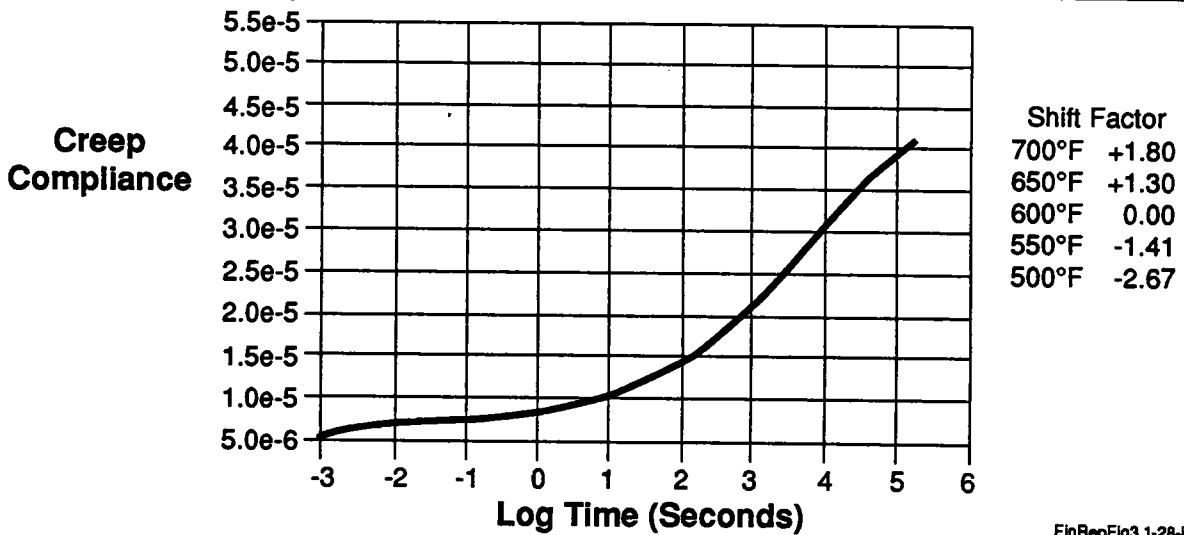
# Creep Compliance at 1500 psi



## Shifted Data



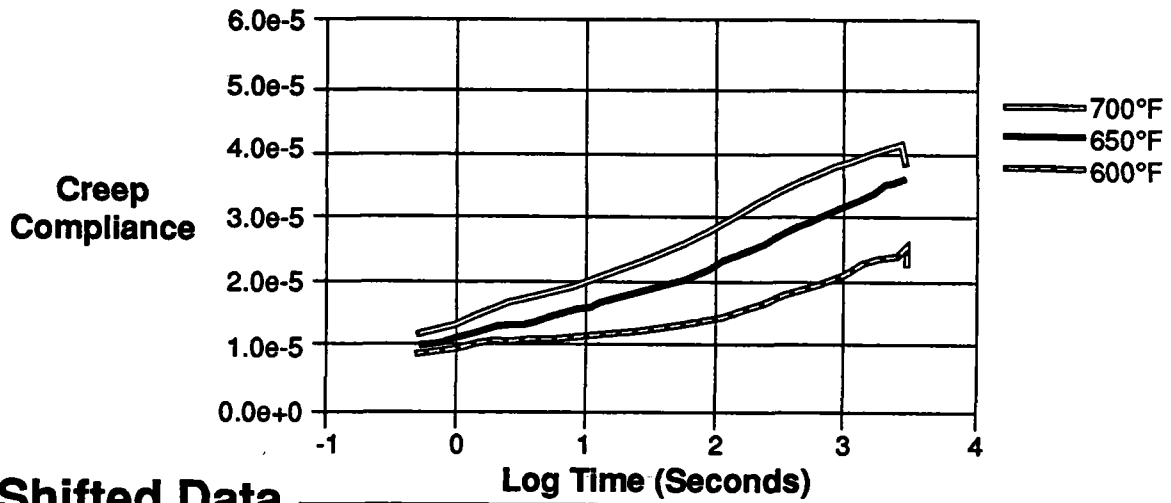
## Master Curve



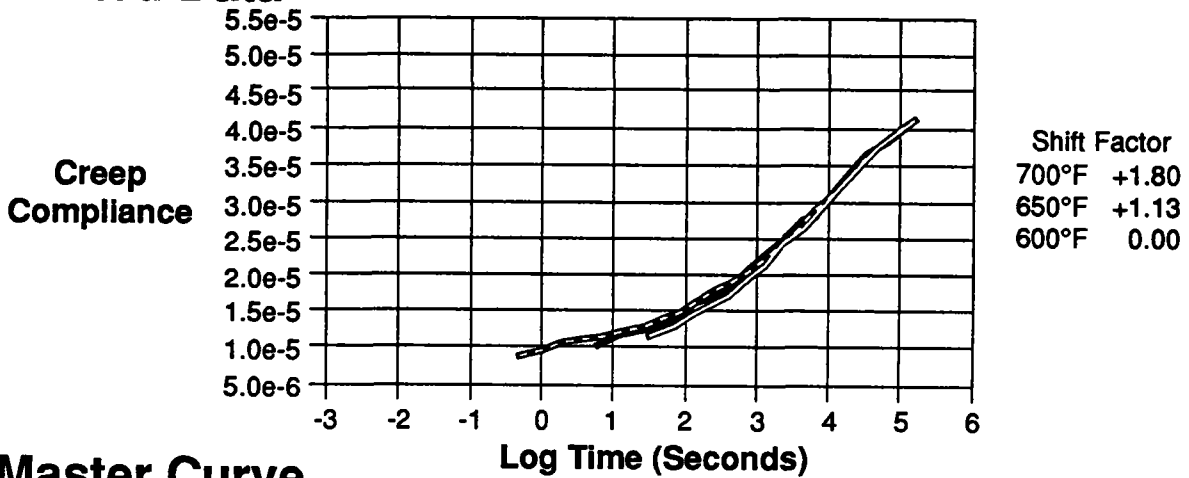
FinRepFig3.1-28-13.0

Figure 23 Master Creep Compliance of Kapton at 1,500 psi

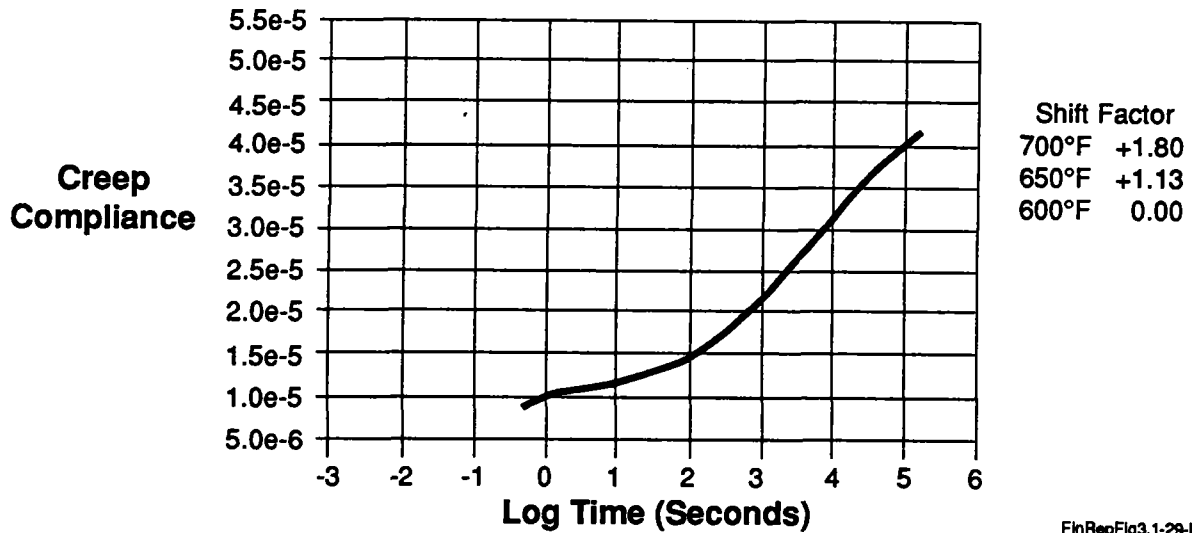
## Creep Compliance at 1200 psi



## Shifted Data



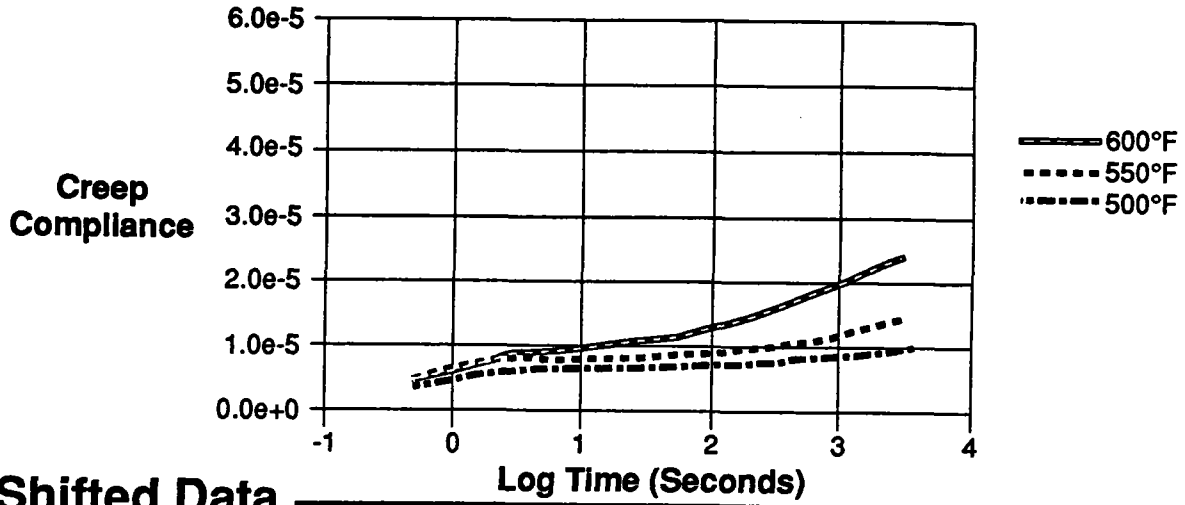
## Master Curve



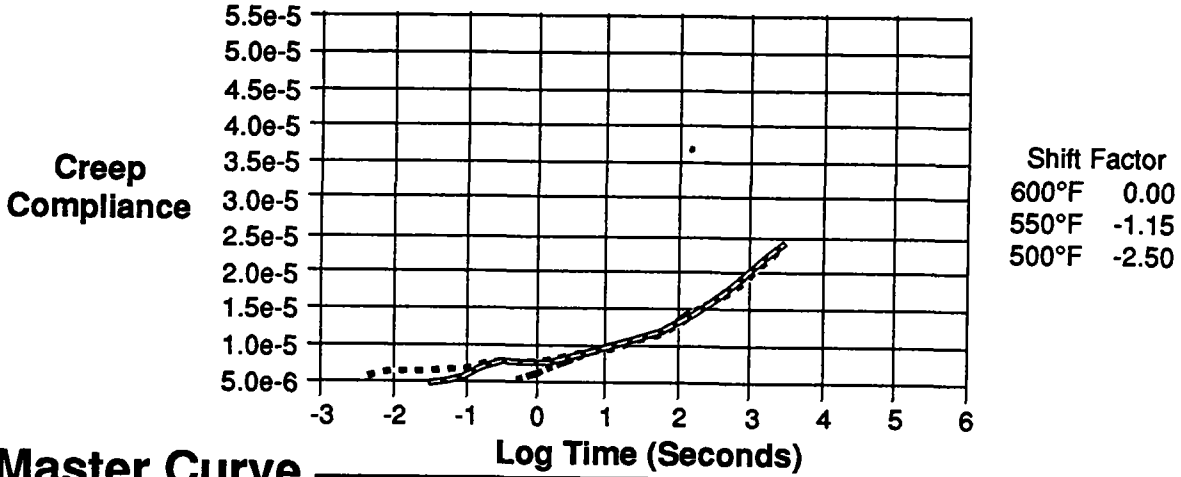
FinRepFig3.1-29-B.0

Figure 24 Master Creep Compliance of Kapton at 1,200 psi

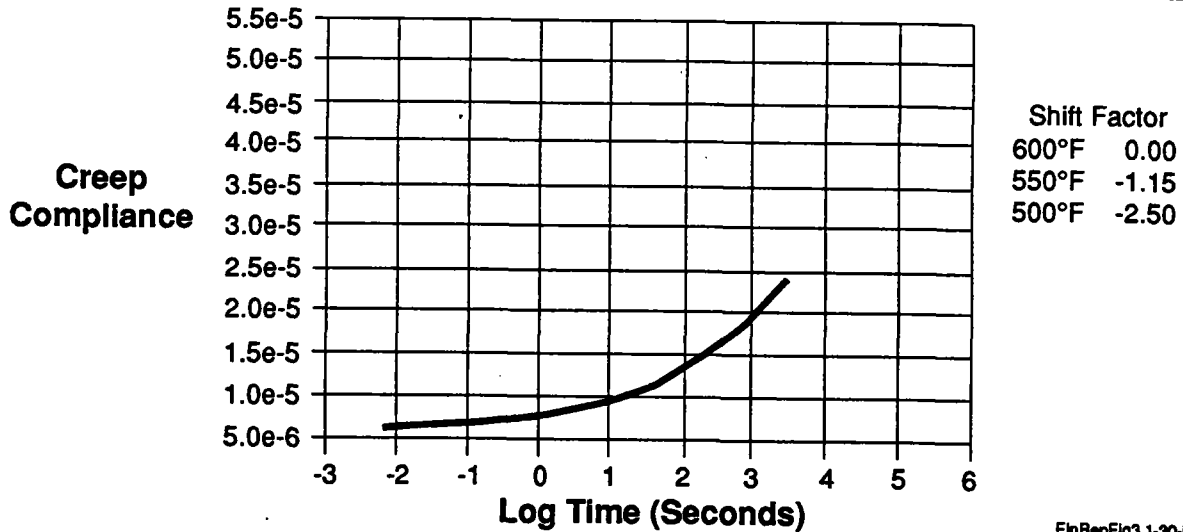
## Creep Compliance at 2000 psi



## Shifted Data



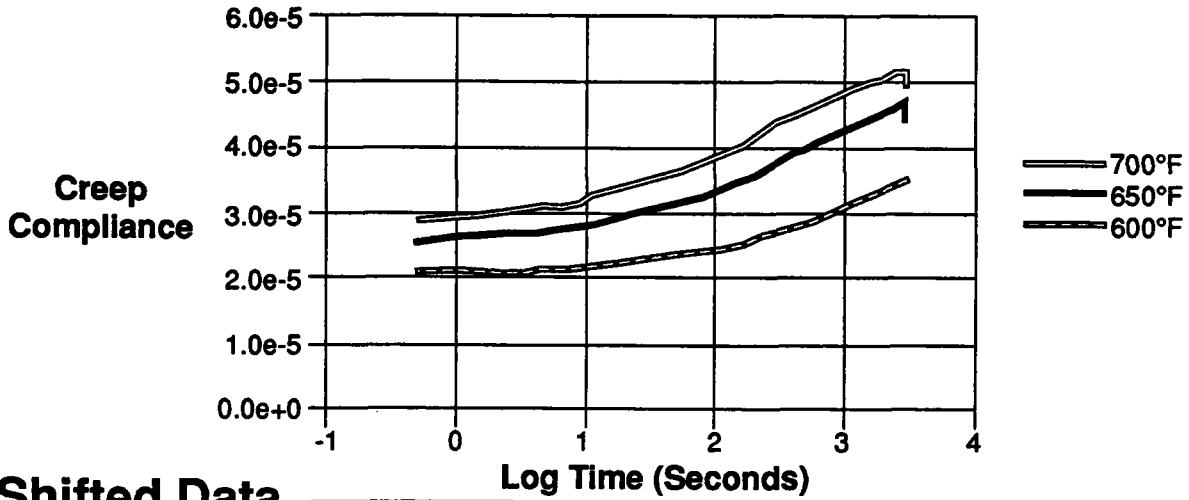
## Master Curve



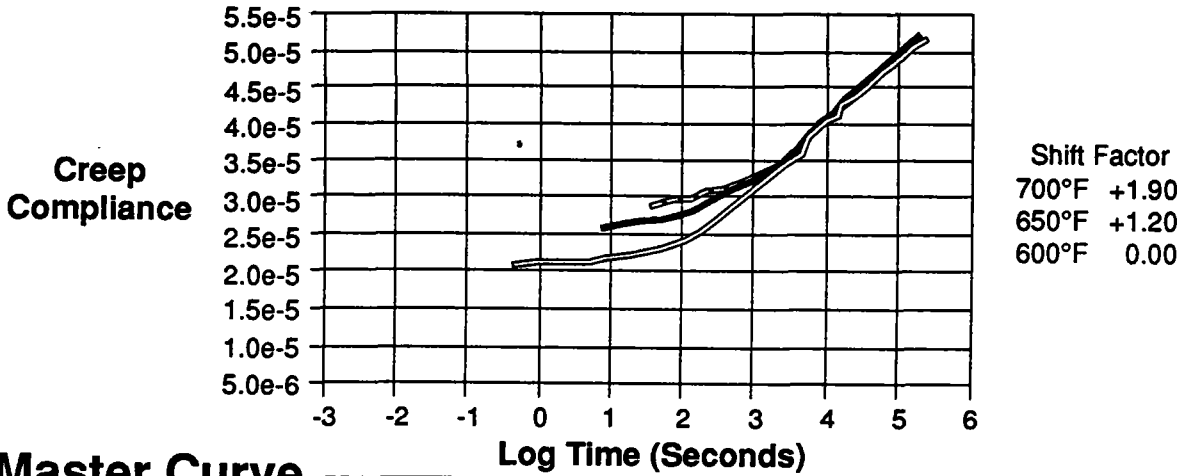
FinRepFig3.1-30-13.0

Figure 25 Master Creep Compliance of Kapton at 2,000 psi

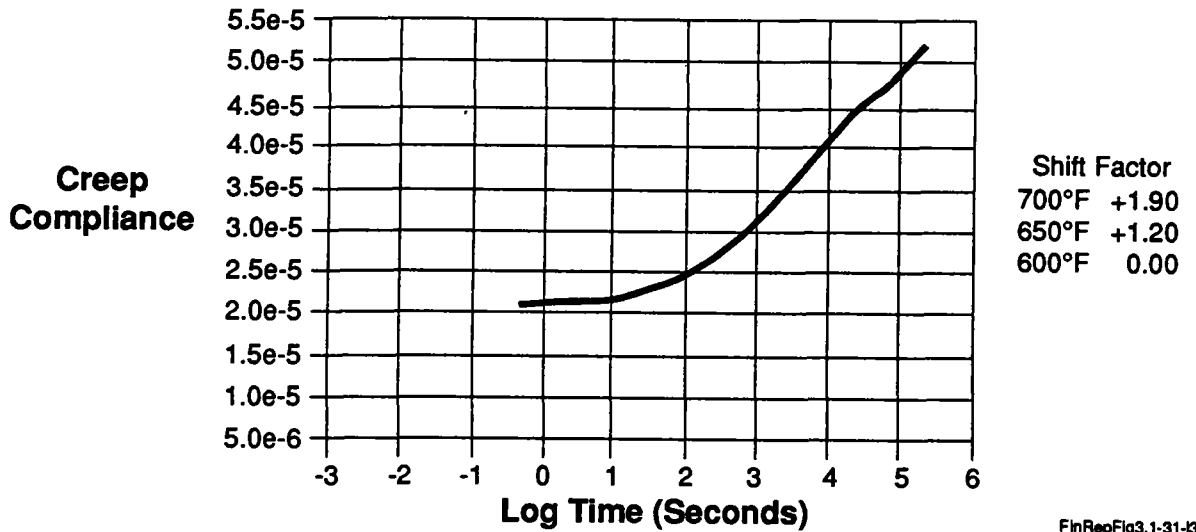
### Creep Compliance at 500 psi



### Shifted Data



### Master Curve



FinRepFig3.1-31-3.0

Figure 26 Master Creep Compliance of Kapton at 500 psi

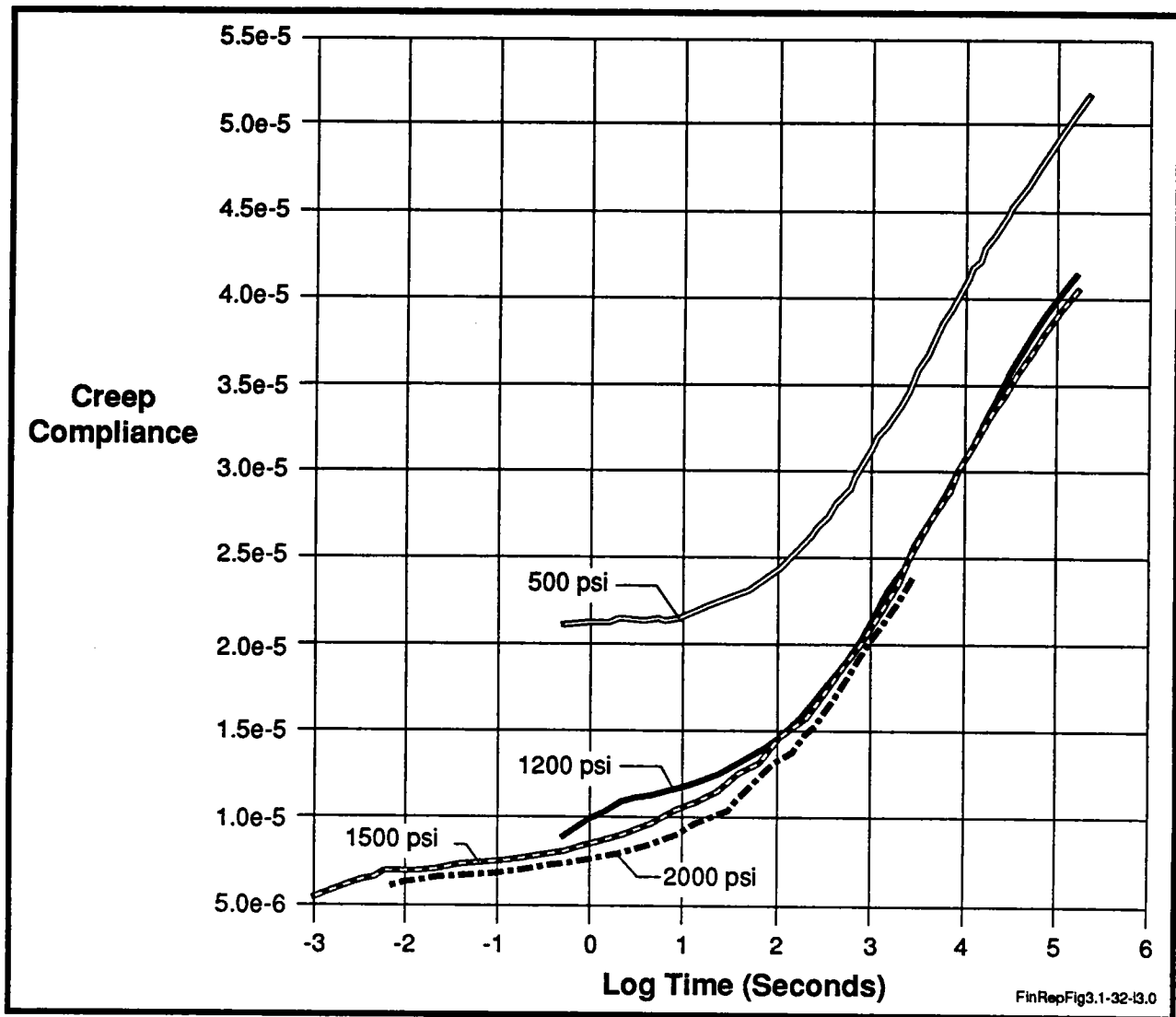


Figure 27 Master Creep Compliance Curve

calculation of the final shape and stability of the creep-formed reflectors. Schapery (1) characterized non-linear materials by expanding methods in linear theory to non-linear theory by the use of vertical shift factors in creep compliances along with the horizontal shift factors in thermologically simple materials for time-temperature equivalence.

The constitutive laws for isothermal conditions were modified to incorporate a time-temperature equivalence relationship. Initially, the effect of a uniform temperature was addressed. The relaxation modulus and creep compliances

at a base temperature  $T_0$  were defined.

$$G(t, T_0) = G(t) = L(\log t)$$

The shift function  $D$  was defined for a thermologically simple behavior to take the form

$$G(t, T) = L(\log t + D(t))$$

where

$$D = \log(D(t))$$

The reduced time  $u$  was then defined by:

$$u = tD(t)$$

The reduced time functions allowed us to pass from the constitutive equations at the base temperature  $T_0$  to any constant temperature  $T$ .

The constitutive equations for a variable temperature field  $T(x, t)$  required further modifications to the isothermal viscoelastic equations. The reduced time  $u$  was generalized, consistent with the time-temperature equivalence. The thermal expansion coefficient was then taken into account in the dilational response of the material. The reduced time for transient problems included a dependence on both position and time. A "pseudo-temperature" was developed which included thermal expansion. The results of the development indicated that the instantaneous stresses at each material point of the body are functionals of the preceding local strain and temperature history. Muki and Sternberg (2) indicate that the functionals are linear in strain but non-linear in temperature. Application of the time-temperature shift factor was applied to creep data as well as relaxation data. The relaxation data curve yielded an indication of long term stability of the creep-formed reflector.

### **3.1.3.5 — NASA / Langley Developed Polyimide Materials**

The extensive creep testing conducted in this effort led to the results that different thicknesses of Kapton, and different brands of polyimide, display markedly different viscoelastic properties. Also it was demonstrated that Kapton film of thicknesses greater than 0.5 mil display such a low creep compliance as to be practically non-creep-formable. Kapton 0.5 mil in thickness which has been subjected to prior creep-forming and annealing processes also displayed a lower creep compliance. These results led to the evaluation of polyimide films developed by NASA Langley research center. The film material from NASA is received in solution form and can be cast on mandrel substrates and cured to fabricate

double curvature membrane.

The 6F+BDAF polyimide (Reference NASA Technical Memorandum 876501, "Optically Transparent/Colorless Polyimides") was made by LaRC from 2, 2-bis (3, 4-dicarboxyphenyl) hexafluoropropane dianhydride (6F) and 2, 2-bis [ 4-( 4-aminophenoxy ) phenyl ] hexafluoropropane (BDAF), which was obtained from commercial sources and purified. The material was one of a family of films evaluated and reported in the referenced memorandum. "A need exists for high-temperature (200°-300°C) stable, flexible polymeric film and coating materials that have high optical transparency in the 300-600 nm range of the electromagnetic spectrum for applications on space components such as multilayer insulation blankets, solar cells, and thermal control coating systems."

It was recognized that such a material could have applications also for space inflatable solar concentrators. Such a film would be needed as an optically transparent front membrane needed to form the pressure enclosure. It could also be used as a substrate for aluminizing as the front or rear surfaced reflector element.

Upon investigation, it was found that the family of materials evaluated included both heat imidized and chemically imidized films. The chemically imidized is reversible; it can be redissolved and used again.

Further, since the materials may be obtained in solution and then cured, any size/thickness film may be produced, without seams. Since the chemically imidized film is reversible, it may be solvent welded, allowing a very uniform butt joint weld to be made of very thin film. This technique has been used to patch and join 1/2 mil film.

## 3.2 — Reflector Fabrication Processes

The objective of this task was to evaluate key issues of process and assembly technology of inflatable concentrators. The task supported transferring basic materials data generated in Task 1 into the designing, on a sound engineering basis, the concentrator scale models built in Task 4. The fabrication processes originally considered were using the off-the-shelf polyimides. Methods to seam flat sheets and gore segments were considered. Methods to form films using mandrel techniques were also evaluated. Advance mandrel techniques such as geodesic network and liquid spin cast mandrels were considered. Concentrator fabrication techniques using NASA polyimides were discovered during the course of study under this task. The results of this task led to further evaluation of spin and spray cast polyimides in Task 4. Several models were fabricated in Task 4 using the techniques discovered and refined under this task area of reflector fabrication processes.

### 3.2.1 — Seaming of Flat Sheets, Gores and Combinations

The options investigated for creep forming off-the-shelf polyimides into parabolic shapers were:

a. Seam flat sheets together, creep-forming (CF) an entire concentrator simultaneously: involves large deformations, easy/forgiving seaming procedure, good for correcting seam distortion and filling wrinkles/imperfections (for mandrel creep/relaxation forming (CRF), not for pressure CF), but requires large furnace, and may have large spring back and recovery.

b. Seam flat gores into paraboloidal shape, then CF gores into double curvature: requires large furnace, difficult seaming procedure, little imperfection corrective because little deformation especially at seams.

c. CF radial (geometrically identical) gores, precise trim and inch mark peripheries, then seam on a radial mandrel: fairly easy seaming, seams need not withstand CF temperature, furnace and mandrels can be small; little deformation, therefore little imperfection correction, and no seam distortion correction.

As previously determined, pressure sensitive adhesives were unsuitable for long term high stability applications because of their inherent poor ambient-temperature viscoelastic properties, even for seaming previously curvature formed film gore sections. The adhesive of choice for seaming polyimide film is TPI, both for seaming arrays of flat sheets to be subsequently creep-formed in a large furnace and for seaming together already curvature formed gores. One obvious question raised by locally heat cured seams is distortion from local heat shrinkage; however, since heat shrinkage largely arises from relaxation of residual stresses, if the creep-formed gore sections were properly annealed/stress relieved for long term stability, as part of the creep-forming process, they should display no heat shrinkage during seaming operations. Local heat shrinkage during seaming might be a problem for joining flat sheets that were to be subsequently creep-formed, but in that case, heat shrinkage wrinkles/distortions should be automatically removed during creep-forming.

For full size concentrator fabrication the outcome of the final trade-offs between (a) creep-forming the entire concentrator, in a very large furnace, from a flat sheet seamed together from many flat strips, versus (b) seaming together many curved gores previously creep-formed in a small furnace, is not obvious. Method (a) requires an extremely expensive furnace, for 30 meter or larger concentrators, and may require many tries before a defect free film is produced, due to the very large area of film involved; however, the geometry is relatively

simple to deal with, and seaming of flat sheets is an order of magnitude easier than seaming of curved gores. Method (b) allows a large creep-formed concentrator to be built using only a modest size creep-forming furnace, and for this reason is more likely to be chosen for the first attempt at building a full scale concentrator; however, it involves complex, hard to visualize, and very difficult to fixture for creep-forming, geometries of the individual curved gores, especially for the off-axis parabolic configuration. Fixturing for seaming of preformed gores is inherently extremely difficult. SRS has had successful experience in seaming large flat sheets (in fabrication of 20 foot and 50 foot pressure-shaped concentrators) and singly curved meridional gores (in fabrication of 9 foot solar water purification spherical concentrator), using pressure-sensitive tape technology, and successful experience in making straight seams of 3 foot length in flat sheets using heat cured TPI technology, so it is reasonable to expect to be able to extrapolate this experience to TPI seaming of large arrays of flat sheets.

Distortion due to double thickness of a lap seam is a concern both during creep-forming from a large seamed flat sheet and for elastic stretching due to normal operating tension in the case of a concentrator assembled by seaming together precreep-formed gores. The high bond strength of TPI adhesive allows use of seam overlaps as narrow as the practicalities of seaming fixturing will allow. Measurements must be made to allow realistic upper and lower limits to be assigned to the widths of the band of significant distortions to be expected on either side of a seam, as a function of seam overlap width, both for seams made before creep-forming and for films assembled from precreep-formed gores and subsequently tensioned into specularly. The effect on this distortion, of using an embossed heat curing iron which over tensions the seam

longitudinally, is to be evaluated.

Compliance, curvature matching to film support fixtures, and temperature/time uniformity/control are concerns for a seam curing iron for use in seaming preformed curved gores. It is expected that careful "tuning" of the heat inputs, insulation, and heat losses, along the length of a long strip-type curing iron, will give adequate temperature uniformity without recourse to such techniques as circulating liquid or thermostats. The technique of a motor driven embossed heated roller should be investigated and compared with curved compliant strip curing iron techniques. Such variations as a square or hexagonal stepping flat-face curing iron driven by a "Geneva stop" mechanism should be explored.

For pressure CF, seams are a major concern, and must be narrow and linearly pre-overstretched. For mandrel CRF, seams are a minor problem as to distortion effects and seam width. CRF process tends to correct seam distortion/wrinkles.

Seam effects vary directly with in-flight inflation pressure; a major advantage of CF vs. assembly of concentrator from flat sheet gores is that less inflation pressure is needed to achieve proper geometry, which reduces effects of seams and effects of film imperfection thickness variation, and also reduces leakage from micrometeoroid punctures.

### **3.2.1.1 — Seaming of Flat Sheets of Kapton**

Work was done to investigate the effects of seam behavior of Kapton-Kapton lap joints. The objective was to develop the detailed seaming procedures for fabricating large, uniform seams and to characterize the creep behavior and lap shear strength of the seams for creep-forming. Two types of adhesives, TPI and a heat curable polyimide, were tested to determine which was more suited for the seaming technique.

The procedure which was used for the seaming process is as follows: The adhesive was spread over one end of the Kapton; a second sheet was then placed over the adhesive (See *Figure 28*). The seamed area was then placed between two aluminum heat conducting bars with heating elements. A uniform weight was placed on the seaming apparatus and the temperature slowly increased until a final temperature of 400°F was reached. The seam was then cooled back down to room temperature and subsequently removed from the seaming apparatus.

Numerous tests were conducted with both

adhesives at varying thicknesses and seam widths. The seam widths varied from 1/8" to 3/8". The most promising results were obtained from the 1/8" seam using a thin line of the heat curable polyimide. The seams made in this manner appeared much smoother and more uniform with little or no bubbling of the adhesive occurring. The TPI seams produced noticeable bubbling due to the offgassing of the volatiles during the cure cycle.

For pressure CF this is a major concern, e.g., thickness variations or property inisotropies, causing bulges/wrinkles. For mandrel CRF

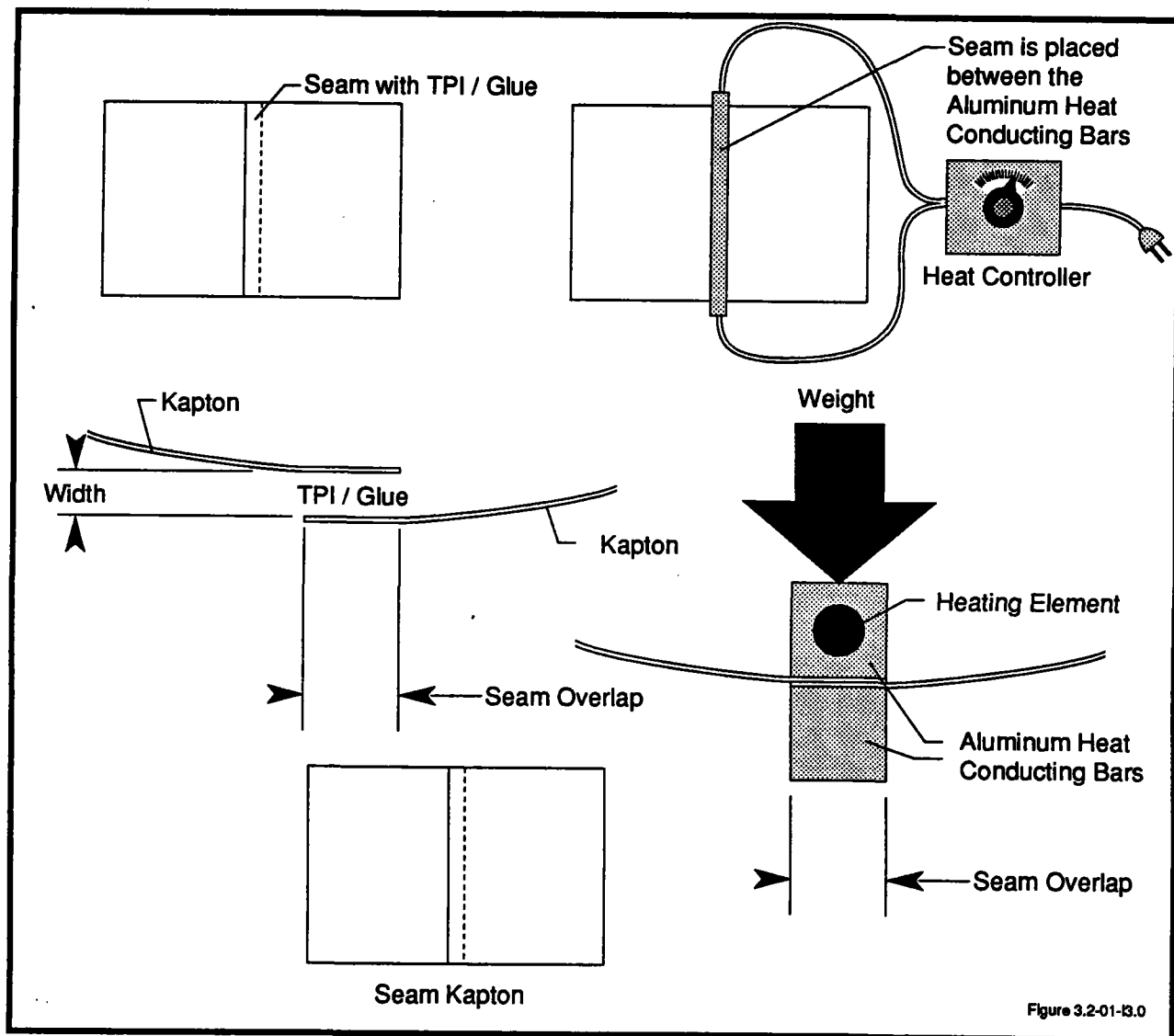


Figure 28 Film Seaming Method

these effects are negligible. Low in-flight inflation pressure of CF concentrator reduces effects of film thickness variations.

### 3.2.1.2 — Long-Term Film Effects

Long-term film effects are a greater concern, for larger deformations; however, mandrel CRF inherently involves long high temperature stabilization/annealing process, which is conducive to high stability.

Inputs were given to Task 1 to perform reasonably long duration recovery tests, at a variety of temperatures, on creep-formed films. Using the Arrhenius-Eyring relations, activation constants were derived and other appropriate analyses performed that allowed theoretical extrapolation/prediction of recovery (and other factors affecting dimensional stability) over a period of years at projected operating and storage temperatures.

### 3.2.2 — Reflector Construction Without Seams

Ideally a thin film reflector of any desired size would be constructed to any desired shape without any seams. Currently, large thin film reflectors must be constructed from flat stock material off rolls up to a maximum width of 96". Any double curving of the film must be achieved by processing, such as creep-forming. Gores, flat or doubly curved, must then be assembled to form a large area reflector. Assembly control of all the stresses at the seam is difficult. Even if a completely stress free, wrinkle free seam is achieved, the reflector is no longer homogeneous across the surface. When a stabilizing force is applied to hold or further shape the reflector, this non-homogeneity tends to result in flats or scallops across the reflector, a major source of figure error.

SRS investigated materials recently developed at the Langley Research Center for application as spray molded reflector film of any

shape and size. One type material was developed for use as a binder for paint pigments used to coat space radiator surfaces. It is used with a solvent thinner and sprayed on, dried, and removed as a film from the mold surface. No curing at elevated temperatures is required. Characteristics of this and others in this family of materials are described in NASA Technical Memorandum 87650, Optically Transparent/Colorless Polyimides. The one currently under evaluation as a film is Polymer 6F - BDAF. These films were formed with the material and successfully removed from water and glass molds. Presently, samples were aluminized to evaluate the optical surface qualities.

A small 6 inch parabolic glass cast polyimide model was constructed. The material used was an insoluble heat cured (at 450°F) polyimide material with similar properties of Kapton. A sodium silicate release agent was used on the glass mandrel to permit the film to be removed from the mandrel following curing. Residual stresses in the material caused the outside edges of the cast material to "curl up". Further heat curing was found to relieve the residual stresses induced during the casting process. Further refinements to the processing parameters were subsequently investigated.

A considerable amount of interest and effort has been applied to the spray-casting, spin-casting, and doctor blading methods of forming a film on a mandrel. It is a very appealing concept, as to formation of seamless films of arbitrary shapes and arbitrary thicknesses, in polyimide of properties resembling Kapton.

Previous mandrel casting work had largely involved chemically imidized solvent soluble 6FDA+4BDAF polyimide. The same film-forming techniques were applied to heat-imidized insoluble BTDA+4,4ODA polyimide. Processing techniques were similar except that the chemically-imidized material was heated only to about 200°F during film hardening (by

solvent evaporation) whereas the thermally imidized material was heated to 600°F during cure. The chemically imidized film acquired strong residual stresses during the mandrel constrained one dimensional shrinkage during drying, contributed to by the fact that it began to acquire considerable strength before its solvent-evaporation shrinkage was completed. By contrast, the thermally imidized material did not acquire high strength until after drying-shrinkage was complete, i.e., during subsequent high temperature imidization. However, even if fully annealed by prolonged exposure to the 600°F curing temperature, upon subsequent cool down of film (yet bonded to the mandrel) it must closely track the mandrel in thermal expansion coefficient, (especially in the 400°F to 600°F range, where the film is able to creep rather rapidly) or else it will "freeze in" substantial residual stresses. Films of heat cured polyimide typically have shown evidence of high tensile stresses upon removal from glass or silicate coated aluminum mandrels, and also have displayed high stresses with respect to fibers of graphite, Kevlar, and fiberglass imbedded in them prior to heat curing. Polyimide thermal expansion coefficient nominally ranges from  $2 \times 10^{-5}/^{\circ}\text{C}$  at ambient temperature to  $4 \times 10^{-5}/^{\circ}\text{C}$  at 300°C, perhaps favoring use of vespel bulk polyimide, silicate coated for film part off, as mandrel material.

Soluble polyimide (of interest to drying-rigidized film supporting structures) was found not to adhere well to heat cured polyimide film. Mixtures of TPI with soluble polyimide, heat cured, were found to make a seemingly satisfactory adhesion promoting primer coat when applied to heat cured films. Under some conditions, adhesion of a second layer of heat cured polyimide applied to a previously heat cured polyimide film appeared marginal, perhaps also requiring a TPI primer coat. TPI is an excellent adhesive and has been used to form films

by itself, but it is not desirable for that purpose because it is very difficult to part off the mandrel, it is considerably more brittle than the other polyimides, and it is strongly inclined to form bubbles during heat up.

It was found convenient to color the resin with Shachihata blue stamp pad ink before applying it to the mandrel, to facilitate visual detection of thin spots in the film during application of the liquid. This ink did not appear to affect the process behavior or properties of the film after curing. The blue color of the film changes to green as imidization occurs, due to the heat-cured polyimide developing its characteristic amber color. Such pigmentation of the film may have useful applications for selection of film absorptivity/emissivity, for in-space thermal control purposes.

### **3.2.3 — Mandrel Film Curvature Forming Techniques**

Creep/relaxation forming inherently involves use of accurately configured mandrels. Spray in spin casting of polyimide precursor, on mandrel, followed by high temperature cure and active release from mandrel, eliminates seams. However this process has difficult mandrel part-off, requires very large vacuum metallization facility, and places much more stringent requirements on mandrel surface finish and adhesion properties, than CRF.

#### **3.2.3.1 — Fabrication of Reflector Models Using Creep and Relaxation Forming Techniques**

It was decided to study relaxation forming of film curvature by stretching a Kapton film over a polished glass mandrel and exposing it to 600°F, removing it, and monitoring film geometry after various intervals of temperature. This was expected to verify predictions of film relaxation behavior based on uniaxial data generated in Task 1.

An 18" diameter glass parabolic mirror with a 22" focal length was used as a mandrel to creep-form a flat sheet of Kapton into a parabolic shape. Three models were constructed using the creep and relaxation forming process with the glass mandrel. The models

were made with the different material configurations listed in *Table 6*.

Each Kapton sheet was attached to a circular aluminum hoop with TPI polyimide glue. The TPI was cured at 400°F. During the cure process the Kapton heat shrunk causing the material to "tighten up" on the hoop. The forming process is shown in *Figure 29*. Initially, the material was placed in the oven with the mandrel placed on top of the material. The oven was then heated to the 600°F creep-forming temperature. The material under the state of stress crept until the mandrel contacted and was supported by the aluminum hoop. The Kapton material then relaxed the induced stresses due to the creep-forming process. The material was then allowed to cool to room temperature following the relaxation process.

A method was developed to inflate the model reflectors with a slight pressure while still on the support hoops. The device constructed inflates the reflector with enough pressure needed to hold its shape for optical measurements. Each formed reflector was inflated and the focal points were measured. The focal points were measured to be 22". The seams did not effect the final geometry of the reflectors. The creep-forming time and stresses were large enough to enable the seams to take the shape of the mandrel. The appearance of the seams were good with few discontinuities across the seam. Model C was seamed with heat cured polyimide

**Table 6 Material Configurations**

Model	Film	Type of Seam
A	Aluminized Kapton	No Seam
B	Aluminized Kapton	TPI with 1 Seam
C	Un-Aluminized	Heat Cured Polyimide with 4 Seams

Figure 3.2-02-188

in four sections and then formed to the mandrel. The film was aluminized following the forming process. The seams for the model were extremely good and shaped to the mandrel quite well.

A parabolic plaster cast mandrel was used in the creep-forming process and results similar to the glass mandrel were achieved. Finally, a plaster cast off-axis mandrel was constructed using computer generated shaped data.

A computer program that was previously developed to analytically describe and plot an off-axis paraboloid was revised in order to obtain the x, y and z coordinates needed for the construction of an off-axis paraboloid frame structure. At various points along the minor axis (y axis) the values for x vs. z were determined. At points along the major axis (x axis) the y vs. z points were calculated. The x vs. z and y vs. z were plotted on graph paper and cut out. The sections were then used to trace the curve on aluminum strips. Again, using the program, the values for x versus y were calculated and plotted on graph paper. This outline for the paraboloid was an ellipse in the x, y plane.

A 12" x 18" x 0.5" pan was filled with plaster and used as the base surface (the x, y plane) for the structure. The outline of the ellipse was then traced on the surface. The various values of y where the x vs. z plots were taken were located. The same process was performed for the

x values where y vs. z was plotted. The aluminum pieces were placed in position forming a structural frame for the off-axis paraboloid model. Again, using plaster, the model was filled and shaped. The model was dried in the oven and shaped with a fine grade polishing agent.

Off-axis reflector models were creep-formed using the plaster cast and shaped mandrel described above. The reflector models were creep-

formed on the mandrel for three hours at 650°F. The dimensions of the mandrel surface were made to yield the following reflector shape geometry:

- Semi-Minor Axis - 5.5"
- Semi-Major Axis - 7.1"
- Focal Length of Parabola - 4.76"

The curvature of the reflector models was compared to the computer generated shape data by using a shaping tool. *Figure 30* depicts a

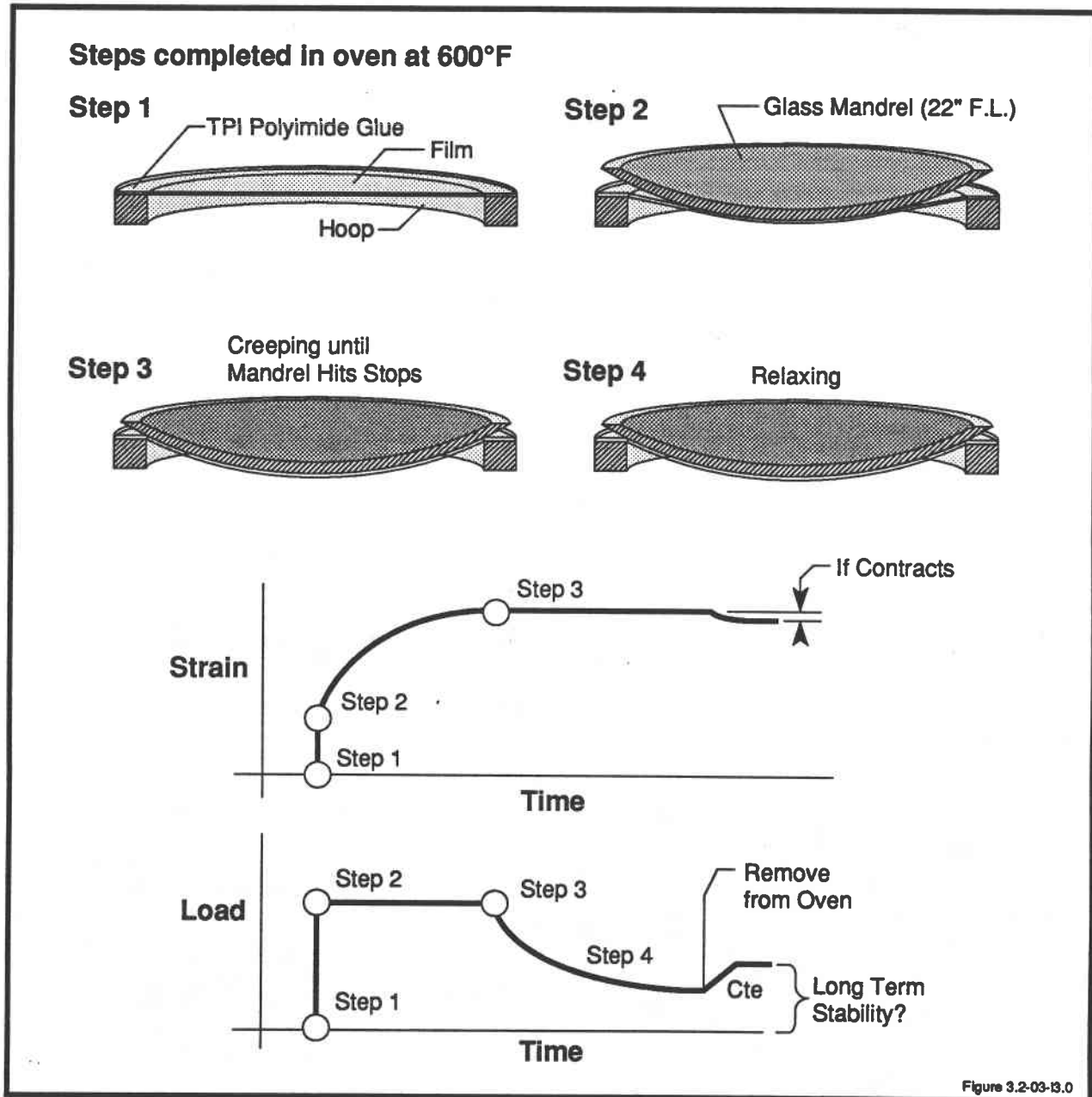


Figure 29 Creep-Forming Process to Mandrel

creep-formed model inflated and compared to shaping tools on both the major and minor axis. It is apparent from the figure that the reflector closely resembles the desired shape to produce the calculated reflector y. Optical methods were used to measure the focal point of the reflector shown in *Figure 31*. A laser ray tracing technique was used to visually indicate the focal point of the off-axis reflector model. The experimental focal point determination closely resembles the analytically calculated results of 4.76". The reflectance of the material was not adversely affected by the creep/relaxation forming process. The mandrel technologies developed for this relatively small model will be expanded to yield larger creep and relaxation formed reflector prototypes.

Large scale reflectors can be constructed using seamed sections of creep-formed Kapton film. The curvature of the film sections can be creep/relaxation formed to a mandrel with the desired curvature. The off-axis reflectors are sections of a larger paraboloid. Gore sections of the reflector can be taken that are identical in curvature but different in size. A single mandrel can be constructed to produce every gore geometrically correct. Slicing the large paraboloid into sections by radial planes, each containing the axis of revolution of the paraboloid, yields identical sections of the paraboloid shown in *Figure 32*. The top view of the paraboloid with the projected view of the reflector is shown in *Figure 33*. The intersection curves of the radial planes

with the paraboloid are identical for each plane. Therefore, using one section of the paraboloid as a mandrel for gore sections will make all sections necessary for the off-axis reflector. By using the mandrel geometry from Section A of *Figure 34*, all sections of the reflector can be formed and seamed together using polyimide seaming procedures developed under this task. Sections B and C in *Figure 34* could be cut to the correct shape and seamed together on the forming mandrel in order for the seams to comply to the correct curvature. For this particular design, creep-forming the gores in only one direction would be necessary.

### 3.2.3.2 — Liquid Mandrel Centrifugal Spin-Casting of Polyimide Film

The availability of the relatively large turntable used for spin casting of polyimide films, and concern about the substantial cost and weight of a precision machined off-axis creep/relaxation-forming mandrel of large size, led

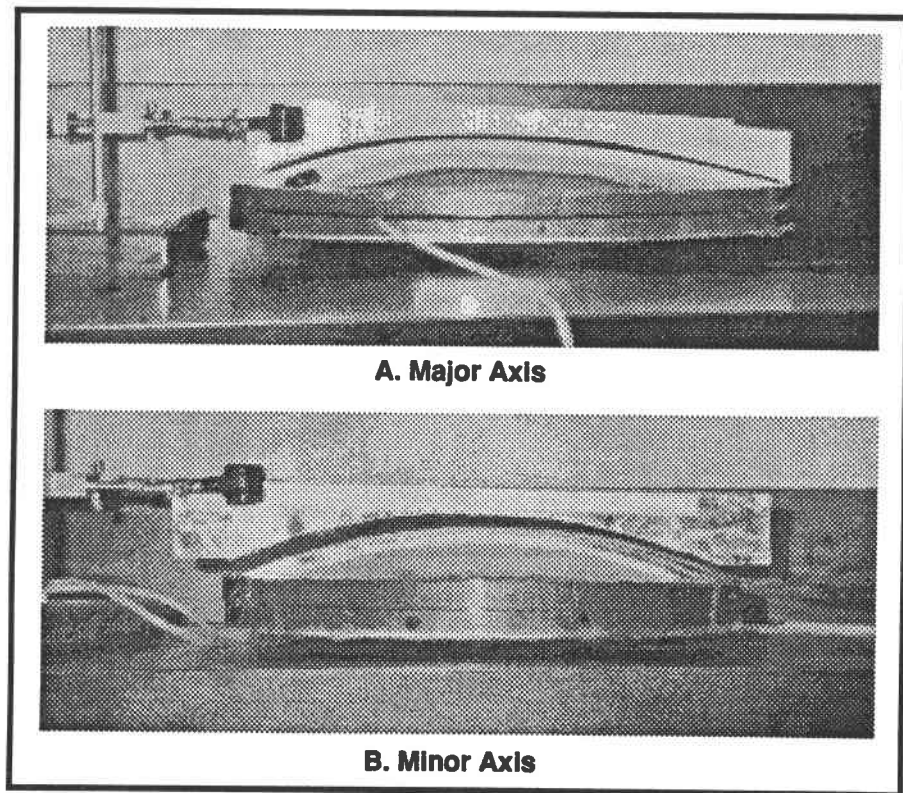
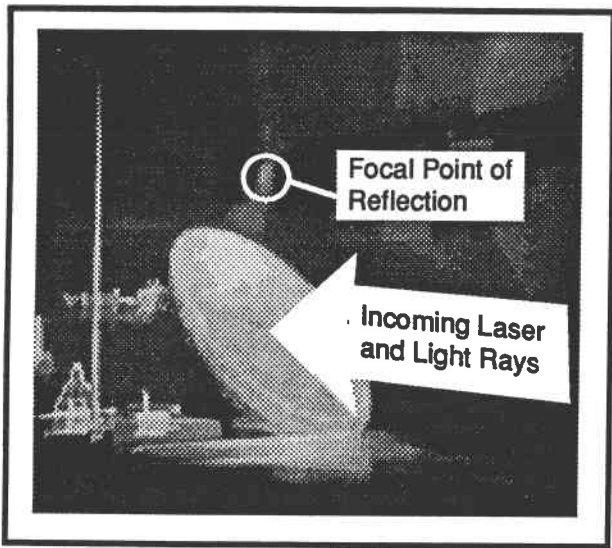


Figure 30 Reflector Compared to Mandrel Shaping Forms



**Figure 31 Optical Investigation of Focal Point for Off-Axis Reflector Model**

to renewed interest in the technique of polymer film casting on a liquid substrate. This technique was employed many years ago for making sub-mil thickness polymer film for the skin of indoor endurance contest rubber-motor

model airplanes to be flown inside such large enclosures as the dirigible hangar at Lakehurst, New Jersey. In that technique, a drop of special "microfilm dope" was dropped on the surface of stationary water in a bathtub. It rapidly spread over the entire surface of the water, then lost its solvent to the water and/or to the air. It then was carefully lifted off by use of a large submerged loop of wire, dried, and applied to the model airplane structure. It is reasoned that, in view of the historical evidence of the practicality of liquid-substrate film casting, if that technique could be combined with centrifugal formation of the liquid substrate surface into a perfect off-axis paraboloid on a suitably controlled turntable, and if the substrate liquid were heated to a temperature sufficient to cure insoluble polyimide, and if air introduction were then used to separate the resulting polymer film from the liquid substrate/mandrel before centrifuge coast-down, a cost-

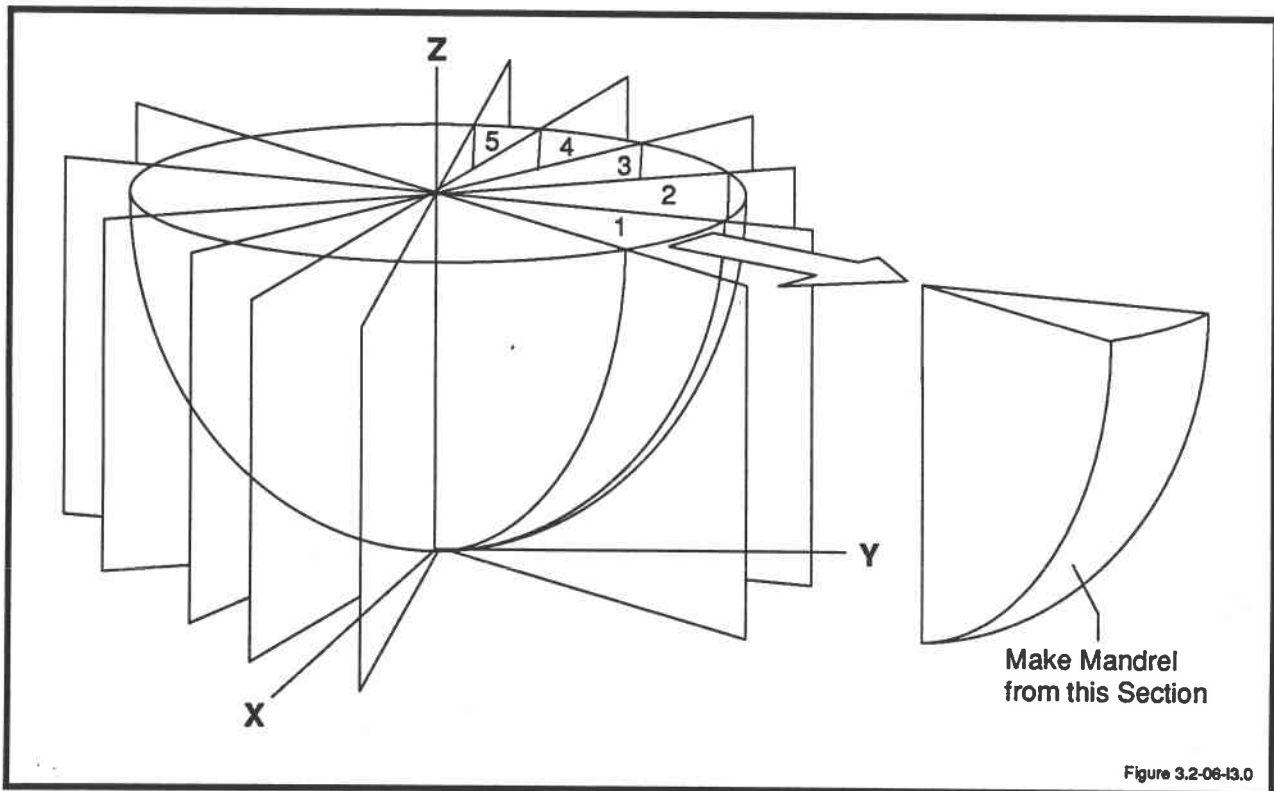


**Figure 32 Slicing Paraboloid by Radial Planes**

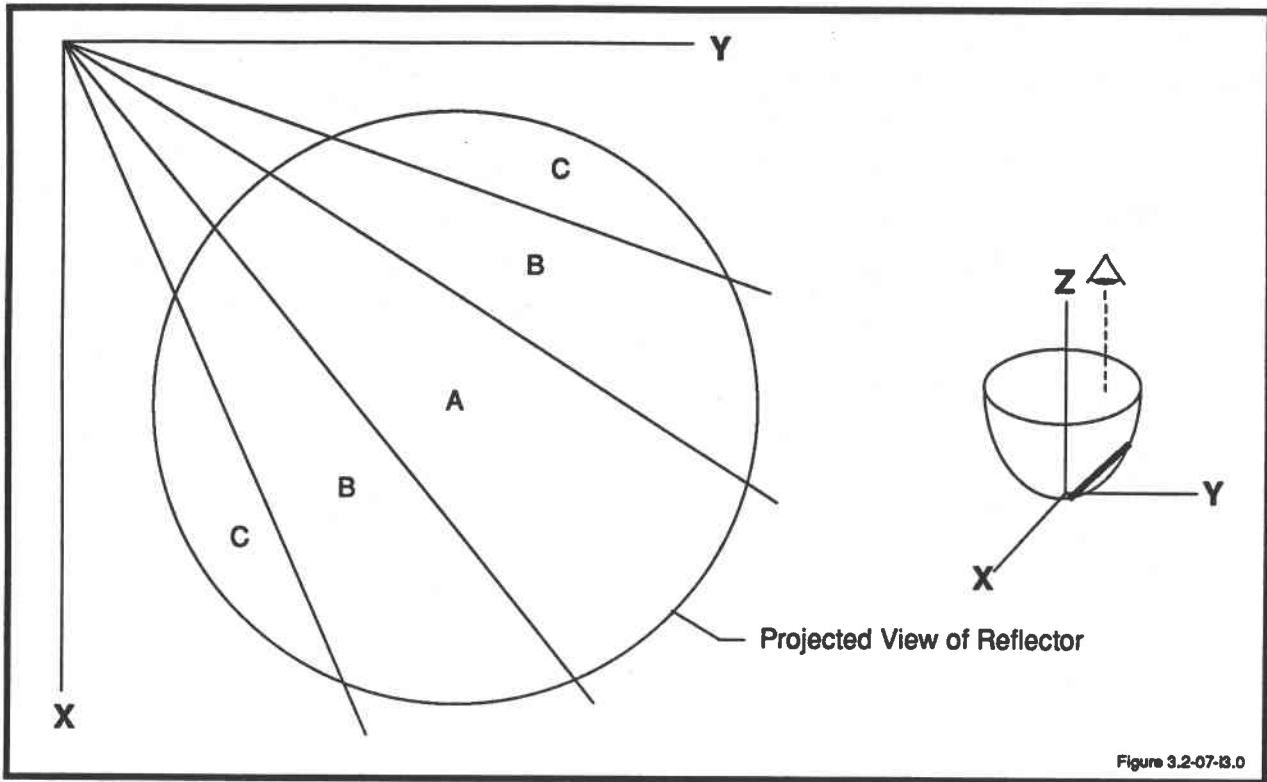


Figure 33 Projected View of Reflector

effective technique for producing geometrically precise paraboloidal seamless polyimide films would result. The substrate liquid would need to be matched to the polymer film precursor liquid (soluble polyimide in diglyme, or heat curable polyimide in DMAC, or epoxy in

MIBK) in the following ways:

- Film precursor liquid must not be significantly/rapidly miscible in substrate liquid.
- Film precursor liquid must wet the surface of substrate liquid.
- Film precursor liquid must be less dense

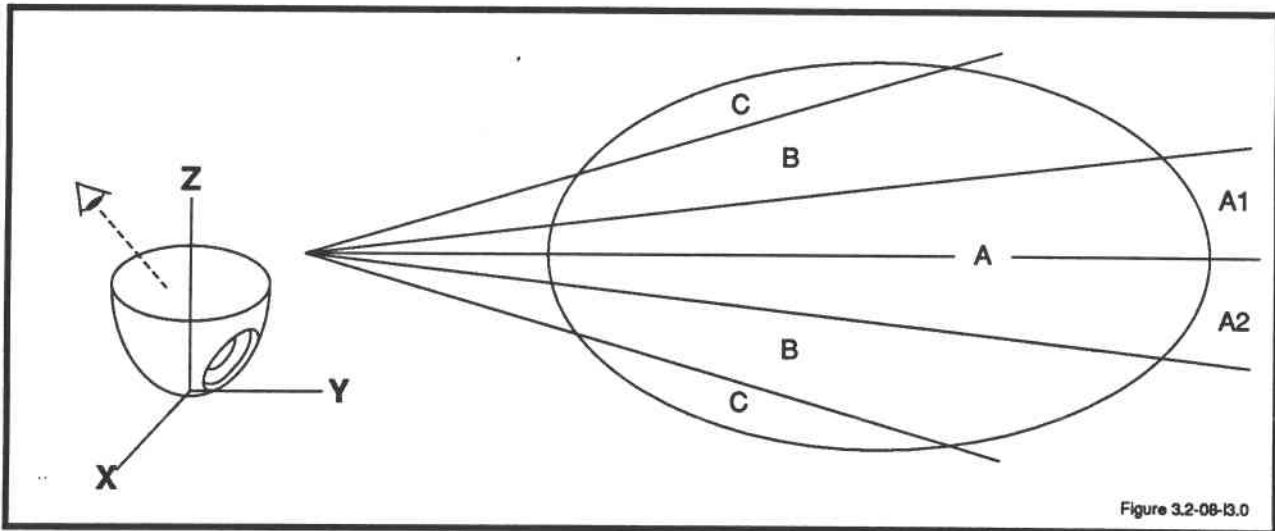


Figure 34 Gore Sections of Off-Axis Reflector

than substrate liquid.

- Solvent phase of film precursor liquid must be higher in vapor pressure than substrate liquid (at the same temperature); substrate liquid boiling point must be higher than curing temperature of film polymer.

The candidate film precursor liquids mentioned above all are based on powerful solvents which are rapidly miscible with water and most other organic liquids. Diglyme mixes rapidly with water, glycerine, petroleum oil, castor oil, and perchloroethylene. It mixes rather slowly with DC 704 silicone oil, and diglyme/polyimide solution dropped on the surface of DC 704 spreads rapidly to form a thin surface film which can subsequently be removed intact. However, miscibility is great enough that the film forming solution loses its solvent to the DC 704 within a minute, too rapidly for well-controlled film formation, and the resulting film looks rather cloudy. Diglyme/polyimide solution dropped on the surface of concentrated sulfuric acid floats on the surface without apparent mixing nor interaction, but it does not wet nor spread across the surface of the acid. In spite of high miscibility of diglyme with water, diglyme/polyimide dropped on the surface of water does not wet the surface sufficiently to spread out into a film. Exactly the same is true of a polyamine liquid (epoxy catalyst). Diglyme does not appear miscible with R6104 silicone liquid, but diglyme/polyimide liquid dropped on the surface of R6104 does not wet it sufficiently to spread out to form a film. However, diglyme/polyimide liquid dropped on the surface of mercury wets the surface of the mercury, spreading out rather rapidly to form a thin film. This film appears to reduce the surface tension of the mercury, but no other interaction between the two liquids is apparent. Mercury is a dangerous material health-wise, especially if heated, but if mercury were used as liquid substrate for film cast-

ing, during most of its time in service its entire surface would be covered with a layer of immiscible polyimide/diglyme liquid, which should serve as an effective vapor barrier to prevent emission of hazardous vapor. As the boiling temperature of mercury is in excess of 600°F, it should be possible to heat it sufficiently to cure films of heat-curable polyimide cast on the surface of the mercury. Low melting point metals such as gallium and Cerrobend might be candidates for spin-casting liquid mandrels, but gallium is too expensive and Cerrobend oxidizes rapidly.

Development of a practical liquid mandrel spin-casting facility for off-axis paraboloidal films would require attention to at least the following points:

- Precise speed control of turntable; preferably by positive selectable gearbox and synchronous motor.
- Liquid mandrel container vessel shaped very nearly to match desired film shape, to allow minimum depth of mercury in vessel.
- Trunnion mount (with viscous damping) to allow vessel to swing upward and downward freely during slip-clutch spin-up and coast down to prevent liquid spillage.
- Mercury circulation/heater/level control system, to heat and cool the mercury and maintain uniform temperature during film curing, and to compensate for thermal expansion of mercury.
- Spray nozzles to distribute the film precursor liquid reasonably uniformly over the liquid mandrel surface while the turntable is in motion.
- Air injection system to separate film from mercury before coast down of centrifuge.

A small film of soluble polyimide was cast on the surface of a pool of mercury, and dried at elevated temperature. The resulting film quality appeared good, as to strength, smoothness, and transparency. Some of the mercury clung rather tenaciously to the film and was difficult to rub off, which was unexpected. It appears

likely that the most serious obstacle to use of this technique for forming doubly-curved surfaces may be the large and powerful in-plane shrinkage of the film as the solvent evaporates. Bonding of the film to container vessel peripheral walls, by local pre-drying, might partially solve the problem, but some distortion of film shape might yet occur. One solution would be to use a Cerrobend (or a similar eutectic alloy) as the liquid mandrel, then allow it to solidify before and during evaporation of the solvent from the film. After film drying, the Cerrobend would then be re-melted to effect heat-curing of the film (in the case of heat-cured polyimide). Another option may be use of a low viscosity slow-curing solvent-free epoxy as film-forming liquid, which should display negligible volume change and consequently negligible in-plane shrinkage during curing. Also, for some epoxies, acetone can serve simultaneously as a thinner and as cure-initiation inhibitor; in such case, the acetone could facilitate wetting and spreading of the epoxy, but the epoxy would not acquire sufficient rigidity to generate shrinkage stresses until the acetone had largely evaporated. Devcon 5 minute epoxy, both with and without acetone thinner, appears to wet the surface of mercury reasonably well. A small very thin film of acetone-thinned Devcon epoxy, displaying somewhat promising properties, was cast and cured on the surface of (stationary) mercury.

A three inch diameter dish of mercury was spun on a turntable to produce a concave paraboloidal surface, and acetone-thinned/inhibited pre-catalyzed epoxy was placed on that surface. The solution failed to wet the mercury sufficiently to form a stable film over the entire surface, although in a similar test using a smaller pool of mercury it had appeared to do so. The large and powerful drying shrinkage of the polyimide solutions of interest seemed to make them unpromising for casting on a

liquid mandrel, even though they wet the mercury very satisfactorily. Attention has shifted to centrifugally cast solid mandrels. Investment-casting wax was centrifugally cast and films of soluble polyimide were cast on its surface. For thin films with short drying times this appeared promising, but with thick films involving long drying times, it became evident that the diglyme solvent of the polyimide was attacking the wax and incorporating significant amounts of it into the film. Also, the wax had unacceptable (about 5%) volume contraction upon freezing, and its free surface developed a matte finish upon solidification (because of its having a crystalline structure).

Cerrobend metal, covered with high-boiling liquid to prevent oxidation, was tried. It displayed very little freeze-shrinkage and produced a macroscopically good paraboloidal shape, but its surface, mirror-smooth while melted, developed a very rough surface from growth of large crystallites/dendrites, upon freezing. It was obvious that the cerrobend possessed a complex phase diagram, and that such materials are less promising than those having a simple phase diagram, for free-surface-critical casting. Sulfur was tried, but it also froze to a matte surface and displayed unacceptable freeze-shrinkage. It was concluded that only materials of amorphous or quasi-amorphous (polymeric) structure could produce the required specular free surface and lack of a "step change" in volume at solidification. Heat-cured two component silicone resin was centrifugally cast, but concentric ridges appeared in the free surface, presumably resulting from the uneven (torch) heating utilized. RTV 60 silicon was cast, in two-inch and eight-inch diameter sizes. The smaller size displayed a specular well-shaped surface, and allowed good films of soluble and heat-cured polyimide to be cast on its surface. The films did not separate during drying nor heat-curing, yet could be easily

peeled off without damage, subsequently. The eight inch diameter mandrel also possessed a specular surface, but displayed concentric ridges suggesting standing waves, excessive effects, or bleed-through of ridge geometry from the underlying pan. Soluble and heat-cured polyimide films were spin-cast on this eight-inch mandrel. Initial film formation was difficult due to poor wetting, but once formed, the liquid films were stable on the RTV60 surface, and dried to form continuous uniform-looking films. They remained in contact with the concave mandrel surface until dry to the touch, but then subsequently as the last fraction of solvent departed, the film stiffness increased sufficiently that the drying shrinkage pulled the films completely free from the concave surface of the silicone mandrel.

A three inch crucible and cover was carved from a magnesite firebrick, and filled with broken soda-lime glass, which was subsequently "melted" with a propane torch, and spun on the turntable. A paraboloidal glass mandrel of promising characteristics was obtained. The rationale for interest in a centrifugally cast glass mandrel is as follows:

- Satisfactory spin-casting and subsequent active (water) mold-release experience obtained with polyimides on glass substrates/mandrels.

- Centrifugal casting of glass has recently been applied successfully to fabrication of large precise astronomical telescope reflectors, reportedly showing a substantial cost and fabrication-time advantage over the traditional cost-and-grind techniques for making large telescope optics.

- Glass is low in cost and has well-known characteristics that can be tailored to cover a wide range of viscosity/temperature curves and thermal expansion coefficients. It produces a specular free surface upon solidification, and by virtue of its high but Newtonian viscosity when soft, it tends to dampen vibrations/harmonics of the turntable mechanical system.

### 3.2.3.3 — Geodesic Network Mandrel Creep/Relaxation-Forming Study

A geodesic network mandrel resembling a dress form or wire basket was made by cutting a 10.5 x 13.5 inch elliptical opening in a 1/16 inch steel plate, placing this plate around an existing plaster off-axis mandrel, and stretching and spot welding .01 inch nichrome wires in a triple lay (equilateral-triangles) pattern over/against the surface of the plaster mandrel and attaching them to the periphery of the elliptical cut-out in the steel plate. A 0.5 mil sheet of Kapton was then bonded to one side of a 10.5 x 13.5 inch aluminum hoop, and a similar sheet was bonded to the other side of the hoop, to form a closed vessel, and a pressurizing tube was attached. This latter assembly was placed flat on the floor of the test oven, with the pressurizing tube extending out through a port in the oven wall, and the geodesic network mandrel was placed down over the hoop-mounted Kapton film assembly. Air pressure was applied and the oven temperature was raised to 660°F. Creep was continued until the film filled or contacted the entire mandrel. Then the film assembly was removed, cooled, and inspected. Line imprints of the mandrel wires were visible at the low-curvature end of the film, in the limp condition, but these completely disappeared under very slight pressurization.

The model looked promising, and appeared to support the concept and did not indicate any basic problems, though it was apparent that the creep process should have been continued longer. A basic premise of this technique is that the stress in a circular edge-supported membrane of constant thickness, subjected to constant pressure, is a linear function of diameter of the membrane (or diameter of any cell of a membrane supported by pressing against a network frame), whereas center-point deformation of such a membrane varies roughly as the square of the diameter of the membrane (or

cell of a network-supported membrane).

#### **3.2.3.4 — Graduated Thickness**

It was conjectured that one practical means for achieving pressure shaped concentrator aberration correction was to seam together suitably-configured gores of differing thicknesses and therefore produce differing deflections under uniform pressure load. Obvious objections to this technique were the step discontinuities in thickness involved and the probable difficulty/expense in procuring film stock manufactured in a wide range of slightly-differing thicknesses. The experience recently gained in spin-casting relatively large seamless sheets of polyimide film of highly-uniform thickness suggests that modest process changes should allow fabrication of large seamless sheets of polyimide film incorporating smooth gradual variations in thickness of arbitrary magnitude and distribution. The analytical model developed in Task 3 could be exercised, given sufficient resources, to specify, either for the fully-elastic case or for the viscoelastic case or for the combined case of elastic configuring followed by heat cure in the pressurized condition, the precise distribution of film thicknesses required to produce the desired concentrator geometry. The case of elastically configuring a dried but un-cured film of heat-curable polyimide, under uniform pressure, then heat-curing it while thus distended, which is the most interesting case, is based on the assumption that all relevant properties of the polyimide, in the dried un-cured state and in the cured state, are reasonably linear or at least very accurately known and repeatable. This process could be applied equally well to symmetrical or off-axis paraboloids. By use of ultrasound or other thickness gauging, coupled with local spray-on adjustment of film thickness, an arbitrarily-precise tailored pattern of thickness variation over the film surface should be ob-

tainable, for a sheet of film of arbitrary size (assuming a flat glass substrate built up of many smoothly resin jointed flat plates of glass).

A small (8 x 8 inch) film of linearly-tapered thickness was fabricated by doctor-blading soluble polyimide resin using tapered blade-guides. This film was subsequently mounted in a 7.5 x 6 inch elliptical frame and pressurized. It qualitatively appeared to support the concept. However, doctor-blading, either linear or rotary as has been employed in our previous spin-casting work, seems much less adaptable to precise and arbitrary thickness tailoring than spray-casting. Furthermore, some temperature elevation for drying acceleration is required. Where film thickness uniformity is desired, slow drying and strong surface tension effects are desirable aids to the long-range leveling of the resin, but these effects make it difficult to maintain a non-uniform thickness distribution of polyimide resin on glass substrate when room temperature drying is utilized. Drying rate and resin viscosity must be adjusted such that short-range leveling occurs, for surface specularity, but long-range leveling is inhibited.

By contrast with other techniques addressed under this contract, this method of film configuring could possibly require no controlled temperature distribution in the processing oven, no previously-configured smooth surface mandrel other than a flat glass plate, and no precision turntable nor rotary high temperature casting furnace. It is anticipated that this concept will be further evaluated as follows:

- Spin-cast, dry and cure a uniform 18" diameter circular film of heat curable polyimide, on a glass substrate. Aluminize it, bond a 16" metal ring to it, remove it from the glass substrate.
- Pressurize this film to f2 configuration, and perform a single-diameter laser ray trace figure configuration.
- Calculate a pattern of thickness adjustment that

should correct the observed figure aberrations.

- Mount film on turntable, and spray on concentric adjustments to thickness (dry and dial indicator measure thickness, iteratively with spraying) until the calculated thickness distribution is obtained. Heat-cure and stress-relieve.

- Pressurize to  $f2$  configuration, and repeat laser ray trace.

- Repeat these steps until a good (10,000:1 CR) figure is obtained. Then measure and map as precisely as possible the actual thickness distribution of the film.

### **Symmetrical Paraboloid, Fully Elastic Case**

A sheet of  $\frac{1}{2}$  mil aluminized Kapton was bonded with TPI adhesive to a 12" I.D. aluminum hoop, and backed with Plexiglass to form a pressure vessel. A pressurizing nozzle and flexible tubing were attached. Templates were laid out on and cut from poster-board, one configured as an  $f1$  parabola (12" diameter, 0.75" center-point depth) and one configured as an  $f0.75$  parabola (12" diameter, 1.0" center-point depth). The vessel was pressurized with air until the Kapton sheet approximated the shape of the  $f1$  template, which was placed diametrically across it.

The  $f1$  template was then replaced with the  $f0.75$  template, and the vessel was pressurized until the Kapton sheet achieved its best fit to the template. Upon release of pressure, the Kapton sheet was seen to have yielded slightly and become slightly loose/baggy in its central region. Warming it with a heat gun caused it to recover its flatness.

Then an annular sheet of  $\frac{1}{2}$  mil Kapton was laid out and cut, of 13" O.D. and 6" I.D. The outer periphery and inner border of this sheet were coated with TPI adhesive, then superimposed (aluminized side outward) on the 12" diameter hoop-mounted Kapton film described above, and heat cured. Then the pressure ves-

sel was reassembled, pressurized, and tested as described above.

The  $f1$  template was then replaced with the  $f0.75$  template, and the vessel was pressurized until the Kapton sheet achieved its best fit to the template. The resulting geometry demonstrated no deviation between the template and the film profile could be clearly discerned within the limits of accuracy of the test (probably about  $\pm 0.01$ "). The cusp-like discontinuity in profile at the step-point in film thickness, clearly apparent in the previous test, was barely visible in this test. Probably the nonlinearity in Kapton properties near the yield point, which the  $f0.75$  test slightly exceeded, accounted largely for this observation. It probably also was a significant factor that a given ratio of peripheral thickness to central thickness of a circular film gives optimum aberration correction only for one value of  $f$  number.

### **Symmetrical Paraboloid, Creep Formed Case**

The plexiglass backplate was removed from the 13" O.D. and 6" I.D. model described above and was replaced with a sheet of  $\frac{1}{2}$  mil Kapton, TPI-bonded to the rear side of the 12" I.D. aluminum hoop. A stainless steel pressurizing tube was attached, and the assembly was placed in an oven. Pressure was applied, and the oven temperature rose steadily to 640°F, at which time the model was removed. Pressure was then released. Under minimal inflation pressure, the single-layer side appeared to have crept to a configuration of approximately  $f0.9$ , and the double-layer side appeared to have crept to approximately  $f1.1$ .

Under pressurizing until the single-layer side achieved its best fit to the  $f0.75$  template. Thus, the deviation from parabolic, at  $f0.75$ , with single-layer film, for the creep-formed case, was significantly less than that for the nominal fully-elastic case probably because of

greater creep in the highly-stressed central region. Because of geometrical factors, points of greatest deviation of pressurized film from paraboloidal shape do not correspond directly to points of greatest stress, and therefore, it is not to be expected that a film which has crept under uniform pressure would have the same geometry as a film which has been elastically deformed under uniform pressure to the same center-point deflection.

During pressurization of the above described creep-formed film, the film was observed to go through a stage of displaying strong parallel ridges, .04" deep, 0.5" peak-to-peak spacing, such as are often seen in creep-formed films. These ridges were completely absent from the limp film before pressurization, and from the fully-pressurized film. They indicate anisotropic recovery of the creep, presumably arising from anisotropies introduced by roll stretching and/or by processing steps done under uniaxial tension, during manufacture of the film. These anisotropies are in themselves a strong argument against using roll-processed film for precise concentrator applications, especially where creep-forming is to be used, but even for fully-elastic deformation applications.

The model was inverted, and pressurized until the double-layer/dual-thickness film achieved best fit to the f1 template. The cusp-like discontinuity was much less evident. Maximum deviation from parabolic was about .04", but part of the deviation appeared due to some film separation from the support hoop.

The f1 template was then replaced with the f0.75 template and the vessel was pressurized until best fit was achieved. The film profile appeared to be very close to the template in shape, but maximum deviation between film and template was about .02".

Qualitatively, looking sideways at the model during full inflation, the profile of the single-layer side looked very much like the arc of a

circle, while the profile of the double-layer side looked very much like a parabola.

#### **Off-Axis Parabola, Elastic Case**

A sheet of 0.3 mil Kapton was bonded with TPI adhesive to a 10.5 x 13.5 inch aluminum hoop. A second sheet of 0.3 mil Kapton extending  $\frac{2}{3}$  the length of the major axis was bonded on top of the first sheet. Then a third sheet of 0.3 mil Kapton extending  $\frac{1}{3}$  the length of the major axis, was bonded on top of the second sheet. Then a sheet of Kapton was bonded to the rear of the aluminum hoop, to form a closed vessel, and a pressurizing nozzle and flexible tubing were attached. Upon pressurizing, an approximate off-axis paraboloidal shape was obtained, but due to many leaks, rips, and repairs, insufficient pressure was applied to allow quantitative measurements.

#### **Off-Axis Parabola, Creep Formed Case**

A film model was placed in an oven, heated to 640°F, and pressurized, until significant creep occurred. Then it was removed, cooled, inflated, and its major axis profile compared to a cardboard template laid out and cut in the theoretically correct shape. Qualitatively, the model profile looked good, suggesting that the 3:1 variation in film thickness from one end to the other end of the major axis is about optimum. A layer geometry is probably appropriate, to give optimum shaping in both major axis and minor axis deviations. However, the amount of creep obtained was only about half that required to match the template shape, and many local deviations were caused by excessive adhesive and rip repairs, so a quantitative measurement was not feasible.

### **3.2.4 — Reflective Coating of Polyimides**

Methods to reflective coat polyimide were investigated. Vapor deposition of aluminum in

a vacuum chamber and electroless silvering were done to develop techniques for coating the reflector models constructed.

### 3.2.4.1 — Aluminum Vapor Deposition

Experiments aimed at aluminizing thin (.2 mil) spray cast polyimide film were done. The film samples (up to 18" diameter) were installed in the vacuum chamber at a distance of 18 inches from the single tungsten filament. The filament was loaded with small pieces of high purity aluminum wire. The chamber was evacuated to about  $5 \times 10^{-4}$  torr, and the filament heated with a high current transformer. A uniform aluminum coat was rapidly deposited. The spray cast film had a smooth, matte surface as a result of the spray process; the aluminum film followed this completely, precluding specular reflection measurements. It appears that when the spray casting process is improved (with better mold surface, solvent concentration, and spray technique) a film quality comparable to that of roll coated Kapton can be achieved. One problem encountered with the spray-cast film was handling, due to its extreme thinness. The .2 mil (.0002") film is probably near the lower limit for safe handling.

Further experimental work is in progress, aimed at depositing both silver and nickel coatings, chemically. This will avoid the need for a very large vacuum chamber, and provide a base metal suitable for applications needing a high conductivity surface. The nickel coating is expected to be easily applied and suitable for plating other metals onto it, while the silver provides a highly ductile, very reflective coating. A thin, transparent over coat can be applied to both protect the silver from tarnish, and somewhat enhance its reflectivity for solar power applications.

Techniques for aluminization (vacuum-evaporation of aluminum) of folded film samples were evaluated. The restrictive sizes (24 inch diameter) of the available coating

chamber required that the film be folded in squares of about 14-15 inches, aluminized, extracted and refolded, then coated in another area. The sample used was about six feet in diameter, and 15 runs were made to aluminize the central portions.

The results indicate that it is acceptable to fold and aluminize large pieces of film. The problems encountered were:

- a. Smoothly folding and supporting the film without wrinkles (which would mask off the aluminum).
- b. Non-uniform deposition due to varying source-film distance.
- c. Non-uniform or discolored film due to differing vacuum pressure at the time of deposition.
- d. Multiple handling of film, because of the many refold cycles.

All of these problems are easily solved, although the handling and folding will always require great care. The film, while less than .001 inch (1 mil) thick, proved very durable and showed no permanent damage due to folding. It was even found possible to use tape to hold the film; the aluminum adherence withstood the tape removal.

It appears that it will be feasible to aluminize large, one piece films using the fold technique. The outstanding facility requirements are:

- The largest practical chamber
- Multiple aluminum sources for uniform film
- Fast recycle time (refold and reload)
- Pressure (vacuum) of  $10^{-5}$  torr or better ( $10^{-6}$  torr preferred)
- Tables, and other large, flat, clean areas to perform folding.

### 3.2.4.2 — Electroless Deposition of Silver

The need for an economical method of applying reflective coatings to the large pieces of

film being produced lead to the selection of chemical silvering. While chemical silvering is a common method of producing second-surface glass mirrors, it is rarely practiced with thin, plastic substrates. Silver is a very good reflector but it suffers rapid degradation when exposed to sulfur-polluted atmosphere. Silvering was selected for evaluation because:

- It does not require large (> 8 foot diameter) vacuum chambers, as aluminizing would
- It can be deposited while the plastic film is still on the substrate
- It could be used as a second-surface mirror, allowing the plastic film to protect the silver
- Experience with and data collected from the silvered film would be valuable, since silver is typically a better reflector than aluminum, it can be protected (with an extra coating step), and would be durable in space with the proper AO coatings.
- Silver coatings can be rapidly stripped and replaced as needed during laboratory testing of films, while aluminizing in a large chamber would be slow and expensive.

The first attempts at silvering polyimide film used the well-known Brashear process, and also the Martin process (see references), which reduce metallic silver from a silver nitrate solution. First attempts gave brilliant, durable films, which indicated the applicability of commercial silvering operations for mirror production. These methods, suitable for large area mirror production, use similar chemical techniques, but are applied with an external mix spray gun. We felt this would give rapid, uniform coverage of large film areas.

The initial trials with spray equipment and a six foot film were relatively unsatisfactory. The film was dull, tarnished rapidly, and was very uneven. After several attempts at spray silvering, the following observations were made:

- Spray silvering appears to work best at relatively high temperatures, 80°F or more

- The spray mixture (silver/reducer ratio) is critical

- Surface cleanliness is very critical,
- Surface preparation, that is "tinning", is necessary
- Handling and cleaning up of waste solutions were quite messy
- Dwell time of the silver/reducer mixture was not adequate to fully deposit the silver on the film; much silver was wasted.

A method of bath silvering of film while supported on the glass deposition substrate was used. Fair reflectance was obtained by forming a retaining wall around the leveled film and mixing the silver/reducer directly on the film. After several trials and refining certain procedures, an effective process was developed.

Peacock Laboratories (see references) was the source of the silvering chemicals. Their silver solutions are more economical than buying the chemicals from a chemical supply company, while assuring adequate purity. The solutions needed are:

- Solution A - Concentrated Silver Solution
- Solution B - Concentrated Activator Solution
- Solution C - Concentrated Reducer Solution
- No. 77 Cleaning Agent
- No. 93 Sensitizing Solution.

In addition, an adequate supply of distilled water is required for diluting the solutions, washing film, and cleaning glassware and bottles.

Following Peacock Laboratories' recommendations, the following procedure were used:

1. Mix one part of solution "A" with 16 parts of water. Add one part of solution "B" and mix thoroughly. Then, dilute to make 32 parts of activated silver solution.

2. Mix solution "C" - one part diluted to make 32 parts of reducer solution.

3. The surface to be silvered is cleaned with distilled water and then washed with a dilute (1-to-5 or -10) solution of #77 cleaner, and rinsed several times with water. Care must be

taken to avoid scratches in the film.

4. Use a 1-to-64 dilution of #93 sensitizer to wet and coat the surface. Do not allow the surface to dry after this step. Rinse off the sensitizer, and keep the surface wet with water.

5. Pour the required amount of activated silver solution (step 1) onto the surface. Eliminate any trapped air bubbles, and use the pouring process to make sure that all remaining water droplets (or sensitizer) are replaced by silver solution. At this point, it seems beneficial to wait a short time (1 to 5 minutes), allowing the silver solution to become uniform and evenly distributed. The activated silver solution should be at least ½ inch deep; 1 inch will give a better thickness.

6. Reduce the silver by applying the reducer (step 2). Starting at the edge, pour a very small amount into the silver, distributing evenly. The objective is to have a 1:1 ratio of silver: reducer evenly mixed and distributed. When the mix is achieved, there is a short, temperature-dependent delay of several seconds to perhaps two minutes before any visible activity occurs. The mixture may be agitated during this time to ensure uniform mixing. When the deposition starts, the solution will rapidly darken with metallic silver, while the surface will become plated with silver. The solutions may be agitated during this time, but avoid any contact or disturbance of the silver film - this will result in a dull, scratched, thin film of silver. The solution will display further changes in color and appearance. It is recommended to leave the solutions in place for at least two minutes after the last color change (to a cloudy, brown appearance).

7. Pour off (or otherwise remove) the silvering solution and wash thoroughly with distilled water, preferably in a spray, to remove all traces of the unused silver compounds. The silver should then be dried with warm air. Avoid touching or scratching.

8. Further protective coatings may be fol-

lowed, for example paint, thin plastic, or copper plating. Take care to avoid dissolving the polyimide film by improper use of solvents.

It was felt that the techniques for electroless silvering of films (Brashear chemical reduction deposition process) left room for improvement in the following areas: (1) ease or convenience of application of uniform high reflectivity film over a large geometry doubly-curved film, either mounted on a forming mandrel or inflated after removal from such a mandrel; (2) reflective film adhesion to the polyimide; and (3) silver film tarnish protection, preferably of such nature as to allow first surface mirror usage.

Both silver and polyimide have a rather low degree of chemical reactivity, so, little opportunity for chemical bond contribution to adhesion exists, and silver film adhesion must depend largely on van der Waals type forces. Therefore, it was felt that every effort should be made to optimize the film deposition process from the standpoint of adhesion. This concern was discussed with Mr. Bob Davey of Peacock Laboratories, supplier of the silvering chemicals used. He expressed the following opinions:

- Silver adhesion to the polyimide should be adequate, though not great.

- Use nonabrasive cleaner and rub with a soft cloth; cleanliness is essential, but it is very easy to scratch the polyimide surface so as to reduce its reflective specularly.

- Double the recommended concentration of sensitizer solution. Its wetting agent will assist in wetting the hard to wet polyimide. Don't add detergents or additional wetting agents to any of the process solutions.

- Warm the silvering solutions moderately, and/or use a warm spray-booth for spray silvering; try to accomplish the entire process, from cleaning to completion of film deposition, in as little time as possible.

• Some people etch (to roughen and oxidize) surfaces of plastics to improve film adhesion, but this is to be avoided if possible, because it typically reduces the reflectivity of the finished film. If you must etch, use a mild caustic.

Small test samples were cut from soluble polyimide film, cleaned initially in isopropanol, then cleaned, each in one of a variety of detergents, swabbing with Q-tip cotton swabs. They were then rinsed in distilled water, sensitized, rinsed, and bath-immersion silvered. The detergents used were: Peacock 77 diluted 5:1 with water (as recommended by Mr. Davey), Peacock 77 undiluted, Peacock 77 diluted 1:1 with isopropanol, Alcojet highly alkaline laboratory dishwasher detergent, Never Fog windshield wetting agent, Sunclear solar still droplet inhibitor, household ammonia solution, and concentrated sodium hydroxide solution. All samples yielded a reasonably uniform, bright film, and no obvious differences in appearance or rate of silvering were noted. Two tests for adhesion were used: (a) rubbing with a dry cotton swab and (b) applying, then peeling off, 3M magic tape. No clearcut differences in film adhesion were noted among any of the samples. For these and some similar samples made subsequently, the following general statements could be made: (a) all thin films/deposits failed the dry swab rubbing test but passed the tape peel test and (b) all thick deposits passed the dry swab rubbing test but failed the tape peel test. One supposes that it merely took longer to abrade through the thicker films in the rubbing test; this test may have tested wear resistance more than adhesion. The thinner films did not appear continuous, and may have occupied merely isolated sites of high activity and adhesion, whereas the thicker films may have grown laterally from such sites, to include intervening areas of lower activity and adhesion. It also appeared that adhesion of thick silver films improved with time after deposi-

tion (some reference to this was seen in the literature, along with some indication that bur- nishing may improve adhesion). This may have been due to evaporation of trapped water mol- ecules or relaxation of stresses due to the depo- sition process, or adjustment of silver atom lo- cations to positions of lowest energy or closest approach to polyimide film atoms. In any case, after drying 1 hour, even rather thick silver films on polyimide marginally passed, or some- times passed, the tape peel test. By compari- son, good quality aluminized Kapton usually (though not invariably) passes the magic tape peel test. As with any electroless plating pro- cess, extreme care in achieving and maintain- ing surface cleanliness and wetting, and plat- ing solutions purity appeared essential to tol- erable film quality.

Both for protection of the silver film against abrasion and excessive tarnishing, when used as a second-surface reflector, and preferably to allow use of the film as a quasi-first-surface reflector, it was desired to find a suitable trans- parent protective overlayer for the silver on polyimide. Typical lacquers optically suitable for that purpose, such as that sold/recom- mended by Peacock Lab., or acrylics such as Krylon and various other brands, invariably contain toluol and/or xylol, which are damag- ing to the soluble polyimide. Peacock Lab. formerly sold a mineral spirit soluble lacquer that would have been compatible with the soluble polyimide, but discontinued it because of the slight amber hue. Mr. Davey of Peacock Lab. said it seems impossible to get a mineral spirit soluble lacquer with fully satisfactory optical properties. In general, one can say that the soluble polyimide of interest is not soluble in, or significantly swelled by, or attached by simple straight-chain hydrocarbons. Simple alcohols are compatible with this polyimide, but not complex or aromatic alcohols; ketones are invariably damaging; simple ethers are

alright but complex ethers are good solvents for it; and halogenated hydrocarbons either swell it or dissolve it. As to lacquer resins that can be used with merely petroleum distillate as thinner, one can list some kinds of polyurethane, and modified linseed oil. Great Day clear aerosol spray enamel of Illinois Bronze Paint Co., containing only simple hydrocarbons as thinner (and probably polyurethane resin) was tested and found compatible with the soluble polyimide film, silvered and/or unsilvered. It did not appear to dissolve, attack, or swell the polyimide or tarnish the silver. It dried smooth and level, though it possessed a faintly detectable amber hue, not quite as crystal clear as an acrylic. Judging by eye, the total visible spectrum reflectance of a first-surface silver film coated with it is probably 95% that of the same film before coating with the lacquer. Thin lacquer greatly improved adhesion of a silver film to a glass slide, and produced substantial, though less marked, improvement in adhesion of a silver film to a sheet of polyimide probably because the silver films were very porous and allowed the lacquer to penetrate to the substrate, and the lacquer had a high adhesion to the glass, whereas it did not have a high adhesion to the polyimide. No material to date has been found which does not dissolve or attack this soluble polyimide, or display a strong adhesion to it. The Great Day lacquer is rated for outdoor use, which implies tolerable resistance to UV and moisture. Various water-based overlayers, namely, sodium silicate, potassium silicate, colloidal silica, and Sunclear, were tried, but they all displayed unsatisfactory adhesion to the silvered polyimide.

An attempt was made to obtain simultaneously both the geometric flexibility of the spray method of applying the silvering solutions, and the convenience and control of the bath method, by use of capillary wicking to position the silvering solutions on the surface to be silvered. Wicks of muslin cloth, Handi-

wipe, Kaydry, and paper towel, were placed on a presensitized glass slide, and silver solution and reducer solution were poured on so as to saturate the wicking. The resulting silver deposits were all too thin, and only the muslin produced a uniform looking (non-mesh-like) film. For silvering a doubly-curved film on a convex forming-mandrel (or such a film, inflated, after removal from such a mandrel), one can visualize temporarily attaching contour terrace fences, to allow concentric pools of silvering chemicals to be used in the bath mode, but this would not be easy. The spray method of applying the silvering solutions appears messy, wasteful of expensive solutions because of rapid run-off, and difficult to cover a large area reflector fully within an acceptable time after application of the sensitizer, though it seemingly works well in moderate scale manufacturing of glass mirrors, where experienced operators get the process going rhythmically. It may yet be the best method for silvering a large doubly-curved polyimide film; probably the film should be rotated slowly on the spin-casting turntable during spraying of the silvering solutions, the temperature in the spin-casting booth (and of the spray-liquids) should be elevated to about 95°F to maximize reaction before run-off of liquids, and the humidity in the spray-booth should be elevated to 95% to prevent drying of some areas while spraying other areas; the spin-casting booth should help retard contamination of the polyimide film between completion of detergent scrubbing and completion of silvering.

The spray technique for electroless deposition of reflective silver coatings on polyimide film was studied on the premise that it is potentially more practical than bath techniques for silvering large doubly-curved surfaces. After acquiring some experience in spray silvering, a comparison test was conducted, in which two similar polyimide samples, mounted on

12 inch hoops, were silvered, one by the spray method and one by the bath method. The resulting silver film deposited by the spray technique looked superior to the bath deposited silver film; and by this time the spray technique had begun to seem easier to use and control than the bath technique. However, considerable unexplained variability was yet being encountered from sample to sample. An additional conversation was held with Mr. Davey of Peacock Labs. He suspected that our major problem was variability in the trace minerals in the bottled distilled water being used, and he recommended use of a demineralizer. This helped somewhat; also changing to an oil less air compressor to drive the spray air brush seemed to help somewhat. One 18-inch hoop-mounted film, spray-silvered, looked very good both as a first-surface and as a second-surface mirror, except for pre-existing scratches. It has not tarnished significantly during two weeks exposure to laboratory atmosphere, though the literature indicates that such films tend to tarnish rapidly, especially from airborne particles, unless overcoated promptly after deposition.

A fresh sample of spin-cast film was made to investigate silvering before separation of the film from the glass casting substrate. Care was taken not to touch the film with any solid object; spray cleaning and spray sensitizing were used, prior to silvering. The film wetted during exposure to the highly detergent cleaning and sensitizing solutions, but de-wetted visibly during the subsequent rinsing operations (using distilled water). It was then spray-silvered. Silver deposition was very nonuniform and adhesion was poor. Ann St. Clair of LaRC, developer of the soluble polyimide, was consulted for recommendations. She said that all polyimides are difficult to metallize by electroless deposition, but that the polyimides which we are using are particularly difficult because the fluorine items make the film sur-

faces intensely hydrophobic and very inert chemically, such that poor adhesion is likely to be more of a problem than poor wetting/nonuniform deposition. She said these materials are difficult to etch chemically; the most promising candidates for etchant being strong alkali, or a mixture of water and solvent in the case of soluble polyimide. She believed that everyone who has successfully electroless plated even conventional polyimides has been forced to resort to mechanical abrasion, typically "rubbing in" the catalyst or sensitizer solution. The literature surveyed had indicated that most industrial electroless plating of plastics relies on chemical etching. This literature also indicated that only a rather small range of types of plastics are practical for electroless plating, and invariably some form of suboptical roughening of the surface is required in order to give high adhesion.

The above mentioned film sample, still attached to the glass substrate, was etched free of silver using nitric acid. Then, one third of it was etched with warm concentrated sodium hydroxide (which appeared to cause a significant lasting improvement in wettability), rinsed, and spray sensitized; a second third of the film was spray sensitized with sensitizer solution containing 30% acetone (any stronger concentration of acetone visibly damaged the surface, any weaker concentration did not appear to affect wettability significantly); the remainder of the film was spray sensitized with the normal sensitizer solution then rubbed gently but thoroughly with a Shurwipe cellulose wiper. The film was then rinsed and silvered. The alkali etched region and the acetone etched region looked nonuniform and blotchy, but the wiper rubbed region looked uniform, specular, and of fully satisfactory quality. Film adhesion was good, for the Shurwipe rubbed region and for the alkali etched region, i.e., capable of passing the Scotch tape peel test, after drying.

The entire film was then etched clean with nitric acid, and the procedure which had been successful with the Shurwipe rubbed region was applied to the entire film surface. This time the entire surface came out nonuniform, with random blotches of thin deposit covering about 20% of the area. Further etching, cleaning, and silvering attempts seemed to indicate that the number and size of the regions which silvered poorly was increasing with time, and also, that adhesion was improving with time, as the surface became progressively more scratched from repetition of the procedure. Neither strong alkali, nor strong acid, nor vigorous rubbing with a Shurwipe, was able to obliterate the poorly-silvering regions/blotches on the surface. It was felt that subsurface electrets, on locked-in electrostatic charges in the highly nonconducting polyimide, might be distorting the auto-galvanic charge exchanges which are instrumental to the electroless deposition process. Grounding of the wiper during rubbing with sensitizer seemed to produce slightly better coatings than insulating the wiper, but not decisively so. Severe etching of the surface with a solvent was tried, but this resulted in destruction of the sample. Fragments of the film were removed, inverted, and taped down, to determine whether long contact with the glass substrate might have produced different silvering behavior than that of the other (air dried) surface of the film. No differences in wetting nor adhesion were noted. Triton wetting agent was added to the rinse water. This seemed to improve uniformity of deposition in some cases, on freshly prepared unrubbed film, but adhesion remained unsatisfactory on such film. Because thin coatings seemed more adherent than thick coatings, deposition in two stages, separated by drying, was tried; no improvement in final adhesion was observed. A strange phenomenon was noted several times, when a rather thick silver coating was applied

to a rather poorly wetted film: The deposit appeared rather white and matte-like and just barely specular, but as spraying proceeded, a sharp transition to a silver colored, specular condition, of much lighter adhesion, began at some points and propagated slowly but with visible speed across the surface of the film, in a manner suggesting a wave front. Various optical polishing agents, e.g., red rouge, black rouge, bornesite, and alumina suspensions, as well as Bon Ami soft abrasive cleanser, were tried as surface rougheners, but typically no clearcut improvements in wetting, silver uniformity, or adhesion resulted, even when abrasion was carried to the point of general reduction in surface specularity and/or visible scratching of the polyimide surface.

An old film sample made from an old lot of the soluble polyimide, which had been dried at elevated temperature, was observed to silver much more easily and uniformly than more recently cast films. Freshly made films dried at low and high temperatures did not display clearcut differences in silver acceptance, and thus failed to support the reasonable hypothesis that trace amounts of solvent in the film were causing the seemingly unpredictable variations in coating quality from film sample to film sample. This casts possible suspicions on lot-to-lot variability of the polyimide resin batches received. Also yet under suspicion is photoelectric formation of subsurface electrets from long exposure to fluorescent lighting.

In any case, the spray applied electroless silver coatings attainable at present on soluble polyimide film seem marginally adequate for the present needs of this project, in reflectance, specularity, uniformity, durability, adhesion, and ease and predictability of deposition. The preferred coating process at present is as follows:

a. Mix Solutions: activated silver: 40 parts deionized water, 1 part Peacock silver A, 1 part Peacock activator B

- Reducer: 40 parts deionized water, 1 part Peacock reducer C
- Sensitizer: 20 parts deionized water, 1 part Peacock sensitizer 93
- Cleaner: 2 parts deionized water, 1 part Peacock cleaner 77.

b. Scrub with cleaner solution, using Shurwipe held in bare hand.

c. Spray rinse with deionized water.

d. Scrub with sensitizer solution, using Shurwipe held in bare hand.

e. Spray rinse.

f. Spray silver plus reducer (dual airbrush).

g. Spray rinse

h. Blow dry with clean dry air.

The silver coating must not be subjected to stress, nor touched with a solid object, until it has air dried overnight; typically such a coating will fail a Scotch tape peel test performed directly after initial drying of the coating, but will pass the same test if allowed to "age" overnight before testing.

As it was felt that the silver spray-coating process had been adequately mastered to metallize a film sample of interesting size, a 4'-6" diameter film was spin-cast. Four successive attempts were made to spray-silver it. Each time, unsatisfactory results were obtained, and some additional factor which seemed to account for the poor adhesion and/or poor uniformity of the coating, was discovered and corrected. Typically, satisfactory coating was obtained on 30% to 60% of the area of the film, but solution run-off from previously-sprayed or subsequently sprayed areas interfered with proper film deposition. A piece of FEP teflon tape was used to patch a hole accidentally torn in the film, and it was visually obvious that

the teflon tape accepted the silver coating much more readily/rapidly/thickly than the surrounding polyimide film. Attempts were made to rework or touch up or complete the silvering of the film when the latter was incompletely silvered due to running out of silvering solution, but these attempts to blend the subsequent coating smoothly with the previously-deposited coating produce very unsatisfactory results, and the solution run-off loosened the previously-deposited coatings. The spray silvering technique was evaluated considering the following:

- A viable process for metallizing large area films must have a large safety margin, must be forgiving of random variations in application conditions over the film area; and if not a simultaneous-over-entire-area process, it must be possible to blend smoothly a subsequent coating with a prior coating.

- Wetting of polyimide is marginal; attempts to chemically etch polyimide or mechanically sub-optically roughen it were unsuccessful; anti-tarnish overcoating either gave a yellowish tinge or interacted with underlying soluble polyimide, and unprotected thin silver coatings are very susceptible to tarnish-through from airborne contaminant droplets or gases.

- By contrast, vacuum aluminization has been demonstrated, on this polyimide material, to give a coating with acceptable uniformity, adhesion, reflectance, durability, and appearance, with no surface preparation required. Unlike electroless plating, the vacuum evaporation coating technique/equipment can be utilized to deposit a wide range of reflective and protective-overlayer materials.

### 3.3 — Refinement of Analytical Model

The objective of Task 3 was to develop/adapt/refine an analytical model of the membrane creep-forming process that would enable thin film solar concentrators to be curvature formed, in a predictable, well defined manner, using the temperature profile controlled uniform pressure creep-forming process. As the project proceeded, the objective (and the analytical model capability) evolved to include description/monitoring of other variations of viscoelastic curvature forming processes such as mandrel controlled creep relaxation forming, and on station mechanical/thermal behavior modeling of operational deployed thin film concentrators.

Analytical modeling techniques capable of supporting the design and analysis of thin film solar concentrators have been developed. The objective of improving Phase I modeling based on a uniaxial Burger's equation describing viscoelastic material behavior was achieved through the development of a detailed finite element model. Major milestones accomplished as a result of the modeling effort to date include; an extensive literature survey resulting in the compilation of a thin film forming library, a review of software applicable to analysis of thin film structures, development of a pre / post-processor, data reduction techniques for incorporating test data into the numerical model, and finite element model development and verification. In addition to model development, techniques and guidelines for numerically efficient implementation have been formulated. The result of this effort is a design tool capable of supporting construction of thin film solar concentrators.

The analytical model developed in Phase I was based on a uniaxial Burger's model. This model served the purpose of quantifying the rheological behavior of KAPTON film and also provided some capability to model the creep-

forming process. In Phase I the creep-forming process was modeled by discretizing the KAPTON film into a series of finite strips and then applying a Burger's model to each strip. The material could be modeled with either longitudinal strips, as shown in *Figure 35* or with transverse strips. The major limitation of this model is that each strip acts independently; the deformation of one strip has no influence on the deformation of the other strips. Therefore, the combination of longitudinal and transverse strains, required to achieve the shape of an off-axis solar concentrator, can not be accurately represented by this model.

For Phase II a more general finite element model was developed to support the creep-forming effort. The finite element model eliminated some of the limitations associated with the finite strip model. In the Phase II model the KAPTON Film was divided into many discrete finite elements. *Figure 35* shows a finite element model of the KAPTON film. Within each of the elements the behavior of the material is governed by a constitutive equation which relates stress and strain. The constitutive equation can be made general enough to include elastic strains, creep strain, and plastic strain. The shape of the finite element made it possible to relate material strain within the element to the relative displacement of discrete nodes located on the element. By combining the constitutive equation and the nodal displacement/strain relationship, equations can be derived which relate nodal point forces to nodal point displacements. Therefore, if the forces applied to the film are known, the displacement of the film can be calculated. The major advantage of the finite element model over the finite strip model is that a force applied at any node within the material affects the behavior of all of the material. Therefore, the model deforms as a continuous media and the true state of stress and strain within the material

can be determined. An added advantage of the finite element model is that the displacement of the nodes are solved for directly. Therefore, it is relatively easy to determine if the particular set of loading conditions being modeled has produced the desired off-axis reflector shape.

The capabilities of the finite element model allow it to be used as a design tool to support the creep-forming effort. The effects of various factors such as temperature distribution, forming pressure, oven time, and recovery procedure can be parametrically evaluated. The results of the parametric evaluations can be used to estimate the values of the parameters necessary to produce an off-axis reflector.

A list of finite element software packages

was evaluated to determine which software package is most suitable for modeling the creep forming process. Software documentation was obtained and reviewed. Software developers and distributors were questioned regarding the capabilities of various finite element programs. Two software packages, ABAQUS and NEPSAP, were chosen for detailed review.

ABAQUS is a general purpose nonlinear analysis program developed and distributed by Hibbit, Karlsson, and Sorensen, Inc. It has solution algorithms capable of solving problems involving both geometric and material nonlinearities. Data input options are provided for several creep laws that can be chosen to model the material behavior. One of the creep laws available

is similar to the power law that was successfully correlated to material test data in Phase I. ABAQUS also includes well documented results for incorporating user supplied creep laws into the solution. This option allows the creep-forming model to be easily adapted to more complex creep laws if required. Arrangements were made to access ABAQUS on a CRAY computer through Control Data Corporation's Data Services.

NEPSAP is another finite element program suitable for modeling the creep-forming process. NEPSAP is distributed through the Aerospace Structures Information and Analysis Center at

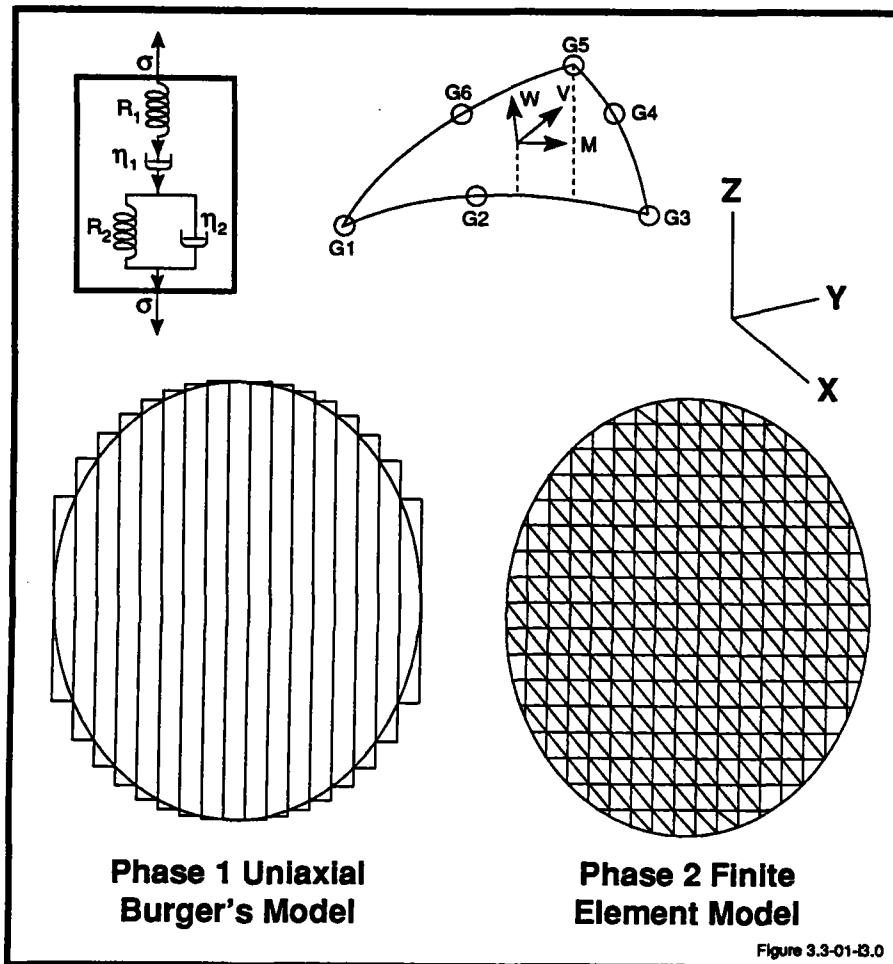


Figure 35 Comparison of Phase 1 and Phase 2 Analytical Models

Wright-Patterson Air Force Base. An advantage of using NEPSAP is that the FORTRAN source code is available. This allows the user to modify the solution routines to be particularly efficient on a specific problem.

Each of the two software packages, NEPSAP and ABAQUS has advantages and disadvantages associated with using them to model creep-forming. However, in the final analysis ABAQUS was chosen as the most suitable software for further model development. Several factors contributed to this decision. One of the primary concerns regarding NEPSAP was that much of the source code was highly machine-dependent and difficult to implement on most computers. The documentation of the machine dependent portions of the code was poor. Therefore, it was difficult to estimate the amount of resources required to develop a model using this software. On the other hand, the ABAQUS software is well documented and more general in terms of capabilities. Therefore, it was felt that ABAQUS provided the most cost effective and technically attractive approach to modeling of pressurized polyimide film at high temperatures. Model development proceeded using ABAQUS.

As part of any large finite element modeling task, having a preprocessor to generate the large amounts of input data can be a valuable tool. A preprocessor is a computer program written to generate and output the large amounts of data in a specified format to be used as input into another program. A preprocessor can generate the node and element data for a finite element model much faster and more accurately than can be done manually. Making large or small changes to a large finite element model is greatly simplified using a preprocessor.

The program to generate the creep behavior finite element model was written in as general a form as possible to allow later revisions. The following paragraphs give a brief description of the capabilities

that were included in the program.

To specify the initial geometry, any major and minor axis could be input to generate either elliptic or circular boundaries. The number of radial and circumferential divisions could be any even number. A spacing parameter allowed the radial divisions to be concentrated to either the inside or outside of the geometry. The origin of the geometry could be located anywhere within the boundary. This allowed the origin to be placed at the point of maximum expected deflection for an off-axis reflector. The origin was not limited to being on the major or minor axis. An option was included in the model to take advantage of symmetry and only create a partial model. This saved computer resources and allowed more detailed models for the same computer time.

To save computer resources in running large finite element codes, efficient node numbering was required to produce a banded stiffness matrix. Generally a stiffness matrix with a smaller band width will run more efficiently. An option was included in the preprocessor to renumber the nodes in a more efficient manner than the program initially used to generate the geometry.

Options for creating four different types of element were included in the program. The four element options included a three point triangle, six point triangle with midside nodes, a quadrilateral element with four sides, and a 15 point solid wedge with midside nodes. The four elements are illustrated in *Figure 36*. The three point triangular element and four point quadrilateral element are linear elements which represent the relative displacements of the element corners with a linear relationship. The six point element with midside nodes represents the relative nodal displacements of the element nodes with a quadratic relationship. The quadratic element can more accurately represent complex strain fields than the linear element. However, the linear element can pro-

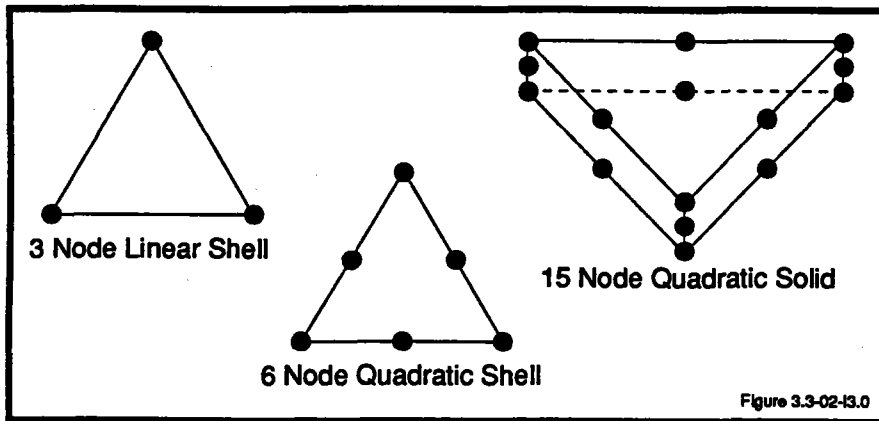


Figure 36 Elements that can be Generated by the Preprocessor

vide the same accuracy as the quadratic element if more elements are used in the model. The 15-point solid was also included in the program because of the different way a solid element handles bending moments from the way a shell element does. The aspect ratio of all the elements is a concern especially for the very thin solid element.

In large finite element models, the best way to check the input data is through plots. An option was included in the preprocessor that efficiently plots the input data on an in-house HP plotter. *Figure 37* gives examples of both on and off-axis models with an elliptic boundary. The radial and circumferential divisions are 8 and 24 respectively. *Figure 37* gives examples of the radial divisions concentrated to the outside and inside. The radial and circumferential divisions used in *Figure 38* are 6 and 12 respectively.

One of the primary interests from the creep behavior model will be the final deflection of the film. An option was included in the preprocessor to be able to compare the finite element model predicted deflections with the e of a perfect reflector. The program prints the difference between actual and ideal deflections.

Since there are two reflector configurations that will be run most of the time, an option for using standard off-axis or standard on-axis default input parameters was included in the pro-

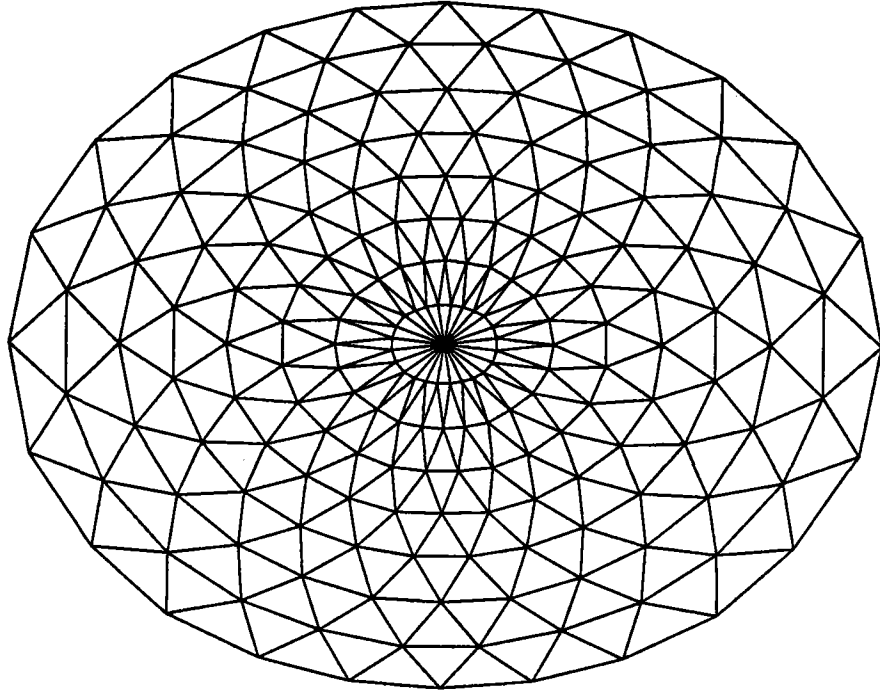
gram. The standard reflector defaults were based on assumptions used in the past for deriving the shapes of on-axis and off-axis parabolic reflectors.

The tremendous amounts of output produced by a large finite element analysis can often make the results difficult to interpret. Therefore, a

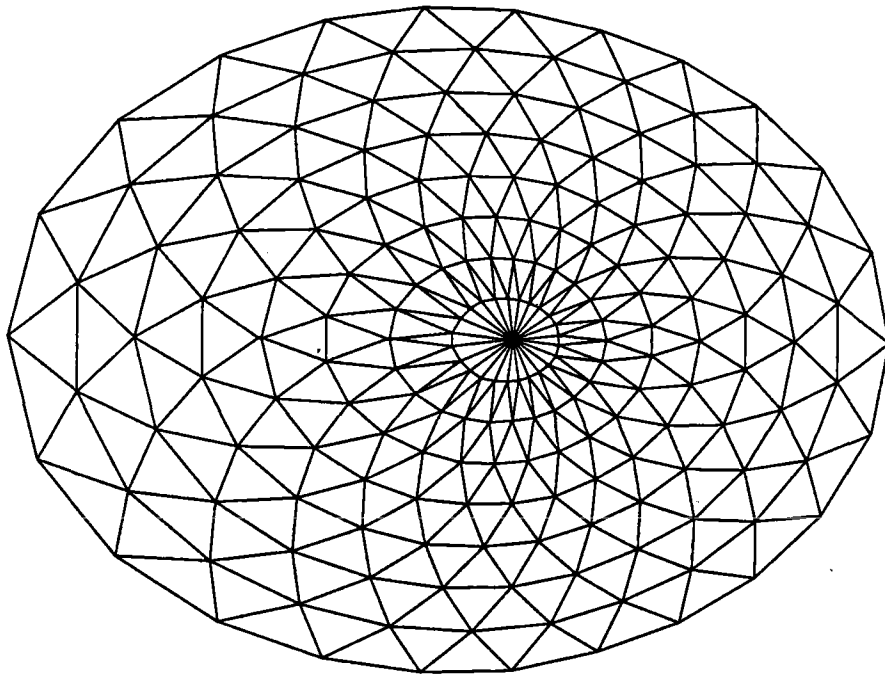
postprocessor has been developed to help interpret the results from the finite element model. The postprocessor compares the shape predicted by the finite element model to the shape of a perfectly formed solar concentrator of the same size. The results are displayed in the form of contour plots representing the magnitude of the differences in the two surfaces. The contour plots provide graphical representations of how the shape needs to be modified. The effect on the shape of changing the design parameters is graphically illustrated by the postprocessor.

The capabilities of the finite element modeling, using the ABAQUS software, were quantified for several aspects of the analysis required to support the development of thin film solar concentrators. Procedures, techniques, and guidelines were established for various aspects of modeling this type of structure. It was demonstrated that ABAQUS could accurately incorporate nonlinear effects and viscoelastic material behavior into analysis of thin film membranes subjected to a variety of thermal and loading conditions.

Accurate modeling of thin film structures in applications such as the forming of solar reflectors is difficult because of the effects of geometric nonlinearity and viscoelastic behavior of the material. To aid in model development, each of these problems were addressed



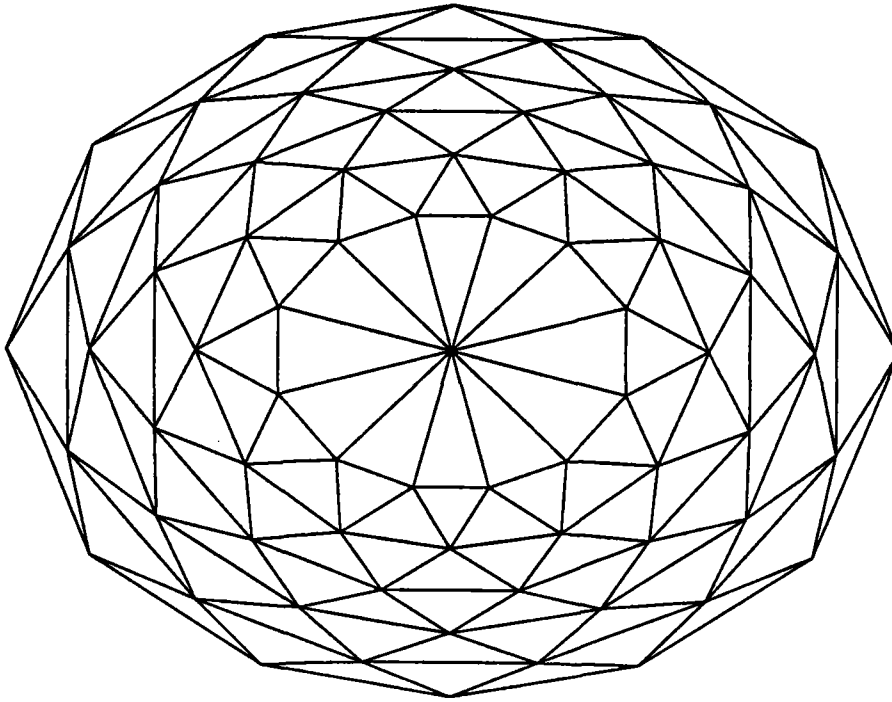
**A. Focus Located at the Center**



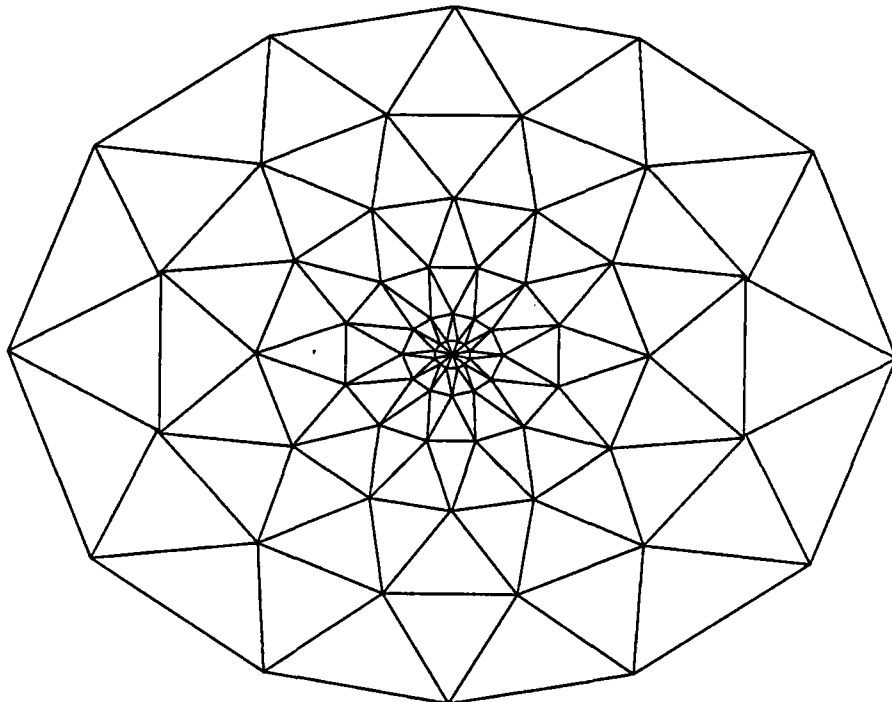
**B. Focus Located at the Point of Expected Maximum Deflection**

Figure 3.3-03-13.0

**Figure 37 Examples of Finite Element Model with Elliptic Boundary**



**A. Shape Factor  $Z=0.5$**



**B. Shape Factor  $Z=1.5$**

Figure 3.3-04-13.0

**Figure 38 Examples of how the Shape Factor  $Z$  Effects  
the Position of Elements in the Finite Element Model**

independently. A set of simplified models were used to evaluate the accuracy of the results for loads producing large deflections. Another model was used to evaluate creep modeling capabilities. The cases modeled were simplified to the point that they can be verified analytically or by testing.

Thin film structures carry transverse loads primarily through membrane stresses and are incapable of supporting significant bending stresses. Therefore, the support reactions must be tangent to the surface of the film. This effect causes the support reactions to be a function of the displaced geometry of the film. In this situation standard small displacement theory, typically used for finite element analysis, is invalid. The ABAQUS software incorporates an iterative solution scheme capable of modeling structures where large deflections introduce geometric nonlinearities. Models were developed to evaluate these capabilities and to establish a procedure for incorporating geometric nonlinearity into analysis of reflector models. For this study, the Kapton film was considered to be linearly elastic. The geometry modeled was a circular membrane supported at the edges. Initially, the film was flat. A pressure load was applied to the film which caused out-of-plane displacements. This geometry was chosen because an analytical solution can be calculated for this case. The primary objectives of this study were to evaluate the software capabilities for handling this type of nonlinear analysis and to develop model building guidelines for incorporation into reflector modeling.

The first concern of any finite element model development is to construct a suitable gridding scheme capable of accurately representing the strain field within the geometry. For this particular structure, the fact that the loading and geometry are axisymmetric with respect to an axis through the center of the membrane would allow the entire structure to be analyzed by

modeling only a sliver of the actual structure. However, modeling of an off-axis reflector requires that at least half of the structure be modeled. Therefore, the test models constructed represented half of the structure. Three basic gridding schemes were used in model development. These schemes are illustrated in *Figure 39*. The first models constructed used three and four node shell elements. It was necessary to use shell elements because the ABAQUS software does not incorporate any true membrane elements. However, it was found that with proper boundary conditions applied, the shell elements could be used satisfactorily. The problem encountered with this type of grid was that as the model was refined by increasing the number of angular divisions in the grid, the elements near the center became either very small or very skewed. Therefore, in order to have an acceptably fine grid on the outer portions of the model, the grid was overly refined near the center. This resulted in an appreciable increase in the execution time of the model with little improvement of solution accuracy. Therefore, grid reduction techniques were employed near the center of the model. The first scheme utilized a combination of three and four node elements to reduce the number of angular divisions near the center of the model. This helped solve the problem of element skewness near the center of the grid but still resulted in very small elements in that region. Finally, a third gridding scheme was conceived which proved to be the most numerically efficient. This grid utilizes all four node shell elements and allows more flexibility in defining the relative coarseness of the grid in different parts of the model.

Benchmark cases were run using all four node element forms of gridding. Several guidelines were developed which are applicable to reflector modeling. The cases modeled used the material properties of Kapton at room tem-

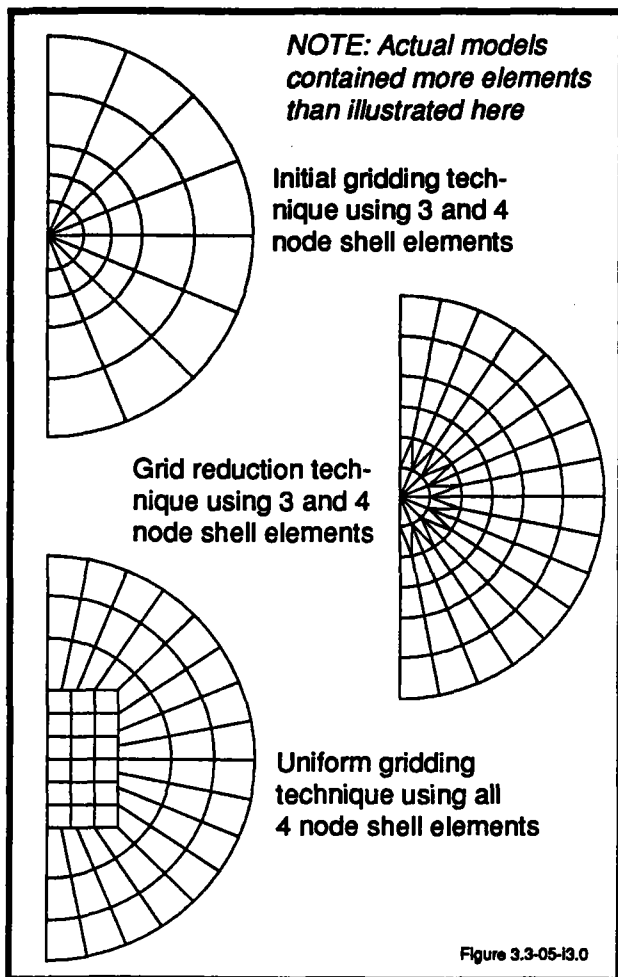


**Figure 39**  
**Finite Element Gridding Techniques**  
**used for Membrane Analysis**

perature: elastic modulus - 430,000 psi; Poisson's ratio - .34. The material was 0.005 inches thick and the diameter of the membrane was 30.0 inches. The applied pressure was 0.1 psi. The maximum deflection, which occurs at the center of the membrane, can be calculated analytically by the methods presented in Timoshenko's *Strength of Materials*. The best results were obtained when using a grid consisting of 338 nodes and 336 elements. Half of the membrane was modeled. This resulted in a maximum ratio of element size to membrane radius of nine percent and the minimum ratio was two and a half percent. Using this grid, the model results agreed with the analytical

solution for the maximum deflection to within three percent. With this grid the solution converged in 30 iterations. Further model refinement resulted in only small increases in accuracy and relatively large increases in computational time. Therefore, it is felt that the element size ratios stated above are numerically efficient and suitable for reflector modeling.

In addition to gridding requirements, the membrane models also led to the development of other procedures applicable to reflector modeling. In the first simulations conducted using this model, the membrane was initially assumed to lie in a single plane, i.e., it was perfectly flat. This resulted in highly nonlinear behavior of the support reactions in the first iterations of the solution. This phenomenon occurred because a membrane has no bending stiffness. Therefore, the in-plane loads would have to approach infinity to support a transverse load for a perfectly flat membrane. As a result, a large number of solution increments were required to reach a converged solution. This problem was addressed by building the model with a very small amount of sag built into the geometry of the unloaded membrane. It was found that a large reduction in the number of iterations required to obtain a converged solution was achieved with little effect on the accuracy of the results. In fact, since finite element models approach the exact solution from the side of being too stiff, the initial sag actually slightly improved the results.

The boundary conditions applied to the model were also found to affect the convergence rate of the solution. Theoretically, a membrane should have the same deflection regardless of whether the edges are clamped or pinned. However, since shell elements were used in the model, boundary conditions were important. In a forming process the edges of the membrane will most likely be clamped. Therefore, in the first runs the rotations at the

outer edge of the models were constrained. This procedure led to convergence problems and diagnostic warnings of excessive rotations in the shell elements. Much better convergence rates and results were obtained when the edges were modeled as pinned. This approach is realistic and does not conflict with actual conditions in a forming process because the Kapton film behaves like a true membrane.

Based on the results obtained from the modeling discussed above, it is felt that the finite element models using the ABAQUS software can adequately model the effects of nonlinear geometry associated with forming of thin film solar reflectors.

In addition to complications associated with large deflections, a reflector model must also be capable of handling viscoelastic material behavior. There are several ways to address this problem using ABAQUS. The software

has provisions for incorporating arbitrary, user-defined time dependent constitutive relationships into the solution procedure. There are also several widely used creep laws already incorporated into the software. It was decided to evaluate the time hardening form of the creep rate equation found in ABAQUS. The power function relates deviatoric stress level and time to the creep strain rate. Temperature dependence is introduced by inputting the material constants in tabular form as a function of temperature. An interpolation algorithm is used to evaluate material constants for values which lie between specified values. The form of the equation is shown below.

$$\dot{\epsilon}_{cr} = Aq^n t^m$$

where:

$q$  = equivalent deviatoric stress

$t$  = time

$\dot{\epsilon}_{cr}$  = strain rate due to creep

$A, n, m$  = material constants

A simple test case was developed to further investigate the suitability of this type relationship for application to thin film solar reflector analysis. The grid used for the model is shown in *Figure 40*.

The model was constrained in the longitudinal direction along the upper boundary and loaded along the lower boundary to produce the desired stress level. A comparison of the results obtained from the ABAQUS model to actual test results is shown in *Figure 41*. The creep test data shown is for creep tests conducted with a stress of 1200 psi and temperature of 600°F, 650°F, and 700°F. The test data plotted for 600°F and 700°F was obtained by averaging the results for three separate creep tests for each of the temperatures. The tests were normalized by shifting the time scale to zero at the point the load was applied to the specimen. The specimens were unloaded at slightly different times, which resulted in a slight distortion of the data after the time the

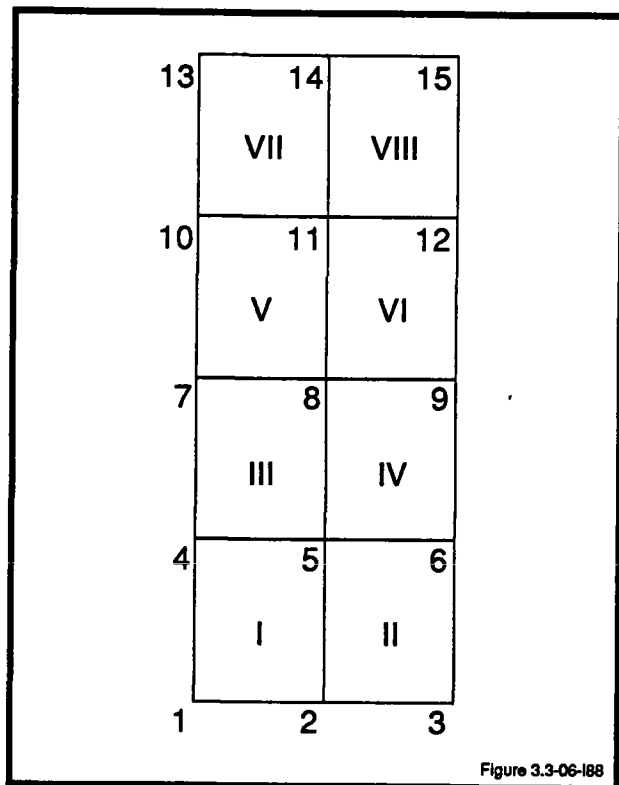


Figure 3.3-06-188

**Figure 40**  
**Finite Element Model of Uniaxial Test**  
**Specimen using Four Node Shell Elements**

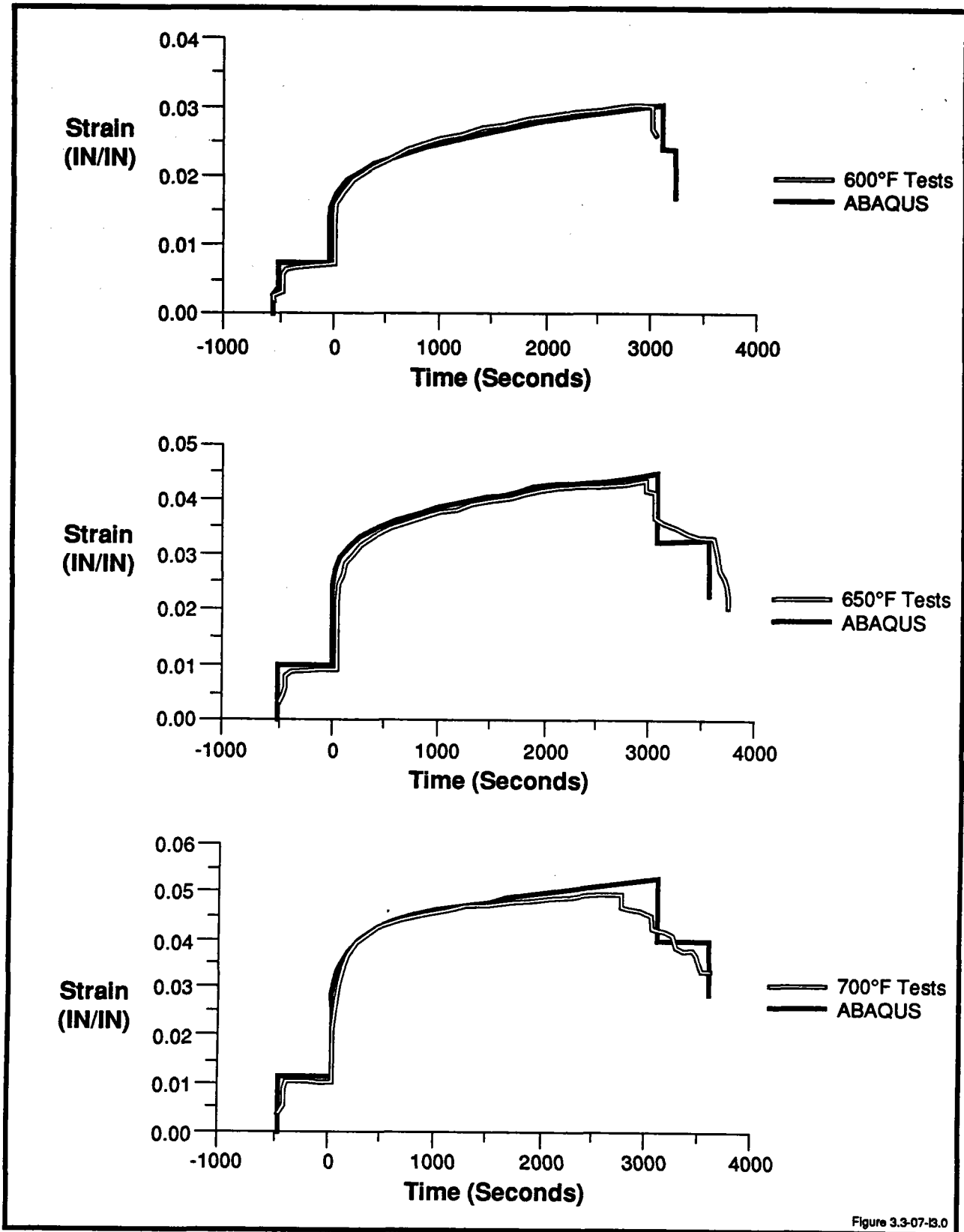


Figure 3.3-07-3.0

Figure 41 Comparison of Results from ABAQUS Simulation and Uniaxial Creep Tests for 1,200 psi Stress

specimen was unloaded. It can be seen from the figure that excellent results were obtained from the ABAQUS simulation for the initial thermal expansion and for the creep behavior of the film. The test data was reduced in order to obtain the following material constants which were used in the model shown in *Table 7*.

The method for reducing the data to obtain the creep rate material constants was the logarithmic curve fitting method. A logarithmic curve fit was performed on the actual strain versus time data. The strain rate was then analytically evaluated for each case. The stress hardening parameter, *n*, was assumed to be one. This is a valid assumption for many materials. This assumption states that the material behaves as a linear viscoelastic material. A review of the creep test data shows that Kapton behaves as a linear viscoelastic material with deviation from this assumption being noted only for very low stress levels. *Figure 42* shows a comparison of the actual test data to the curve generated by the curve fitting. This test data corresponds to creep tests performed at a stress level of 500 psi.

The form of the equation generated by curve fitting is shown below.

$$E = K_1 t^{K_2}$$

This equation is differentiated in order to obtain the strain rate equation needed for the finite element model.

$$\frac{dE}{dt} = K_2 K_1 t^{K_2-1}$$

$$K_2 K_1 = A q^n$$

$$K_2 - 1 = m$$

The stress and stress hardening parameters are known. Therefore, *A* and *m* can be calculated for each case.

Initial simulations using this method resulted in a large overshoot in the creep strains predicted by ABAQUS. The

problem was identified as being related to the fact that ABAQUS treats the creep strain and elastic strain separately. The test data that was being reduced contained both the instantaneous elastic strain and the time dependent creep strain. To overcome this problem, the test data was normalized with respect to the strain recorded at 1.5 seconds after loading. This strain was subtracted from the remaining test data and the time scale was shifted to make time zero correspond to 1.5 seconds. A standard logarithmic curve fit was then applied to the shifted data to obtain the material creep constants. ABAQUS results using these constants were very good for the initial portion of the creep curve. However, the model tended to slightly overshoot the creep curve for the latter part of the test data. It was found that this problem could be corrected by increasing the value of *m* predicted by the curve fit by five percent. This had little effect on initial creep strain predicted by ABAQUS and improved the overall results.

*Figure 41* illustrates how well the ABAQUS creep results agreed with the test data. However, because of the distortion of the test data caused by averaging of test data from tests which ended at different times, the figure does not show how well final permanent strain remaining in the specimen after it was cooled and unloaded was predicted. To evaluate how well the permanent strain was predicted, data from individual tests were examined to determine the amount of elastic recovery after loading. The model results compared well to the test data for the cases of 600°F and 650°F.

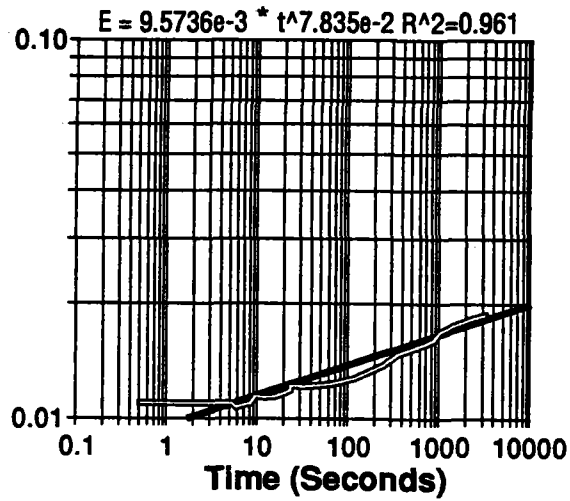
**Table 7 Materials Constants**

Temp (°F)	a(in/in/°F)	E(psi)	A(in/in/sec)	n	m
600	1.34429E-5	1.925E5	3.321E-7	1.0	-0.6708
650	1.6687E-5	0.972E5	5.720E-7	1.0	-0.7214
700	1.767E-5	0.902E5	9.238E-7	1.0	-0.7761

Figure 3.3-08-dr2

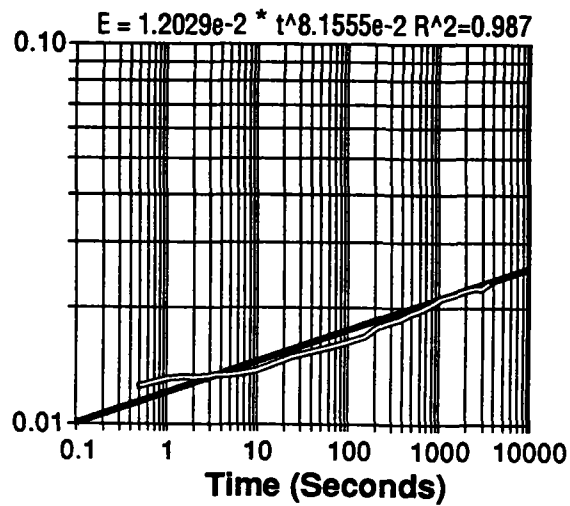
Test - KH505T-600

Strain



Test - KH505T-650

Strain



Test - KH505T-700

Strain

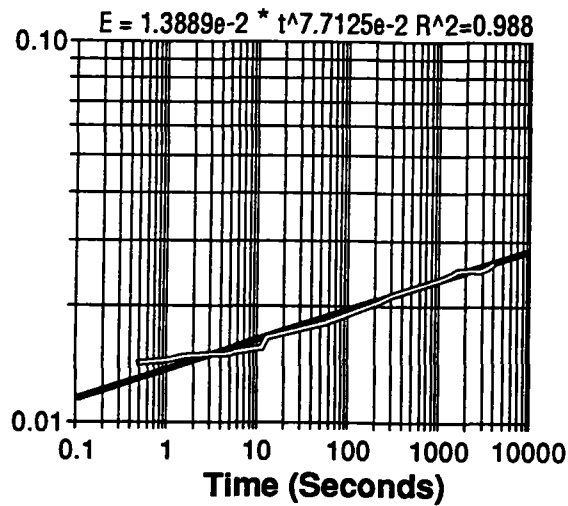


Figure 3.3-09-13.0

Figure 42 Comparison of Actual Test Data to Logarithmic Curve Fits for a Test at 500 psi Stress

For the 700°F case the model over predicted the amount of elastic recovery in the film. This was possibly due to some physical change that occurred in the material between the temperatures of 650°F and 700°F.

Based on the results discussed above, it is felt that the time hardening form of the creep law can be applied to the analysis of Kapton reflector structures.

The results from the creep modeling tests were incorporated into the membrane model to investigate how the model could be used to analyze a reflector. The membrane model was subjected to various temperatures and allowed to creep under a pressure loading. The membrane displacements, as a function of time, were

observed. The model behaved as was expected; however, there is currently no data available to verify the results.

The studies that were conducted have shown that ABAQUS modeling can be used as a powerful tool for analyzing reflector forming or other aspects of thin film reflector design. It is felt that the modeling techniques have been refined to the point of being applicable to actual design problems. At this time, various prototype model forming techniques are being explored by reflector design team. For this reason, no further finite element modeling is planned until forming procedures are refined and problems are identified which require the support of the finite element model.

### 3.4 — Reflector Models

The objective of this task was to design, fabricate, and evaluate thin film concentrator physical models by use of the technology established in Tasks 1, 2, and 3, as a verification/demonstration of that technology. This technology can then be applied to the large size fabrication of thin film concentrators using the procedures developed. Spin casting and thermal forming of 1 meter and larger symmetrical models were made. One symmetrical model was reflective coated using vapor deposition of aluminum. An off axis mandrel was also fabricated for spin and spray casting of NASA polyimides.

#### 3.4.1 — Reflector Models Constructed

The reflective film fabrication process options delineated under Task 2 are directly relevant to the design of a physical scale model. Techniques developed in Task 2 were used to fabri-

cate and test several models. The models were fabricated using thermal forming technique with spin cast polyimide materials supplied by NASA/Langley.

Thin polyimide films 1.125 and 0.5 mils thick were produced up to seven and one-half feet in diameter on a flat substrate. A six and one-half foot diameter, 0.5 mil film was removed from the substrate while attached to an aluminum ring. *Figure 43* is a photograph of this sample. Thickness uniformity over the surface measures better than  $\pm 0.05$  mils which was the accuracy limit of the measurement device used. Specular reflective quality appeared equal to or better than commercially available polyimide films. Although the objective is to produce a seamless reflector of any size including diameters of 30-40 meters, seams in the reversible polyimide have been made by solvent welding. Seams of an extremely homogeneous nature have been produced. No adhesive, overlap, or tape is needed. The film

was produced from chemical imidized 6F+4-BDAF powder obtained from LaRC. Additional development in solvent welding of polyimides is needed to fully define the processes.

The objective of the thin film spin-casting effort is to produce the required size of reflector film without any seams. If seams are unavoidable for a particular design, solvent welding is to be used to obtain a seam as homogeneous in nature as the rest of the film.

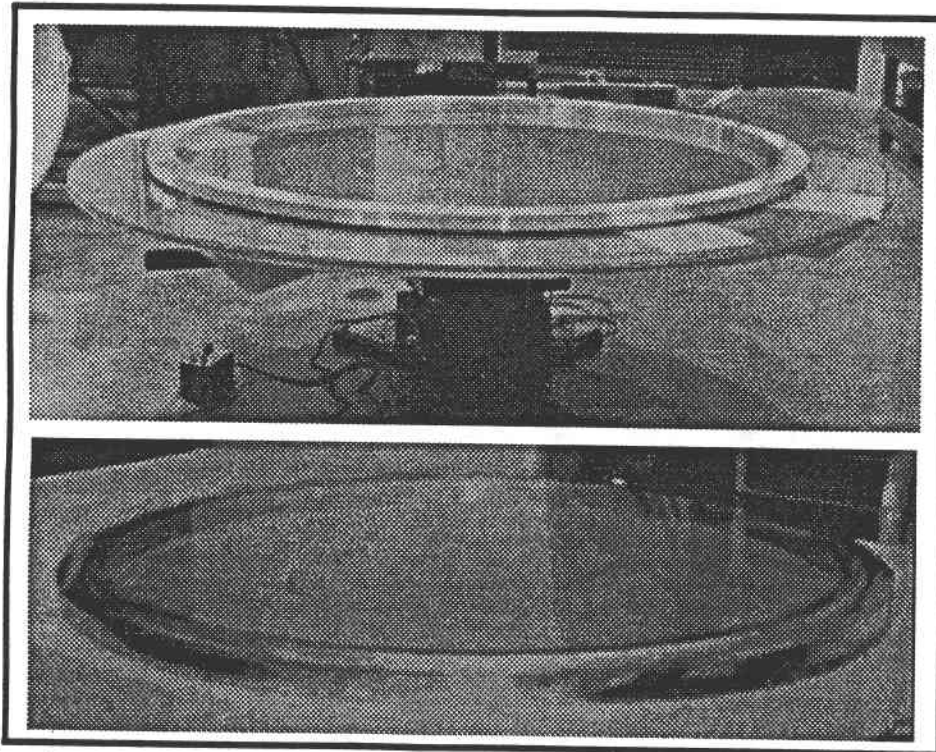


Figure 43 Spin Cast Polyimide Film Mounted on Aluminum Support

**Table 8 Symmetrical Models Constructed**

Test Article	Material	Status
4 foot flat with step and repeat vapor deposition	Reversible polyimide	Failed during testing
4 foot, creep formed	Recycled film	Ruptured during forming
4 foot, creep formed	"New" reversible polyimide	Tested
4 foot, creep formed	Heat immidized	Tested and results
5 foot spin cast flatg	Reversible polyimide	Clear, good film

Table 3.4-01-13.0

Films obtained from this process are usable as flats, as pressure shaped disks obtained from an initially flat film, or as heat/stress crepted preshaped disks (including shaping against a mandrel). Both symmetrical and off-axis parabolic and spherical reflectors may be obtained. In the spin-casting process, the thickness of the film is varied by varying the viscosity of the solution used. The surface smoothness, the characteristic that controls the achievable specularly of the reflector, is controlled by the substrate surface quality upon which the film is cast and the film stress provided while in the operational configuration.

A clean room enclosure for the film spin-casting table was designed and fabricated. This enclosure provided temperature and humidity control and continuous positive pressure atmosphere during film-casting and curing processes with support air passing through a 100,000 class filter. A clean room environment is necessary for film spin-casting because the film "attracts" minute dust particles during the curing process. When the film is cured and dry, entrapped dust particles cause surface imperfections.

### Symmetrical Model Construction

Several four foot diameter symmetrical thin film reflector model were constructed and

tested. A summary of the symmetrical models constructed is shown in *Table 8*.

The first model constructed consisted of a thin film membrane with a vacuum deposited aluminum coating stretched across an air pressure/heat formed plexiglass dish as shown in *Figure 44*.

The reflector membrane is 1/2 mil clear polyimide

spin cast, with no seams, from a solution of the LaRC 6FDA + 4BDAF. The film was cast on a five and one-half foot diameter piece of glass.

The film was held at the edge, released from its glass substrate and epoxyed, while in tension, to the plexiglass dish. This was the first attempt to vacuum deposit the aluminum in a step and repeat process. Several lessons were learned. The most significant problem was the vacuum seals used. Where the gaskets overlapped on sections already aluminized, gasket residue discolored the front surface side of the reflector. Too great adherence of the gasket to the fresh aluminum can result in peel of the aluminized surface. Where the gasket contacted the film prior to its being aluminized, residue later prevented good adherence of the aluminum to the film. An alternate gasket material and appropriate gasket cleaning between aluminization steps could correct these problems in the future. The 1.2 meter (48 inch) diameter symmetrical reflector model failed during optical testing. The reflector membrane which was attached to a pressure/heat-formed plexiglass dish was 1/2 mil spin-cast polyimide film which was aluminized in a step-and-repeat aluminization process. The volume between the film and dish was evacuated during optical testing to focus the reflector. The film

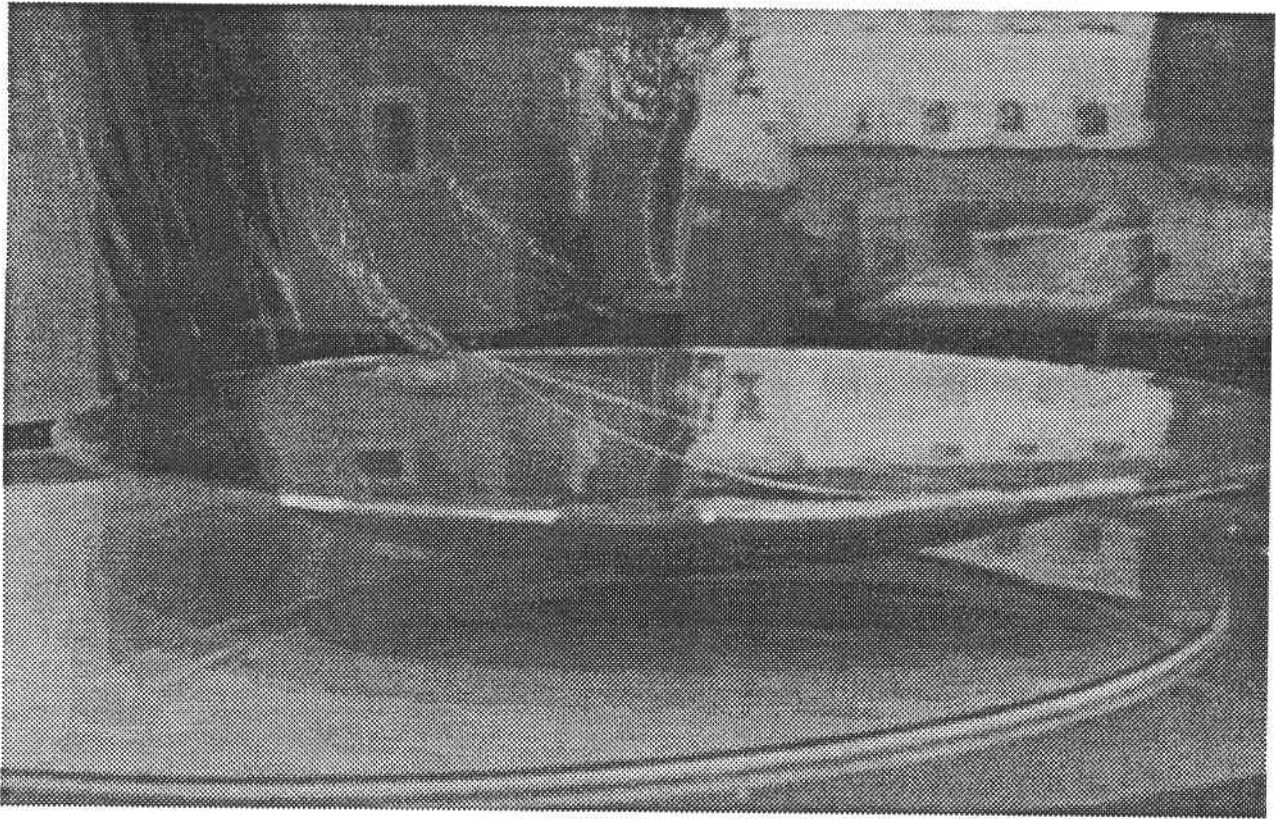


**Figure 44 Vacuum Deposited Aluminum Thin Film Polyimide.**

ruptured before meaningful optical figure data was obtained. The cause of the rupture was over stressing of this thin film.

A second 1.2 meter (48 inch) diameter symmetrical model was constructed using the re-dissolved film that ruptured during testing and additional polyimide (LaRC 6FDA + 4BDAF) material to make the film thicker. This model consists of the following major components:

- Reflective film (nonaluminized);
- Plexiglass back dish; and
- Machined 4 feet diameter aluminum film and back dish support ring.

An additional plexiglass back dish, was thermally formed in the 6' x 8' film creep-forming oven from  $\frac{3}{8}$ " thick bronze color material. This dish was fabricated to provide higher dimensional accuracy than the plexiglass dish used on the first symmetrical model. It was found that the dish used on the first model in which

the film was attached directly to its shoulder ring surface, caused distortions in the film because the shoulder ring was not flat enough and the dish would distort under its own weight when mounted in its support stand.

In this model, the reflective film is attached to a machined aluminum ring, for dimensional stability, and the plexiglass back dish is attached to the opposite side of the aluminum ring. When the volume between the film and back dish is evacuated via a port through the aluminum ring, the film is "focused" in a manner that simulates on-orbit deployment using a jettisonable front inflatable film membrane. The film on this model was not aluminized because: (1) the feasibility of the step-and-repeat aluminization process was previously demonstrated; and (2) the extensive time required for aluminization with the currently available equipment.

The film for this symmetrical model was

spin-cast in the dehumidified, filtered clean room enclosure, and a smooth, uniform, clear film achieved. Only one small, non-fatal defect was found. The film thickness near the edge (at 25-1/2" radius, about 2" inside the spun edge) was 1.7 mils thick.

The film was removed from the glass plate and epoxied to the aluminum support ring (48" I.D., 54" O.D., and 2" thick). As a trial of the figure measurement technique, and to get a baseline for this mirror, the ring was clamped to a plexiglass dome, sealed, mounted in the test position, and fitted to the vacuum pump/manometer. After about 1 hour of careful pumping (at about 1" H<sub>2</sub>O pressure) the film was judged to be stabilized, and the optical figure was examined. As usual, about 70% of the inner surface was spherical (i.e., about 35" diameter), while blending into an outer zone of progressively shorter radius of curvature. This is consistent with an ablate spheroid, or an ellipsoid with the optical axis being the minor axis. Several sets of data were taken at different locations along the optical axis, and are reported .

The film/ring was assembled to a 1/4" aluminum plate; this time a 1/8" thick, 1" wide silicone rubber gasket was used to prevent air leakage rather than silicone caulking which was used previously. The assembly was installed in the oven, and allowed to heat up to 360°F (air temperature) and 350°F (ring temperature), taking overnight (about 16 hours) to reach stability. The air was to pass through about 40 feet of copper tubing, in the oven, to preheat it.

When the creep-forming was attempted, the pressure was gradually increased, and the film formed a bubble. The pressure required was much higher than expected, and the film deflection appeared roughly proportional to pressure. At about 6 psi, on the regulator gauge, the film ruptured very near or at the ring. The film then relaxed back to flat. No creep-form-

ing had occurred.

The conclusions on what caused the film rupture are:

1. It appears undesirable to heat the film for any extended period before creeping; the "cooking" seems to set the film in a physical state that does not creep.

2. The film was thicker than the Kapton films used before, and evidently quite strong.

3. Future work should be done with a "green", i.e., uncured, fresh film.

4. Mounting and handling techniques now appear to be adequate; control of film properties seems to be the only remaining issue.

A third 1.2 meter (48 inch) diameter symmetrical model was constructed by spin casting. The film for this model, also composed of a solution of LaRC 6FDA + 4BDAF, was spin cast to a thickness of one mil for added strength. While mounted on an aluminum support ring which had an aluminum back plate attached, the film was creep-formed to a depth of five inches. The cast film is depicted in *Figure 45*.

Subsequent to creep-forming, the center section of the film was aluminized using the vacuum chamber apparatus. It was then attached to the plexiglass dish after the ruptured film was removed.

### Optical Testing of Membrane

The mirror, mounted on the plexiglass dome, was tensioned with 0.75 inch of water pressure as indicated by manometer. Little change in figure was observed after the mirror became smooth; therefore at these pressures there is little stretching of the membrane. Observation of the focus achieved near the center of curvature (radius was measured at 89.13 inches) indicated that the central 32 to 36 inches was a reasonably accurate reflector, with most of the light from a small (~0.04") point source concentrated within about .3 to .4 inch. Light from

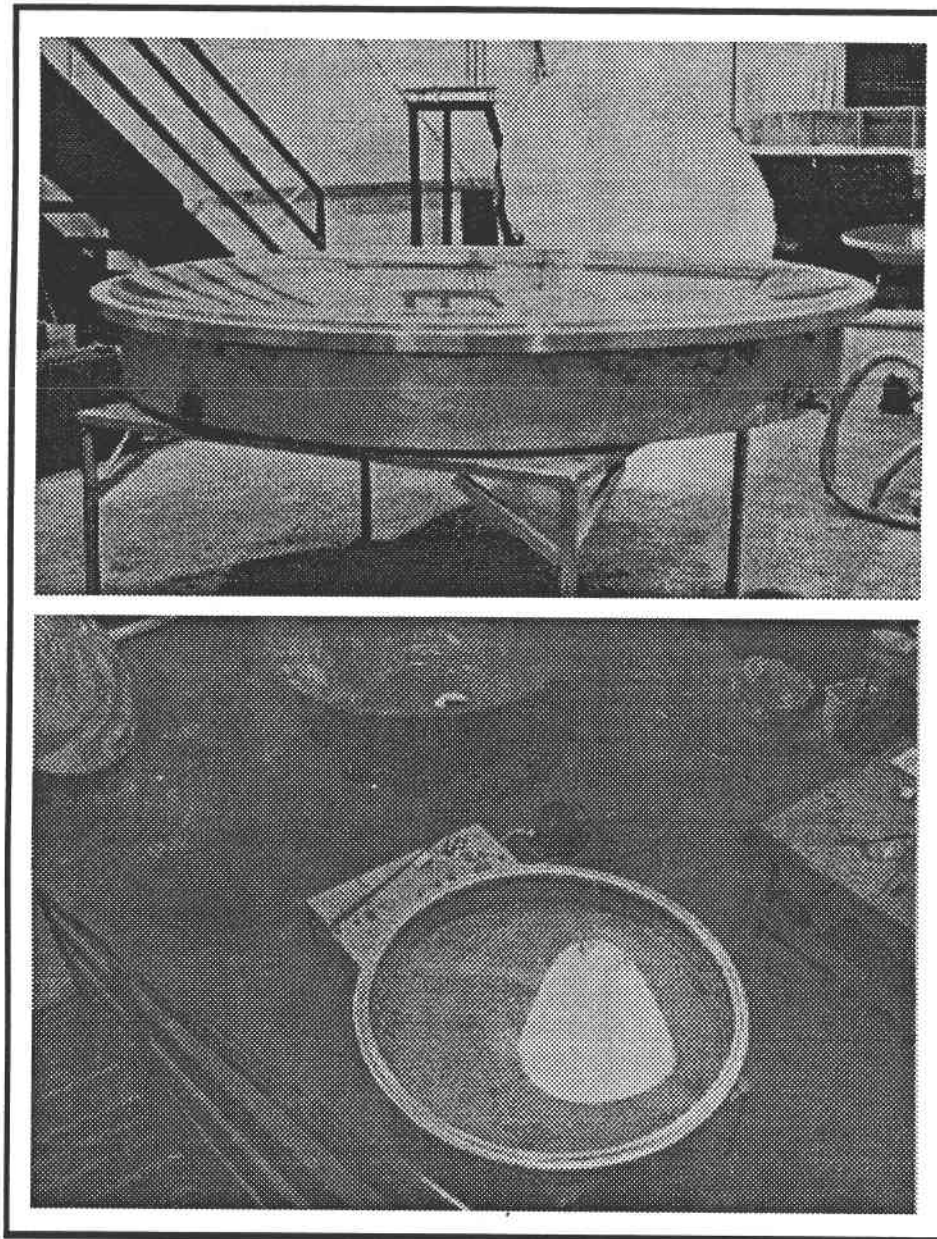


**Figure 45 Formed Thin Film Membrane Using NASA Polyimide**

the outer regions came to a shorter focus, and observation using a mask with a 4" center-to-center array of  $\frac{3}{4}$ " holes (about 125 were used) indicated that wrinkles near the edge contributed to scatter in the outer zone, that is, between about 16 and 24 inches off-axis.

Since the slope and surface errors observed were beyond the limits of the precision measuring setup, a mechanical profiling method

of the two radii of the mirror that were observed. A negative slope error indicates a shorter focus at the point of the error.

The sign and magnitude of the slope errors can be varied by choosing another radius of curvature as a reference. This can be done to lessen the total plotted error but the variation from point-to-point will remain. Figure 46 and Figure 47 indicate that the inner 32 to 36 inches

was used. The depth of the curved mirror was measured with a depth micrometer at carefully located radial increments. The error in depth measurement was approximately  $\pm 0.005$  inch, and in radial location, approximately  $\pm 0.015$  inch. These errors were due to the necessary care in avoiding puncture of the film by the measuring tool. The inner, 36" diameter was checked at 2 inch increments of radius; then at 1 inch increments to the edge.

The radius of curvature used was based on the depth of curve at the vertex (center). This value was slightly less than the distance to the center of curvature as estimated using the point source for smallest focus.

*Figure 46 and Figure 47* provide the measured slope errors

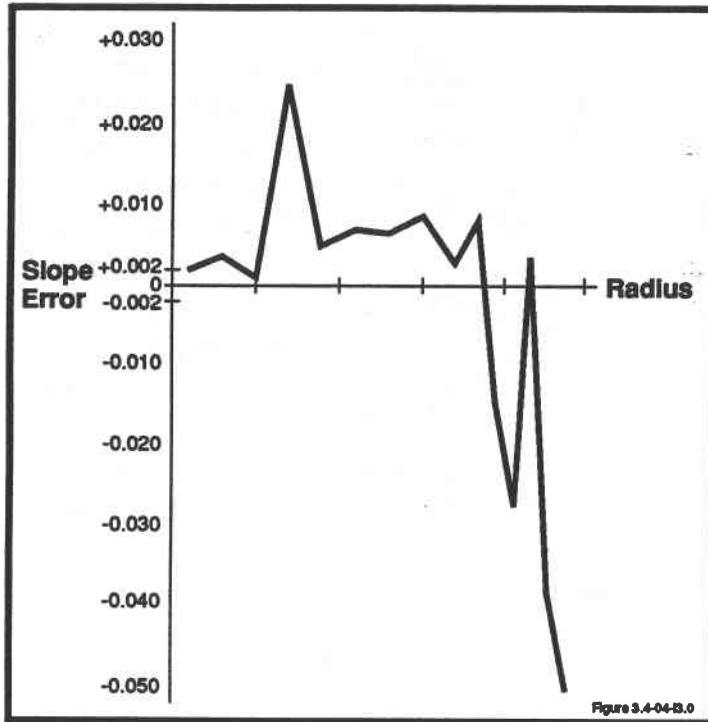


Figure 46 Slope Error along Radius 1

of the mirror were close to a sphere, with slope errors in the .010 or lower range. Therefore, errors were on the order of 30 minutes (1/2

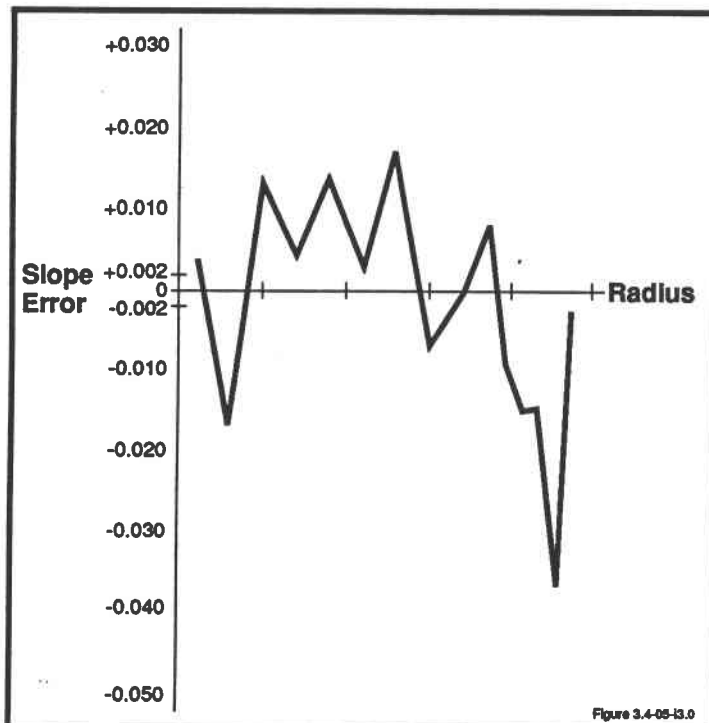


Figure 47 Slope Error along Radius 2

degree). The outer zone confirmed initial observations as to wrinkles and shorter focus.

Figures 48 and Figure 49 provide the measured surface error, referenced to the central radius of curvature. The points plotted represent the difference between the observed coordinates of a surface point and the theoretical coordinates of a reference sphere. Figures 48 and Figure 49 indicate that a slightly longer radius of curvature could have been used to give a better fit, but the important characteristic of these figures is the difference between the plotted curve and a straight line (the horizontal axis represents the reference sphere). Again, the figure of the mirror varies fairly smoothly out to about 16"-18" from the center.

Based on these observations, it appears that the present technique works toward an approximate spherical mirror, with a "turned-up" edge, of shorter focus. A parabolic mirror would go the other way, that is, "turned-down" relative to a sphere. These observations indicate that edge effects in creep-forming and mounting of the film limited the observed surface accuracy.

### Off-Axis Model Mandrel Design Selection

Several off-axis creep-forming mandrel concepts have been investigated resulting in detailed evaluation and conceptual design of a geodesic network mandrel and a solid full surface metal mandrel. Excessive three dimensional tolerance requirements for the geodesic network stringer attachment points tend to eliminate this concept to produce a model of practical size. The weight of a solid full surface mandrel is of some concern rela-

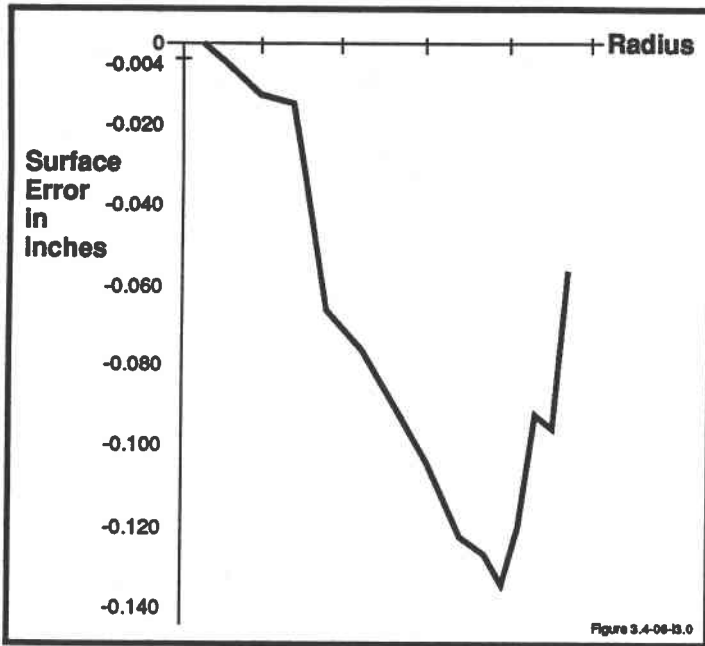


Figure 48 Surface Error along Radius 1

tive to handling difficulties during the creep-forming process; however, a mandrel made of aluminum does appear to be manageable with the existing facilities and equipment. The specifications for an aluminum mandrel are :

$$R_m = \text{Semi-Minor} = 17.3278''$$

$$R = \text{Semi-Minor Axis} = 13.6078''$$

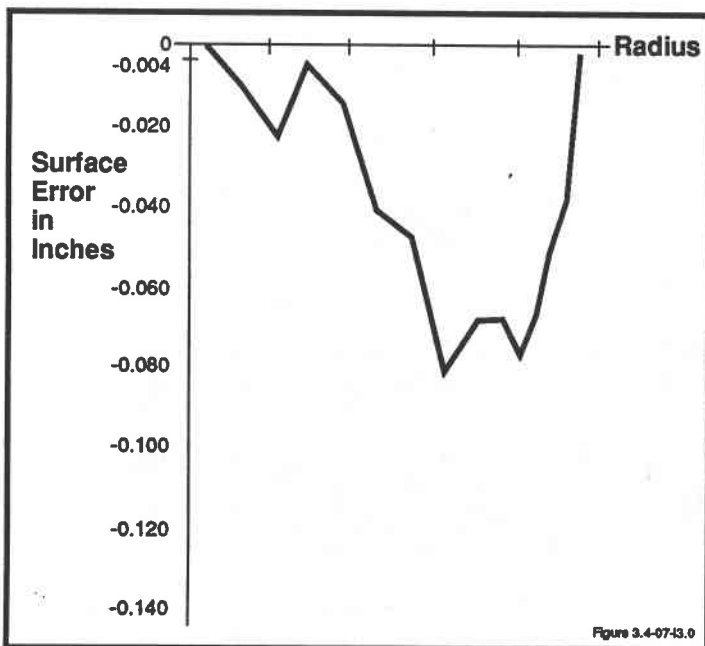


Figure 49 Surface Error along Radius 2

$Z_f = \text{Focal Length} = 12.0000''$   
 $A_p = \text{Angle of Planar Surface} = 38.25$   
 degrees

$$D_{max} = \text{Maximum Depth} = 2.8443''$$

The mandrel that was machined is shown in *Figure 50*.

### 3.4.2 — Application of Reflective Coating to Spin-Cast Soluble Polyimide Film

An apparatus was assembled for step-and-repeat aluminization of arbitrarily large films. Subscale tests proved the feasibility of the concept in principle, and fullscale model film aluminization subsequently demonstrated its practicality. The following key technical observations were made in the course of set-

up and check-out of the apparatus shown in *Figure 51*.

- Relatively large high-conductance by-pass tube interconnecting the chamber volumes or opposite sides of the film being metallized is required to prevent harmful level of pressure differential across the film during roughing pump-down and during chamber venting.

- Unless all sources of outgasing are meticulously eliminated, it is necessary to mask-define the edges of the area being metallized, by a sharp-edge close-contact mask, because where the aluminum vapor stream is of low intensity, e.g., where partially shadowed by the chamber peripheral flange and seal-face gap, especially when near strong outgas plume areas/sources such as seal-flanges tend to be, a brownish discolored edge/border of the aluminum deposit is produced. Careful masking allows highly reflective coatings with non-discolored borders to be deposited at significantly lower vacuum levels

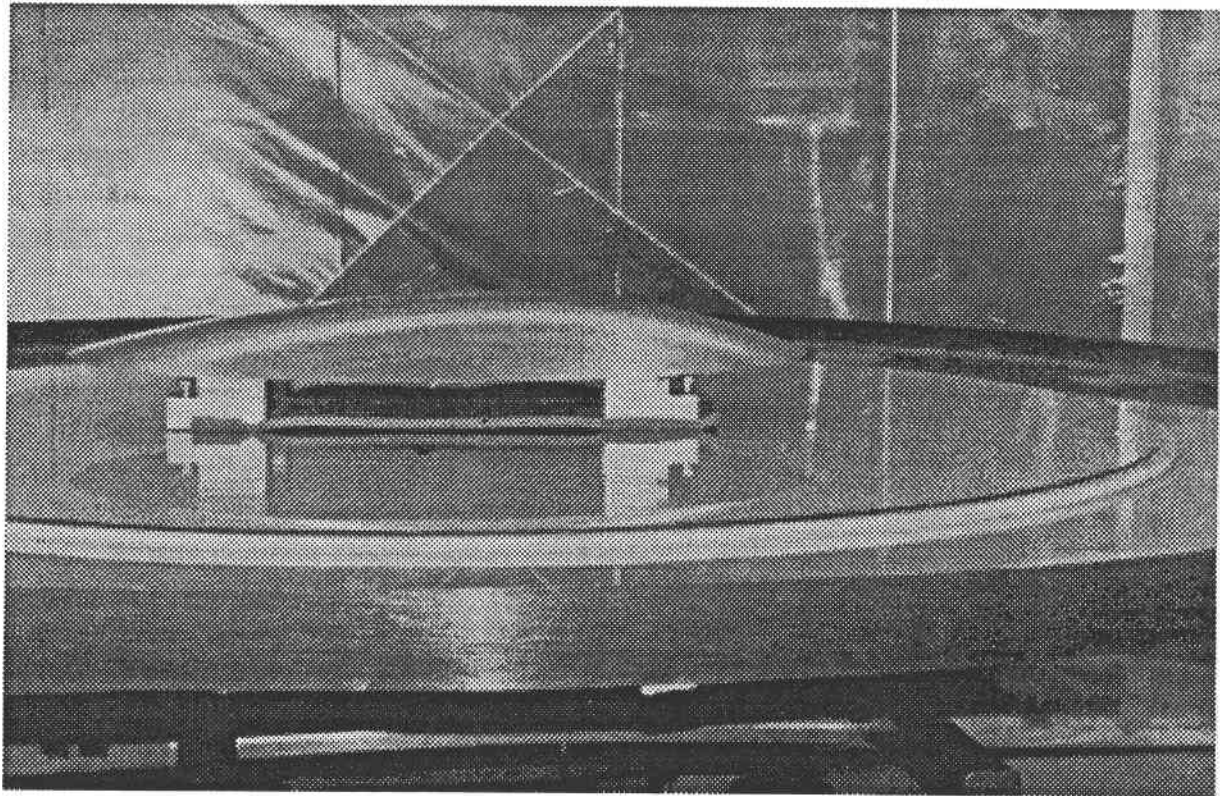
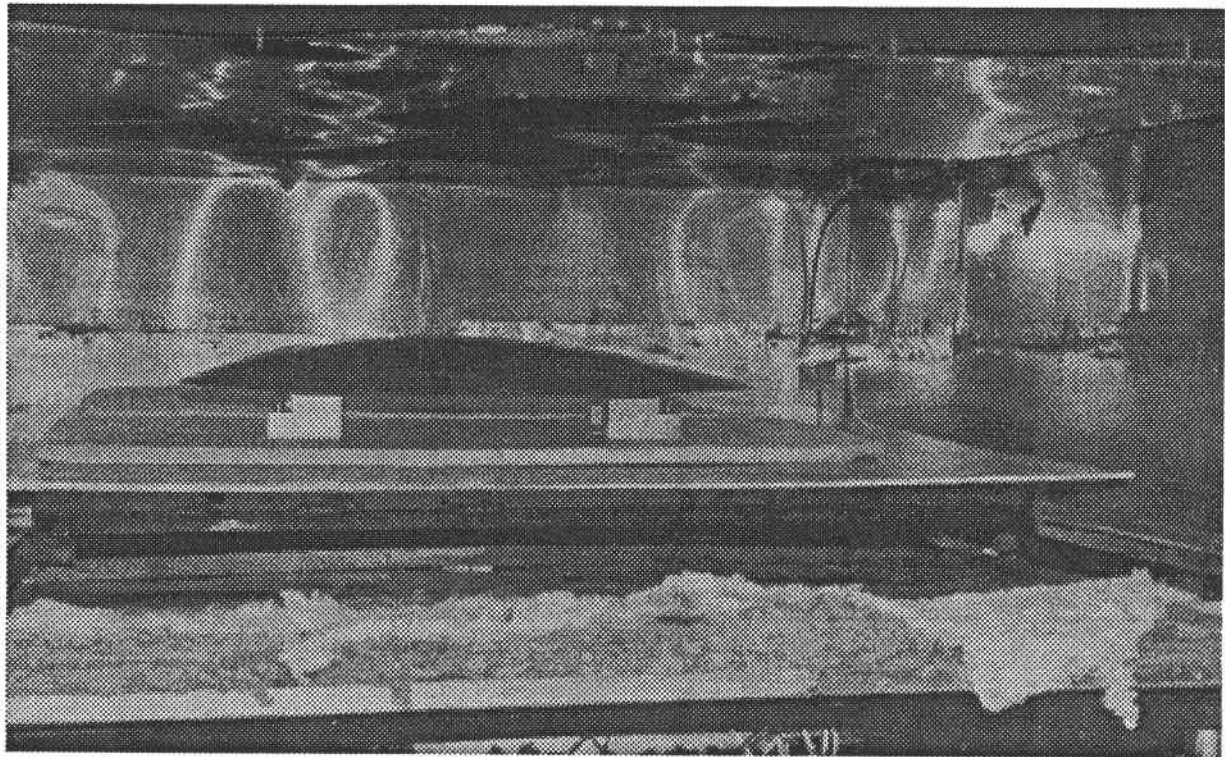


**Figure 50 Machined Off-Axis Mandrel for Film Casting.**

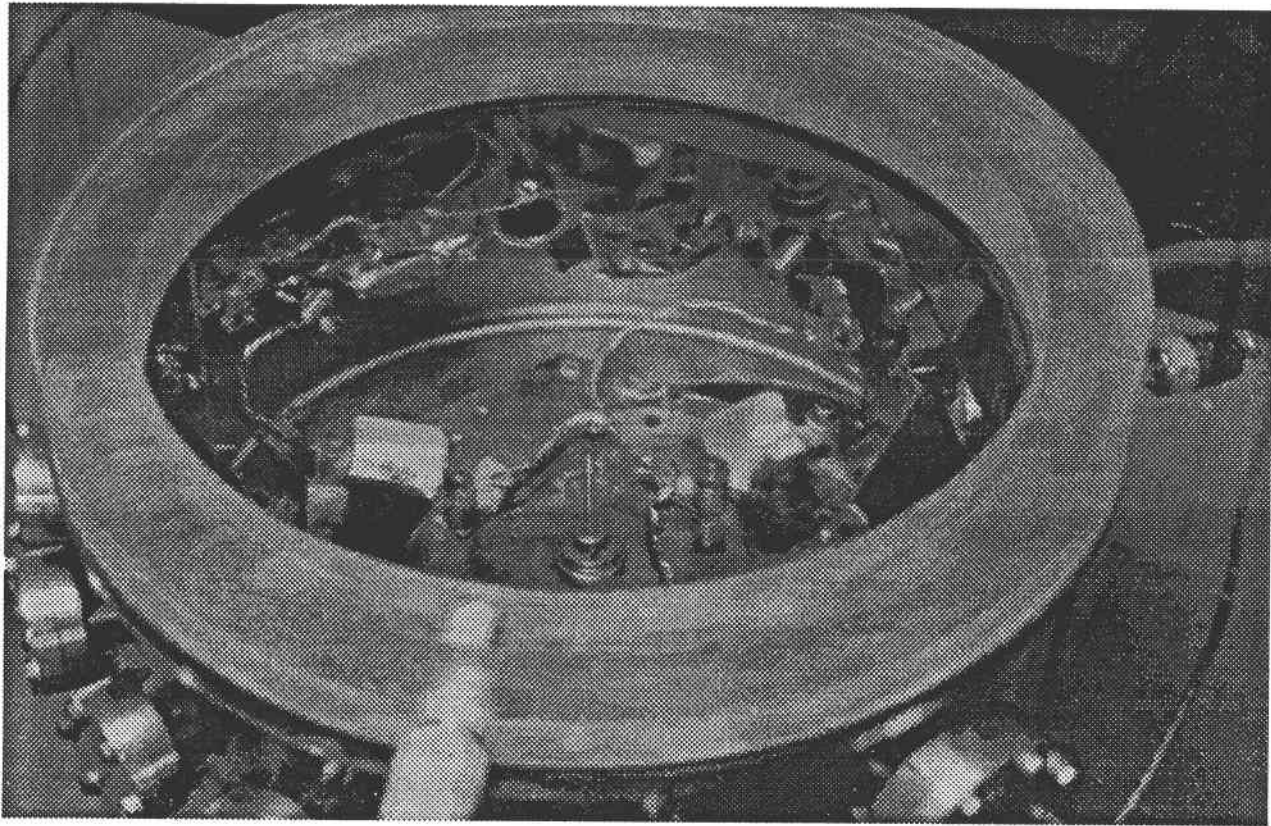


**Figure 51** Aluminum Vapor Deposition Chamber for Step and Repeat Process.

than are otherwise permissible.

**Preliminary Preparations:** The stainless steel chamber was thoroughly cleaned. Four high current electrical feedthroughs were mounted on the appropriate ports to provide filament power. A rotary feedthrough in the chamber rotates a shelter to cover the filaments so that the aluminum charge may be "pre-fused" without coating the target. This helps assure a clean coating. The use of three filaments provides a uniform, heavy aluminum film over the whole sample.

**Processing:** Before mounting the sample to be coated, the filaments are checked for burn-out or other damage, and replaced if necessary. Each filament is loaded with three or four aluminum wire "horseshoes". These are handled (like the filaments) with gloves and tweezers to avoid contamination. The cleaned test substrate is mounted, and the system

pumped.

Using the shuttle to avoid premature aluminization, the filaments are heated, in turn, to melt the aluminum over the tungsten coils. When the vacuum is as low as possible, each filament is brought to aluminizing temperature, and an opaque film produced. The filaments usually are good for three to five shots. When the chamber and contents are clean, the vacuum approaches  $2 \times 10^{-5}$ .

The sequential firing of three filaments causes signs of overlap, or discoloration in the coating in the areas where the filaments overlap. To eliminate this, all three were driven in series, simultaneously. This gives a very uniform appearing coating.

A polyimide film was cast on a five and one half feet diameter circular glass substrate and is shown in *Figure 52* mounted on an aluminum supporting ring. Also shown in the photo-

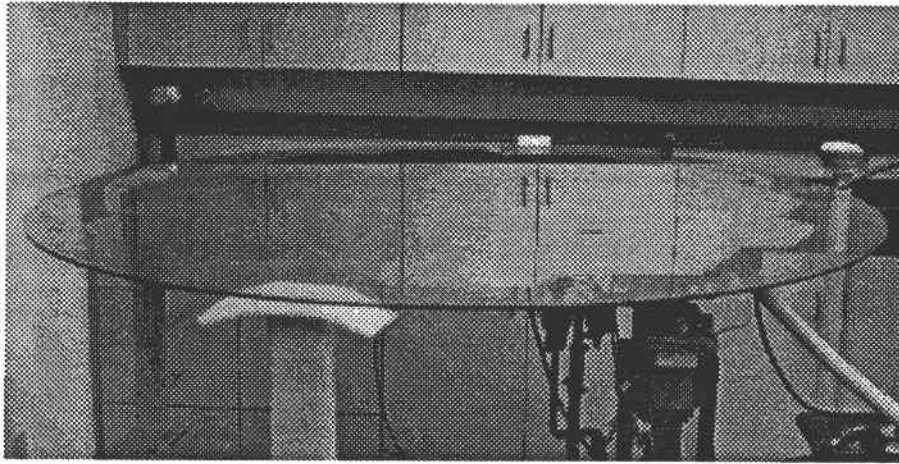


**Figure 52 Polyimide Film Mounted on Glass Substrate.**

graph in Figure 52 are hexagonal index markings that were drawn on the glass using a template on the side opposite the film to facilitate alignment with a hexagonal mask in the vacuum chamber, that reduces shadowing during the aluminization process.

The film, while still on the glass substrate, was installed on the vacuum chamber film side down, for initiation of the step-and-repeat aluminization process as described in Section 3.1. The photograph in *Figure 53* shows the film/glass sitting on the vacuum chamber subsequent to aluminization of the third hexagonal element. These photographs illustrate the step-and-repeat film aluminization process.

### 3.4.3 — Optical Testing Apparatus

The surface accuracy testing is done over an array of points on the surface of the mirror, measuring the slope error at each. *Figure 54* shows the geometry of the test. The test is performed near the center of curvature, which facilitates

adjustment and measurement, and obviates the need for parallel light, long optical benches, lasers, and beam splitters. The slope error is measured directly by means of a theodolite, mounted on an adjustable slide. A point source of light is placed on the optical axis, *inside* the center of curvature, and the conjugate

focus is observed, *outside* the center of curvature. Based on the geometry of the mirror, either a spheric, or the desired parabolic shape, the location of the conjugate focus is easily calculated for various points on the mirror.

**Geometric Characteristics:** Assuming a perfect mirror, any given point on the mirror at distance,  $y$  (off axis), will bright light from the source at  $F_1$  to a focus at  $F_2$ . Since the point  $F_2$  is easily calculated from the equation of the (perfect) mirror, the angle  $\phi$ , of the observed point is also easily calculated. When the actual focus,  $F_3$  is found, the difference between the observed angle,  $\phi^1$  and the expected angle,  $\phi$

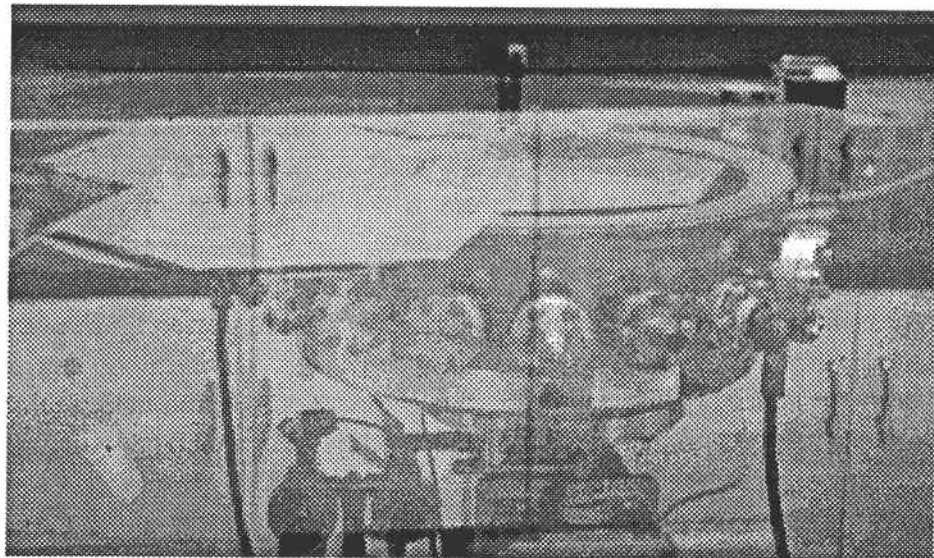


**Figure 53 Aluminized Sections of Reflective Polyimide Mounted on Vacuum Chamber**

immediately gives the third angle of the triangle  $F_3$ - $P$ - $F_2$ . By the laws of reflection, this angle is exactly twice the slope error at point  $P$ .

The difference between the angles  $\phi$  and  $\phi_1$  can be readily observed by the theodolite at  $F_3$ , or the angle  $2d$  can be calculated by geometry from the radius of curvature,  $R$ , the coordinate of point  $P$  ( $y$ ), and by measuring the distance  $F_3$ - $F_2$ . The two methods can be used simultaneously to provide a check.

**Apparatus Setup:** The theodolite is mounted on an x-y table, to provide for measuring the distance  $F_3$ - $F_2$ , using the longer axis; and to provide location of the theodolite on axis, using the shorter travel of the y-axis. The x-y table is very rigid to provide repeatable location, and is provided with dial readout to .001 inch and scale readout for inches and tenths. One dial evolution is .050 inch travel.

The adjustment of the test requires that the x-axis of the table be parallel to the optic axis of the mirror. This is achieved by adjusting the relative locations of the mirror and the x-y table. The axis of the mirror passes through the center of the theodolite, so that x-axis translation maintains the theodolite on the mirror axis. In the case of irregular surface errors, a combination of x and y translations may be needed to locate the aberrant focus at  $F_3$ . The

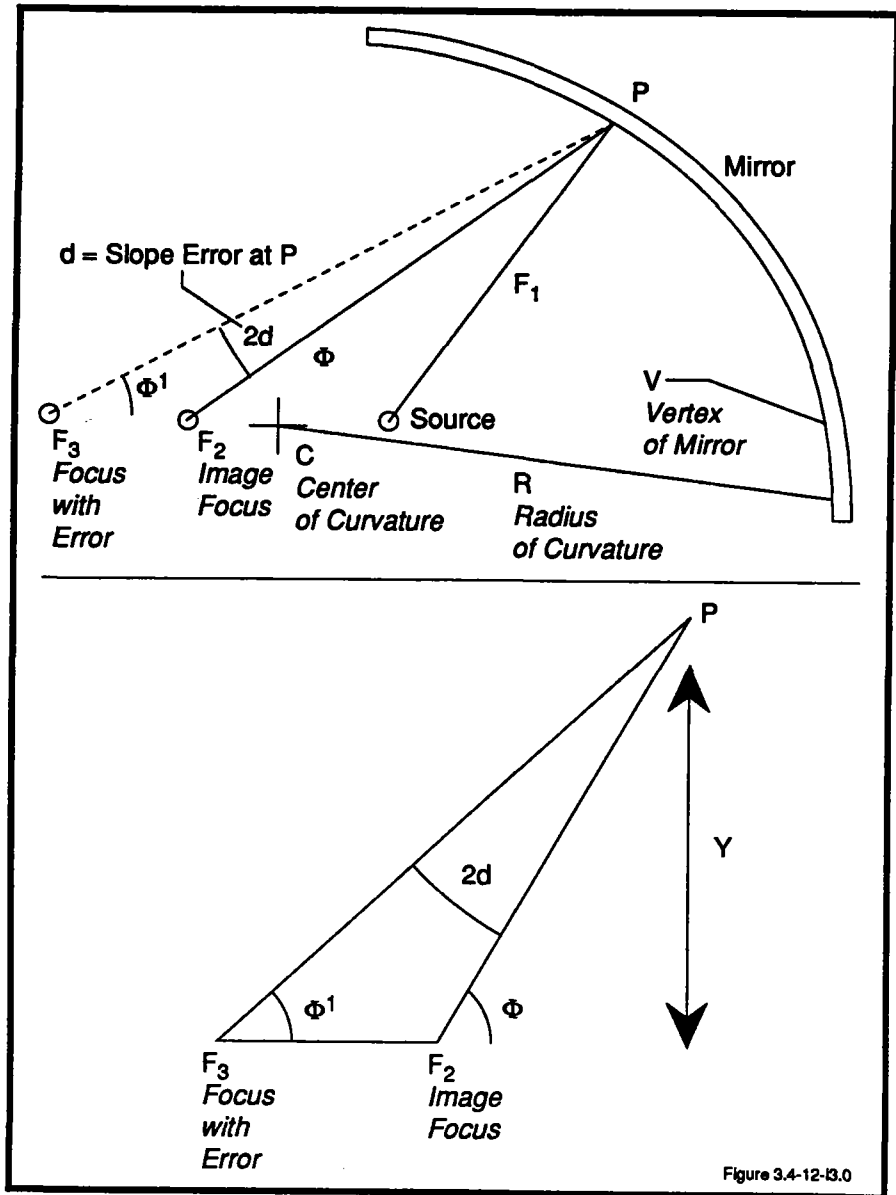


Figure 54 Geometry of Optical Testing of Primary Mirror

reduction of data in this case is facilitated by the ability to measure  $x$ ,  $y$ , and  $\phi$  precisely.

The point source of light is located on the optical axis, inside the mirror's center of curvature. The theodolite is used to center and adjust the position relative to the x-axis, and a steel tape is used to measure the distance from the source to the theodolite and to the mirror. The theodolite is also used to check these distances by angle measuring techniques and the geometry of the setup.

To localize the points on the mirror being measured, several methods are possible as indicated below:

A. Physical marks on the mirror, i.e., with ink or paint,

B. Purely by coordinates, that is, using length and angle measures to identify each point, and

C. A physical grid, or mask, consisting of small holes in an opaque material to define and identify points.

Method A is rejected here because of the danger to the thin film and the need to repeat a tedious measure-and mark process for each mirror tested. Method B is useful, but rejected here because of the uncertainty as to mirror accuracy and the possibility of confusion. Method C is selected and implemented by means of a plastic screen with a square array of holes, placed in front of the mirror under test. The size of the holes provides adequate visibility and location of the point being measured, while eliminating contact with the thin film. The sensitivity of the test can be appreciated by the following example:

- $R = 96''$
- $F_1 = 80''$  (source-mirror distance)
- $F_2 =$  approximately  $120''$  (theodolite-mirror distance).

A movement (along x-axis) of 2 inches corresponds to a slope error, at P, of about .096 degrees, or 346 seconds, or 1.7 millirad. Since the x-y table can be located to nearly .001 inch, and the theodolite is capable of near 1 seconds, the precision of measurement is capable of meeting the expected errors in the mirror.

### Film Thickness Measurement

The thickness of thin films (less than .001 inch, 1 mil) is difficult to measure with ordinary micrometers or dial indicators. For example, a very fine dial indicator may read to .006" total, with divisions at .00005" increments (50 millionths). A film of 1/2 mil thickness, gauged

between a dial indicator and a surface plate would read .00050 inch, accurate within  $\pm 10\%$  or better if functional divisions were estimated. Ideally, the dial indicator is used as a comparator against a standard in order to get the best accuracy. With a micrometer, it is difficult to get uniform force and avoid twisting the film between the anvils.

A simple, accurate interferometric method is shown in *Figure 55*. Two optical flats are used, with the upper one having an edge contact with the lower. The film sample under one edge establishes a narrow air wedge between them. As shown in the figure, fringes can be observed where the two reflected light rays interfere, at integral multiples of half the wavelength ( $\lambda/2$ ) of the monochromatic light used. These fringes look like those in the top view, that is, alternating bright and dark lines. These are easily photographed for a permanent record.

A useful light source for this test is a mercury vapor light, filtered to isolate the green, 546 nanometer wavelength. A half wavelength is then equal to a difference in the optical path of the air wedge, of 10.75 millionths of an inch. As an example, a specimen of film was used and 45 fringes counted (fractions were ignored, but may be estimated). Then,  $10.75 \times 10^{-6} \times 45 = 4.838 \times 10^{-4}$  inches, or just under 1/2 mil to within about 2%. The limits on accuracy are primarily in counting fringes and fractions thereof, and in application of pressure to the top flat to compress the film. Although *Figure 55* shows the use of two common shop type, round flats, square or rectangular flats work quite well; indeed, two pieces of selected plate glass also work, although the fringes may not be straight. It is interesting that this kind of test can be done with such accuracy from simple materials, as opposed to very expensive mechanical means. The reason, of course, is that the light source provides the precision, repeatable length standard, not a precisely made machine.

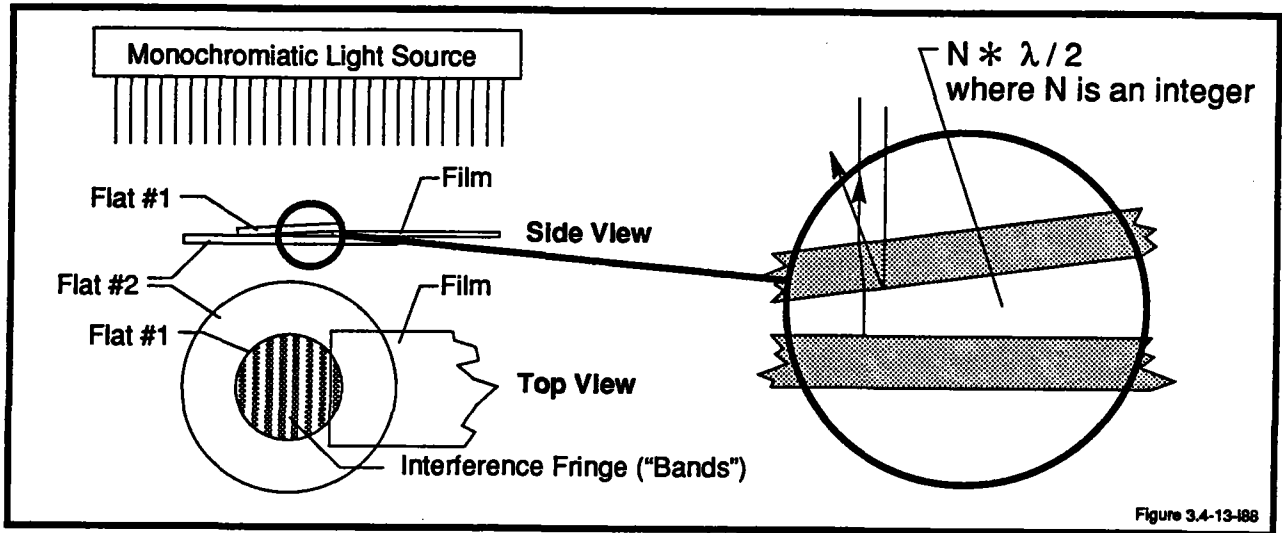


**Figure 55 Thickness Measurement of Polyimide Film.**

### 3.5 — Thin Film Heliostat for the Solar Laboratory

An additional effort was added to the original contract. The objectives of the additional work were to: 1. Demonstrate the capability to spin cast and coat large polyimide reflectors, 2. Develop, fabricate and deliver spin cast reflectors for use as a heliostat at the Phillips Solar Lab. The work was included in Task 4 of the original effort as shown in *Figure 56*. The work performed enabled the advancement of casting and reflective coating large one piece concentrators. The procedures developed as a result of this program will be used in future programs for fabrication of concentrators for solar thermal propulsion. The following section describes the work that was performed under the contract modification.

#### 3.5.1 — Thin Film Casting Equipment Design and Fabrication

The equipment required to cast, cure and silver the thin film membranes included a clean room

ventilation system, a curing oven, and a spin table. A large curing oven was designed, fabricated, and installed for the casting and curing of the polyimides. A clean room ventilation design was included in the curing oven. The existing spin table mechanism was modified and enlarged to enable casting of large membranes.

The oven has dimensions of 21' x 21' x 6' has a maximum temperature capability of 550°F. The oven's construction is modular in order to facilitate possible future expansion and portability. The oven uses a forced convection heating system and includes a fresh air exchange system to reduce off-gas buildup. *Figure 57* is a floor layout of the SRS High Bay area where processing occurred. Complete design details of the oven are shown in *Appendix B*. The oven and spin mechanism used for the effort is shown in *Figure 58*.

#### 3.5.2 — Heliostat Structural Design

The design of the heliostat support structure included both the tensioning structure for the

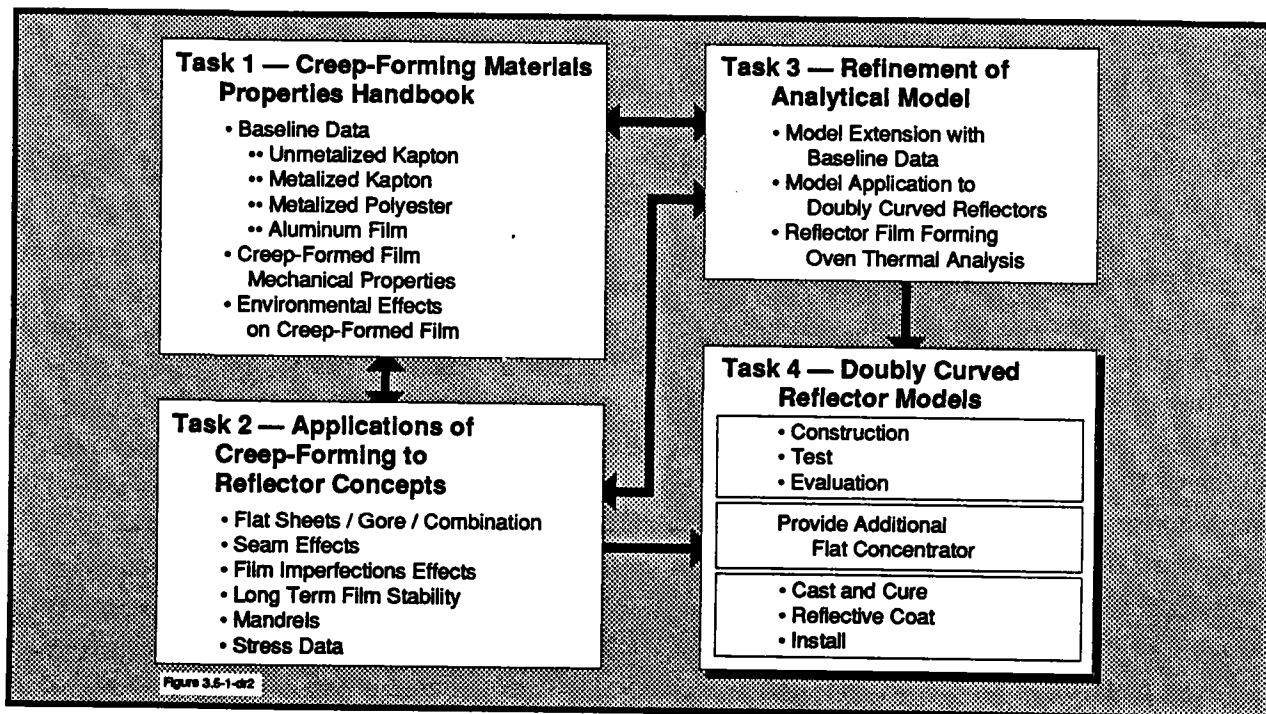


Figure 56 Original Phase II Task Flow

stretched membrane and the interfacing of the tensioning structure with the heliostat structure located at the Solar Laboratory. Originally a design was made to interface with the heliostat hub located at the Lab. During the course of the effort, the heliostat was upgraded at the Lab. The original designs presented in this report are for the hub design heliostat that is currently not in use. A revised design was made to interface to the new heliostat at the Solar Lab.

### 3.5.2.1 — Design of Triangular Segment Support Frame

The design of the triangular tensioning structure was developed by fabricating scale models of the designs and analysis of the full scale layout. Testing of the models was performed at SRS's facility. The passive tensioning design was fabricated and successfully used to tension and support the membranes cast in the laboratory. The following section describes the models that were built and the final design selected.

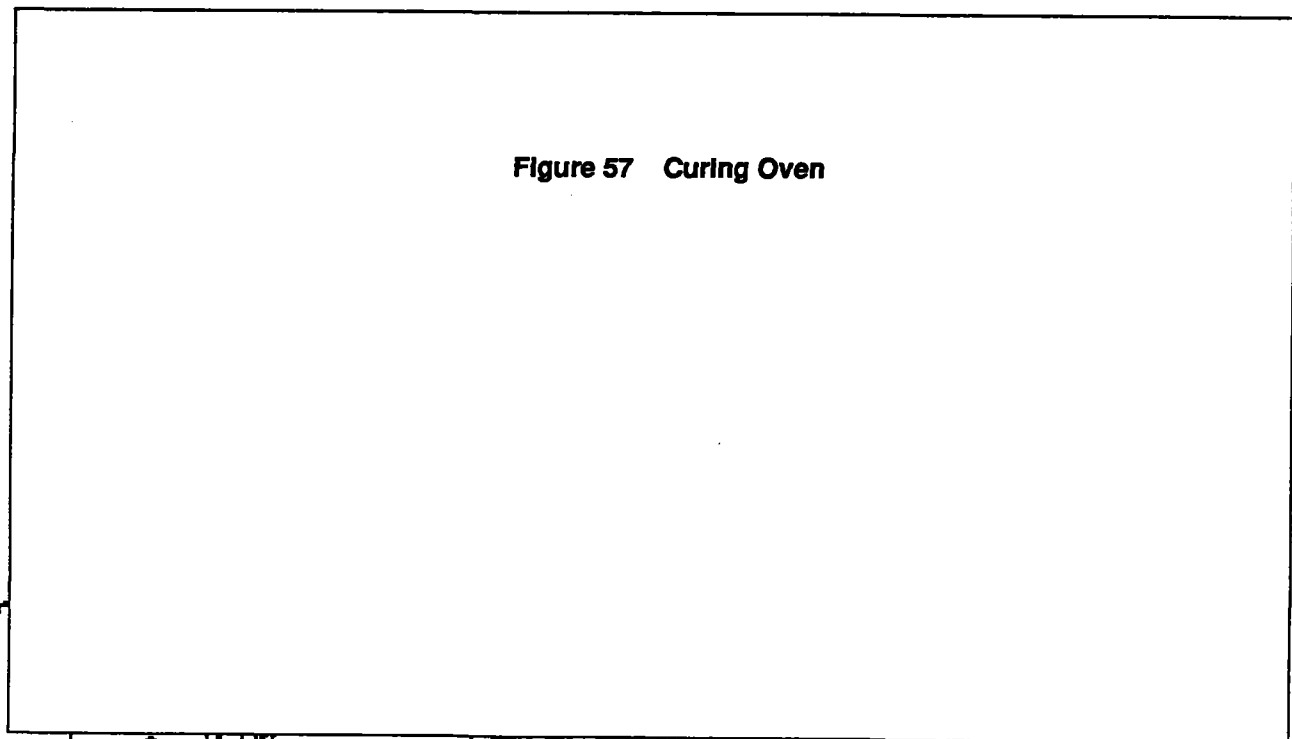
Several design options were considered and are presented in *Appendix C*. A scale model of a triangular segment was constructed using a Option A design shown in *Figure 59*. The model was built using 1" thin-walled aluminum tubing sections 3 feet long, as the side-rails, and ¼" foam-board as the plenum rear plate. A wide fillet of flexible silicon adhesive was used as flexible seal boot between side-rails and back-plate, to seal the plenum. A ½ mil polyimide film was stretched under very low pre-tension and epoxy-bonded to the side-rails of the assembly, while the side-rails were held bowed inward by the turnbuckles. After epoxy-hardening, the turnbuckles were driven outward, to straighten the side-rails and tension the film. Satisfactory, uniform appearing tensioning was obtained in the central region, out to about 5" from each corner. Then, small jack-screws were installed, at each corner, between points about 3" from each end of each

side-rail. Actuating these jack-screws provided satisfactory tensioning out to within 2" of each corner. It appeared that the concept of hinge-joints at each corner of the frame does not allow satisfactory tensioning of the film in the corner regions.

A scale model embodying the general concept of Option 3D as shown in *Figure 60* was built, using 1" thin walled aluminum tubing sections 3' long, as the side-rails, bonded with silicone adhesive to a ¼" foam-board plenum rear plate. The tensioning concept used is shown in *Figure 60*. Five push-screws and five pull-screws were distributed along each side-rail. The pull-screws were actuated, the silicone (acetic cure) film-bonding adhesive was placed, and the frame was brought down onto the polyimide film, stretched on, taped to flat plywood at rather low pre-tension. Upon hardening of the silicone adhesive and trimming of the film, the pull-screws were released and the push-screws were activated. Satisfactory and uniform-appearing tensioning was obtained over the full expanse of the film. The compliant nature of the silicone film adhesive appeared to be advantageous; however, curing was incomplete and the bond began to fail, limiting attainable tensioning.

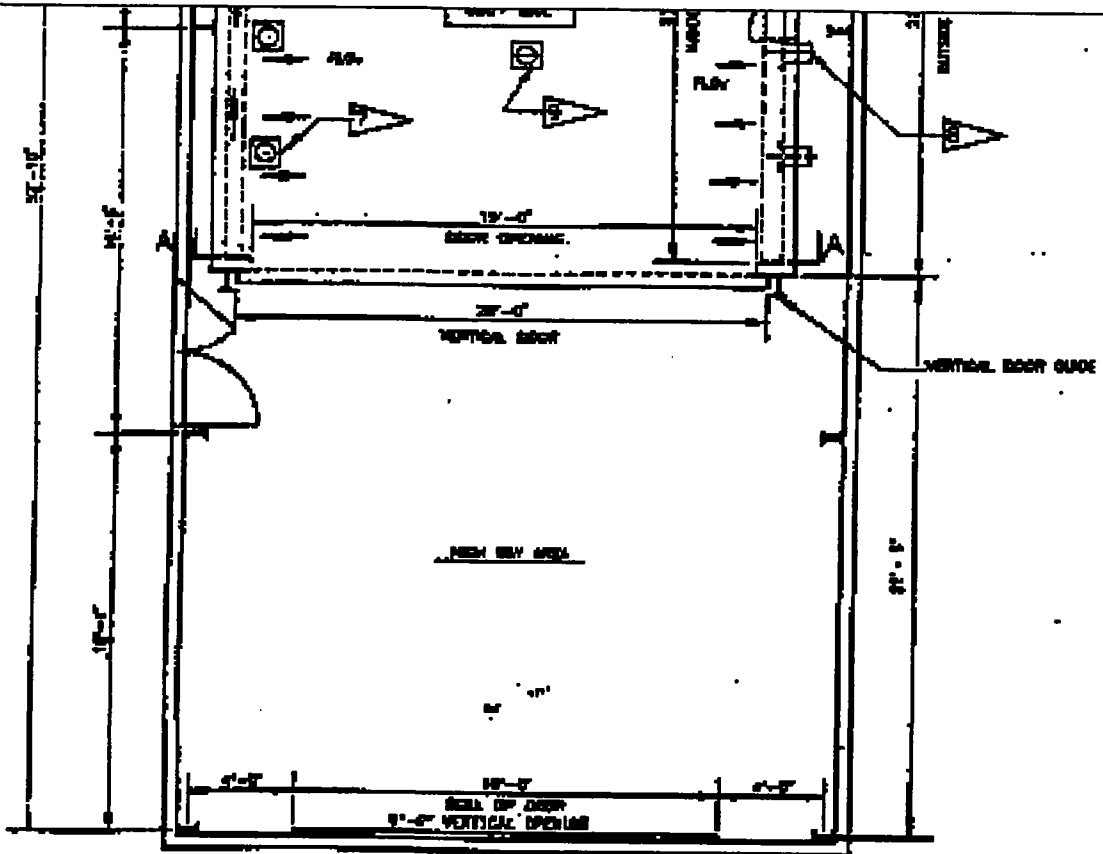
Both of the preceding models were taken outdoors on a moderately windy (estimated 15 knot gusts) day, and sunlight was reflected from them onto a wall 85' distant. Option 3D performed slightly better than Option A. Their resistance to rippling from wind eddies was fair, but their tendency to go concave under steady wind load was poor, due to leaky plenums. This test was inconclusive, as to the need for a wind-shield. There was some concern about thermal warpage of the side-rails of a heliostat triangular segment, and thermal bulge of the honeycomb backing-plate of the wind-resisting behind-film air plenum chamber. The significance of bulging of the plenum

Figure 57 Curing Oven



RETURN AIR DUCT

NETS



ELECTRICAL CONTROL PANEL



PLAN VIEW

# Back of 11x17 Foldout

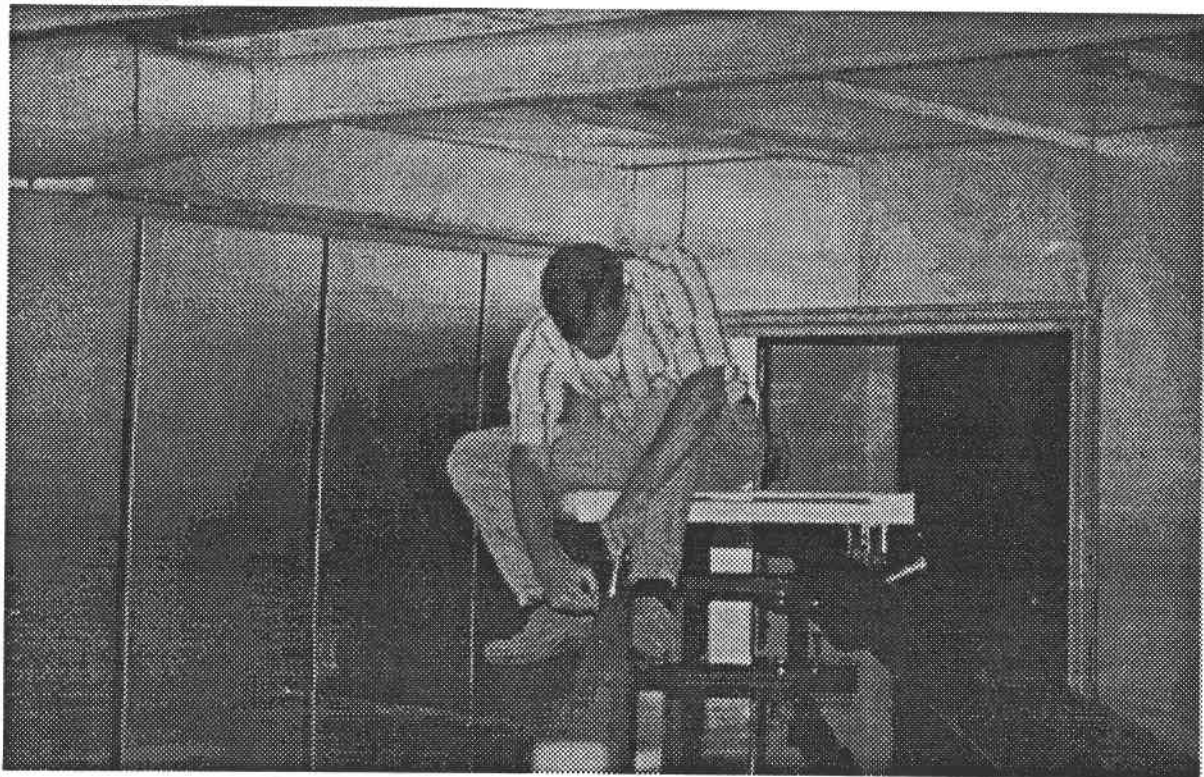
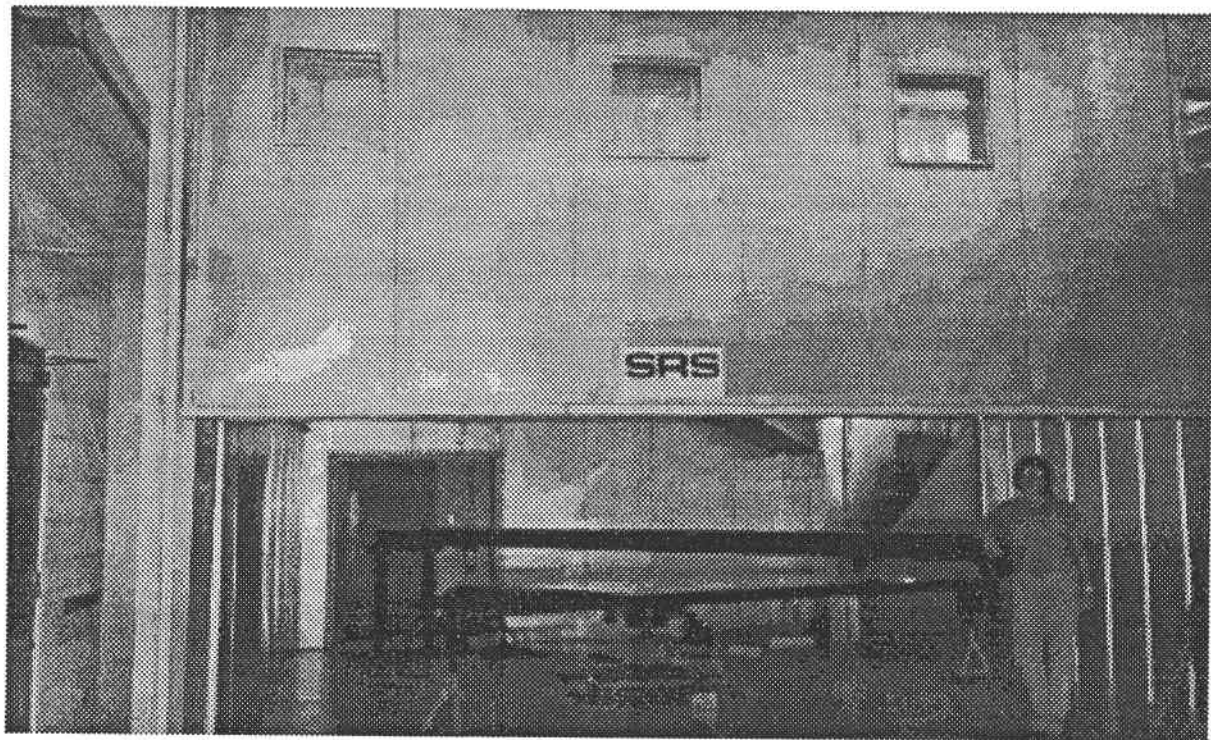


**Figure 58 Spin Table and Track System**

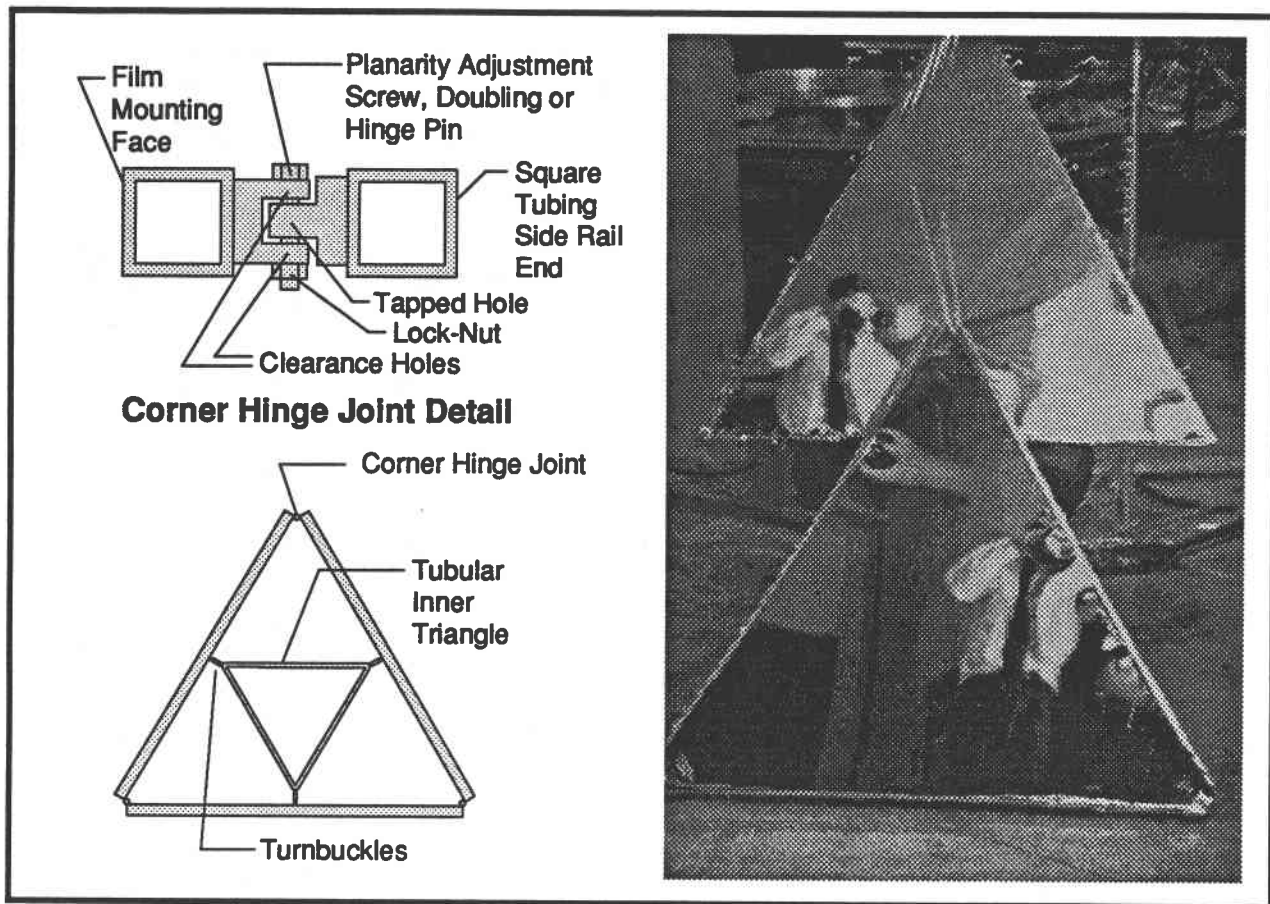


Figure 59 Scale Model of Helioostat

back-plate is that it sets a lower limit on the depth of the plenum, and the ability of the plenum to dampening wind-induced ripples is a very sensitive function of plenum depth. Also, a deep plenum can cause heliostat focusing as a result of temperature changes in the plenum air. Also, bulging of the plenum back-plate would transfer directly into bulging of the film, because of the sealed nature of the plenum as required to resist steady wind loads.

As noted above, the Option 3D model used a compliant silicone film-bonding adhesive of air-activated (acetic) cure. Its compliance seemed to have potential value, but its air-activated cure would require excessive time for cure completion, in the geometries of interest. Internally catalyzed (2-component) silicone, RTV609, was tried for the same application. It was found to bond fairly well to heat curved polyimide, but not to

silvered polyimide, nor to aluminum. Priming the silvered polyimide and the aluminum with a thin layer of air-cured (acetic) silicone adhesive, allowing this layer to cure fully, then applying RTV60, assembling the joint, and allowing the RTV60 to cure, appeared to produce a strong, compliant bond between aluminum and silvered polyimide.

A scale model of the most likely configuration was designed for fabrication and evaluation. *Figure 61* depicts the scale model fabricated. The complete design of the segment is shown in *Appendix D1*. The use of the spring-rail mounting of the films is considered necessary in order to maintain film tension reassembly constant in the presence of large humidity coefficient of film strain, substantial thermal expansion mismatch with aluminum structure, and uncertain ambient-temperature creep of

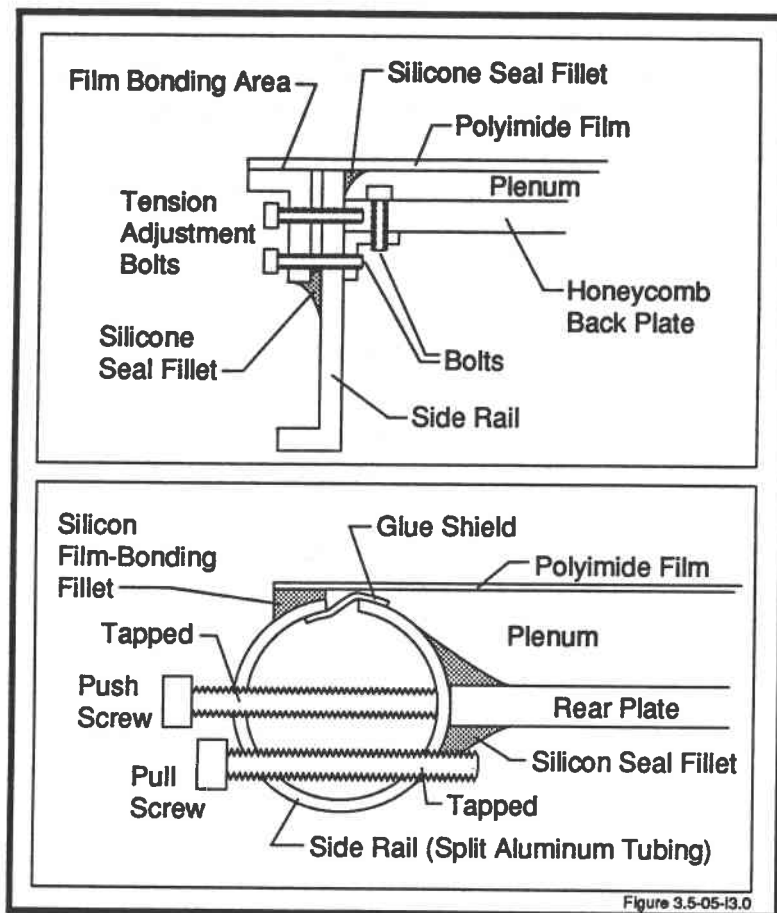


Figure 60 Scale Model of the Option 3D Concept

film over the operational lifetime. The design offers the back-up possibility of after-installation boosting of film tension without removing the mirror triangular segments from the heliostat. This is accomplished by inserting tension-booster bolts into pre-drilled/tapped holes in the side rails, working only from the underside of the heliostat.

The aluminum mock-up was made to study (1) the attachment of the aluminum channel side rail to the honeycomb back-plate, (2) the attachment of the film-tension-control spring-rail to the channel side-rail, (3) the means of pre-tensioning this spring-rail, and (4) the use of epoxy filleting to attach the film to the spring-rail. Use of epoxy filleting rather than face-bonding allows the epoxy bond to be placed in several sections, at different times,

whereas a face-bond must be done simultaneously in its entirety. Also, the filleting concept is less likely than the conventional face-bond concept to produce epoxy run-out and consequent non-planarities as the spring-rail rotates in response to hygroscopic and thermal expansion/contraction of film. Epoxy agents to attach the film to the tensioning structure were investigated. Shell Epon 828 resins with two candidate hardeners were evaluated. The hardeners Epon V40 and V50 were selected for evaluation based on discussions with the technical expert at the Shell Chemical Company. A 50/50 mixture of Epon 828 with V40 was selected as the best material for bonding the film to the structure. The material was cured at an elevated temperature of 350° F for 1 hour. Longer cure times at lower temperatures will be used for the full

scale heliostat. Fillers to thicken the epoxy were also tested. CABOSIL and aluminum oxide powder were mixed with the epoxy. CABOSIL was selected to be the best filler for the bond segment.

The final design of the tensioning structure is shown in *Appendix D2*. The tensioning structure and honeycomb aluminum backplate are depicted in *Figure 62*.

### 3.5.2.2 — Heliostat Interface Designs

The thin film heliostat is approximately the same size as the existing heliostat, therefore, the loads on the main heliostat structure were not expected to be increased by the modification. Therefore, the approach used in this effort is to design separate film support frame to which the film will be attached. Appropriate struc-

tural interfaces and adjustments were designed to attach the film support frames to the existing heliostat structure. Analysis of the existing structure was performed to identify hard points as the structure for attaching the film frames.

The major design concerns that were addressed for the design of the film frames were stiffeners, thermal effects, and joint design. Very small deformations in the support geometry can cause large distortions in the film. Therefore, the frames were designed stiff enough to support the film and wind induced loads with negligible deflection. Both the flexural and torsional stiffness are important. High flexural stiffness was required to keep the frames from deforming due to wind loads. Torsional stiffness was required to keep the frames from twisting.

After careful consideration of the modification to the existing heliostat structure, it appeared that a considerable amount of both design time, fabrication time, and installation was be required. At best, there is doubt that the modified substructure could be adapted to a thin-film reflective membrane system of mirrors. SRS designed a truss type structure to be installed on the spare hub. With this hub, the truss structure could be installed on top of the hub with an added support plate, clips, and fasteners. The existing bolt holes along the periphery of the hub could be used to distribute the truss loads. The truss has a significantly higher structural inertia to wind loads. The new truss structure could be fabricated in sections and installed to the space hub, leaving the existing mirror intact for continued use. The "droop" at the outer extremes of the existing mirror could be improved, once removed from the pedestal and brought inside for modification. This may not be required if the truss structure is satisfactory.

A hexagonal shaped heliostat structure is depicted is shown in *Figure 63* and *Figure 64*. To provide the necessary stiffness, a truss type beam

is required to prevent deflections normal to wind loads. The design accommodates wind loads of 30 mph (44 fps) with transient gusts to approximately 42 mph. A thin film passive tensioning method was designed that acts like a fixed spring and which provides constant tension to the membrane, regardless of changing temperature, humidity, and wind conditions.

A new heliostat was installed at the Solar Lab after the design was completed for modifying the hub of the original heliostat. SRS designed the interfaces for the new heliostat structure installed by Applied Thermal Systems (ATS). The *Appendix D2* depicts the final design for interfacing the stretched membranes to the heliostat structure.

### 3.5.2.3 — Windshield Discussion

The design of a windshield for the stretched membranes can be designed primarily to reduce the wind loading effects on the reflective surface. Originally it was anticipated to use an additional spring on the film tensioning structure. This design caused interfacing problems for assembly currently designed. The windshield would also be difficult to remove from the structure if desired. An alternative design was to make the windshield a separate structure above the tensioning structure and membrane. This method allows for the removal of the windshield if desired. The material used for the windshield needs to be as transparent as possible. The candidate material for a windshield is a transparent polyester with an acrylic UV resistant overcoat. The design of a windshield was out-of-scope of this effort. Subsequent studies should address the use of a windshield.

### 3.5.3 — Thin Film Process Development

The procedures developed under this effort demonstrated that thin film polyimides can be cast into large one piece concentrators. Reflec-

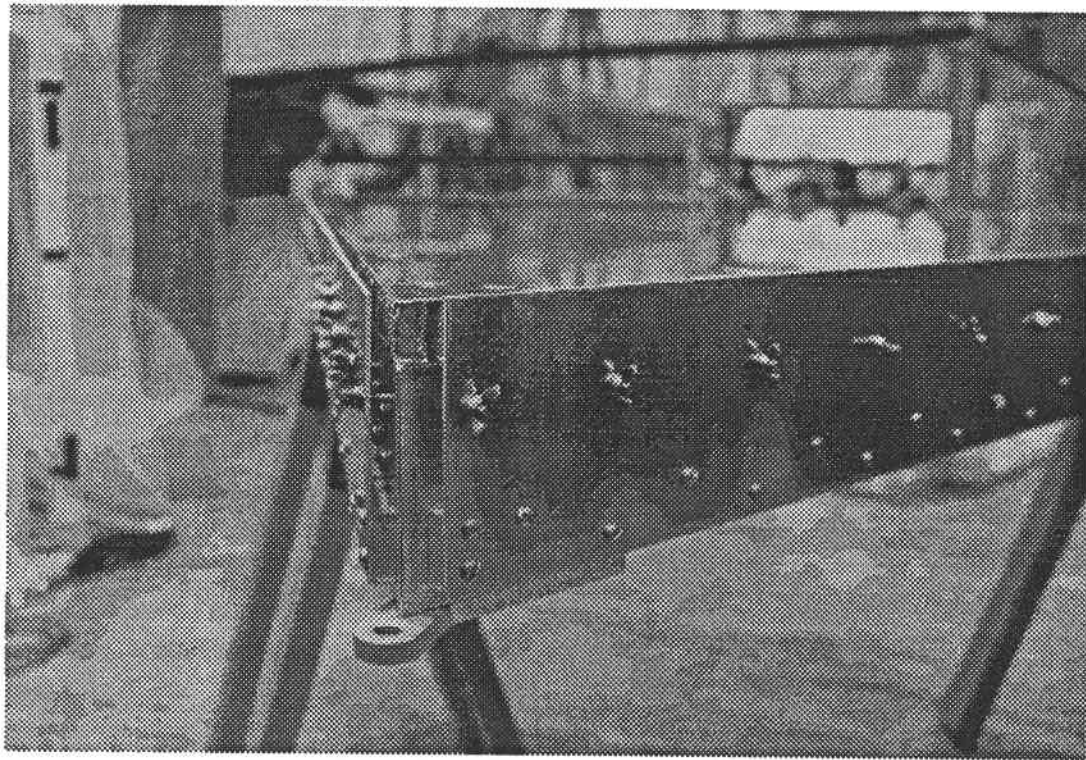
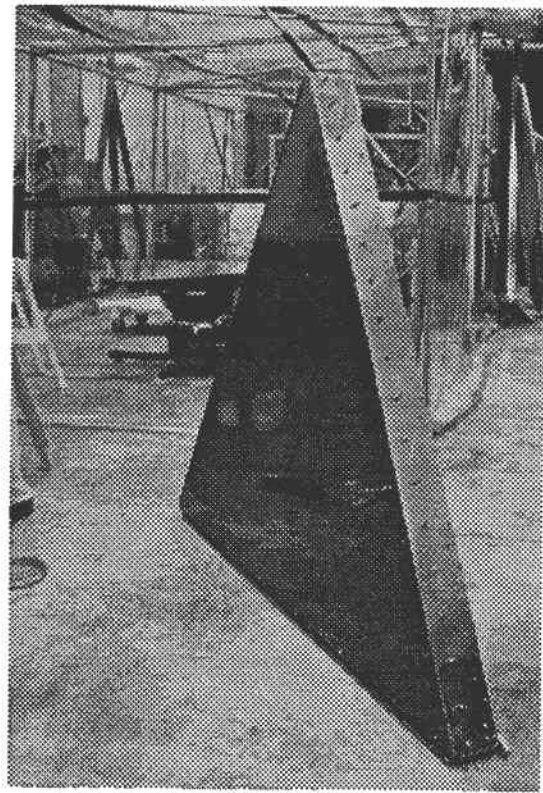
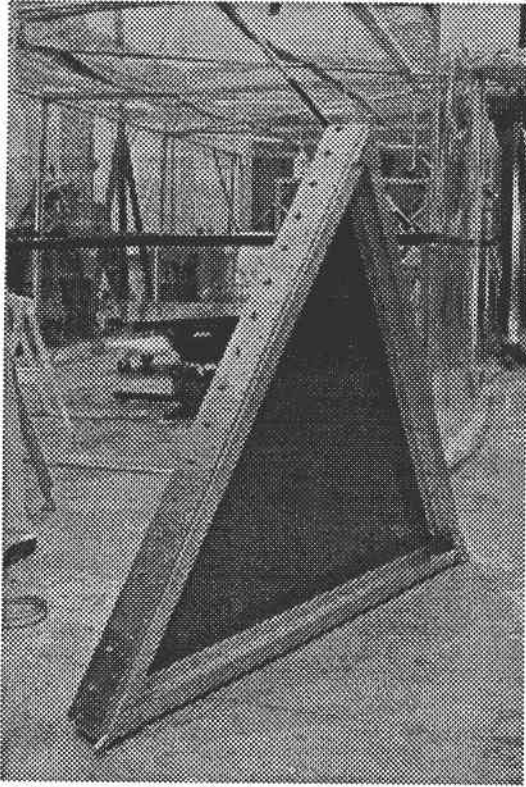


**Figure 61 Heliostat Test Article**

tive coating processes were developed to chemically silver the thin films in a cost effective manner. The processes and technologies for casting and coating larger diameter films were refined under the effort. The complete fabrication procedures were demonstrated by cast-

supplemented with dedicated sprayers for sensitizer, detergent, and rinse-water. A line water-demineralizer was installed. Suitable protective clothing was obtained.

Uniform reflective coatings of good specularity and fairly good adhesion were ob-

tained on polyimide film, using the Peacock H300 silvering system. The Peacock H30 system was also evaluated, but it produced inferior results. It was concluded that the streaking problem previously



Figure 62 Tensioning Structure

ing large diameter thin film segments and mounting the segments on the tensioning structures fabricated. The following section discusses key issues that were addressed in the research.

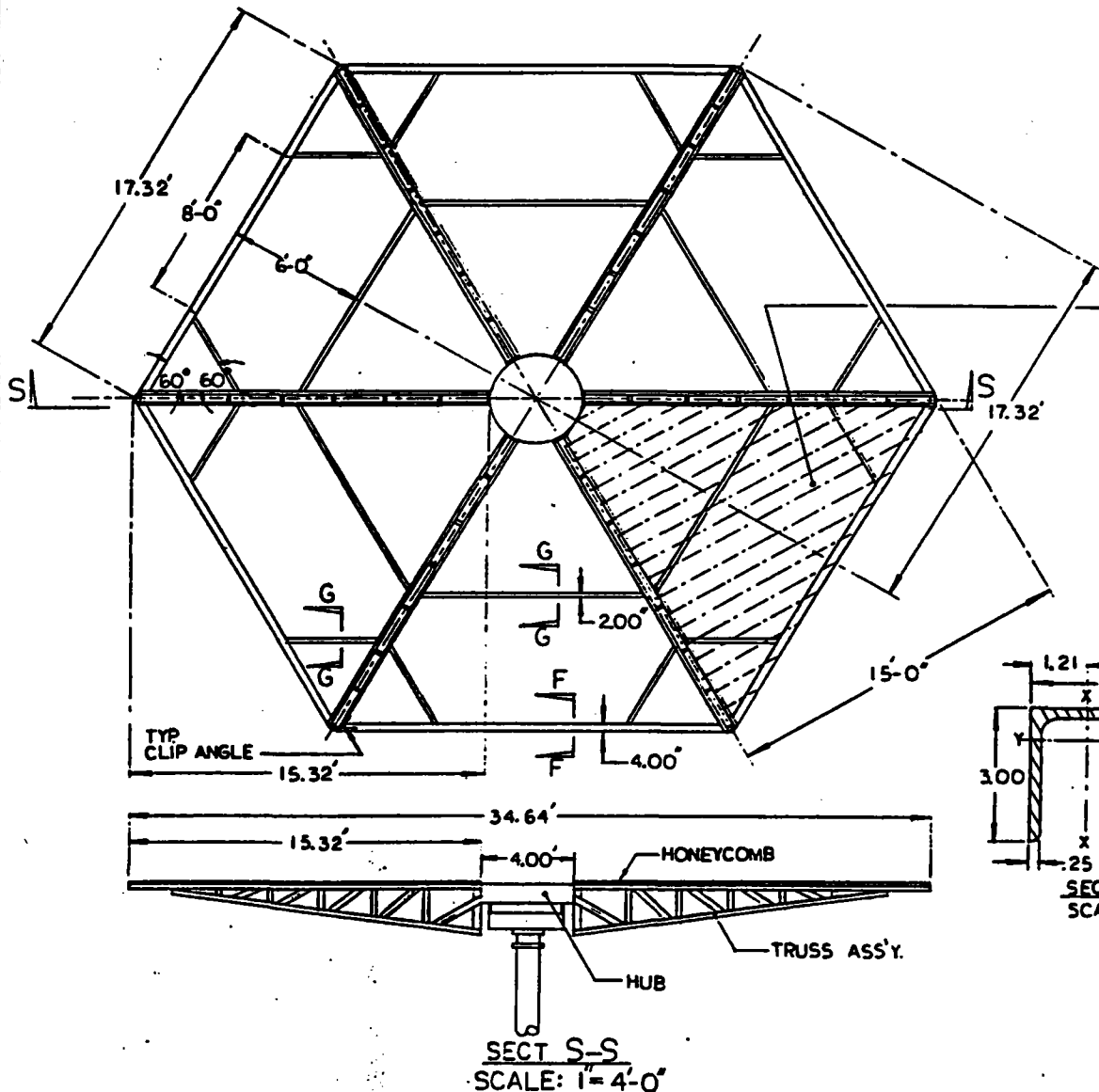
### 3.5.3.1 — Evaluation of Electroless Spray Silvering

In order to better evaluate electroless spray silvering as a candidate reflective coating for the film heliostat, a silvering station was designed and set up. A booth was constructed of clear plastic film stretched over a PVC conduit frame, with an exhaust fan connected to the facility exhaust system. A shower-curtain backing, drain vessel, and adjustable rack for holding films to be silvered, were installed. The existing silvering equipment was installed,

experienced with this technique was probably partially due to incomplete rinse-off of the sensitizer before applying the silver, and due partly to the fact that the silvering spray-gun had been used to apply the sensitizer, thereby contaminating the spray-gun. It became possible to silver 1 meter by 1 meter sections of polyimide with no significant streaking. This was achieved without use of the rapid flush-off of silvering solution running down over previously-silvered areas, which had previously been considered necessary, and which would have posed a major concern for silvering heliostat segments.

Adhesion of the silver coating, adequate when dry but rather poor when subsequently exposed to water, remains an area of concern. In one experiment, a silver coating on

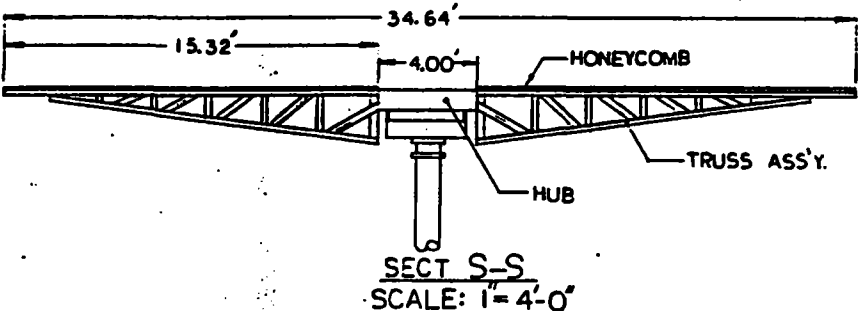
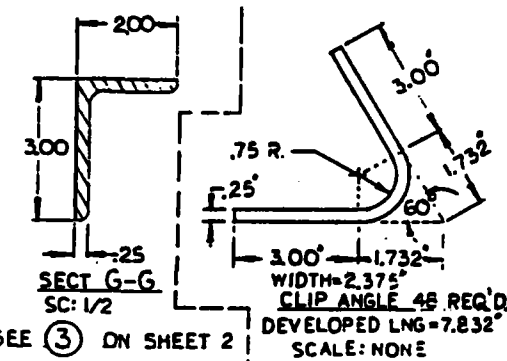
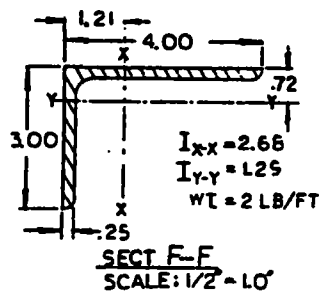
PART NO.	REV	REVISIONS				
		ZONE	SYM	DESCRIPTION	DATE	APPROVAL



ALUM. CORE  
HONEYCOMB  
2" THK, 6 LBS/FT<sup>3</sup>  
TYP. 6 PLS.

**NOTES**

- STRUCTURAL WEIGHTS**  
 EACH TRUSS 185 LBS ± 6 = 1,110 LBS  
 EACH HONEYCOMB SECTION 130 LBS ± 6 = 780 LBS  
 CROSS BRACING TOTAL = 378 LBS  
 EACH THIN-FILM TENSIONING STRUCTURE 65 LBS ± 18 = 1,170 LBS  
 TOTAL WT. OF STRUCTURE = 3,438 LBS  
 EACH TRUSS MUST SUPPORT 1/6 TOTAL WT. = 573 LBS
- TOTAL EXPOSED SURFACE AREA TO WIND LOAD, AS ASSUMED TO BE NORMAL TO SURFACE**  
 AT 30 MPH, F = 2.525 LBS/FT<sup>2</sup>  
 AT 40 MPH, F = 4.4489 LBS/FT<sup>2</sup>  
 TOTAL SURFACE AREA = 700 FT<sup>2</sup>  
 TOTAL FORCE AT 30 MPH = 1,970 LBS ± 8 = 328 LBS  
 TOTAL FORCE AT 40 MPH = 3,500 LBS ± 6 = 583 LBS  
 EACH TRUSS SHARES 1/6 OF TOTAL WIND LOAD



99

Figure 63  
Truss Assembly  
(Concept No. 2)

APPLICATION				DO NOT SCALE DRAWING		SIGNATURE		DATE	
THIS ITEM IS USED ON SUBASSEMBLIES				UNLESS OTHERWISE SPECIFIED DIMENSIONS ARE IN INCHES. TOLERANCES ARE		G.C.C.		1-21-91	
DRAWING NO	PER ASBY	NO. OF ASBYS	TOTAL	JUN =	JULY =	P. GIEROW		TITLE	
				JULY =	AUGUST =	DR. STRESS		TRUSS ASSEMBLY	
						J. MOORE		CONCEPT NO. 2	
						APPROVED BY		SIZE CODE IDENT. NO.	
								C 9V959	
								DWG. NO.	
								5289-02-800-2	
								REV	
								SCALE NOTED	
								SHEET 1 OF 2	

polyimide film, given a protective overlayer of soluble polyimide, came off in its entirety with the overlayer, when immersed in water (in this case the overlayer was excessively thick, so that the powerful drying-shrinkage of the soluble polyimide created a high shear stress). A sample of silvered polyimide was sent to Aerospace Corporation in order to measure the silver thickness. The average silver thickness was reported to be 1,728 angstrom.

The reflective coating of the polyimides was done by using a silvering solution supplied by Peacock Laboratories. The film is silvered before being attached to the tensioning structure. A sensitizer is used to fully "wet" the thin film before applying the silver solution. The "wetting" of the film is necessary in order for the silver to adhere to the polyimide. After the film has been sensitized the film is fully washed with deionized water. The silver solution is then applied with a dual nozzle spray gun. One nozzle of the gun sprays a reducer and the other nozzle sprays an activator with silver. When the two materials are sprayed together the silver precipitates out of solution and adheres to the polyimide surface. The process is done with the film on the spin table. The silver is applied while the table is rotating. After the silver has been applied the film is washed and dried. This process has resulted in a good reflective coating on the polyimide.

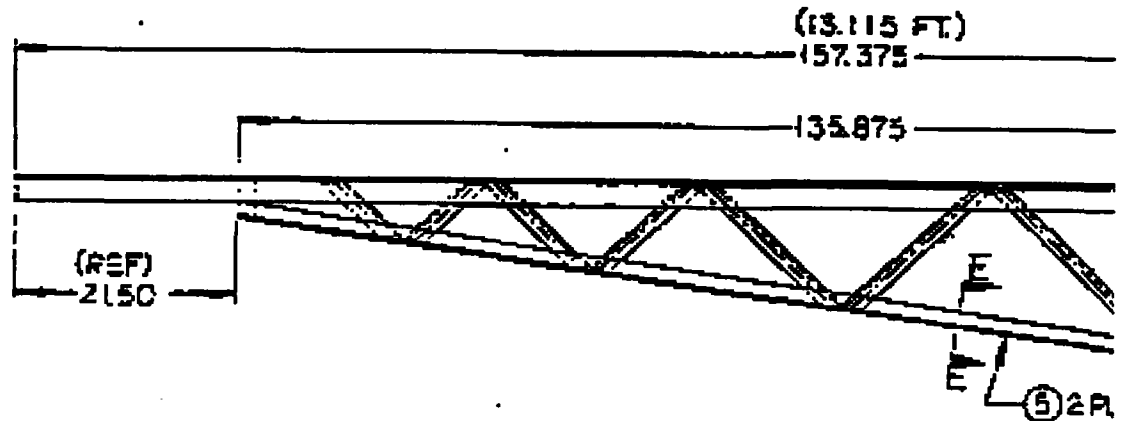
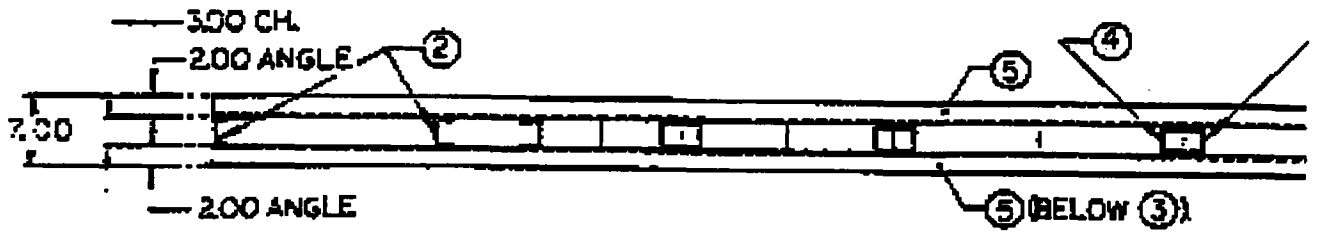
### 3.5.3.2 — Protective Coverings

For the heliostat application the silvered film must be protective coated with a clear overcoat to prevent oxidation of the silver. Several types of overcoats were tested with limited success. Originally, it was anticipated to use a front surface mirror and that a clear overcoat would be required. Due to problems in overcoats, a decision was made to use a clear polyimide and silver the backside of the mirror. As a result of this change, an optically clear

overcoat was not required. The following section does summarize work done to develop a clear overcoat and is presented as a study result.

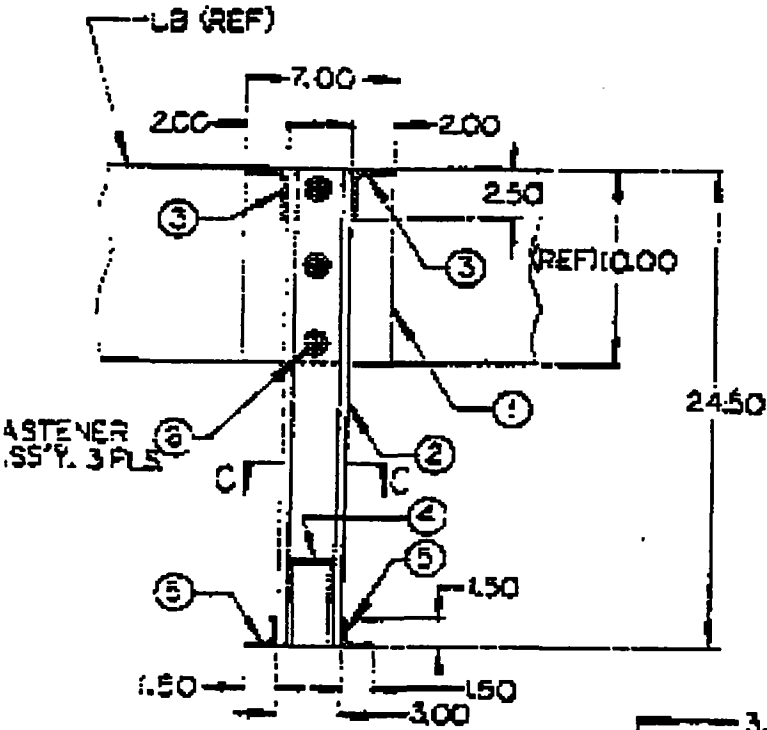
Peacock Labs (the silver supplier) recommended protective overlayer, Coppertite lacquer. Un-thinned and thinned coppertite was spin-cast over silver coating on polyimide film. It was observed to produce a slight yellowing of the silver, even when thinned to  $\frac{1}{3}$  and  $\frac{1}{2}$  its as-received concentration. It was then found that the Coppertite thinner, without the lacquer, produced the same yellowing, except the yellowing disappeared upon evaporation of the thinner. It was found that acetone behaved similarly. These experiments were done under laboratory fluorescent lighting. When repeated under incandescent lighting, no yellowing was seen. When viewed in sunlight, the Coppertite lacquer coating appeared perfectly clear. The same was found to be true of chemically imidized polyimide thinned to low viscosity with diglyme and spin-cast on silver-coated polyimide film as a protective overlayer candidate. This polyimide overlayer displayed too strong a drying-shrinkage and too low an adhesion to the silver, to be viable as a protective overlayer. It was concluded that the strong line-spectrum of the laboratory fluorescent lighting caused the slight yellow appearance of all the overlayer candidates, and that overlayer appearing perfectly transparent in sunlight should be considered as viable candidates, with fluorescent-lighting appearance being used for worst-case comparisons. This illustrates that photometric measurements rather than visual estimates must ultimately be used. Clean epoxy/acetone solution, spin-cast, also appeared to be a viable overlayer candidate, as did clear lacquer spray, and polyurethane coatings. 3M Corporation applies acrylic overcoats to their ECP 305 films which do not exhibit this tarnished appearance. Through discussions with a technical representative at 3M we found

Figure 64 Truss Assembly No. 2

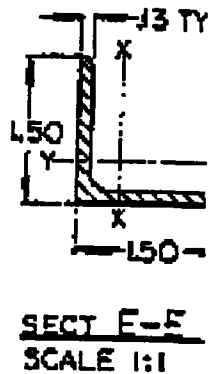
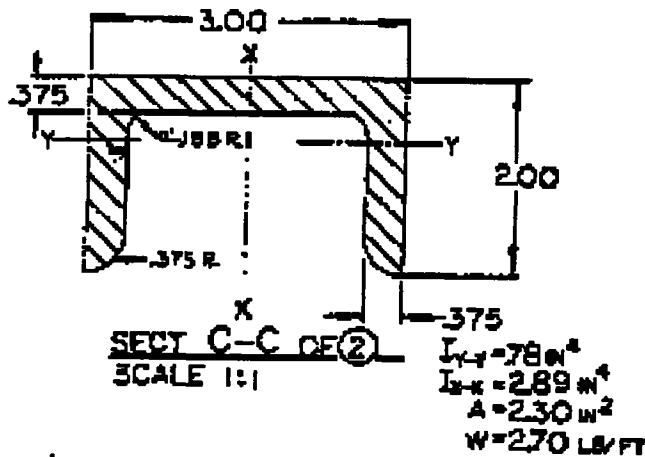
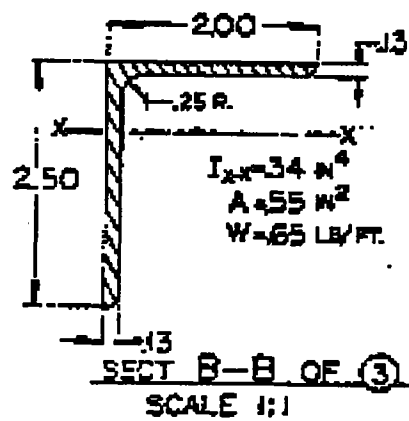


TRUSS ASSEMBLY (5289-02-80)

ONE OF SIX  
SCALE 1:10



SECT A-A  
SCALE 1:5



**Back of 11x17 Foldout**

that they had developed proprietary methods to eliminate the oxidation of the silver because of the overcoat. Their methods used a chemical overcoat over the silver before applying the acrylic. Non-organic substance  $\text{SiO}_2$  is used in industry to sputter protect overlays on silvered materials.

The final protective coating chosen was spray cast silicone. The transparent polyimide was silvered and then a thin layer of silicone was sprayed over the silver coating. The protective coating tended to darken the silver coating but this was on the rear surface of the mirror and did not effect the front surface of the polyimide.

### 3.5.3.3 — Sputtering Coating Study

Electroless plating tends to be a less robust process than vacuum evaporative plating and sputtering, i.e., it is much more sensitive to random variations in conditions, specifically surface cleanliness. In electroless plating, the plating atoms strike the surface to be plated, at room temperature, i.e., energy of the order of .025 electron volts per atom, which is inadequate to knock loose surface contaminants monolayers, or even thick layers. In vacuum evaporation, the plating atoms boil off of the vapor source at a temperature of at least  $1500^\circ\text{C}$  and strike the surface to be plated, with energy on the order of 0.25 electron volts per atom, which is sufficient to dislodge all but the most tenacious contaminants (provided they are not in the form of thick layers). In sputtering, clumps of the plating atoms strike the surface with sufficient momentum to penetrate even thick contaminant layers, interspersed with strong impacts from the high energy ions of the glow discharge, such that intense surface cleaning occurs simultaneously with plating deposition. By adding vigorous hand-rubbing to the cleaning and sensitizing steps of electroless silvering, the robustness of the process ap-

pears to be increased sufficiently to be somewhat competitive with vacuum evaporative plating. Silver sputtering was done in the SRS chamber in the event electroless spray silvering failed.

The SRS vacuum system was fitted with an argon supply, high voltage feedthroughs, and a current-limited high voltage AC power supply. Silver electrodes were mounted to the feedthroughs, a vacuum was pumped, argon was admitted to maintain pressure at approximately 100 microns, and glow discharge was maintained such that silver was sputtered onto a Kapton film sample mounted near the electrodes. Deposition rate appeared to be about 500 angstroms per minute. Adhesion and specularly of the coating were fair. The test indicated that about the same degree of subtleties are involved in sputtering as in vacuum evaporative metallization and in electroless spray silvering, and that sputtering does not offer a "short-cut" to heliostat metallization.

There are two basic candidate concepts for metallizing a heliostat segment by sputtering. *Concept A* - use the large vacuum chamber available at Phillips Lab, setting up a sputtering source assembly capable of metallizing one entire heliostat triangular segment simultaneously. This sputtering source would consist of an array of parallel silver wires 1 inch apart, suspended 1 inch above the heliostat film to be metallized, an alternate wire of the array would be connected to opposite terminals of a 5000 VAC transformer (wire a, c, e, etc. connected to terminal X, wire b, d, f, etc. connected to terminal Y). *Concept B* - develop a travelling head sputter, connected to the vacuum system by a large-diameter flexible tube; the inner sputtering chamber would be surrounded by a force-balance chamber pressurized with argon so as to allow the head to be moved easily across the surface of a spin-cast film not yet released from the glass casting-substrate; dry teflon O-ring seals under light pressure would

isolate the inner and outer chambers.

Both Concepts (A) and (B) would require a substantial development effort to implement them for this application, even though sputtering is a well-established technology. Concept A has the strong logistics disadvantage of requiring substantial development and set-up activity in a chamber and facility not under the control of SRS nor the Solar Lab. Concept A, unlike Concept B, could be used for metallizing the film after the latter was mounted on the heliostat segment frame, but this would require temporary venting of the airtight plenum chamber between film and honeycomb backing-plate. Concept B has more developmental costs and risks than Concept A, and would at best be a very slow process, since the movable sputtering head could not plate a large area at one time, due to the vacuum force which would break the glass substrate if a large-area head were used. Furthermore, since the Concept B process would need to be performed before the film was removed from the spin-casting substrate, it could not be used for not fully transparent film materials unless the film were transferred from the casting substrate to an intermediate frame and then retransferred to the heliostat segment frame (introducing an undesirable complexity). In the normal sequence, the film is transferred directly from the spin-casting substrate to the heliostat segment frame, with the plenum back-plate of the frame facing the film.

Thus, if either Concept A or Concept B were developed to fully satisfactory status as metallizing techniques, they would create substantial problems or limitations for other aspects of the heliostat program. Therefore, in view of the fact that the SRS learning-curve for the electroless spray silvering process reached an acceptable confidence level, and the fact that sputtering is extendable directly to metallization of seamless films of seemingly arbitrary size with limitation by available vacuum chamber size,

it seems advisable to consider sputtering as a back-up option, not to be developed further.

The same can be said of vacuum evaporative plating, which resembles Concept A sputtering as to pro's and con's. Evaporative plating of a large heliostat segment would require either a very good vacuum ( $10^{-7}$  torr) to get sufficient mean-free-path to use a single vapor source, or would require a very complex multiple-source array in order to metallize satisfactorily at the  $10^{-5}$  torr vacuum unlikely to be attainable in a larger chamber containing a heliostat segment of considerable outgassing capacity.

#### **3.5.3.4 — Spin-Casting Substrate Joint-Filler Study**

It was assumed that a spin-cast heliostat triangular segment, of approximately 16' x 16' x 16' size, would need to be cast on a substrate assembled from several sheets of glass due to the unavailability of a large single sheet of glass. Also the inconvenience and risk of handling such a large, heavy, fragile item if such a sheet were available would be difficult. In addition, further extension of spin-casting technology to very large sizes, which is one of the ultimate goals of this project, requires that a substrate built up of multiple sheets of glass be used. A metal substrate, e.g., aluminum honeycomb, coated with a surface-smoothing and water-release agent such as spin-cast potassium silicate solution or RTV60 silicone, was considered, but metal sheets are not available in greater widths than glass, warp-free joining of the large metal sheets is not straightforward, warpage in the film bake-out furnace would likely be more severe than with glass (except in the case of Invar), and use of glass substrates represents proven technology.

Glass plates joint filler options considered included: silicone compliant filler, tape or strap bridge; filled epoxy filler, silicate-bonded filler, and no filler. Leaving of an unfilled minimum-

width crack between adjacent plates of glass was dismissed without trial. It might give good results for a small-scale test, where gap width could be kept to less than 2 mils, but for large sheets, tolerance stack up would inevitably cause gaps wide enough to interfere with drying of the overlying film.

Joint-bridging Kapton tape, and heat-curved polyimide-bonded aluminum foil strips and stainless steel foil strips, were tried, bridging a  $\frac{1}{16}$  inch gap between 2 glass sheets. Upon spin-casting polyimide on this test substrate, it was observed that the aluminum wetted faster than the glass, causing run-out. The stainless steel wetted slower, causing a depression in the casting puddle periphery, and the Kapton wetted about the same as the surrounding glass. After spin-casting and heat-curing the film, the film could not be released from any of the gap-bridging tapes. Upon repeating the test, using a potassium silicate coating as a release-agent, it was found that the edges of the tapes invariably produced lines of thinning and weakness in the resulting film. It was concluded that deviations from substrate planarity in a concave direction, tending to cause local thick areas in the film, are acceptable, but deviations in a convex direction, tending to cause local thin/weak areas in the film, are unacceptable.

Filling of the  $\frac{1}{16}$  inch gap between the 2 test glass plates with aluminum-filled epoxy was tried. This produced a local perturbation in wetting, during spin-casting of the film, and the film could not be released, after heat-curing, from the epoxy.

Filling of the  $\frac{1}{16}$  inch gap between the 2 test glass plates with compliant silicones was tried. Air-cured (acetic) silicone caulk, RTV615 clear silicone and RTV60 red silicone, were tried. The air-cured silicone and the RTV615 grossly de-wetted during spin-casting of heat-curable polyimide, whereas the RTV60 wetted almost the same as the surrounding glass. Adhesion

of the film to the RTV60 was less than to the glass, but it seemed adequate for the joint-filler situation. Repeated attempts were made to learn how to use RTV60 for this application, but the results were inconsistent; in general, it appeared that wetting of the RTV60 by the polyimide film precursor liquid was marginal, and typically produced local thinning of the film over the joint. It had been assumed that the compliance of the RTV60 was an advantage, allowing the glass plates to shift slightly under thermal loading. It was found that such flexing of the joint ripped the overlying film.

Plaster of Paris was tried, as joint filler. It wetted satisfactorily and released satisfactorily, but caused gross thinning of the overlying film, from casting-resin soak-down into the porosity of the plaster. Filling of the plaster with Ludox colloidal silica after plaster set, was tried; it produced a glassy surface, but it could not be smoothed to planarity after drying, without shattering. Mixing the plaster with Ludox liquid instead of water produced a fairly interesting body with a glassy coating, but it could not be smoothed after hardening, without losing the smooth, rather impervious surface.

At this point it was concluded that an acceptable joint-filler must have the following properties:

- No significant non-planarity.
- No significant porosity.
- Able to be carved/shaved smooth with a razor blade after hardening in the joint.
- Wetting very closely matched to glass, for polyimide film precursor liquids.
- Film release properties closely matched to glass.
- Able to be trowelled in from the top-side of the joint, not requiring access to the under-side of the glass plates.
- Non-compliant; mechanical properties similar to glass; high adhesion to glass.
- No outgassing nor softening during heat-

cure cycle of polyimides.

Sodium silicate and potassium silicate solutions filled with powdered alumina were tried. The sodium silicate, which foams excessively when heated in the unfilled condition (unlike potassium silicate), produced a more porous and slightly less strong body than the potassium silicate. Both of these bodies were heated to redness on a sheet of tantalum, without foaming, cracking, nor losing their adhesion to the tantalum. The  $\frac{1}{16}$  inch gap between the test glass plates was filled with alumina/potassium silicate and oven-dried. The surface of the filler was too hard to smooth satisfactorily without damaging the surrounding glass. A film was spin-cast on this test substrate. Wetting of the filled joint, with the casting liquid, closely matched that of the surrounding glass. Release of the heat-cured film, from the joint-filler, was fairly good, but clouded by the surface roughness of the filler. Significant film thinning due to precursor liquid soak-down into the filler porosity was noted. Replacing of the powdered alumina with powdered dolomite limestone was tried, producing a softer body, but hard for practical smoothing of the filled joint after joint hardening. Replacing the powdered alumina with finely powdered talc produced a joint-filler material which appeared to meet all of the requirements listed in the preceding paragraph. After drying, it can be cleaned easily with a razor blade, and its surface burnished to give a shiny appearance. Rubbing in dry talc after the joint-filler surface has been shaved smooth appears to partially seal its porosity and improve its film-release properties. It does not produce a visible perturbation in the wetting of the substrate during spin-casting, and does not appear to cause a thin/weak area in the film over the joint, but merely a  $\frac{1}{16}$  inch wide stripe of matte surface, in the film. A satisfactory mix of filler "putty" was obtained by mixing 7 parts by weight of powder talc

with 6 parts of 20% solids-by-weight potassium silicate solution.

The joint-filler study has implications for the design of the framework or bed which must support the heat-curing, and, possibly, metallization. Compliant joints would have greatly simplified this matter, but the discovery that the entire glass substrate must remain a rigid monolith means that the entire substrate must be supported in a "fluid-like" cushioned/"floating" manner on a bed of springs with the relatively weak joints reinforced from below with hard fillets of alumina-filled silicate cement.

The final method chosen uses a potassium silicate and talcum mixture. The film above the seamed substance is reinforced with an additional layer of film following casting of the film. This additional layer adds strength to the film around the seamed cast area. The results of the process are that this method will work on the large sections leaving only small mold lines in the film. Multiple casting over the seam did result in degradation and separation of the seam. Additional studies need to be done to improve this area of spin casting.

### 3.5.3.5 — Triangular Substrate Casting

It was determined to be advantageous to cast the heliostat triangular segment films on triangular glass substrates. This minimized waste of film material and minimized size and weight of substrate, and lent itself advantageously to build-up of the substrate from triangular glass plates supported at 3 points.

A triangular test-substrate was made by epoxy-bonding 3 pieces of  $\frac{1}{8}$ " diameter glass tubing to a glass plate, as to form an equilateral triangle with leaky corners. A test-film was spin-cast with this substrate, at 45 rpm, using heat-curable polyimide. The liquid flowed smoothly out to the centers of the glass-tubing "dams", then flowed along these dams, to fill

the corners of the triangle. In order to avoid having to use excess liquid, the spin table had to be stopped a couple of times to redistribute the liquid so as to fill the triangle corner regions fully. The excess liquid departed smoothly via the leaky corners, leaving behind a uniform-appear-

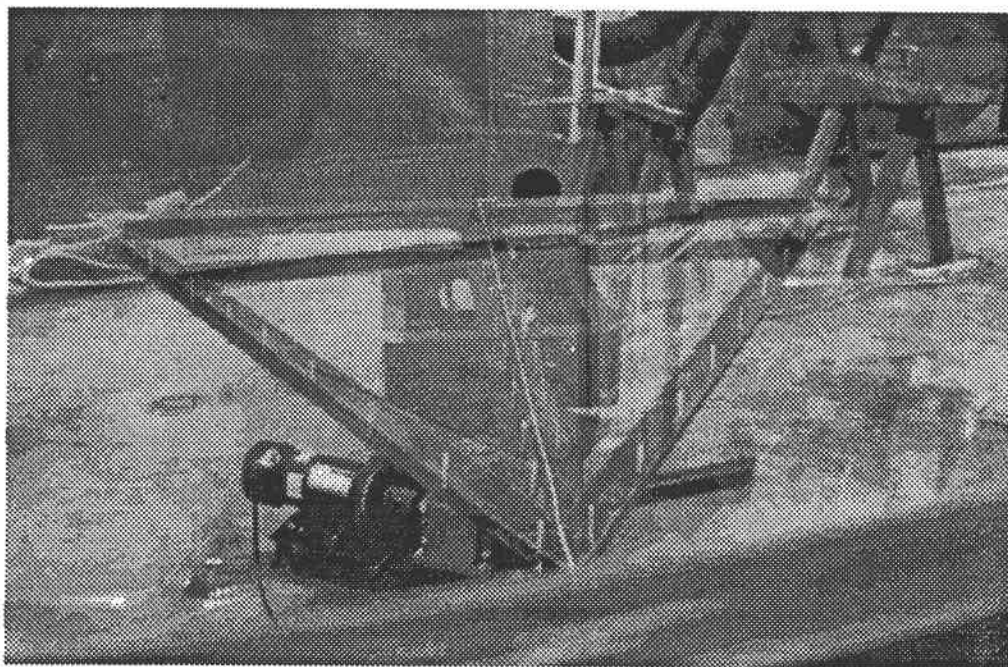


**Figure 65 Seamed Glass Test Article**

ing film. Upon drying, baking, and knife-scoring of the film along/close to the dams, the triangular film was easily released from the substrate. It had been feared that the raised dams would perturb the air-flow during spin-casting, causing non-uniform drying rate and consequent non-uniformities in film thickness, but this did not appear to be a problem. The main difficulty with the technique was that the dams prevented the normal use of a spatula to continually trim/control the periphery of the film precursor liquid puddle as it expands during spin casting.

### **3.5.4 — Fabrication and Installation of the Thin Film Polyimide Heliostat Segments**

Scale process verification was done before the casting of the full size heliostat segment was initiated. The original creep forming oven was used and a ventilated tent area was constructed to cast the films. These processes were done before installation of the oven and modifications to the spin table was started. The silvering process was developed with the scale model fabrication.

*Figure 65 through Figure 68* depict the casting and silvering of the scale test segment.

Several casting parameters were defined as a result of the casting. The film was cast at 90°F and 40% relative humidity. These conditions appear to be the optimum casting conditions for casting and subsequent drying before heat curing in the oven. The viscosity of the casting material was measured using a standard Zahn #2 viscosity cup. The material varies in viscosity with solvent content as well as temperature. The viscosity for the casting was 4:15 Zahn standard minutes at 88°F. The viscosity of the polyimide material used depends on the percent solids of material in solution. The viscosity also changes with the temperature of the material. The final thickness of the film depends on the viscosity of material and the spin table rotation rate. The correct viscosity for casting the films was determined by casting a range of percent solids material on a small turntable. Ranges of solid content tested were 15-23% solid content. Based on the test results it was determined that 21% solid content would yield a film of 1.5 mils thick. The

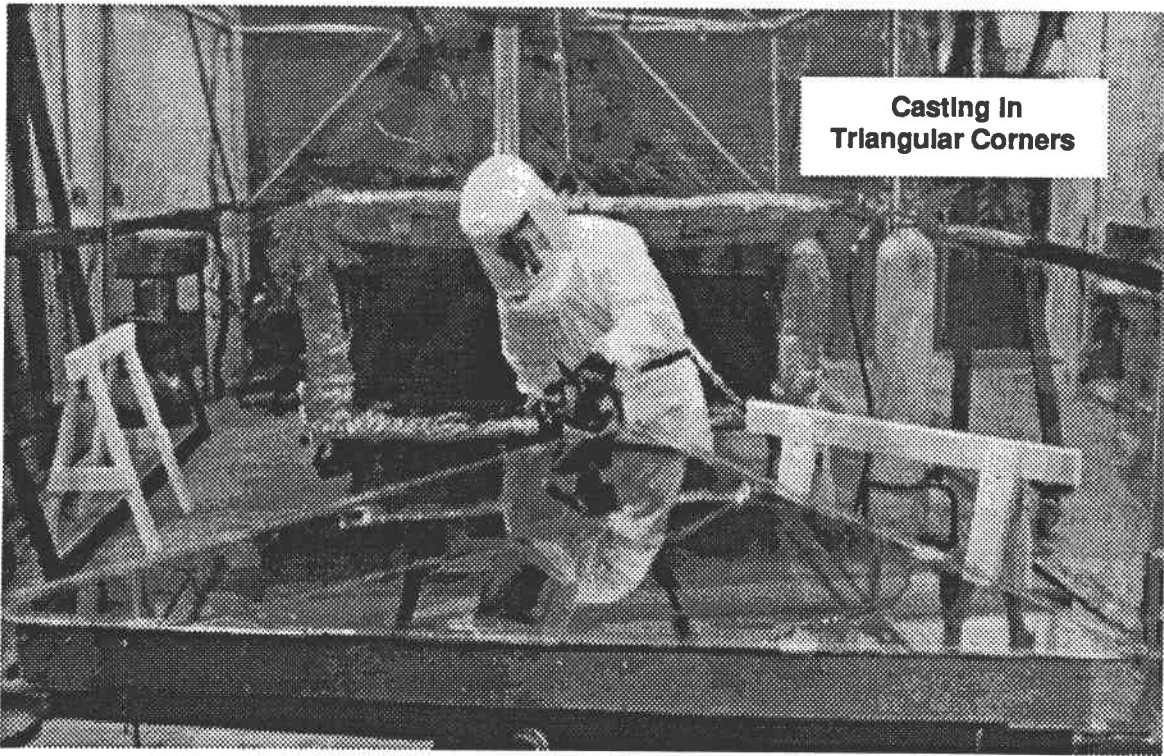
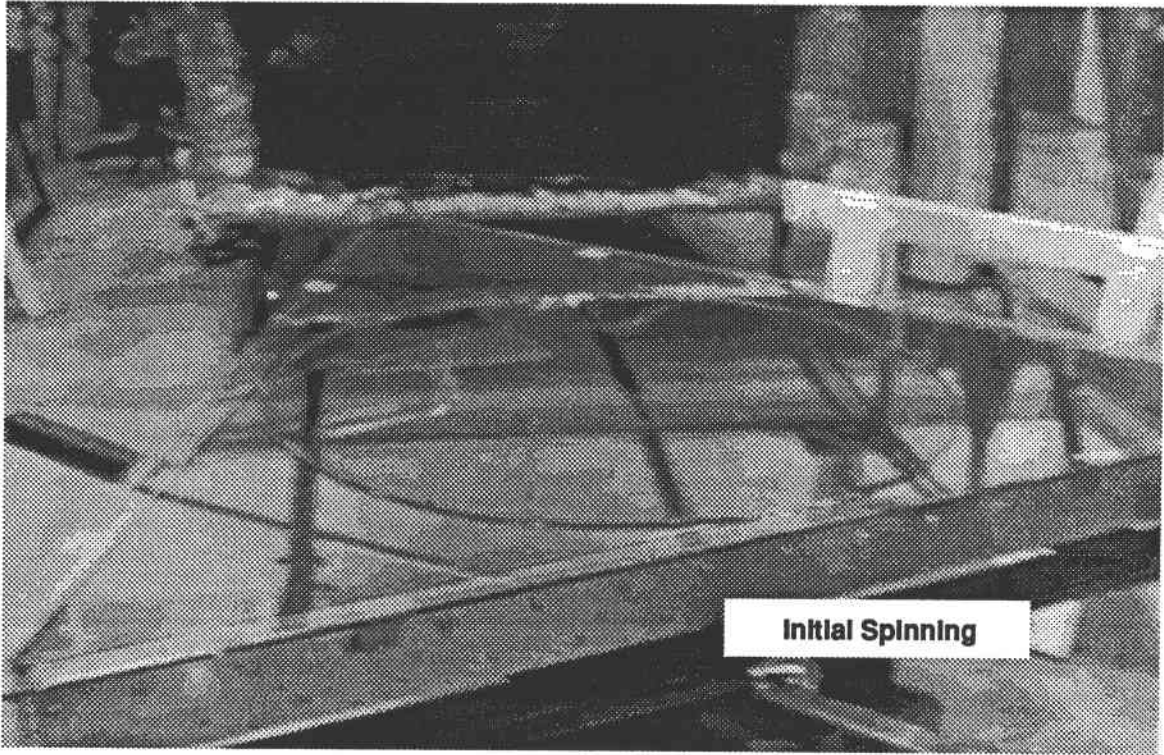
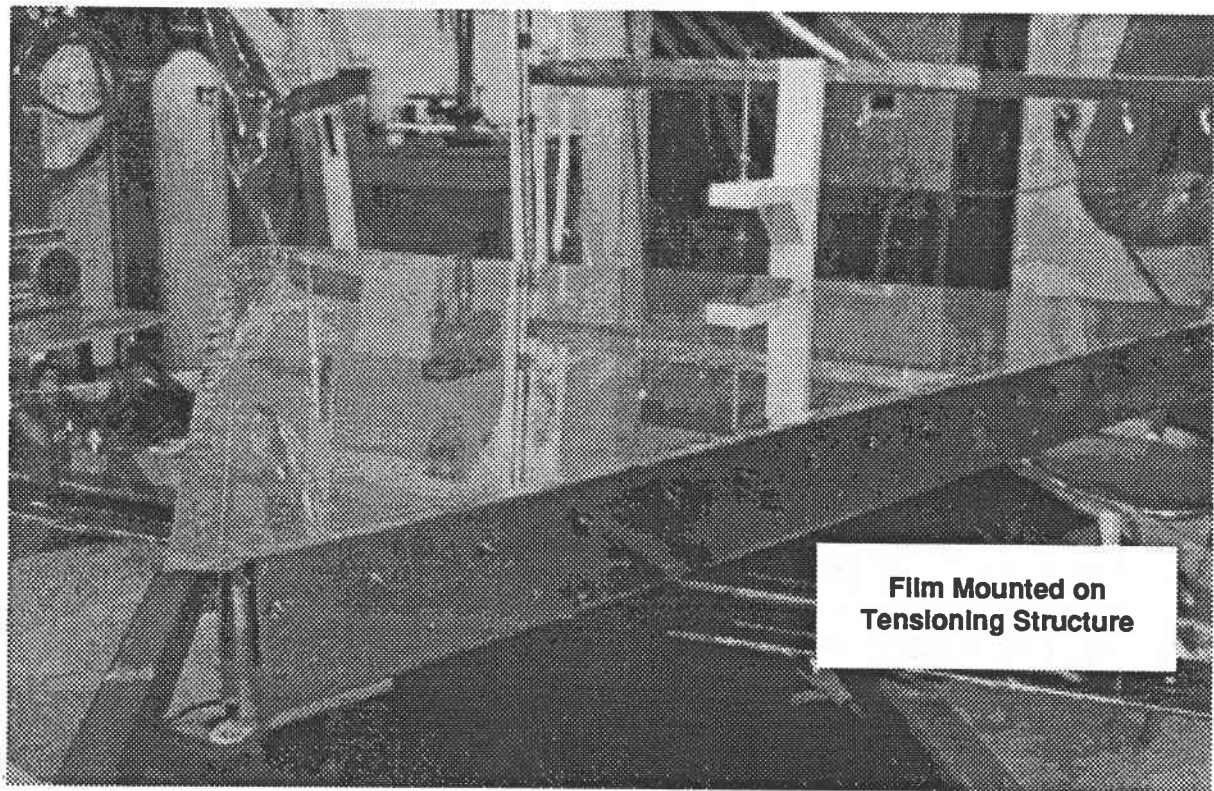
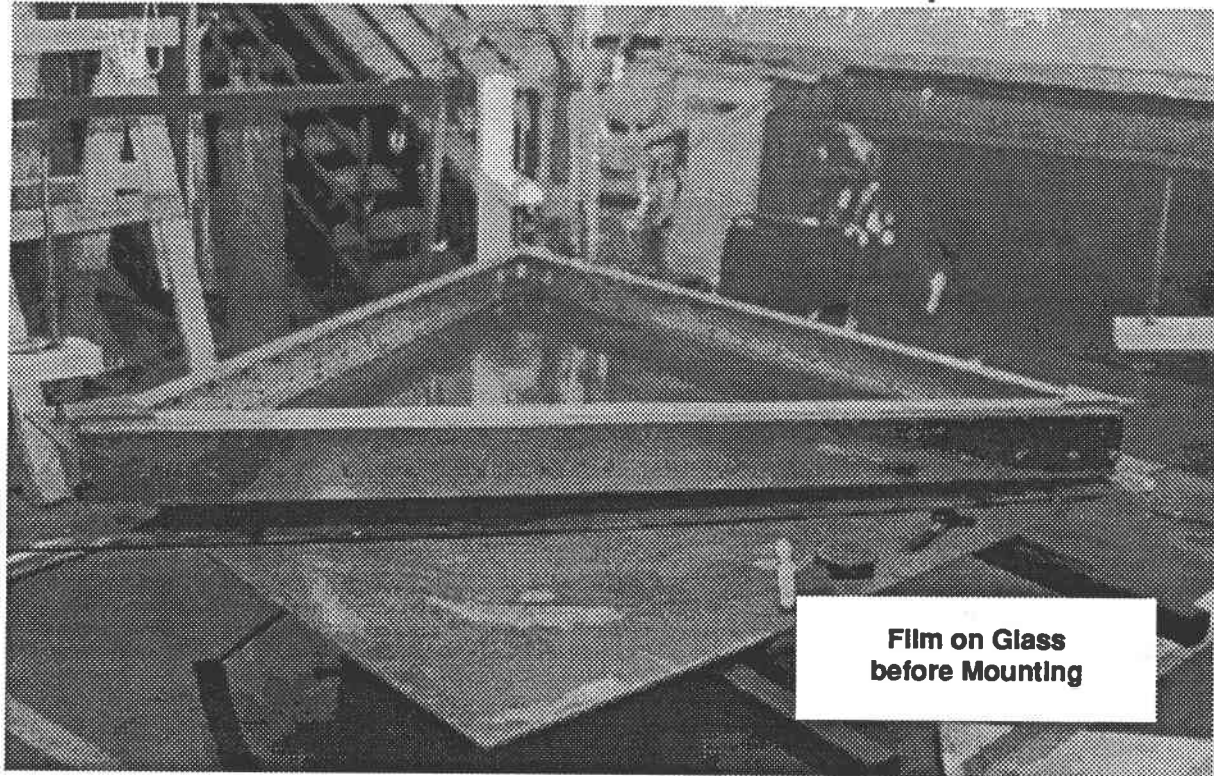
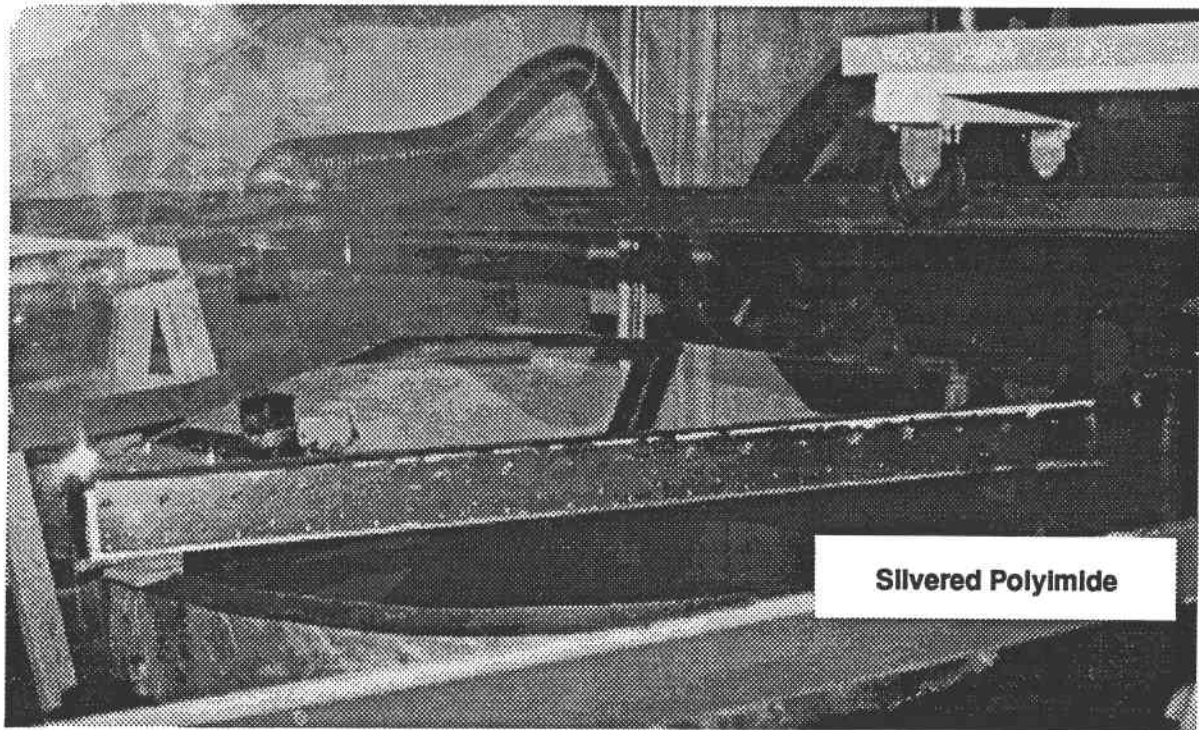
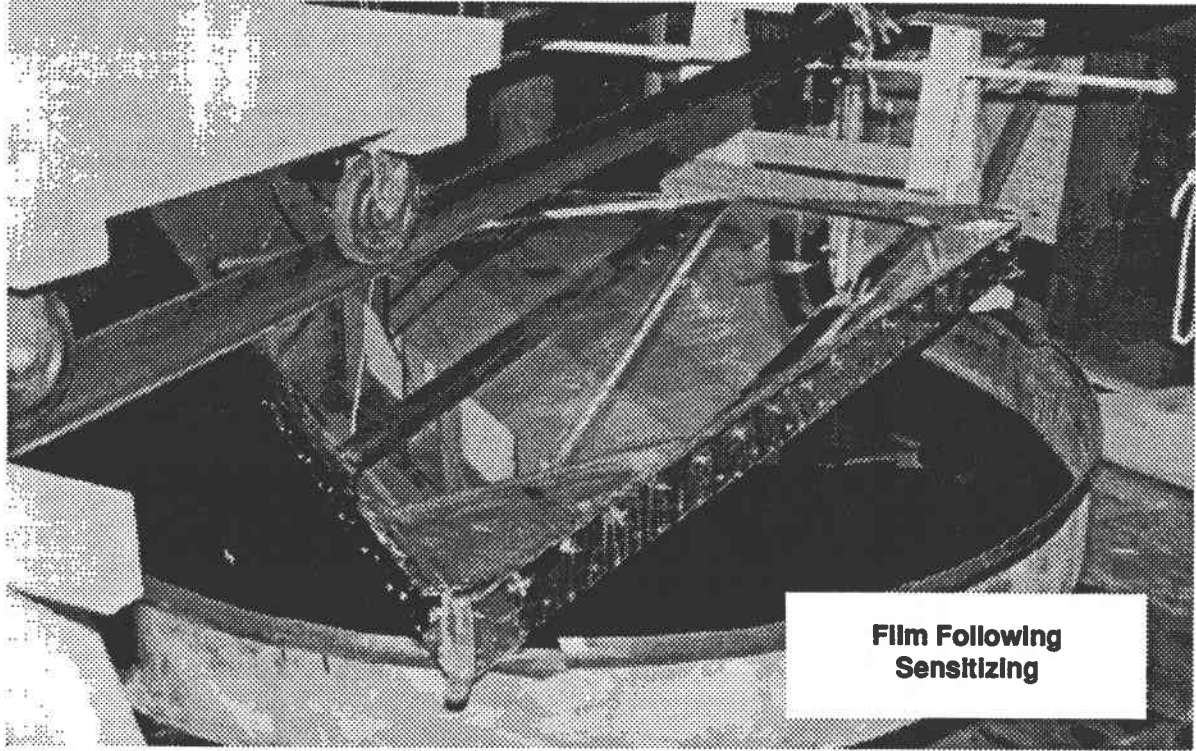


Figure 66 Casting of Thin Film



**Figure 67 Mounting Film on Tensiling Structure**



**Figure 68 Silvering the Tensioned Polyimide Film**

**Table 9 Process Summary for One Segment**

Process	Time	Day
Apply film to spin table and let dry at 85°F, 50% RH.	8 hours	1
Cure film at 100°C, 200°C, 300°C at a minimum of 1 hour each. Let cool.	12 hours	2
Set up silvering equipment and verify	3 hours	3
Spin silvered polyimide and let dry.	4 hours	3
Protective coat the polyimide and cure.	8 hours	4
Mount film to Heliostat with epoxy and cure.	4 hours	5
Remove Heliostat film from glass	4 hours	5
Package test segment.	8 hours	6

Table 3.6-1-dr2

21% solids content was eventually changed during the full scale casting. NASA/ Langley mixed the polyimide material at 21% solid content for the first casting.

The new oven and modified spin table was assembled after sufficient testing was complete on the scale model. The fabrication procedures for the full scale articles and time required for casting/coating and mounting the thin film polyimides are shown in *Table 9*. All safety guidelines were strictly adhered to during the fabrication processes.

*Figure 69* shows the casting glass mounted on the spin table. The glass was filled in between the seams with a potassium silicate and talc solution. The complete table is leveled both statically and dynamically in order to spin cast the glass properly. The first casting of a 21% solids content polymer was cast with a total of 4000ml of material. The viscosity and spin rate determines the final thickness of the material. The viscosity of the 21% solids material

worked well on the smaller test cases. The spin rate for the full scale was not large enough to “force” the material to the edge of the spin table. The first casting revealed that a larger amount of material was needed for the full size. A 21% solids and 8000ml of material was used on the second casting. The film was cured at 560°F. The film when cooled sheared small portions of glass slivers and tore near the potassium silicate/talc seam on the glass. The film when removed was measured to be 4 mils thick. The initial viscosity of 21% solids had to be reduced to obtain a thinner film. The 4 mil thickness had an extremely large drying shrinkage that accounted for the shearing of the glass. The high cure temperature also resulted in large stresses around the glass seam portion of the casting surfaces. Following discussions with NASA it was determined that a cure temperature of 420°F for 8 hours will fully imidize the material. A new seaming method with RTV615 silicone was chosen for the sub-

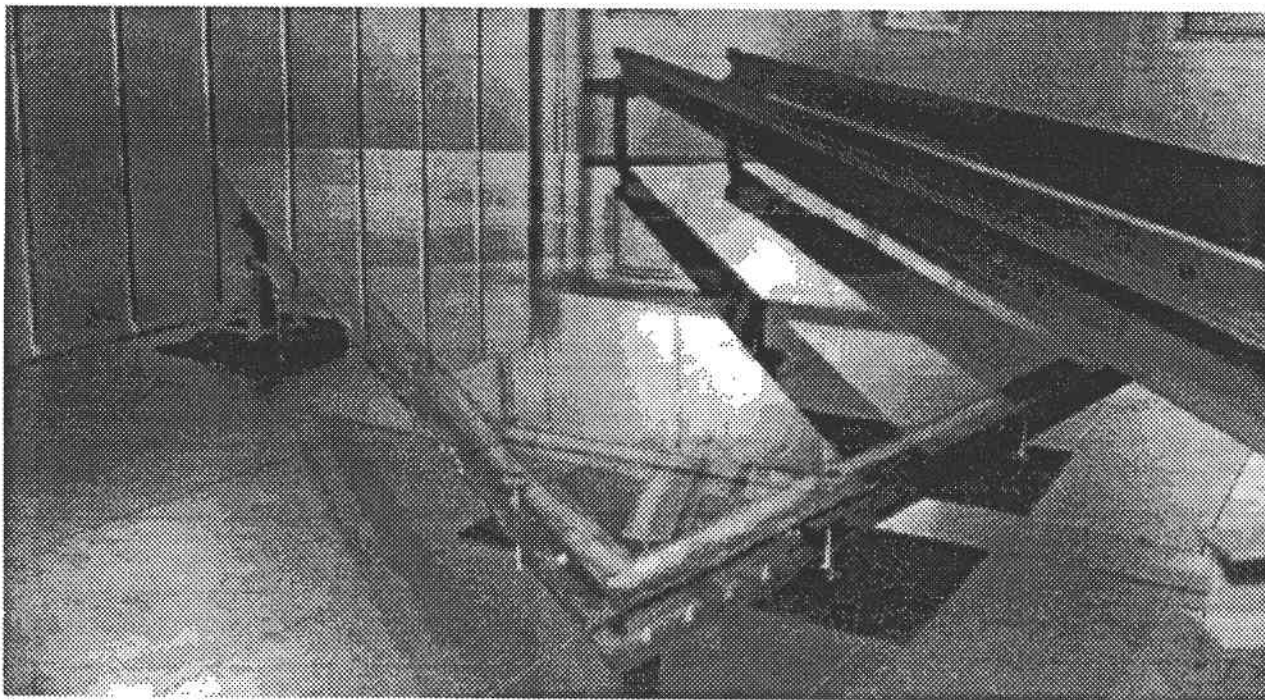


**Figure 69 Casting Glass**

sequent castings.

The third casting was done with 18% solids. The film was cast and cured successfully. The film was silvered following the cure cycle. Tears were initiated during the silvering process as the material released from the casting substrate when water was applied to the film for silvering. This problem was discussed with NASA at the progress review. It was decided that the film should be released evenly from the glass before silvering to avoid an uneven release that could result in tears. The fourth casting was done with reused material to test new procedures. The casting was done while waiting for new polyimide solution from NASA. The film recycled had absorbed too much water and did not cure properly resulting in an unusable film. The fifth film was cast successfully using the procedures refined from the previous castings. The film released and was successfully silvered. The casting and silvering process is shown in *Figure 70* thru *Figure 74*. Seam problems still existed but were repaired using silvered tape. The film was then

protective spray coated with RTV615 silicone and mounted to the tensioning structure. The film when tensioned resulted in good reflectivity and performed acceptably in the sun as shown in *Figure 75*. Additional films were cast using the procedures developed. Problems were encountered during the casting of the fourth heliostat segment. The glass casting table was damaged by the flaking of pieces of glass. This made the casting table unusable. Three heliostat segments were completed and packaged for delivery. The shipping of the segments was designed as shown in *Figure 76*. Installation support was provided at the Phillips Laboratory.

### **3.5.5 — Summary of Lessons Learned Under Heliostat Contract**

The following is a list of observations made after completing the fabrication of the heliostat segments:

Electroless spray silvering of polymer film works well on a large scale, if all key process

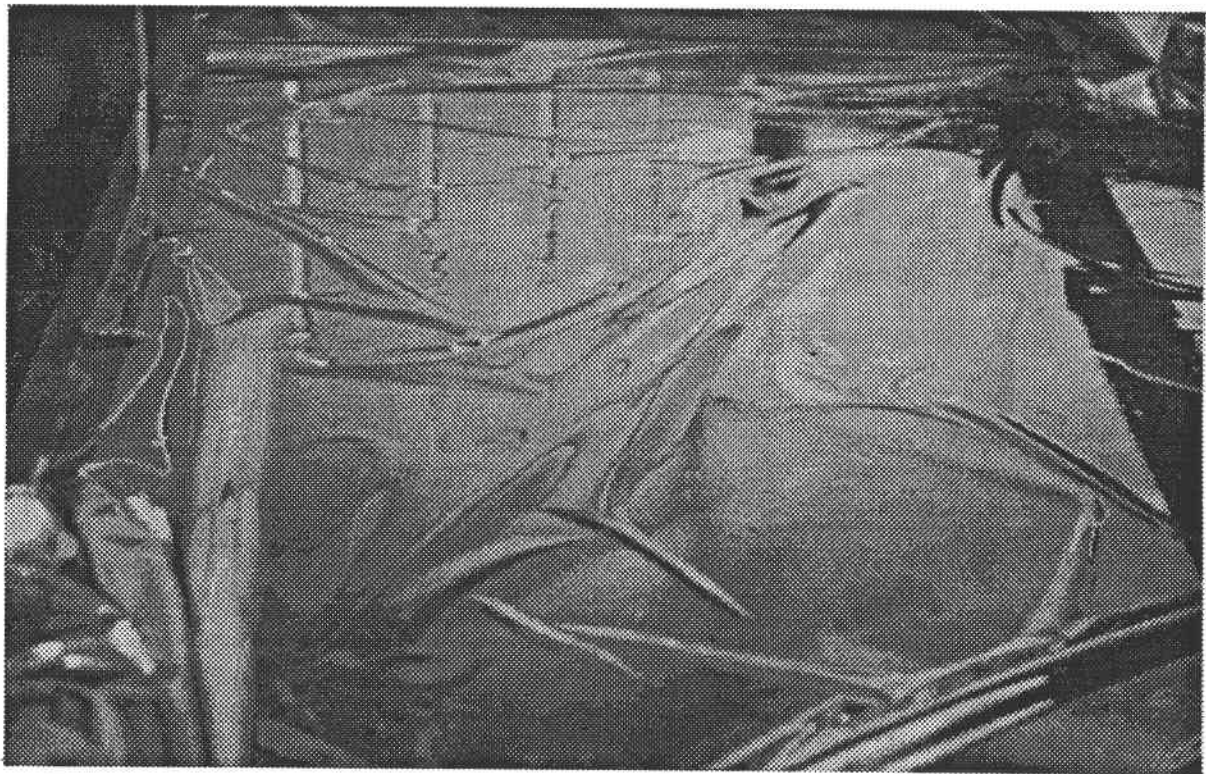
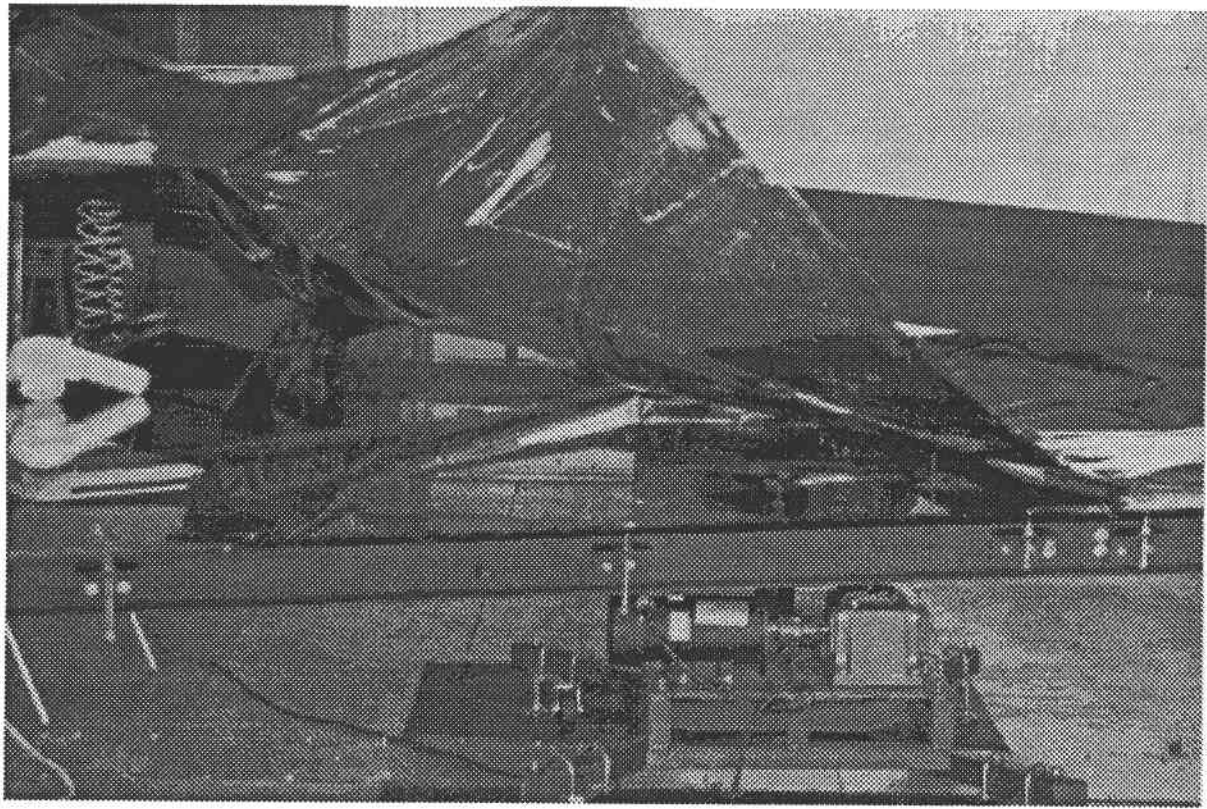


**Figure 70 Release of Silvered Film from Glass**

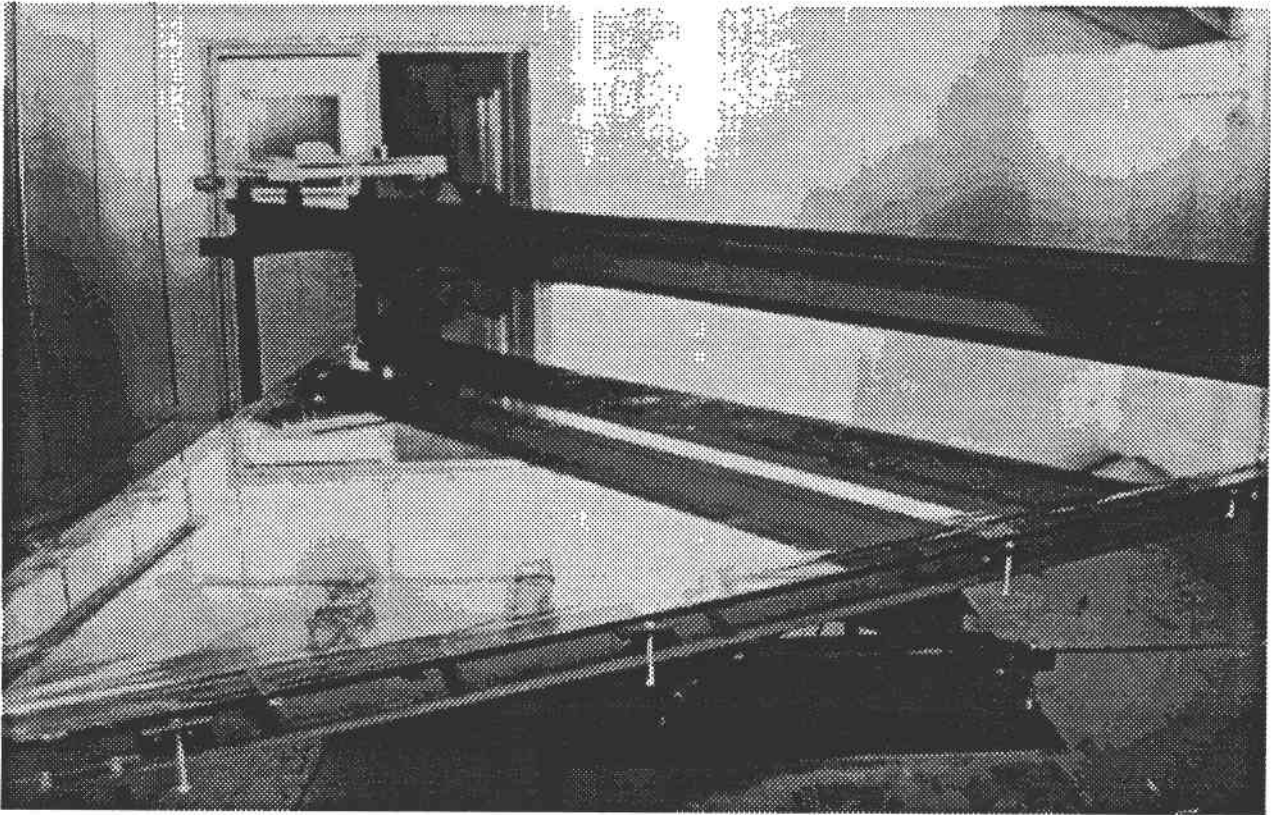


**Figure 71 Tensioning Silvered Film on Glass**



**Figure 72 Honeycomb Support Structure**

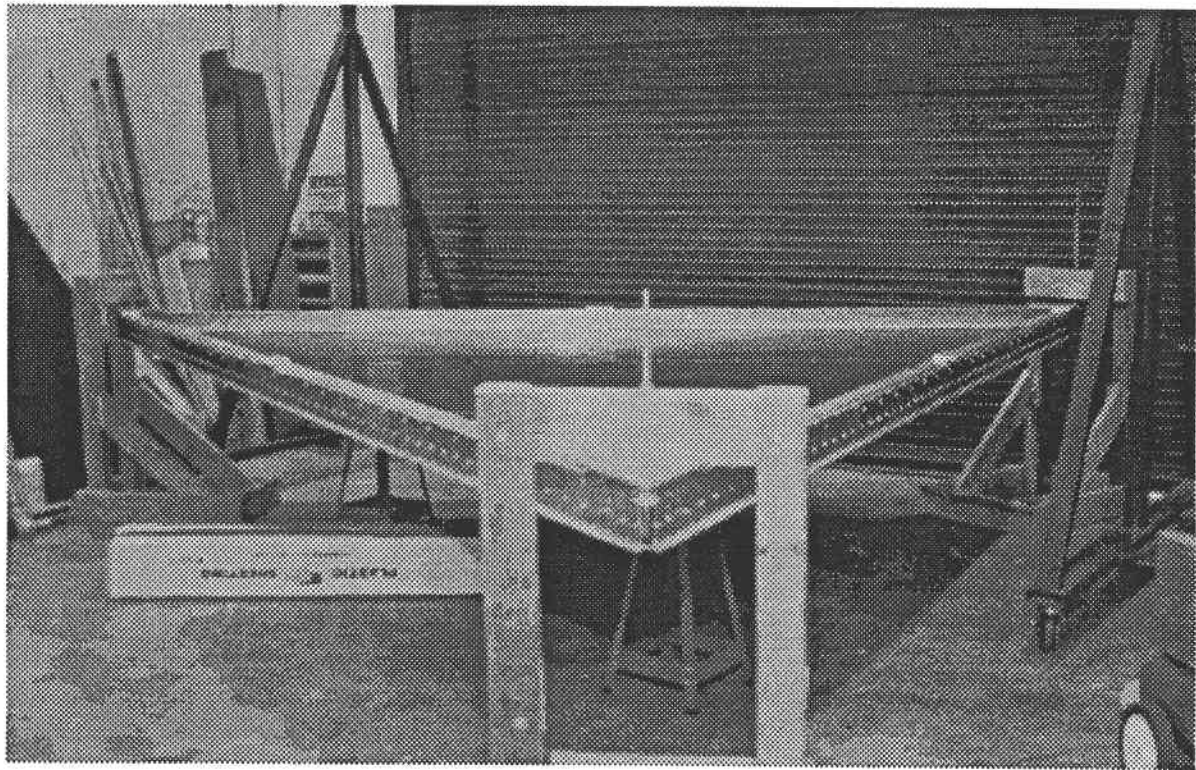
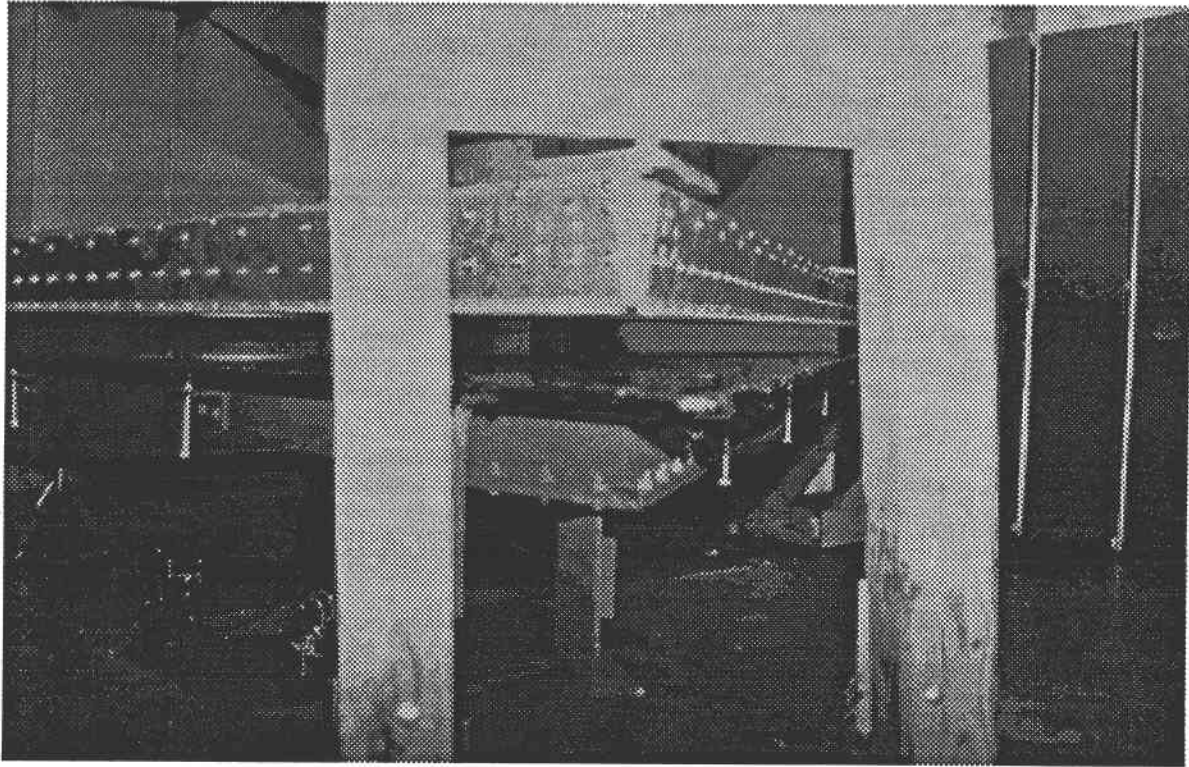


**Figure 73 Film Mounted on Tensiling Structure**

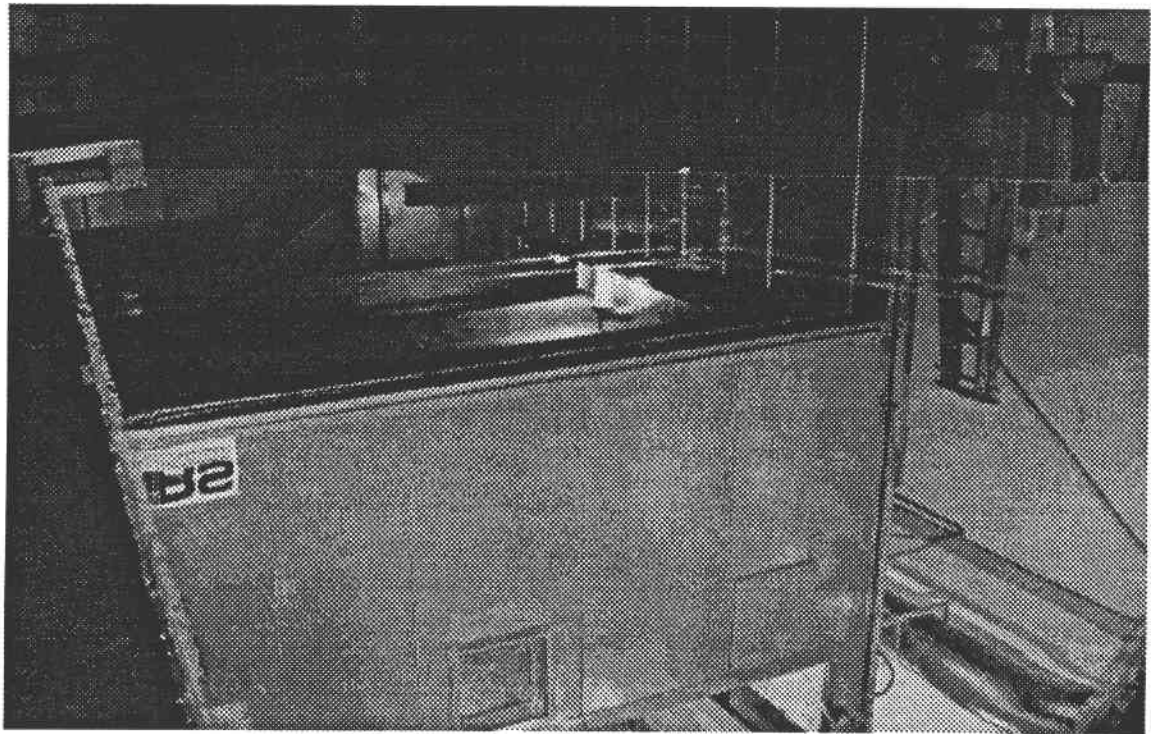
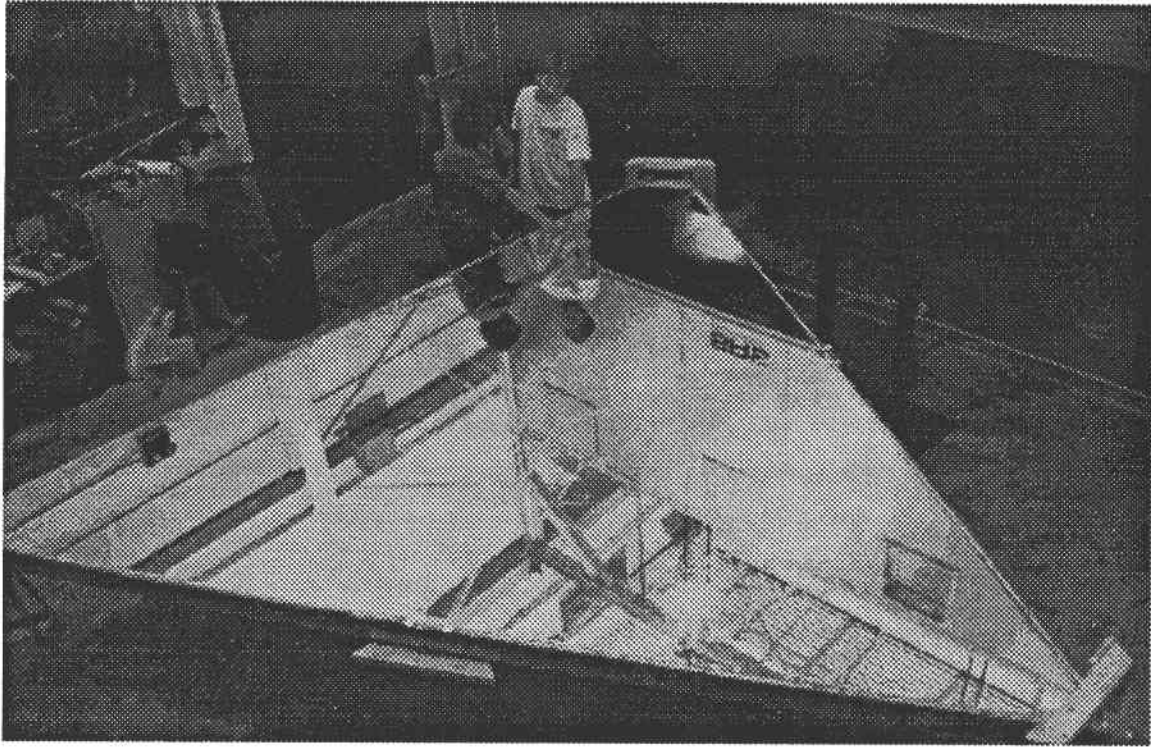


**Figure 74 Stretched Membrane Heliostat**

parameters are attended to. The silvering process works best in the second-surface configuration. Silicone is an acceptable but non-optimum protective overlayer for the silver coating.

The film tensioning and support frame work design used worked well. The epoxy film attachment techniques used seemed to hold satisfactory. The results of the work led us to

believe that a film heliostat of this design will be more planar initially, and especially after several years in service, than a glass heliostat. However, environmental effects require that some sort of windshield be used and require replacement every 1-3 years. Also methods to replace the reflective film every 3-4 years may be needed.

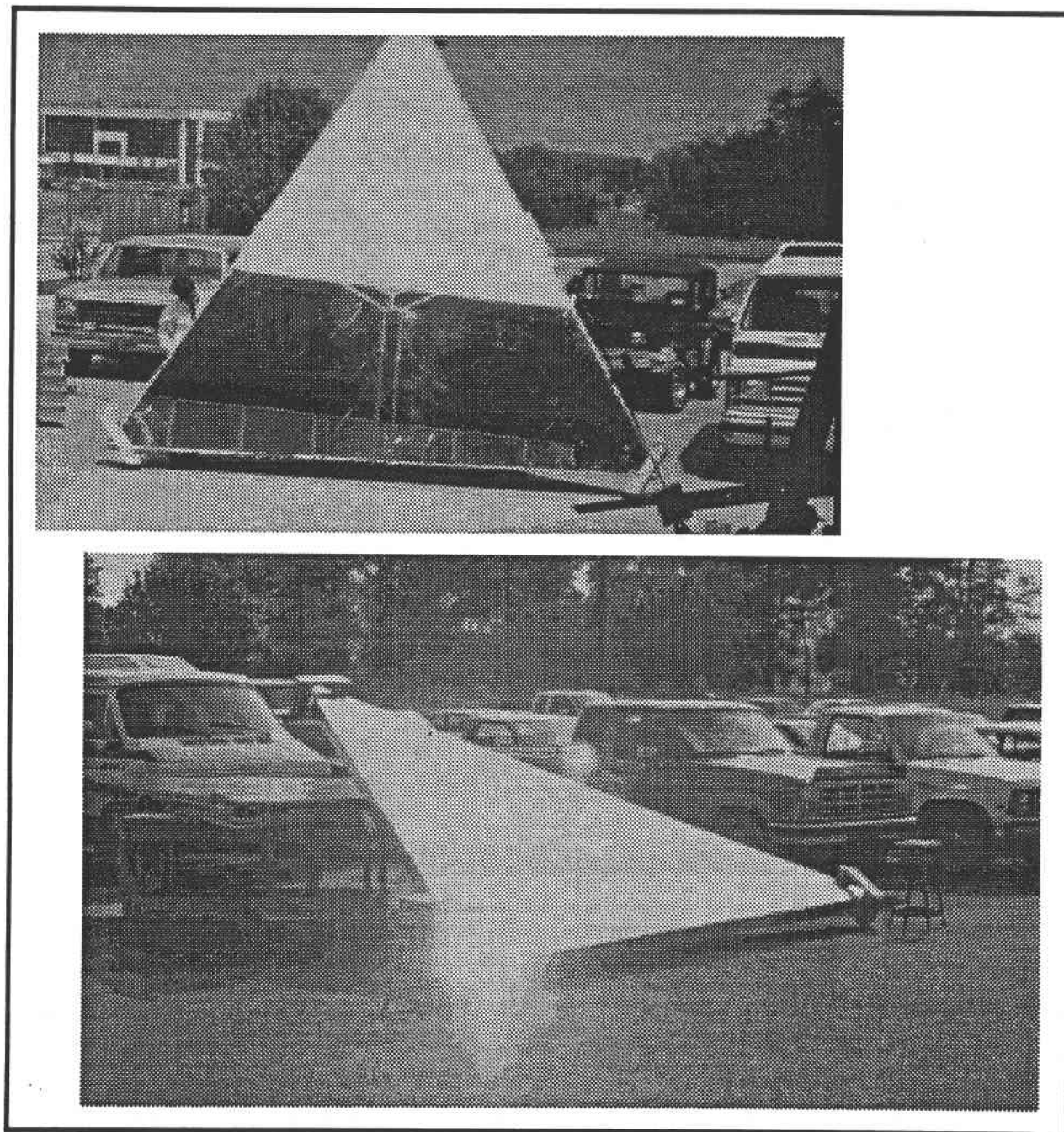
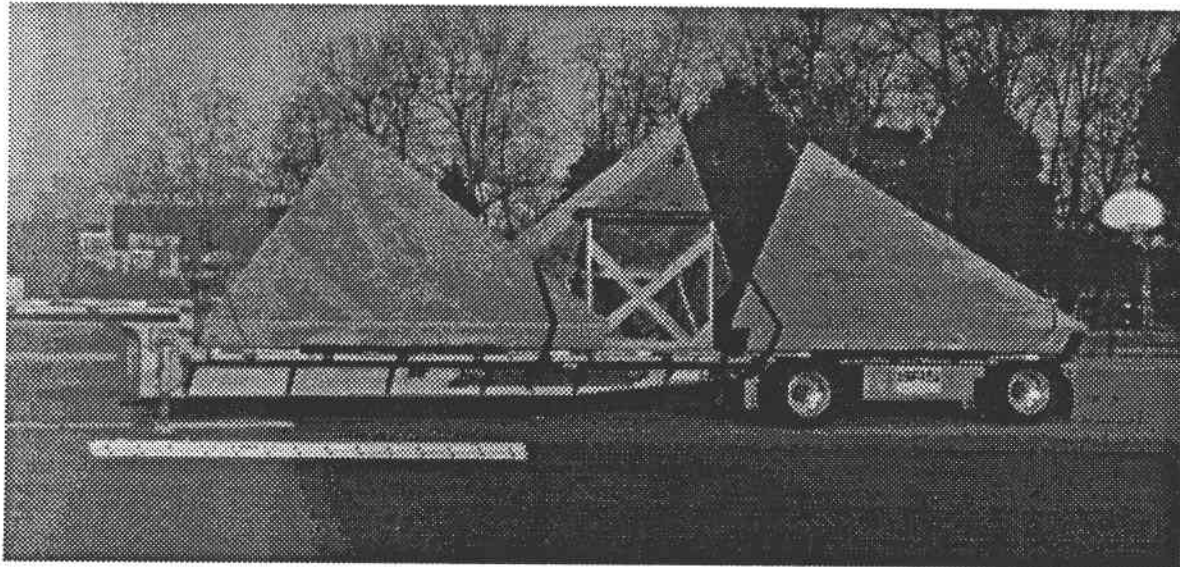
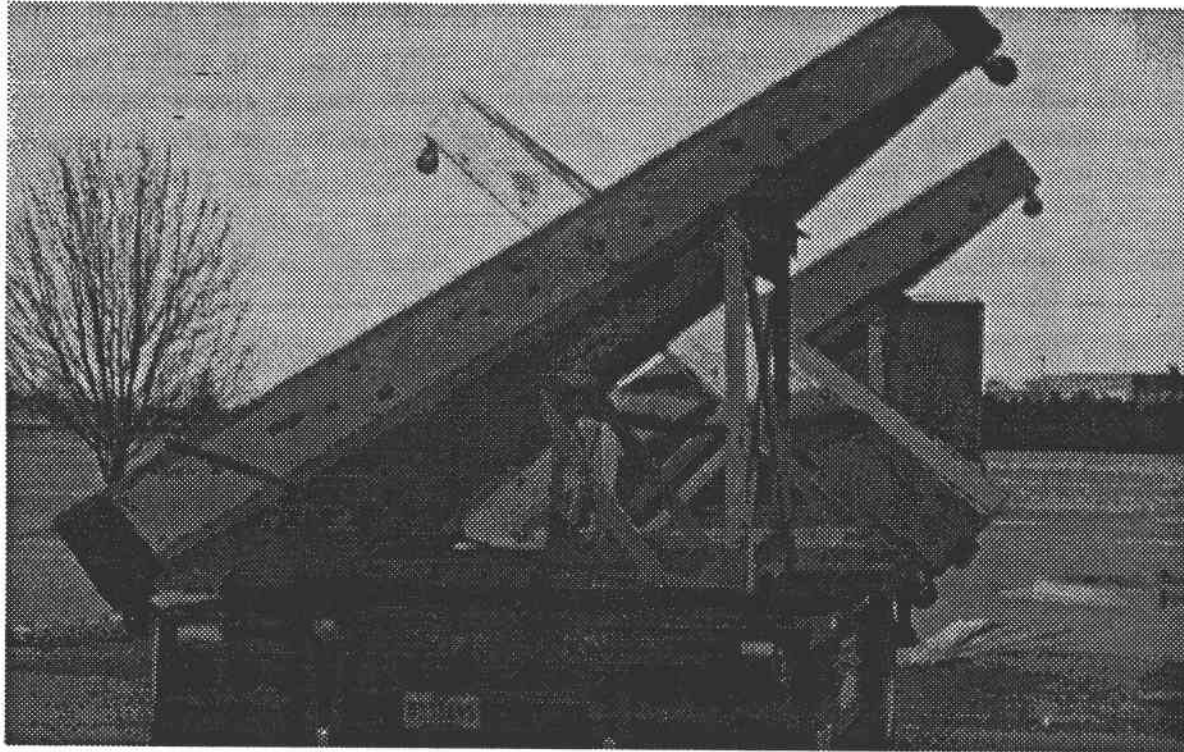


Figure 75 Reflectivity Demonstration



**Figure 76 Segments Ready for Transportation**

The NASA Langley 6F+APB film is only the first generation of optically clear polyimides. The material is too prone to spontaneous tears at thin highly stressed areas. The material is also too brittle and rather difficult to process. Improvements are needed in these

films as the research progresses.

Glass casting substrates lose their ability to water release heat imidized films cast on them after three to six castings. This is probably caused by water-leaching of the water sensitive free alkali from the surface layers. The

film subsequently begins to pull up chunks of glass, in a spalling pattern during the film release. Alternative casting substrates and release agents should be identified.

Techniques satisfactory in small scale models for joining multiple plates of glass to form a large substrate are not satisfactory for use with a large multi-sheet glass substrates. The larger substrates include large thermal expansion stresses and difficulty in supporting and planarizing large heavy glass plates.

The spin casting process for film fabrication is not satisfactory for use with large multi-sheet glass substrates. The glass substrate possesses non-planar and non-homogeneous joints between sheets for sizes larger than 2.5 meters in diameter. Alternative manufacturing methods such as spray casting have demonstrated improved process control for casting films 1 mil in thickness.

### 3.5.6 — Installation and Testing of the Heliostat Segments at the Solar Laboratory.

The three segments that were fabricated at SRS were installed at the Solar Laboratory and limited test data was gathered to determine the performance of the stretched membrane heliostats. Problems were encountered with the polyimide film when it was exposed to water during an extended rain storm. The film loosened in the heliostat frame beyond the capa-

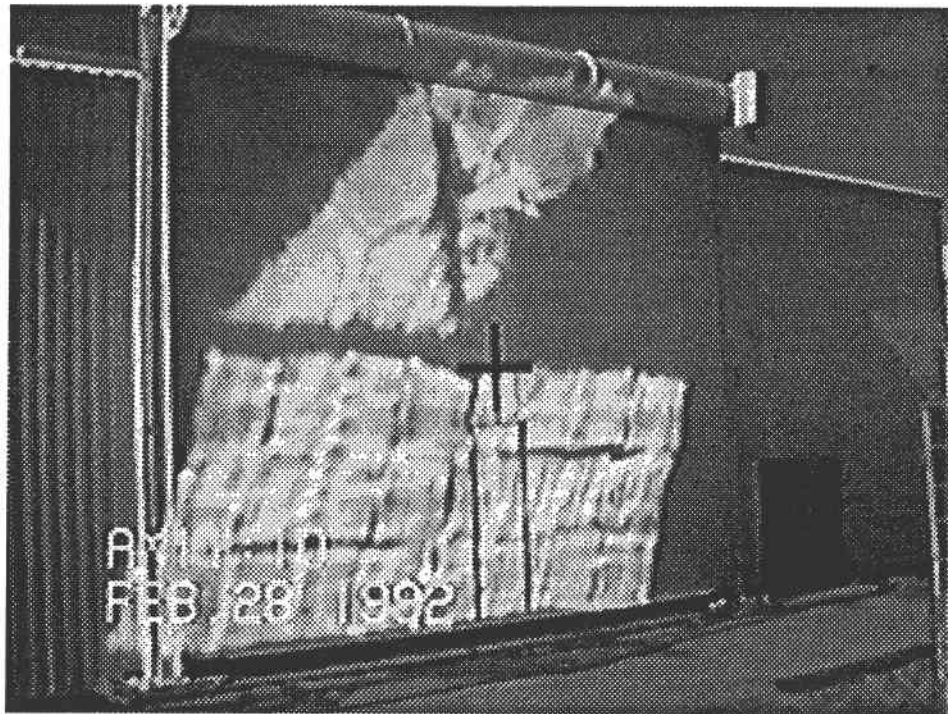


Figure 77 Image of Heliostat Segment from Stretched Membrane and Glass Panels

bilities of the tensioning device. A silicone coating that was cast on the back of the film material to protect the silver from tarnishing adhered to the honeycomb frame during the rain storm. Two of the films failed when the membranes began to dry after the rain subsided. The membranes began to tighten up and the silicone “stuck” to the honeycomb resulting in tearing of the film.

An image test was performed with the remaining segment and is shown in *Figure 77*. The reflected image of the heliostat segment tested was encouraging. The tensioning structure design works extremely well for tensioning the films in a planar configuration. A good reflected image is shown in the figure. The good image is a result of a planar stretched membrane film segment. A relative comparison can be made between the glass segments and film segment. The glass segments reflections have noticeable “valleys” where dark lines are seen. The stretched membrane results were

promising for future use of new polyimide materials as stretched membrane heliostats.

A failure analysis was conducted in parallel with NASA/LaRC to investigate the reason for the embrittlement of the polyimide and hygroscopic absorption problems. After extensive curing and testing of polyimide samples the following conclusions were made:

Failure of the segments was a result of degradation of the polyimide film material due to inclement weather conditions. (High wind and several days of rain). If the film had the correct material properties it would not have expanded and became loose and attached to the surface of the honeycomb. Studies at NASA/LaRC suggest that curing temperatures had a significant effect on the polyimide material properties, specifically, the water absorption that was apparent during the rain storms at Edwards. The material used was 6F+APB heat imidized in DMAC solvent. If insufficiently cured, the DMAC is not removed. This results in a hygroscopic partially cured polyimide with undesirable mechanical properties. The insufficient cure time was a result of other factors which were considered more important at the time of processing. High drying shrinkage of the film at the high temperatures caused spalling of the glass substrate after several cure cycles. The spalling caused the film to bond to the glass during the cure process resulting in tears while releasing the film from the glass. These considerations with the processes led to

the decision to not cure at elevated temperature for extended times. Therefore, the last two segments (which failed) were not cured at the extended high temperature cure.

Film thickness was also a factor in our inability to remove the solvent from the film. Five mil film thicknesses were measured in some locations. This film thickness was a result of the casting process. Extended cure times and even higher temperatures would be needed to fully cure a film five mils thick. Future use of the heat imidized polyimide would require that films three mils and less be made for heliostat purposes.

Reduced temperature chemically imidized film materials have been developed that do not require the high temperatures of heat imidized film. These materials were not available at the time the heliostats were cast. The material does not need to be heat imidized at 575°F but only solvent cured for extended time at 350°F. Chemically imidized films at these lower cure temperatures do not have as large a drying shrinkage as the heat imidized film. The lower temperatures and drying shrinkage significantly reduce the casting surface spalling problems that were encountered at higher cure temperatures. The results from this work led to the development of new curing procedures for heat imidized film and also led to the selection of chemically imidized film for the fabrication of solar collectors.

## 4.0 — Conclusions

The objectives of this Phase II Small Business Innovative Research Program were to support the solar thermal propulsion program through advancing: polyimide materials, fabrication technologies, analytical modeling of concentrators, and construction of models of doubly curved off-axis parabolic solar concentrators. To meet these objectives innovative techniques were used to develop a materials testing apparatus for evaluation of candidate polyimide materials to be used for inflatable concentrators. The results of the material testing led to the selection of NASA Langley polyimide film as opposed to commercially available polyimides. The characterization testing of commercially available films revealed that the material properties of the films varied from batch to batch and varied in thickness. The NASA polyimides are available in solution form and can be cast on parabolic shapes to form the desired concentrator shape. The use of polyimide films in solution form is a dramatic step in being able to control the fabricated shape and on-orbit configuration of inflated parabolic shaped concentrators.

Fabrication studies were performed in parallel with the materials testing of the thin film polyimides. Studies concerning the specific problem areas of forming technologies were done. Advances were made in the reflective coating techniques of the polyimides by using electro-less silvering methods as well as sputter coating and vapor deposition processes. Preliminary mandrel fabrication and creep-form-

ing methods were also evaluated and used in studies for fabrication of models delivered to the Phillips Laboratory.

This research also supported the development of an analytical model to support the forming processes of viscoelastic dependent film forming processes. The model will continue to support the solar thermal program as it is expanded to predict on-station mechanical and thermal behavior of operational deployed thin film concentrators.

Finally, this research was concluded by applying the technology developed under this contract to construct scale models of inflatable concentrators and to expand the casting and forming techniques to large scale processes. The expanded casting facilities and techniques were done under an additional effort. The effort included fabrication of large (5 meter) triangular heliostat sections. The casting and curing of these segments required demonstration of fabrication methods which are equivalent to the methods needed to fabricate the near term flight test article for the solar propulsion vehicle. This effort also demonstrated the reflective coating of large transparent polyimides.

The research objectives of the this funded effort have been met and the success of the technologies developed under the effort are being continued under Department of Defense and commercial funding to fabricate inflatable concentrators for solar thermal propulsion and communication purposes.

# **Appendix A**

**Details of Qualitative and Exploratory Creep Testing**

# Details of Qualitative and Exploratory Creep Testing

## A.-1 — General

A number of tests were performed using the uniaxial creep test apparatus, with the objectives of checking out the apparatus and test procedure, familiarizing the test personnel with the same, and answering some questions about Kapton creep behavior that could bear on the design of the formal tests. All tests were performed with the temperature chamber (nominally at 600°F, with test specimens consisting of 1 inch wide ribbons of 0.3 mil thick Kapton film, and with a load calculated to produce

1,500 psi stress in those test specimens. Specimen strain was recorded as a function of time, on a strip-chart recorder. A typical strain versus time curve obtained (Test J. as described below) is traced in the following *Figure A.1*, with test inputs and specimen responses noted in the curve. Sections of the curve were cut out, as indicated, to get the curve on the page. A light pre-tensioning load, less than 1% of the creep load, was applied at all times to minimize the effect of wrinkles.

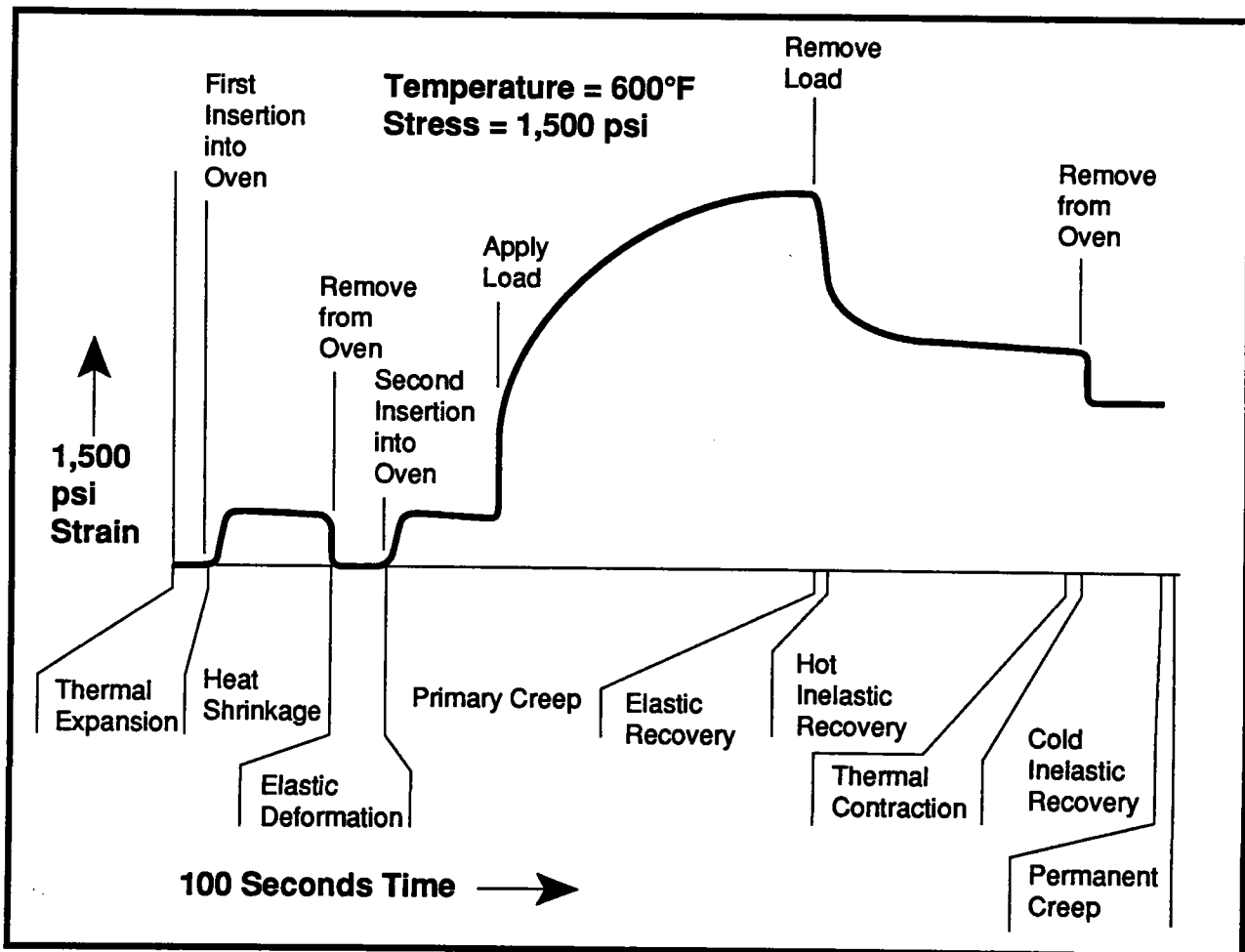


Figure A-1 Tracing of Typical Strain versus Time Curve (Test J)

## A-2 — Tests Descriptions and Observations

### Test A

**Objective:** Baseline data on creep and related parameters

**Material:** Lot 2 Kapton, Cut perpendicular to roll axis.

**Test Time-line:** Apply even, heat shrink .500 sec.; apply load, creep 500 sec.; remove load, hot recover 500 sec.; remove oven.

**Observation/Comments:** Heat shrinkage roughly equal in magnitude to the thermal expansion, i.e., about 0.7%, was observed. The time-constant of the heat shrinkage appeared to be the same as that of the hot creep-recovery, i.e., about 300 sec., which should be true because Kapton heat shrinkage has been reported to consist of hot recovery of room temperature creep, or more properly, room temperature relaxation of the tensile stresser imported in wrapping the film in its packaging roll. Time constant for sample heat-up upon slide-on of the oven (i.e., laterally rolling the oven along its track such that the stationary test sample passed through the narrow vertical slot in the oven side wall facing the testing machine, as judged by thermal expansion, appeared to be about 10 sec. Time constant for sample cool-down upon slide-off of oven appeared to be about 20 sec. (the oven circulating fan undoubtedly accounted for this difference). For all these tests. the slot in the side of the oven was closed by a double "brush" of fiberglass fibers taped to each side of the slot, with cut-outs in the fibers to avoid bumping the film or extensometer arms while sliding/rolling the oven laterally to cause the sample to enter the oven. This "brush" allowed considerable air leakage, but not enough to prevent stable oven operation. (Previously, a solid sliding door with cut-outs to clear the loading arms and extensometer arms was used to minimize air leakage through the oven wall slot,

but it was found that opening and closing of this door, at sample insertion, caused excessive excursions in oven temperature, making it difficult to provide a "step change" in sample temperature). Test A experienced some slippage in extensometer grips at the film sample, at the time of load application, and during ambiguous manual joining of the wench, indicating that a rather snug amount of pressure was needed at extensometer grips. No evidence of failure initiation was seen in subsequent tests, as result of excessive extensometer grip pressure, and no evidence of extensometer grip slippage was seen subsequently.

### Test J

**Objective:** Note effect of film roll direction.

**Material:** Lot 2 Kapton, cut parallel to roll axis.

**Test Time-Line:** Same as Test A.

**Observations/Comments:** Strain versus time curve (traced in Figure A-1 above) looked much like that for Test A, except for lack of grip slippage, and except that heat shrinkage was only about one third as great as that noted in Test A. Since Kapton typically is supposedly isotropic before being roll packaged for shipment, this confirms that its heat shrinkage is mainly due to relaxation of residual stresses from the predominately linear winding-on-roll stretching of the film during packaging.

### Test B

**Objective:** Note effect of different lot of Kapton.

**Material:** Lot 1 (that used in all Phase I testing) Kapton, cut parallel to roll axis.

**Test Time-Line:** Same as Test A.

**Observations/Comments:** Strain/time curve looked much like that for Test J (See Figure A-1) except that thermal expansion and creep rate seemed considerably higher. It was postulated that there may be large batch-to-batch

differences in Kapton; subsequent tests did not support this hypothesis. Thickness measurements of film, using a micrometer, seemed to indicate substantial point-to-point thickness differences, percent-wise, in the 0.0003 inch thick film; subsequent film thickness measurements with a constant pressure dial indicator set-up did not support the manual micrometer measurements, and seemed to indicate a thickness variation no greater than about  $\pm 10\%$ , which would not account for the variations in creep rate seen in this and subsequent tests, and obviously should not cause the thermal expansion variation that invariably accompanied the creep-rate variations. The calibration of the extensometer LVDT and recorder were checked, and did not appear to have shifted. Some indication of uneven gripping at the specimen loading clamps was seen, and these jaws were cushioned with clamped-on multiple layers of 1 mil Kapton. Marking of the film near the loading grips and extensometer grips prior to testing gave assurance that no significant grip slippage was occurring; yet the inconsistent readings continued. The obvious reason for them was not discovered until the final set of tests (Test M) of this series was performed; namely, the oven was turned on at random periods of time before the tests, and as soon as the oven controller indicated that the oven temperatures had stabilized, testing was begun. To make up for the considerable heat losses through the sample entry slot, a 1,000 watt booster heater had been placed downstream of the regular heating elements, and this booster brought the air temperature up very fast, indicating to the control thermocouple, located close to the heating elements air chute, that operating temperature had been reached, long before the oven walls had reached steady-state. Moving the control thermocouple farther downstream, reducing the power of the booster heater after heat-up had occurred (which also was found to

dampen out the considerable short-term fluctuations in air temperature near the sample, as discovered by probing the oven with a 30 AWG thermocouple), and allowing 1 hour for oven stabilization to occur, after turn-on, eliminated this data inconsistency problem. The presence of this problem during all the qualitative testing, however, detracted very little from the qualitative information gained, and it motivated evaluation and/or correction of several potential problem areas.

### **Test C**

**Objective:** Note effect of aluminization on Kapton.

**Material:** Aluminized Kapton, cut parallel to roll axis.

**Test Time-Line:** Same as Test A

**Observations/Comments:** An initial thermal expansion nearly twice that seen in the preceding tests was observed. However, the corresponding thermal contraction upon removal of the oven was no greater than that for the nonaluminized Kapton. The sample was very wrinkled, prior to the test, and very smooth after the test; it was concluded that the apparent high thermal expansion was merely the relaxing of the wrinkles as the sample heated up, under the slight pre-training load. No other clearly apparent difference in behavior, compared to the non-aluminized Kapton, was perceived.

### **Test D**

**Objective:** Compare 2,000 sec. creep with 500 sec. creep.

**Material:** Lot 2 Kapton, cut parallel to roll axis

**Test Time-Line:** Same as Test A except creep 2,000 sec.

**Observations/Comments:** Strain/time curve looked much like that of Test J, (See Figure A-1) except as follows: at about 900 seconds after application of the load, the creep curve

lost its curvature (primary creep), and remained perfectly linear (secondary creep) as far as it would be judged by a straight edge, for the remaining 1,100 sec. of creep-time. Phase I data had indicated that the transition from primary creep to secondary creep typically required about 3,000 sec. The probable explanation for this difference is that the Phase I test apparatus had an inherent slow specimen heat-up rate that masked the primary/secondary transition, whereas the Phase II apparatus has a very rapid specimen heat-up rate. The creep-strain hot recovered in 500 sec., in Test D, amounted to 24% of the total creep strain accumulated during the creep period. This contrasts with 43% hot recovery of total creep-strain, in Test J, and 40%, 41%, and 36% respectively in Tests A, B, and C. (The slightly lower recovery, 36%, seen in Test C as compared to Tests A, B, and J raises a question as to whether the film metallization could have caused it.) Thus, Test D appeared to indicate that secondary creep is substantially more permanent than primary creep. This raised the question, does recovery have a primary and secondary region, or is it merely an immense exponential time constant curve as one would assume? Test L was performed subsequently, to answer that question.

### **Test I**

**Objective:** See whether high humidity in oven could cause high temperature hydrolysis damage to Kapton film.

**Material:** Lot 2 Kapton, cut parallel to roll axis

**Test Time-Line:** Same as Test A except direct steam from a 900 watt water boiler into the temperature chamber before and during test.

**Observations/Comments:** Upon application of the load, the film sample broke promptly; seemingly from propagation of a defect at one edge of the specimen. A second film specimen was mounted, and tested without failure. For

various reasons the atmosphere control in the oven was poor, and the amount of steam present at any time is not accurately known. This sample showed a normal looking hot recovery curve, almost linear rather than the inverse-exponential seen in all the other tests, starting recovery at a slower rate as time preceded. Hot recovery in 500 sec. equalled only 23% of 500 sec. creep. It was an unrealistic test intended to study an extreme situation, but its results, even through anomalous, suggested that the magnitude of effects of normal fluctuations in testing room humidity should be measured, in formal testing.

### **Test H**

**Objective:** Note effect of repetition of creep cycle.

**Material:** Lot 2 Kapton, cut parallel to roll axis.

**Test Time-Line:** Apply oven, heat shrink 200 sec; apply load, creep 500 sec; remove load, hot recover 500 sec; remove oven, cold recover 100 sec.; apply load, creep 500 sec.; remove load, hot recover 500 sec.; remove oven.

**Observations/Comments:** Creep during first creep cycle was 1.95%; hot recovery following that creep was 0.9%. Creep during second creep cycle was 1.20%; hot recovery following that creep was 0.66% (smaller numerically than that of the first cycle, but larger percentage wise, which one expects because some of the first cycle creep, as well as all of the second cycle creep, is now furnishing impetus for recovery). The second creep cycle was flatter than the first cycle creep curve. This raises the questions, (a) if there had been no hot recovery after the first creep cycle, i.e., if that creep had been "frozen in" by removing the oven before removing the load, would a subsequent creep cycle merely take up where the first creep cycle curve left off? and (b) if there had been "complete" hot recovery or annealing after the first

creep cycle, would a subsequent creep cycle curve look just like the curve of a new piece of material? Test H2 was then performed to answer question (a), and test L was performed to answer question (b) (rather, the second half of Test L; the first half of Test L addressed the question raised by Test D).

## Test H2

**Objective:** Note effect of frozen-in creep strain on subsequent creep behavior.

**Material:** Lot 2 Kapton, cut parallel to creep axis.

**Test Time-Line:** Apply oven, heat shrink 200 sec.; apply load, creep 500 sec.; remove oven, cool 100 sec.; remove load, cold recover 500 sec.; apply oven, heat shrink 100 sec.; apply load, creep 500 sec.; remove oven, cool 100 sec.; remove load, cold recover 500 sec.

**Observations/Comments:** It was interesting to observe that the elastic recovery upon removing the load at room temperature, both cycles, was substantially smaller than the elastic deformation upon applying the load at 600°F, for both cycles. This illustrates the fact that Young's modulus of elasticity is, at 60°F, roughly twice its value at 600°F. It was interesting to note that the heat shrinkage rate at the start of the second creep cycle, before application of the load, was about 5 times the heat shrinkage rate at the start of the first creep cycle; the second cycle heat shrinkage represented the recovery attempt of the frozen-in first cycle creep. As expected, the second cycle creep looked almost like a continuation of the first cycle creep, as if the removal of the oven, freezing-in of the creep, removal of the load, re-applying of the oven, and re-applying of the load, had not intervened; the extent to which this was not true appeared to exactly equal the amount of heat shrinkage that occurred between the applying of the oven and the applying of the load at the start of the second creep cycle. As to room temperature recovery of the fro-

zen-in non-annealed creep strains after the first and second creep cycles, it was so slow that it could not be distinguished from thermal contraction as the specimen cooled.

## Test L

**Objective:** (a) Determine shape of long-term hot recovery curve; (b) Determine effect of long hot recovery on subsequent creep cycles.

**Material:** Lot 2 Kapton, cut parallel to roll axis.

**Test Time-Line:** Apply oven, heat shrink 200 sec.; apply load, creep 500 sec.; remove load, hot recover 5,280 sec.; remove oven, cold recover 100 sec.; apply oven, heat shrink 100 sec.; apply load, creep 500 sec.; remove load, hot recover 500 sec.; remove oven.

**Observations/Comments:** Section (a), initial creep and recovery cycle: Creep strain was 2.1%, total hot recovery was 1.2%, and to the extent that recovery was complete, the 62% time constant of hot recovery was 350 seconds. By the end of the 5,280 sec. of hot recovery the recovery rate had slowed to about 1% of its initial value, and appeared to be asymptotically approaching a total recovery of 1.3% to 1.4%, as a proper inverse-exponential time constant curve, but a considerably larger hot recovery time would be required to rule out the possibility of observer prejudice. Section (b), second creep and recovery cycle: The long hot recovery/annealing did not return the material to the pretest condition, as to creep compliance; the second creep cycle curve looked almost like a continuation of the first creep cycle curve, as if no long hot recovery process had intervened between them. Second cycle 500 sec. creep was 0.45%, and second cycle hot recovery was 0.22%. This rather high ratio of second cycle recovery to creep, and the low second cycle creep compliance, suggests that the 5,280 sec. first cycle hot recovery was not nearly complete. However, an alternative, more attractive explanation is that

the first creep cycle had oriented the polymer chains, permanently increasing the elastic modulus in the strain direction, and that not all of this preferential orienting represented a thermally unstable condition.

### **Test E**

**Objective:** Study cold stability and hot stability of quenched or frozen-in creep strain.

**Material:** Lot 2 Kapton, cut parallel to roll axis.

**Test Time-Line:** Apply oven, heat shrink 200 sec.; apply load, creep 500 sec.; remove oven, quench 100 sec.; remove load, cold recover 500 sec.; apply oven, hot recover 500 sec.; remove oven.

**Observations/Comments:** There appeared to be some observable cold recovery, after "quench" following the creep cycle, but its magnitude was so small, or rather, its rate was so slow that it could not be distinguished from sample cool-down thermal contraction. A further cold-recovery test of at least 24 hours duration is indicated, or rather, a family of recovery tests (for frozen-in creep), at temperatures of 100°F, 200°F, and 300°F, from which the Arrhenius-Eyring recovery activation energy can be calculated. Upon reinsertion of the sample into the oven, after the 500 sec. cold recovery, hot recovery occurred at about the same rate as if the intervening quench and cold recovery had not occurred; in fact, the 500 sec. hot recovered strain, about 50% of the 500 sec. creep strain, was slightly higher than the hot recovered strain of the tests that didn't have the creep-freeze-in quench.

### **Test F**

**Objective:** Study cold stability and hot stability of creep-strain when creep is followed directly by an annealing or stress relaxation cycle at constant strain, followed by a quench or freeze-in of that strain.

**Material:** Lot 2 Kapton, cut parallel to roll axis.

**Test Time-Line:** Apply oven, heat shrink 200 sec.; apply load, creep 500 sec.; hook loading arm to fix strain at that level, relax 500 sec.; remove oven, quench 100 sec.; remove load, cold recover 100 sec.; apply oven, hot recover 500 sec.; remove oven.

**Observations/Comments:** The load, as measured by the testing machine load cell, relaxed to about 70% of its initial value during the 500 sec. constant strain-stress relaxation period; this suggests a relaxation of 62% over a time constant of about 1,200 sec. Insufficient time was allowed, for cold recovery, to detect any. Post relaxation post-quench hot recovery was 23% of the 500 sec. creep strain, which is about the same amount of recovery, percent-wise, as was obtained in Test D where a 2,000 sec. creep time was used. This suggests that constant-strain relaxation following creep is a good process, where it can be applied.

### **Test G**

**Objective:** Study cold stability and hot stability of creep-strain when creep is followed by gradual cool-down with load applied (slow quench).

**Material:** Lot 2 Kapton, cut parallel to roll axis.

**Test Time-Line:** Apply oven, heat shrink 200 sec.; turn off oven, let it and specimen cool down in temperature (at average rate of 20°F per minute) with load applied, for 800 sec.; remove oven, then remove load, cold recover 400 sec.; apply oven, hot recover 500 sec.; remove oven.

**Observations/Comments:** This is a conceptually ambiguous process involving a compromise between hot relaxation and quenching, but it has been used successfully in creep-forming off-axis parabolic reflector films in the past. The 500 sec. hot recovery obtained, after the slow quench process, was 21% of the 500 sec. creep, which suggests a more stable film than that resulting from the other creep cycles tested.

However, this data is ambiguous because the hot recovery tests were performed as soon as the oven controller reached stability after the oven cool-down, as it had not yet been discovered that an additional 50 minutes was required for the effective oven temperature to reach steady-state; and recovery rate, much like creep rate, has been seen to be sensitive to the average oven temperature.

## **Test M**

*(as referred to in the discussion of Test B above)*

**Objective:** To find the cause of the creep rate variability observed in the preceding test

**Procedure:** Fiber test specimens were cut, side-by-side, from the same sheet of Kapton, and tested one after the other, for 100 sec. heat shrinkage, 300 sec. creep, and 100 sec. hot recovery.

# **Appendix B**

## **Curing Oven**

- **Original Layout for Test 6156-02**
- **Oven Specifications**
- **Oven Layout**
  - 6156-500**
  - 6156-600**
- **Request to Cast Films**

# Specifications for the SRS Curing Oven

## 1 — General

One (1) curing oven (to be heated electrically) will be fabricated at the oven manufacturer's plant facilities using plant labor, tooling, jigs and fixtures as necessary and furnishing all structural, mechanical and electrical materials necessary to provide a total oven system for SRS Technologies at 990 Explorer Boulevard in Huntsville, Alabama. The oven will be delivered from the manufacturer's plant site to SRS at the address above, installed and checked out in the SRS High Bay area for compliance to the Specifications, using oven manufacturer's labor, supervision and small tools as required. Prior to delivery, the oven shall be checked out for mechanical fit-up. Other items such as the blower motor/fan assembly, electrical heater unit/s and electrical power controls shall also be checked for proper operation. The SRS drawing 6156-600, dated 3-5-91 supersedes any previous drawing, and shows the general arrangement of the oven and oven components and the location within the SRS High Bay area. SRS personnel will be available for consultation on a daily basis during oven assembly/installation.

## 2 — Design Specifications

**a. Function:** Curing of polymer, flexible, thin-film membranes.

**b. Oven Operation Time:** Periodic; not production line. Nine and a half (9 1/2) hours, of which approximately five and a half (5 1/2) hours is allowed to bring the oven up to curing temperatures, and four (4) hours at the required temperature for the curing cycle.

**c. Method of Heating:** Electrical heaters located in the plenum within the oven in a closed-loop recirculated forced air duct system.

**d. Operating Temperature:** Up to 570°F, continuous.

**e. Oven Size:** See SRS drawing 6156-600. The oven shall have inside clear dimensions of 21'x21' of floor space, and head room clearance of 8' minimum. The oven manufacturer shall determine the overall exterior height necessary to provide the 8' minimum interior head room. Overall outside dimensions not to exceed 22'x22' of floor space. Exception: heating duct system as shown.

## 3 — Mechanical

### a. — General

In general, the oven shall be modular in construction, i.e., side panels, corners, top panels, floor panels, doors, etc., are to be separately manufactured components that fit in place at assembly. All exposed welds shall be ground smooth. Sharp edges where exposed to personnel shall be ground smooth. Components are to fit into the manufacturer's floor channels in place on the high bay concrete floor. The floor channels in turn are to be anchored to the concrete floor. Methods, other than floor channels may be at the manufacturer's option, but shall insure that the oven is securely fastened to the concrete floor. The oven roof panels shall be structurally supported by a system of I-beams or a single I-beam to support the roof weight. Roof panels shall be of the removable type with latching fasteners as far as practical. High temperature flexible gaskets shall be provided to minimize dust entry and heat loss. Lifting eyes shall be provided at each of the roof panels for removal by hoist. The oven shall be provided with a vertical door at one end with a 6' high by 19' wide door opening. The door shall be supported each side by

I-beam columns for the full vertical travel of the door. The vertical door lifting mechanism shall be motorized, obtaining power from the manufacturer's electrical control box. Switching shall be done from a push-button station located on the exterior wall near the vertical door, or from a push button station located on the front face of the electrical control box. The vertical door shall have 4 each viewing windows, double pane high temperature glass, approximately 18"x18" square, each. This door shall be fully insulated and of the same thickness and same type construction as the insulated side panels.

On the opposite end of the oven, an insulated double door shall be installed for personnel entry. Appropriate seals shall insure minimum heat loss and dust entry. Size of this double door entry is approximately 6' wide by 6' tall. Door latching mechanisms shall insure that personnel in the oven during the casting/spraying operation (oven heat not on at this time) may make a quick exit if an emergency should occur. Electrical systems are under separate heading.

### **b. — External Air Ducts**

There is the requirement that a minimum of 9 penetrations be made through the oven walls or roof: 8 each to facilitate the entry and exit of clean, filtered and dehumidified air exchange during the layup operation (spin casting/spraying) of the thin film polymer membrane, where small amounts of product off-gassing occurs. During this time, the oven will not be in operation. One (1) each of the penetrations are to provide a clean air intake into the heater return air duct during oven operation. All penetrations are to be equal in size to accommodate 8" I.D. duct connections. Adapters with sealing flanges shall be provided approximately where shown on the drawing. The adapters shall have manual dampers to control air flow from zero to full.

### **c. — Panels**

The oven panels shall be tongue and groove type with a minimum of 6" insulation. The roof and wall panels shall be fabricated from 20 gauge aluminized steel exterior and interior skin secured to 16 gauge steel formed channels. Thermal expansion of the oven will be accommodated by the tongue and groove panel joints. Oven structural columns and beams as required shall be 10 gauge steel formed sections. Size of the roof and side panels shall be 30" to 33" wide, 6" thick. Floor panels shall be stiffened to accommodate a floor load of 500 pounds per square foot, and will be approximately 21" wide. Floor panels shall be 3" to 4" thick. All panels shall be fully insulated with 6 pounds per cubic foot density industrial insulation. Panels shall be sealed to prevent loose insulation fibers from entering the oven that would contaminate the product. Insulation temperature rating shall exceed 600°F. Where required, flexible high temperature gasket material shall be used for sealing purposes.

### **d. — Doors**

One (1) double opening door for personnel entry shall be an integral part of the oven. Opening size to be approximately 6'-0" wide x 6'-0" tall x 6" thick, fully insulated. The doors will be standard formed and fitted construction properly reinforced to support hinges and latches. The door frame to be fabricated from steel formed sections. All exposed welds shall be ground smooth. Flexible sealing gasket material around the door closures shall be installed. Door latching hardware shall be jam-proof and easily operated from the interior side for quick egress in the event of an emergency. Locking handles shall be provided on the door exterior for safety during the oven curing cycle. Industrial insulation, 6 PCF, shall fill the door panels.

One (1) vertical opening door shall be furnished approximately 20'-0" wide x 7'-0" high above floor level. The oven vertical door open-

ing to be approximately 19'-0" x 6'-0" clear. When in the closed position, the door will be sealed with high temperature flexible gaskets around all sides. The door will be standard formed and fitted steel construction, properly reinforced to support lifting lugs for the opening mechanism. The opening mechanism shall be motorized from building power, obtained from the electrical control box. The door will be held in place by two guides (one on each side) for the fully extent of the vertical travel. This door shall have 4 each viewing windows, double pane high-temp glass, size approximately 18" x 18" each. Construction of the door shall be similar to the insulated side panels, except that additional structural reinforcing members will be required to support the door weight during lift. An integral safety catch will be supplied in each end of the door which will fully support the door when locked in its open position.

#### **e. — Structural Support Columns**

Structural support columns, if required per the manufacturer's recommendations, shall be standard steel formed sections of 10 gauge thickness.

#### **f. — Explosion Relief**

SRS does not anticipate that the oven will be subjected to explosion, due to the manner in which the volatile content of the product, (very small percentage) given off as off-gassing during oven curing, is exhausted out the top of the oven. The exhaust shall be capable of removing the proper amount of product off-gassing/hour. The oven, however, will be in accordance with current OSHA regulations for oven requirements and the National Electrical Code for explosion relief. The hazardous classification is discussed in later paragraphs of this specification.

#### **g. — Ductwork**

The interior ductwork shall be fabricated from 20 gauge aluminized steel. The supply duct

originates at the blower plenum, and is to be approximately 8"x20" or 8"x24" rectangular cross-section. Both the supply duct and air return duct shall be at floor level. The return duct shall be rectangular in cross-section and shall be 8"x20" or 8"x24". Return air duct to the blower plenum is to run vertically from the oven wall and over to the plenum at ceiling height. The spacing of openings in both ducts will be uniform with consideration to localized cold spots. The blower plenum shall be an insulated cubicle to be sized in accordance with the oven manufacturer's recommendations (approximately 3' x 3' square).

#### **h. — Heater Unit**

The oven heater shall operate from 480 volts, 3 phase, 60 Hz electrical power obtained from the electrical control box. The heater shall be sized for 120 Kw power rating, and shall deliver approximately 410,000 BTU/hr. Location of this unit shall be at the top of the plenum, with power connections to be made external to the oven roof. Power connections will be enclosed for safety to personnel. Heater controls shall be within the electrical control box and shall be a phase-fired, 3-phase solid state closed-loop control system. Temperature sensors located within the oven at one location shall feed back temperature data to the control system. The closed-loop control system shall be fail safe in the event of sensor malfunction and shall shut the oven down. Redundant temperature sensors shall be installed in the control system to insure safe operation.

#### **i. — Blower Fan**

The blower shall be located very near the bottom of the plenum, pulling return air across the electrical heater and discharging through the oven inlet duct. The blower shall be a squirrel cage design, belt-driven from a pulley external to the oven. Bearings shall be high-temperature. The blower shall operate from a motor-

driven belt external to the oven. The drive motor shall obtain 3-phase, 480 volt, 60 Hz power from the electrical control box. In the event the blower malfunctions, the control logic shall turn the heater unit off. The blower shall be rated for 10,000 CFM of air flow. The drive motor shall be rated for 7 1/2 HP. The drive belt/pulley arrangement shall be enclosed with a sheet metal cover for personnel protection.

#### **j. — Internal Oven Lights**

The oven manufacturer will install as part of the oven two high temperature illuminating fixtures inside of the enclosure. The fixtures will be located near the top of opposite walls and will provide reasonable illumination of the entire volume. The fixtures will be rated for and installed as required for a Hazardous Class 1 Division 2 area and will be rated at approximately 300 watts each.

#### **k. — Electrical Control Box (Enclosure)**

The electrical controls shall be contained within a NEMA 1 Enclosure with a hinged door for maintenance purposes. A dust tight gasket shall surround the door opening. A cooling fan with an air filter intake may be required to reduce the internal temperature of the control components. This requirement shall be at the manufacturer's recommendations. The box shall be equipped with a main circuit breaker disconnect with locking handle. Conduit hubs or conduit knockouts shall be provided at the top and bottom of the enclosure for power input, heater power and drive motor power. Primary oven controls (push buttons, etc.) shall be located on the front panel of the enclosure, with indicating lights. Size of the enclosure shall be the responsibility of the oven manufacturer. Adequate space and component arrangement within the enclosure shall be such that adjacent components do not overheat. SRS shall supply power to the control box via conduit and wiring from the building power main

distribution vault. Wiring will be sized to deliver 3-phase, 480 volt, 60 Hz, 175 amp per phase to the control box. Temperature feedback control sensors shall enter the control box via suitable connectors. The oven installer shall run power from the control box to the drive motor, vertical lift door, oven interval lights, and heater, and to other oven locations as required. The control system will require a step-down power transformer internal to the box to provide low voltage power to the control circuitry. The approximate location for this electrical control box is shown on the SRS drawing.

### **4 — Hazardous Classification and Operations**

The oven enclosure will be used as a multi-purpose facility. In one mode of operation, the oven enclosure will be used in spray casting or spin casting (pouring) of the liquid polymer over or onto a shaped surface which will form the thin-film membrane. In its second mode of operation, the oven enclosure will be used as a film curing area operating up to a temperature of 600°F. In a third mode of operation, the enclosure will be used as film coating facility. More specifically, a silver reflective coating followed by a clear protective coating will be applied onto the film surface. Because of the existence of flammable gases or vapors that are off-gassed during most of these processes, the enclosure will be classified as a Class 1 location under NFPA code 497A (*Classification of Class 1 Hazardous (Classified) Locations for Electrical Installations in Chemical Process Areas, 1986 Edition*). During all film operations, the oven enclosure will be maintained as a Division 2 location by preventing ignitable concentrations of gases or vapors through positive mechanical ventilation. The enclosure will also be subject to type Z purging prior to oven systems operation or opening of the vertical lift door in order to insure a nonhazardous environment. In order to com-

ply with the requirements in NFPA Standard 496 (*Purged and Pressurized Enclosures for Electrical Equipment, 1989 Edition*) a positive pressure ventilation system will be installed and used as follows.

An existing clean air supply will be integrated with the batch oven to provide both a positive pressure atmosphere within the oven enclosure as well as a forced mechanical ventilation system. The air supply will also provide for Type Z purging of the enclosure. The unit will supply the proper CFM into the fresh air intake ports on the oven as described in section 3b. The supply must be able to maintain positive pressure of at least 25 Pa (0.1 in. water) above the surrounding atmosphere during operation as well as provide a minimum outward velocity of 0.305m/sec (60 fpm) through all openings capable of being opened (not including the vertical lift door). A pressure drop below the 25 Pa mark is permissible while personnel doors are open.

The ventilation system will be operated continuously during any and all film process operations performed inside the oven enclosure. In order to properly purge the enclosure, the ventilation system must also be operated at maximum capacity for a minimum of 10 minutes prior to the initialization of the film curing operations (i.e. turning oven on) as well as between the completion of any operation and the opening of the vertical lift door unless conditions are known to be nonhazardous. This purge time requirement will provide a minimum of ten enclosure volumes passing through the enclosure. In the event that the oven has been in operation, the ventilation system should be operated after oven shut-down for at least 30 minutes before the door can be opened in order to cool the oven interior. This ventilation operation procedure will insure a nonhazardous environment at all times within the oven enclosure.

The ventilation system will be operated in

different modes as required during the different processes which are performed in the enclosure. During all film casting operations, enclosure purges, and film coating processes, the ventilation system will operate at maximum potential. In this mode, the purge air will enter through the four inlet fittings in the top of the enclosure. Inside the oven, ductwork will distribute the airflow evenly and smoothly down over the working area. During film curing operations, the four fittings mentioned above will be closed off and purge air will enter the oven through the return duct just in front of the heating plenum so that it will mix with the return air and be heated before it enters the main oven enclosure volume. The purge air supply will operate at a lower capacity than before and the exhaust dampers will be throttled down in order to maintain a 0.1 Pa positive pressure environment. The purge air inlet used during the curing process will be closed during all other processes. All exhaust air will exit from four ducts which are tied into the return air duct well before the heating plenum.

During film casting operations, the amount of flammable gases or vapors must not exceed at any time the capabilities of the ventilation system to maintain an inignitable concentration of the gases or vapors. Spray systems which are being looked at for the spray casting operation are of the HVLP or equivalent type. Information on this area is preliminary and not yet required in the process. When the spray equipment is defined, it will provide an adequate safety margin as required.

The oven builder will provide the following safety items as part of the oven:

- a. Warning nameplates on vertical lift door and control panel to indicate that the ventilation fan must operate for at least 10 minutes following film casting operations or for at least 30 minutes following oven operation before opening vertical door un-

less interior is known to be nonhazardous.

- b. Warning nameplate on control panel to indicate that ventilation fan must operate for at least 10 minutes prior to oven start up.
- c. A safety interlock circuit for the oven control which will prevent oven operation in the event of a ventilation system failure. Ventilation system failure will be detected at the fresh air inlet of the oven and will be indicated by a visible alarm on the oven control panel. A timer circuit shall also be implemented in this safety interlock which will prevent initialization of oven operation until the ventilation system has been operating for at least 5 minutes.

In addition to the above listed requirements, the following considerations must be addressed where applicable.

- a. All exhaust ducts shall be constructed of noncombustible materials.
- b. The electrical power for the ventilation system shall be supplied either from a separate power source or from the enclosure power supply prior to any service disconnects to the enclosure.
- c. The enclosure shall be of substantial noncombustible construction and shall be reasonable tight. Gaskets are permitted.
- d. The source of air shall be free of hazardous concentrations of flammable vapor or gas, contaminants, and any other foreign matter.
- e. Airflow through the enclosure shall be as uniform as possible so as to avoid air pockets.
- f. Air discharge from the enclosure shall be to an area classified as nonhazardous or Division 2.